The lysosomal storage disease fucosidosis:

Towards enzyme replacement therapy

Dissertation

zur Erlangung des
Doktorgrades der Naturwissenschaften

der Fakultät für Chemie
der Universität Bielefeld

vorgelegt von

Heike Wolf

Bielefeld, September 2016

1. Gutachter	Prof. Dr. Torben Lübke Fakultät für Chemie, Biochemie I Universität Bielefeld
2. Gutachter	Prof. Dr. Gabriele Fischer von Mollard Fakultät für Chemie, Biochemie III Universität Bielefeld

Tag der Abgabe: 06.09.2016

Danksagung

Die vorliegende Arbeit wurde in der Arbeitsgruppe Biochemie I an der Fakultät für Chemie der Universität Bielefeld im Zeitraum von Oktober 2013 bis September 2016 erstellt. Mein besonderer Dank gilt meinem Doktorvater Prof. Dr. Torben Lübke. Er hat mir stets hohes Vertrauen entgegen gebracht und mir damit die Möglichkeit gegeben, mich wissenschaftlich frei weiter zu entwickeln. Ich bedanke mich für sein hohes Engagement und seine Unterstützung. Vor allem in der Endphase meiner Promotion habe ich seinen kritischen Blick und seine stete Diskussionsbereitschaft schätzen gelernt.

Bei Prof. Dr. Gabriele Fischer von Mollard bedanke ich mich herzlich für die Übernhame des Koreferats.

Mein besonderer Dank gilt Prof. Dr. Thomas Dierks, der mir die Möglichkeit gab, diese Arbeit in seiner Arbeitsgruppe anzufertigen. Ich bedanke mich für seine stete Unterstützung und Diskussionsbereitschaft. Vor allem in der Endphase meiner Promotion waren seine Hinweise sehr hilfreich für mich.

Dr. Markus Damme danke ich dafür, mir die Grundlagen der Immunfluoreszenzfärbungen näher gebracht zu haben. Die gemeinsamen Arbeiten und Diskussion zu neuropathologischen Fragestellungen haben mir sehr geholfen. Ich danke ihm für seinen unermüdlichen Einsatz und seine Hinweise, die dieses Projekt vorangebracht haben.

Im Besonderen danke ich auch Prof. Dr. Renate Lüllmann-Rauch für die Übernahme der licht- und elektronenmikroskopischen Untersuchungen der *Fuca1*$^{(-/-)}$-Mäuse. Ihr unendlicher Erfahrungsschatz und ihre vielen Hinweise waren für mich sehr lehrreich.

I would like to thank Prof. Dr. Rudi D'Hooge and Dr. Stijn Stroobants for performing the behavioral analysis of the *Fuca1*$^{(-/-)}$ mice.

Furthermore I am deeply grateful to Dr. Hans Christian Beck for analyzing the storage material of the *Fuca1*$^{(-/-)}$ mice by mass spectrometry.

Mein Dank gilt den Mitarbeitern der Zentralen Tierhaltung der Universiät Bielefeld, im besonderen Christiane Grebe und Marion Knufinke für die Pflege der Mäuse. In diesem Zusammenhang möchte ich mich auch bei Dr. Axel Ziesenis, als Leiter des Maushauses, für seine stete Hilfsbereitschaft bedanken.

Ich bedanke mich bei Claudia Prange, Kerstin Böker und Mai-Britt Ilse für die hervorragende Unterstützung bei Experimenten, die reibungslose Abwicklung von Bestellungen und ihren unermüdlichen Einsatz, mit dem sie das Labor am Laufen halten.

Mein besonderer Dank gilt der gesamten Arbeitsgruppe Biochemie I, namentlich Dr. Md. Sarfaraz Alam, Christian Bartz, Tobias Beuel, Mareile Boschanski, Dr. Eva Ennemann, Marcel Freye, Marcus Gerlach, Dr. Björn Kowalewski, Tobias Krüger, Arne Linhorst, Phillipp Neuhaus, Andrea Nolting, Dr. Karthikeyan Radhakrishnan, Christof Trabszo, Dr. Michaela Wachs, Dr. Stafanie Weiland und Dr. Elena Wiegmann für die nette Arbeitsatmosphäre und die immer neuen Wendungen, die das Laborleben bereit hielt. In diesem Zusammenhang möchte ich mich auch bei allen Kollegen der Arbeitsgruppe Biochemie III für die stete Unterstützung und kollegiale Atmosphäre bedanken. Mein besonderer Dank gilt auch René Kottkamp, Marcel Strüve und Michael Weber, die mit ihrem Engagement das Gelingen dieser Arbeit vorangebracht haben.

Für die morgendlichen Kaffeerunden und den interdisziplinären Austausch bedanke ich mich bei Angela Kralemann-Köhler. Für all die kleinen Späße und unterhaltsamen Geschichten danke ich ihr recht herzlich.

Mein besonderer Dank gilt meiner Familie, für ihre Unterstützung und vot allem für die Geduld, die sie mir entgegen gebracht haben.

Als letztes möchte ich mich noch bei Marko bedanken, dafür, dass du immer für mich da warst, für deine allgegenwärtige Unterstützung in allen Höhen und Tiefen. Ich bewundere deine Geduld und dein Durchhaltevermögen, mit dem du all meine Macken ertragen hast. Du bist großartig!

Veröffentlichungen

Originalartikel

Heike Wolf, Markus Damme, Stijn Stroobants, Rudi D'Hooge, Hans Christian Beck, Irm Hermans-Borgmeyer, Renate Lüllmann-Rauch, Thomas Dierks and Torben Lübke (2016). *"A mouse model for fucosidosis recapitulates storage pathology and neurological features of the milder form of the human disease"*. In: Disease models & mechanisms.

This work was supported by Alexion Pharmaceuticals, Cheshire, CT, USA.

Posterbeiträge

Heike Wolf, Markus Damme, Stijn Stroobants, Rudi D'Hooge, Hans Christian Beck, Renate Lüllmann-Rauch, Thomas Dierks and Torben Lübke (2015). *"Targeted disruption of lysosomal α-fucosidase leads to a severe type of fucosidosis in mice"*. ESGLD-meeting, Naples, Italy.

Heike Wolf, Markus Damme, Stijn Stroobants, Rudi D'Hooge, Hans Christian Beck, Renate Lüllmann-Rauch, Thomas Dierks and Torben Lübke (2015). *"The lysosomal storage disease α-L-fucosidosis: Towards enzyme replacement therapy"*. Science-fair contest, Bielefeld University , Germany.

Contents

Summary

Fucosidosis is a rare lysosomal storage disease caused by the deficiency of the lysosomal glycosidase α-L-fucosidase resulting in the accumulation of fucosylated glycocompounds. Human fucosidosis patients are mainly characterized by progressive mental retardation and neurological deterioration leading to premature death. In this study, the generation of a constitutive fucosidosis mouse model is reported. The gene for the lysosomal α-L-fucosidase (*Fuca1*) was disrupted by gene targeting resulting in the complete absence of α-L-fucosidase activity in *Fuca1*$^{(-/-)}$ mice. The phenotype of the mouse model closely resembled that of a milder form of the human disease and due to animal welfare, the *Fuca1*$^{(-/-)}$ mice had to be euthanized at 9 - 11 months of age. A lysosomal storage pathology was detected in nearly all investigated organs of the mouse model, e. g. in liver, kidney, spleen as well as in the CNS, and was characterized by foam-like storage vacuoles to variable degree. An immense accumulation of water-soluble fucosylated glycocompounds was demonstrated and the glycoasparagine Asn-GlcNAc-Fuc was identified as main storage material in kidney and brain and was also excreted with the urine of the *Fuca1*$^{(-/-)}$ mice. The neuropathological alterations of the mouse model were analyzed in more detail, as these are the leading symptoms in human fucosidosis. The *Fuca1*$^{(-/-)}$ mice exhibited neuroinflammatory signs including prominent micro- and astrogliosis and suffered from progressive loss of Purkinje cells. Particularly the latter might contribute to behavioral abnormalities of the animals including progressive coordinatory and motor deficits as well as a reduced overall activity and cognitive impairment.

In order to enable the development of an enzyme replacement therapy (ERT) for the fucosidosis disease, an expression system for the production of the human α-L-fucosidase was generated in CHO-K1 cells. While a purification strategy for the His_6-tagged enzyme was established using a Ni^{2+}-affinity chromatography followed by a strong cation exchange chromatography, the purification of the untagged α-L-fucosidase was more challenging and needs further efforts. Finally, a *Fuca1*$^{(-/-)}$ mouse was intravenously treated with purified His_6-tagged enzyme resulting in an efficient uptake of the recombinant α-L-fucosidase into visceral organs and in a complete clearance of storage material in the spleen. These preliminary results provide promising data with regard to develop an ERT also for human fucosidosis patients.

Zusammenfassung

Fucosidose ist eine seltene lysosomale Speichererkrankung. Sie wird durch die Defizienz der lysosomalen Glykosidase α-L-Fucosidase verursacht, sodass es zu einer Anreicherung von fucosylierten Glykokonjungaten kommt. Die Leitsymptome humaner Fucosidose-Patienten sind eine fortschreitende mentale Retardierung sowie eine Verschlechterung neurologischer Fähigkeiten, sodass die betroffenen Patienten frühzeitig versterben. In der vorliegenden Arbeit wird die Generierung eines konstitutiven Fucosidose Mausmodells beschrieben. Dafür wurde das Gen für die lysosomale α-L-Fucosidase (*Fuca1*) gezielt zerstört (*gene targeting*). Der resultierende, vollständige Verlust der Enzymaktivität der α-L-Fucosidase führt zu einem Phänotyp des Mausmodells, welcher stark dem einer milderen Form der humanen Erkrankung ähnelt. Die *Fuca1*$^{(-/-)}$-Tiere mussten aus Tierschutzgründen im Alter von 9 - 11 Monaten euthanasiert werden. In nahezu allen untersuchten Organen, z. B. in der Leber, Niere, Milz und auch im ZNS, wurde ein lysosomaler Speicherphänotyp mit unterschiedlich vielen Speichervakuolen festgestellt, welche ein schaumartiges Aussehen aufwiesen. Dabei akkumulierten fucosylierte Glykokonjungate in großen Mengen. Das Glykoasparagin Asn-GlcNAc-Fuc, welches auch mit dem Urin der Tiere ausgeschieden wurde, wurde als Hauptspeichermaterial. Desweiteren wurden die neuropathologischen Veränderungen des Mausmodells detailliert untersucht, da diese die Leitsymptome humaner Fucosidose-Patienten darstellen. Im Gehirn der *Fuca1*$^{(-/-)}$-Mäuse wurden entzündliche Prozesse in Form von Mikro- und Astrogliose sowie eine progressive Degenerierung von Purkinje-Zellen festgestellt. Vor allem letzteres könnte zur Entwicklung von Verhaltensauffälligkeiten der Tiere, wie progressiven Koordinations- und Bewegungsschwierigkeiten, einer verminderten Aktivität sowie einer geringeren kognitiven Leistungsfähigkeit beitragen.

Um die weitere Entwicklung einer Enzymersatztherapie (*enzyme replacement therapy*; ERT) zu ermöglichen, wurde für die humane α-L-Fucosidase ein Expressionssystem in CHO-K1-Zellen etabliert. Für das His_6-getaggte Enzym konnte erfolgreich eine Aufreinigungsstrategie mittels einer Ni^{2+}-Affinitätschromatographie und einer starken Kationen-Austauschchromatographie erarbeitet werden. Die Entwicklung einer Aufreinigungsstrategie für das ungetaggte Enzym erwies sich als schwieriger, sodass hier noch weitere Studien nötig sind. In einem finalen Experiment wurde einer *Fuca1*$^{(-/-)}$-Maus die aufgereinigte, His_6-getaggte α-L-Fucosidase intravenös appliziert, welche dann vor allem in viszeralen Organen nachweisbar war, was in der Milz zu einem vollständigen Abbau des Speichermaterials führte. Diese ersten Experimente liefern vielversprechende Daten in Hinblick auf die Entwicklung einer ERT für humane Fucosidose-Patienten.

1 Introduction

1.1 The lysosome

Lysosomes are specialized, membrane-enclosed organelles and represent the main degradative compartment in eukaryotic cells. Initially, lysosomes were described by Christian de Duve as membrane-enclosed vesicles which sedimented during differential cell centrifugation together with a subset of acidic hydrolases (de Duve et al. 1955) and represent the terminal degradative compartment of eukaryontic cells (de Duve 1963). More recently, it was recognized that the lysosome is not only the terminal compartment of catabolic processes but also participates in the regulation of signaling, nutrient sensing, antigen presentation and programmed cell death (Fraldi et al. 2016, Carmona-Gutierrez et al. 2016). Until now, more than 60 soluble (Lübke et al. 2009) as well as more than 100 lysosomal transmembrane proteins (Schwake et al. 2013) have been identified, although the analysis of the lysosomal proteome is still ongoing. The soluble proteins are mainly acidic hydrolases which degrade macromolecules like proteins, oligo- and polysaccharides, complex lipids, RNA and DNA. The resulting monomers (amino acids, monosaccharides, fatty acids, cholesterol and nucleotides) leave the lysosome through specific membrane-bound efflux transporter proteins and can be re-utilized in biosynthetic processes within other cell compartments. Hence, the lysosome has an important impact on the regulation of the cellular homeostasis (Micsenyi and Walkley 2013). The lysosomal hydrolases are characterized by an acidic pH optimum (acidic hydrolases) and the lysosome itself exhibits an acidic luminal pH which is maintained through ATP-dependent proton pumps (Cuppoletti et al. 1987).

The uptake of compounds into the lysosome is mediated by three major pathways: a biosynthetic, an endocytotic and an autophagic pathway. Lysosomal proteins are synthesized at the rough endoplasmatic reticulum (rER) and are further transported towards the lysosomal compartment via the Golgi apparatus and endosomes (see also section 1.1.1). Extra- and intracellular material that is designated for further degradation reach the lysosome via en-

docytosis and autophagy, respectively (Micsenyi and Walkley 2013). In case of endocytosis, extracellular material is invaginated into transport vesicles at the plasma membrane of the cell, either receptor-mediated or receptor-independent, and is further transported towards the lysosome via early and late endosomes (van Meel and Klumperman 2008). Intracellular material reaches the lysosome by autophagy, which can be further divided into macroautophagy, microautophagy and chaperone-mediated autophagy. Macroautophagy describes the formation of a double membrane which engulfs cytosolic material or entire organelles and the further generation of autophagosomes. The invaginated material is recognized by adaptor molecules like heat-shock proteins that mediate their specific uptake into the autophagosome (Micsenyi and Walkley 2013). In contrast, microautophagy does not involve the *de novo* generation of double membrane structures but rather mediates uptake of cytosolic material into lysosomes by a pinocytosis-like process (Platt et al. 2012). Chaperone-mediated autophagy targets selectively proteins containing a KFERQ motif for proteolysis. The proteins are recognized by the Hsc-70 chaperone, which promotes protein unfolding. The lysosome-associated membrane protein type 2A (Lamp2A) mediates the further transport of the targeted proteins across the lysosomal membrane (Dice 2007).

1.1.1 Synthesis of lysosomal proteins

The expression of many lysosomal proteins is regulated by the transcription factor EB (TFEB). Due to lysosomal stress or nutrient depreviation, cytoplasmic TFEB becomes activated by phosphorylation and is transferred into the nucleus, where it promotes the transcription of genes harboring a CLEAR (coordinated lysosomal expression and regulation) element. The phosphorylation is carried out by the rapamycin complex 1 (mTORC1) kinase, which is a master regulator of cell homeostasis and growth (Bar-Peled and Sabatini 2014) in dependency of e. g. the availability of amino acids. The latter is sensed in the lysosome by the lysosomal nutrient sensing machinery (LYNUS), a multi-protein complex consisting of e. g. the *v*-ATPase (Fraldi et al. 2016). In cells with sufficient amino acid levels, the *v*-ATPase promotes the GTP-loading of different GTPases, which results in the recruitment of mTORC1 to the lysosomal surface and its activation leading to promoted cell growth, whereas autophagy is inhibited. At the lysosomal surface, mTORC1 kinase phosphorylates TFEB at Ser^{211}, which results in the retainment of the transcription factor in the cytosol. Under nutrient-depreviative conditions, mTORC1 is inactivated, resulting in the dephosphorylation of TFEB and its translocation into the nucleus, where it promotes the transcription of genes for many lysosomal proteins

and autophagy-related proteins (Bar-Peled and Sabatini 2014). Moreover, the expression of several proteins associated with proper lysosomal function (e. g. receptors essential for lysosomal targeting: MPR300 and MPR46) is also regulated by TFEB, whereas the lysosomal α-L-fucosidase, which is the focus of this work, is expressed independently from TFEB regulation (Sardiello et al. 2009). Recently it was demonstrated, that the transcription factor E3 (TFE3) acts in a similar manner as TFEB. TFE3 is also regulated by the mTORC1 pathway and promotes transcription of genes harboring CLEAR elements (Martina et al. 2014).

Lysosomal proteins are synthesized at the rough endoplasmatic reticulum (rER) and the nascent peptide chain is co-translationally translocated into the ER lumen. This process is mediated by a *N*-terminal signal peptide of 15 - 30 amino acids, that is proteolytically cleaved after ER translocation. During the further transport of lysosomal proteins through ER and Golgi, the proteins are post-translationally modified, e. g. most soluble lysosomal hydrolases receive a mannose-6-phosphorylation (M6P) signal which is specifically recognized in the *trans*-Golgi network and directs lysosomal targeting. (see also section 1.1.2; Braulke et al. 1987).

Most lysosomal proteins are highly *N*-glycosylated, a co-translational modification that is also important for proper protein folding, oligomerization, quality control and further transport (Braulke et al. 1987). *N*-glycans are attached to asparagine residues at the outer surface of proteins within the recognition motif Asn-X-Ser/Thr, where X stands for any amino acid except proline. Initially, the oligosaccharide chain is synthesized on a lipid anchor (dolichol phosphate) and consists of two *N*-acetylglucosamine, nine mannose and three glucose residues. After transfer of the oligosaccharide chain to the protein, the three terminal glucose as well as one mannose residue is cleaved off by the sequential action of α-glucosidases I and II and the α-mannosidase I. The glycosylated proteins are transported to the Golgi apparatus, where the *N*-glycans are further trimmed, but the core-structure consisting of two *N*-acetylglucosamine and three mannose residue is always maintained. In parallel, different saccharide residues can be added, so that the final *N*-glycans are divided into a mannose-rich, a complex and a hybrid type (figure 1.1): Lysosomal proteins exhibit mainly mannose-rich *N*-glycans consisting of two *N*-acetylglucosamine core-residues followed by a variable number of mannose-residues. The complex type *N*-glycans contain the core-saccharide unit described above which can be extended by mannose, *N*-acetylglucosamine, galactose and sialic acid. Moreover a fucose residue can be added α1-6 at the *N*-acetylglucosamine linked to the asparagine residue or at the peripheral residues α1-3 / α1-4 to *N*-acetylglucosamine or α1-2 to galactose. The hybrid type is a mixed *N*-glycan, where one antenna is composed of a mannose-rich *N*-glycan and

another antenna belongs to the complex *N*-glycan (Kornfeld and Kornfeld 1985).

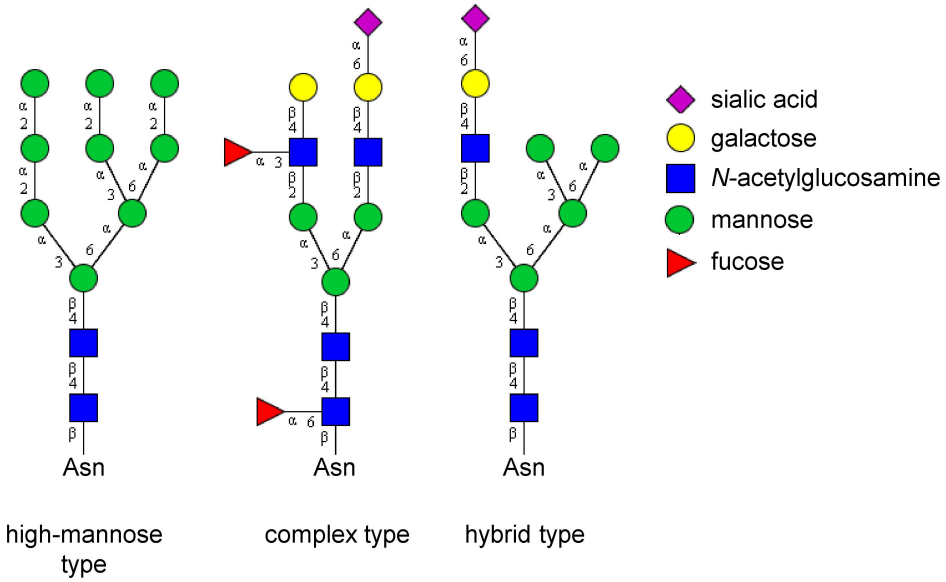

Figure 1.1: *N*-glycan structures
N-glycans can be separated into a high-mannose type and a complex type. Moreover, hybrid type *N*-glycans exhibit properties of both, high-mannose and complex type *N*-glycans. Modified from Kornfeld and Kornfeld (1985).

1.1.2 Targeting of proteins towards the lysosome

Most soluble lysosomal proteins are targeted through the mannose-6-phosphate (M6P)-dependent pathway (figure 1.2). The M6P residue is added to high-mannose-type *N*-glycans in the Golgi apparatus. In detail, the UDP-*N*-acetylglucosamine 1-phosphotransferase (GNTP) transfers a *N*-acetylglucosamine-1-phosphate to the C6-position of selected mannose residues in the *cis*-Golgi network (Pohlmann et al. 1982, Kornfeld and Mellman 1989). The GNTP specifically modifies *N*-glycans of lysosomal enzymes which are recognized by lysine residues at the protein surface near the *N*-glycosylation site (Braulke and Bonifacino 2009). The *N*-acetylglucosamine is subsequently removed by the *N*-acetylglucosamine-1-phosphodiester α-*N*-acetylglucosaminidase (uncovering enzyme, UCE) in the *trans*-Golgi network, resulting in the exposure of the M6P residue (Coutinho et al. 2012b). Two specific M6P receptors (MPRs) are present in the *trans*-Golgi network: the cation-independent MPR with an molecular weight of approximately 300 kDa (MPR300) and the cation-dependent 46 kDa MPR (MPR46). Both receptors bind the M6P residue with high affinity at almost neutral pH and direct the further

transport of lysosomal proteins in clathrin-coated vesicle towards the late endosomes. Due to the acidification in late endosomes, the cargo is released from the receptors which are recycled to the *trans*-Golgi network, whereas the M6P modified proteins reach the lysosomal compartment probably by fusion of late endosomes and lysosomes. Interestingly, although both receptors recognize the same sugar moiety, they exhibit different binding affinities towards lysosomal proteins, which is probably caused by individual structures of the proteins

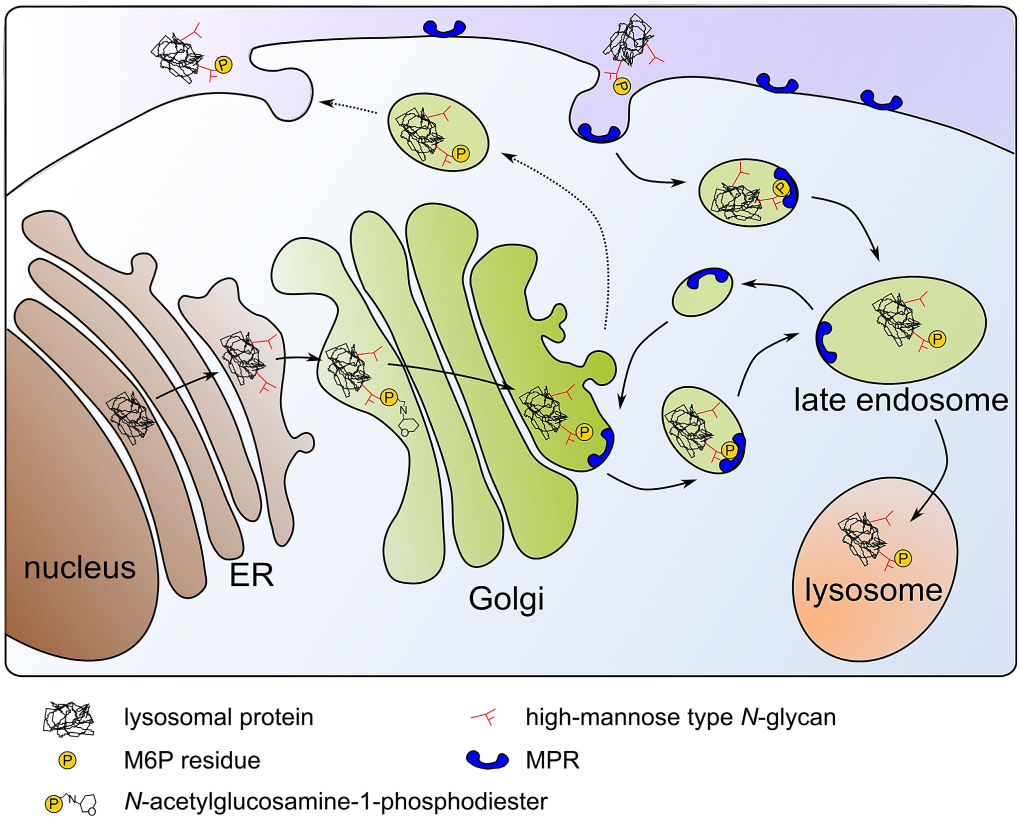

Figure 1.2: MPR-dependent targeting of soluble proteins towards the lysosome
Newly synthesized lysosomal proteins are co-translationally translocated into the rough endoplasmatic reticulum (ER), where they are glycosylated. The proteins are further transferred towards the *cis*-Golgi network, where a *N*-acetylglucosamine-1-phosphate is added on high-mannose type *N*-glycans by GNTP. The lysosomal proteins are further transported towards the *trans*-Golgi network, where the *N*-acetylglucosamine is removed by UCE resulting in the exposure of the M6P residue, which is recognized by MPRs. The MPRs direct the transport of the proteins into late endosomes, where the cargo is released from the MPRs due to the low pH value. The receptors are recycled to the Golgi, whereas the soluble lysosomal proteins reach the lysosomal compartment by fusion of late endosomes and lysosomes. A part of the newly synthesized lysosomal proteins escape the MPR recognition in the *trans*-Golgi network and is secreted. These proteins can be recaptured by MPRs located at the cell surface and are also transported towards late endosomes and lysosomes.

(Coutinho et al. 2012b). Besides their localization in the *trans*-Golgi network and in late endosomes, both MPRs can be also found at the plasma membrane of cells, but only the MPR300 is able to mediate the endocytosis of M6P-modified proteins (Braulke and Bonifacino 2009). This fact is of special importance, as approximately 5 - 20 % of all newly synthesized lysosomal proteins escape the lysosomal targeting in the *trans*-Golgi network and are initially secreted (Markmann et al. 2015). At the plasma membrane, they can be recaptured by the MPR300, a mechanism which is also the basis for an enzyme replacement therapy (section 1.2.1).

Besides the M6P-dependent pathway, some soluble lysosomal proteins reach the compartment by other routes. It was shown, that the lysosomal integral membrane protein 2 (Limp2) mediates the transport of the β-glucocerebrosidase (Reczek et al. 2007), whereas sortilin is a receptor for the accessory proteins prosaposin and GM2 activator protein (Coutinho et al. 2012a) and participates in the lysosomal transport of the cathepsins D and H (Canuel et al. 2008). More recently, the Lrp1 and the LDL receptor were found to be involved in the lysosomal targeting of the cathepsins B and D (Markmann et al. 2015). In contrast, the lysosomal targeting of the α-L-fucosidase is strictly dependent of the MPR-pathway (Kollmann et al. 2012, Markmann et al. 2015).

In contrast to soluble proteins, lysosomal membrane proteins contain a sorting signal in their cytosolic tails, which is based either on a dileucine motif ([DE]XXXL[LI], X stands for any amino acid) or on a tyrosine rich signal (YXXØ, Ø stand for a large hydrophobic amino acid). The sorting signal is recognized by specific adaptor proteins mediating the lysosomal targeting either directly in the *trans*-Golgi network or the membrane proteins are first secreted and then recaptured at the plasma membrane (Braulke and Bonifacino 2009).

1.2 Lysosomal storage disorders

Lysosomal storage disorders (LSDs) are a class of more than 50 inherited, monogenetic diseases that are caused by an impaired lysosomal function (Hopwood 2013). 85 % - 90 % of all diagnosed cases are due to the deficiency of a single lysosomal hydrolase (Winchester 2013a) resulting in progressive accumulation of undegraded macromolecules inside the lysosome (primary storage material). Thereby, the function of the entire endosomal-lysosomal system is impaired leading to an decreased autophagic flux and the accumulation of toxic

substances which can initiate cellular apoptosis. Moreover, LSDs result not only in the accumulation of macromolecules, but also in a reduced efflux of monomeric compounds out of the lysosome and in a disturbed cellular homeostasis leading to metabolic insufficiency and cellular stress (Platt et al. 2012). The immense storage burden of the endosomal-lysosomal system often leads to an impaired function of other lysosomal proteins, which results in the accumulation of secondary storage material, which is not a substrate of the deficient enzyme itself (Micsenyi and Walkley 2013). During disease progression, these pathologic events result in cell and multisystemic tissue dysfunction (Hopwood 2013).

LSDs can be divided into different subtypes according to the accumulating storage material: sphingolipidoses (e. g. GM1-gangliosidosis), mucopolysaccharidoses (e. g. MPS I), glycoproteinoses (e. g. fucosidosis, section 1.2.3) and neuronal ceroid lipofuscinoses (e. g. CLN1 disease). Novel classifications are based on the kind of the deficient protein, where LSDs can be due to defects in soluble lysosomal hydrolases, soluble lysosomal matrix proteins (non-enzymatic), lysosomal membrane proteins or non-lysosomal proteins (Winchester 2013a).

LSDs are inherited in an autosomal recessive manner except Danon, Fabry and Hunter disease, which are X-linked (Wraith and Beck 2013). Each LSD itself is a rare disease, but in combination they have an incidence of $1:5000$ (Lübke et al. 2009, Coutinho et al. 2012b) to $1:7000$ live births (Hopwood 2013, Micsenyi and Walkley 2013). Moreover, the number of undiagnosed or miss-diagnosed cases might by very high, particularly in non-industrial countries. Most LSDs are characterized by a broad spectrum of clinical presentations, although neuropathological alterations of the CNS resulting in physical and mental deterioration are very common features of this group of diseases. Moreover skeletal malformations, cardiac diseases, current respiratory infections as well as organomegaly (enlargement of visceral organs like liver, kidney, spleen) are often observed (Wraith and Beck 2013). The clinical onset as well as the rate of disease progression often differ between patients of a single LSD. Infantile onsets are often connected with severe disease progression leading to death within the first decade of life, whereas patients with an adult onset may live until the third or fourth decade of live (Hopwood 2013). The initial LSD diagnosis is mainly based on the clinical presentation, whereas the individual disease is then often identified by biochemical methods, e. g. the detection of accumulating substrates which are also excreted into the blood or urine of the patients. Finally the disease has to be confirmed by the absence of enzymatic activity (in case of a deficient hydrolase) or by molecularbiological analysis of the affected gene and identification of the disease-causing mutation (Winchester 2013b).

1.2.1 Treatment of lysosomal storage disorders

Even today, the treatment of LSD is challenging, as there exists no cure and in most cases even no specific therapy for the single LSDs is available. Nevertheless, symptomatic therapies improving the LSD symptoms can provide great support for patients and their families, e. g. skeletal malformations may be corrected by surgery (Cox 2013).

Bone marrow transplantation (BMT) is a classical treatment for LSDs, where haematopoietic stem cells (HSCs) are engrafted into the immuno-suppressed recipient and may complement the lacking enzyme activity. The transplanted cells secrete the deficient enzyme, which can be endocytosed by the patient's cells e. g. via the M6P-dependent pathway. However, the effects of a BMT is dependent on the type and the stage of the disease as well as on the specific glycosylation and modification of the enzymes and the secretion capacity of the enzyme-producing cell line. BMT can have beneficial effects on visceral symptoms, but the effects on bone diseases and neuropathological symptoms vary (Matzner 2005). As the BMT-related mortality risk is high, the search for alternative therapies is ongoing (Cox 2013).

The most common treatment for LSDs is enzyme replacement therapy (ERT), which was first suggested by de Duve (1964). ERT is based on the MPR300 localized at the plasma membrane of cells. As mentioned in section 1.1.2, extracellular proteins harboring a M6P modification can be recognized by the MPR300 and are further endocytosed and transported towards the lysosome (Braulke and Bonifacino 2009). Hence, recombinant proteins can be administered intravenously during ERT, are endocytosed and can correct the deficiency of the lysosomal protein (Coutinho et al. 2012b). The aim of the ERT is to reverse or at least to stop the progression of the LSD phenotype and to degrade the accumulated storage material. The first ERT approaches were performed in the 1970s, when human enzymes which were purified from e. g. placenta were used (Desnick and Schuchman 2002). Today, the enzymes are recombinantly produced in e. g. CHO cells and are purified from cell culture medium (Jayapal et al. 2007). ERT is a well proven therapy for LSDs and is commonly used for treatment of e. g. Gaucher and Fabry disease, for MPS I, MPS II, MPS VI and Pompe disease (Cox 2013). Although an ERT might reverse years of substrate accumulation, it is no cure and the recombinant enzyme has to be administered life-long (Desnick and Schuchman 2002). Moreover, ERTs have some limitation regarding the biodistribution of the administered enzyme. Only minor amounts reach the so-called "hard-to-treat" tissues like muscle cells, bones, lungs and particularly the CNS, as the intravenously injected enzyme is unable to cross the blood-brain-barrier (Bur-

row and Grabowski 2013, Acosta et al. 2015, Condori et al. 2016). In this context, ERT was initially used for treatment of LSDs without neurological participation and no improvement of neurological symptoms was observed in ERT-treated MPS I, MPS II and MPS VI patients (Beck 2009). This limitation might be prevented by intrathecal administration, although it bears a high risk for CNS infections (Burrow and Grabowski 2013). In addition, preclinical studies using fusion constructs with so-called "Trojan horses" have shown great potential. The lysosomal enzmes are fused to proteins, which are transported across the blood-brain-barrier and might mediate also the uptake of the lysosomal enzyme (Boado et al. 2011, Acosta et al. 2015, Condori et al. 2016). Due to the intravenous injection of the enzymes, the ERT often leads to development of antibodies, which might result in allergic reactions and / or neutralize the enzyme. This might be prevented by premedication with antihistamines or in severe cases by administration of methotrexate. However, in most cases the antibody titer decreases over time and patients start to tolerate the recombinant enzyme (Desnick and Schuchman 2002).

Substrate reduction therapy is another treatment option for LSDs and aims to reduce the synthesis of the accumulating storage material by administration of small-molecule inhibitors. Moreover, the current investigations on pharmacological chaperones are promising. Here, LSDs resulting from a mutation influencing the folding or stability of the lysosomal enzyme are addressed. After binding to the chaperone, the enzyme is stabilized and may display a residual activity sufficient to improve the LSD pathology (enzyme enhancement therapy EET; Beck 2009, Cox 2013, Burrow and Grabowski 2013).

In the future, the most promising treatment seems a gene therapy. Here, induced pluripotent stem cells (iPSCs) are generated from the patient's fibroblasts, are genetically manipulated and re-transferred into the patient, thereby avoiding graft-versus-host reactions. However, further studies are necessary, as rejections of autologous transplanted iPSCs were observed in mice. During *in vitro* culture of the iPSCs, the patients' mutation in the affected lysosomal gene can be corrected e. g. by homologous recombination or knock-in of the functional gene (Burrow and Grabowski 2013).

1.2.2 Glycoproteinoses

Glycoproteinoses are a subgroup of LSDs that result from defects in glycoprotein metabolism leading to accumulation of oligosaccharides and / or glycopeptides (table 1.1). They all are rare diseases and represent less than 10 % of all LSDs with a combined incidence of 1 : 100 000

(Malm et al. 2013). Most of the glycoproteinoses are caused by deficient lysosomal glycosidases that are involved in the degradation of *N*-glycosylated proteins, which is a highly ordered process. These participating exoglycosidases degrade *N*-glycans in a sequential manner, that is given by the structure of the *N*-glycan and, hence, the deficiency of one glycosidase leads to a termination of the *N*-glycan degradation and accumulation of defined oligosaccharides and glycopeptides (Winchester 2005).

The degradation of *N*-glycans is a bidirectional process and happens sequentially from the reducing and the non-reducing end of the *N*-glycan (figure 1.3). The first step is the proteolysis of the polypeptide of the glycoprotein by different lysosomal proteases (cathepsins) resulting in the release of the *N*-glycan that is still connected to the asparagine residue. This intermediate state is a prerequisite for the further degradation of the *N*-glycan, that is dependent on free α-amino and α-carboxyl groups of the asparaginyl moiety. The next step is the removal of any fucose residue (terminal or core-fucose; section 1.1.1) of complex or hybrid *N*-glycans catalyzed by the α-L-fucosidase. A deficiency of this enzyme results in the LSD fucosidosis (see section 1.2.3) and the accumulation of fucosylated glycocompounds (Winchester 2005). The removal of the asparagine is blocked in the presence of a core-fucose residue, that sterically inhibits the aspartylglucosaminidase (Noronkoski and Mononen 1997). The core-*N*-acetylglucosamine is removed by the endo-β-*N*-acetylglucosaminidase (chitobiase) from the reducing end of the *N*-glycan. Interestingly, the deficiency of the chitobiase does not result in an LSD, as the core-*N*-acetylglucosamine can also be removed as the final step from the non-reducing end of the *N*-glycan catalyzed by the β-hexosaminidase. The

Table 1.1: Lysosomal storage disorders caused by defects in glycoprotein metabolism

disease	deficient enzyme	major storage material
fucosidosis	α-L-fucosidase	glycopeptides
aspartylglucosaminuria	aspartylglucosaminidase	glycopeptides
sialidosis	neuraminidase (sialidase)	oligosaccharides
GM1-gangliosidosis	β-galactosidase	gangliosides
galactosialidosis	protective protein (cathepsin A)	oligosaccharides
Sandhoff disease	β-hexosaminidase	gangliosides
α-mannosidosis	α-mannosidase	neutral oligosaccharides
β-mannosidosis	β-mannosidase	neutral oligosaccharides
Schindler / Kawasaki disease	α-*N*-acetylgalactosaminidase	glycopeptides

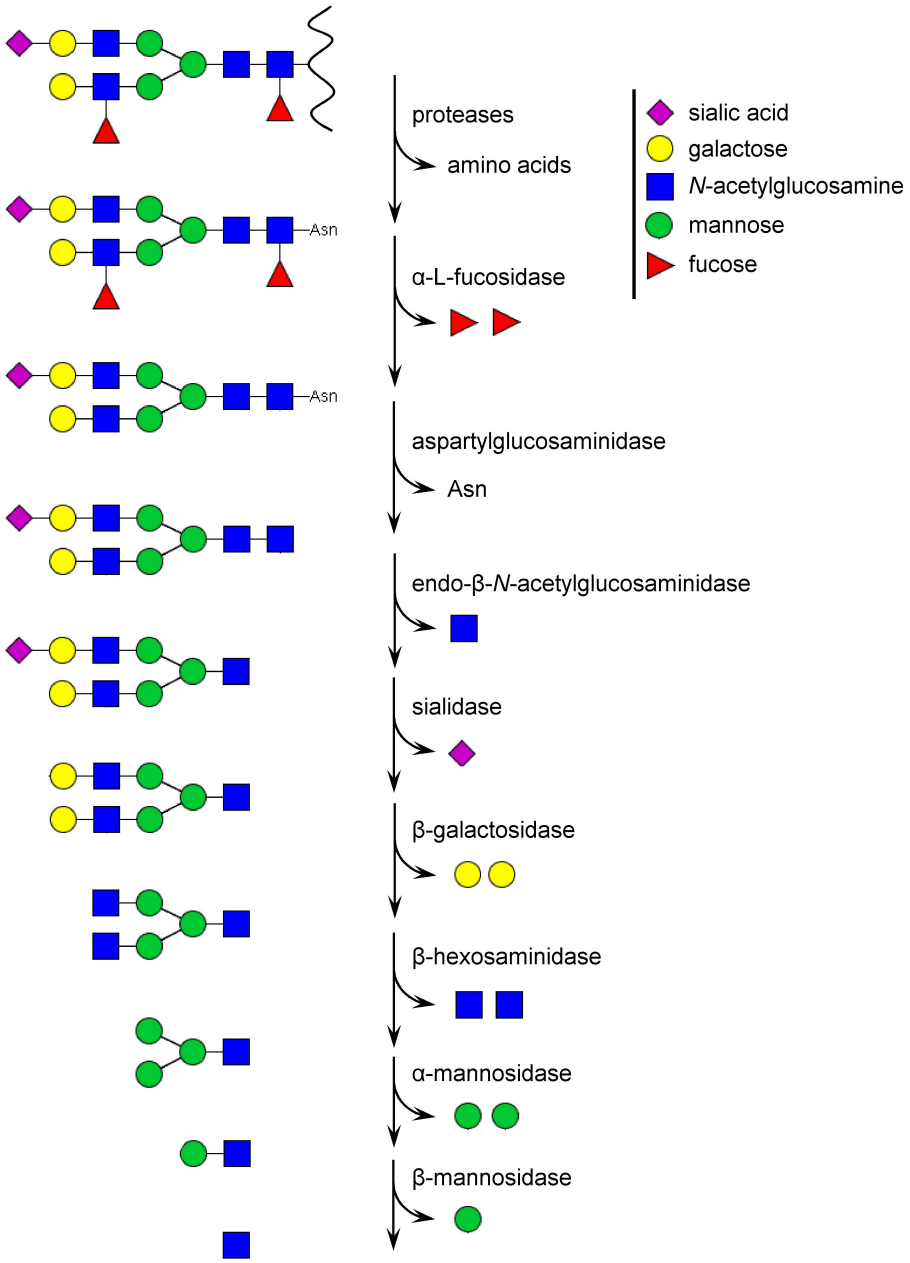

Figure 1.3: Degradation of *N*-glycans
Complex *N*-glycans are degraded bidirectional from the reducing end as well as the non-reducing end. The single exoglycosidases act in a sequential manner. The deficiency of one glycosidase leads to termination of the *N*-glycan degradation, so that the residual *N*-glycan is accumulating in the corresponding LSD (see also table 1.1). Modified from Winchester (2005).

residual *N*-glycan is degraded from the non-reducing end. In case of a complex or hybrid *N*-glycan, sialic acid, galactose, *N*-acetylglucosamine and mannose residues are removed by

the sequential action of the lysosomal enzymes sialidase, β-galactosidase, β-hexosaminidase, α-mannosidase and β-mannosidase. Again, a prerequisite for this degradation is the removal of terminal fucose residues by the α-L-fucosidase. In case of a high-mannose type *N*-glycan, the α- and β-mannosidases as well as the β-hexosaminidase are required (Winchester 2005). The deficiency of one particular enzyme leads to the corresponding LSDs, which are listed in table 1.1. Of note, β-hexosaminidase and β-galactosidase are also participating in the degradation of glycolipids and, hence, the major accumulating storage material in Sandhoff disease and GM1-gangliosidosis are gangliosides, even though oligosaccharides are also accumulating (Clarke 2013). Moreover, the LSD galactosialidosis is caused by the combined deficiency of sialidase and β-galactosidase resulting from mutations in the gene encoding the protective protein cathepsin A. Cathepsin A forms a multi-enzyme complex with both glycosidases and directs their transport towards the lysosome as well as their intralysosomal activation and stable conformation (d'Azzo and Bonten 2013). In contrast, the β-*N*-acetylgalactosaminidase is participating in the degradation of *O*-linked glycans and its deficiency results in the Schindler disease, which is characterized by the accumulation of glycopeptides linked to serine or threonine residues (Winchester 2005).

1.2.3 Deficiency of α-L-fucosidase results in fucosidosis

The α-L-fucosidase (EC 3.2.1.51) is a lysosomal hydrolase that was first mentioned by Levvy and McAllan (1961). The enzyme is encoded by the *Fuca1* gene located on chromosome 1 (1p34), which includes eight exons. The α-L-fucosidase consists of 439 amino acids and an additional *N*-terminal signal peptide of 22 amino acids, that is cleaved off after co-translational import into the ER. The enzyme contains two active site residues, D230 and E294 (Liu et al. 2009; there referred to as D225 and E289) and cleaves glycosidic bonds, in which L-fucose is linked to galactose (α1-2, α1-3 or α1-6), *N*-acetylglucosamine (α1-3, α1-4 or α1-6) or to glucosamine (α1-3) (Willems et al. 1991). α-L-Fucosidase has already been purified from various human tissues, e.g. placenta (Wiederschain et al. 1971), kidney (Wiederschain et al. 1973) and liver (Robinson and Thorpe 1973, Alhadeff et al. 1975a, Alhadeff and Freeze 1977) and was shown to form homooligomers (Chien and Dawson 1980, Alhadeff et al. 1975a, Turner 1979). Up to seven isoforms of the α-L-fucosidase were isolated from human liver and could be separated from each other by starch gel electrophoresis (Turner et al. 1974, Alhadeff et al. 1974b). The isoforms exhibited distinct glycosylation patterns that differed in their degree of sialic acid content resulting in a slightly altered α-L-fucosidase activity, isoelectric

point and pH optimum (Alhadeff et al. 1978) as well as in different retention volumes of the isoforms during size exclusion chromatography (Alhadeff 1978).

The deficiency of α-L-fucosidase causes the LSD fucosidosis (glycoproteinosis; OMIM 230000) that leads to the accumulation of fucosylated oligosaccharides, glycoproteins and glycolipids (Willems et al. 1991). The enzyme is participating in the degradation of complex *N*-glycans. Here, the presence of a core-fucose residue sterically inhibits the subsequent removal of the asparaginyl residue by aspartylglucosaminidase (Noronkoski and Mononen 1997) and, hence, the deficiency of α-L-fucosidase leads to an accumulation of fucosylated glycoasparagines (Yamashita et al. 1979, Michalski and Klein 1999). Moreover, several oligosaccharides harboring terminal but no core-fucose residues were found to accumulate in human patients (Tsay et al. 1976, Tsay and Dawson 1976, Nishigaki et al. 1978, Michalski and Klein 1999). Here, the core-unit of the *N*-glycan (asparaginyl residue and the first *N*-acetylglucosamine) could be removed, whereas the degradation from the non-reducing end of the *N*-glycan was prevented by the presence of terminal fucose residues. A considerable proportion of the accumulating glycopeptides as well as oligosaccharides is also excreted with the urine and can be used for initial diagnosis by thin-layer chromatography (Willems et al. 1991, Michalski and Klein 1999). In addition, α-L-fucosidase is involved in the degradation of fucosylated glycolipids harboring terminal blood group antigens (H-, A- and B-antigens as well as Lewis antigens; figure 1.4). The H-antigen was found as the major storage material in the liver of fucosidosis patients along with the Lewis^x antigen (Dawson and Spranger 1971, Tsay et al. 1976, Michalski and Klein 1999). At the microscopic level, the accumulation of fucosylated glycocompounds results in the formation of foam-like storage vacuoles in multiple organs of human patients, which appeared mainly empty in light microscopy analysis, indicating water-soluble storage material. However, electron microscopy revealed also granular or lamellar inclusions of moderate electron density, indicating highly heterogeneous storage material (Willems et al. 1991).

Fucosidosis is an ultra-rare disease and only about 120 individuals suffering from that disease have been reported until now. The first two patients, two italian sibs, were described by Durand et al. (1966) and suffered from progressive mental retardation and neurological deterioration leading to death before the age of 5 years. The disease was initially reported to exhibit Hurler-like (MPS I) symptoms. Two years later, van Hoof and Hers (1968b) discovered a disease-causing deficiency of α-L-fucosidase in several tissues of three patients suffering from similar symptoms. The disease was then designated as mucopolysaccharidosis F (MPS F; van Hoof

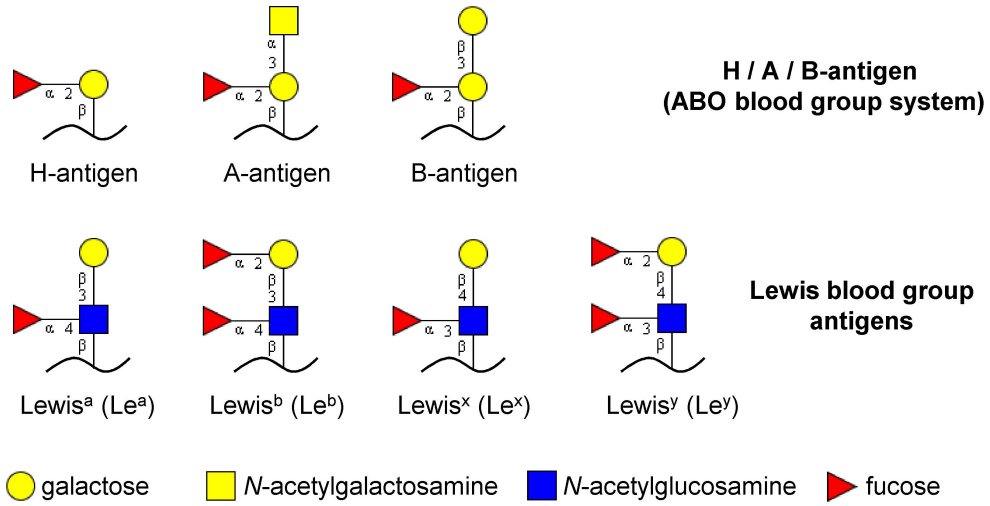

Figure 1.4: Structures of antigens containing L-fucose residues
The structures of antigens containing L-fucose residues are shown (H-, A-, B-blood group antigen as well as Lewis blood group antigens). The antigens can occur as terminal moieties on glycoproteins and glycolipids. Modified from Stanley and Cummings (2009).

and Hers 1968a). In parallel, Durand et al. (1968) also identified an α-L-fucosidase deficiency in his first two patients along with an accumulation of fucosylated glycoceramides and recommended the term fucosidosis for this disease. Symptoms of fucosidosis are progressive mental retardation, neurological deterioration, coarse facies appearance, growth retardations, dysostosis multiplex and angiokeratoma corporis diffusum. Frequently, patients also develop visceromegaly and suffer from seizures (Willems et al. 1991). Fucosidosis is inherited in an autosomal recessive way (Willems et al. 1991). A severe form of the disease is known, where the clinical manifestation starts in early childhood and the patients often die before the age of ten years. A milder form of fucosidosis develops more slowly and patients may survive until the third or fourth decade of life (Kanitakis et al. 2005). Also an intermediate form is known, reflecting the continuous clinical spectrum of the disease. However, no strict relationship seems to exist between the genotypic condition and the phenotypic manifestation, as clinical variability was found in patients carrying the same disease-causing mutation (Willems et al. 1999). Most of the patients were found to harbor homozygous mutations, indicating a high rate of consanguinity in fucosidosis (Willems et al. 1999, Malm et al. 2013). Until 1999, 22 disease-causing mutations were identified, of which four were missense mutations and 18 were inactivating mutations including several nonsense mutations, deletions, insertions and a splice-site mutation (Willems et al. 1999) resulting in a complete absence or severely diminished ($<5\,\%$) α-L-fucosidase activity (Willems et al. 1991). About 120 fucosidosis cases have

been reported world-wide, but the incidence might be much higher, particularly in some regions of Southern Italy and in the Mexican-Indian populations of New Mexico and Colorado in the United States (Willems et al. 1991), in Cuba (Menéndez-Sainz et al. 2012), in United Arab Emirates (Al-Jasmi et al. 2013) and in Tunisia (Turkia et al. 2008).

Until now, there is no therapy available for fucosidosis. In a few cases, BMT was performed and resulted in a slight improvement of neurological symptoms. However, graft-versus-host complications were also observed (Miano et al. 2001). The neurological manifestation of the disease was extensively characterized in a naturally occurring dog model in English Springer spaniel (Kelly et al. 1983, Kondagari et al. 2011b, Fletcher et al. 2011, Fletcher et al. 2014), which closely resembled the human disease and was also used for ERT studies by intracisternal enzyme infusion (Kondagari et al. 2011a). In addition, one naturally occurring fucosidosis case in a domestic short-hair cat was reported (Arrol et al. 2011).

1.3 Aims of the study

Fucosidosis is a lysosomal storage disease caused by the deficiency of the lysosomal glycosidase α-L-fucosidase resulting in the accumulation of fucosylated glycocompounds. In human patients, the disease is mainly characterized by progressive mental retardation and neurological deterioration leading to premature death. In order to analyze the pathological cascades underlying the fucosidosis disease as well as to enable the development of therapeutic strategies, a constitutive fucosidosis mouse model was established. One aim of this study is the validation of the *Fuca1* gene knock-out on genomic, transcript and protein level. Moreover, the phenotype of the fucosidosis mouse model will be characterized in detail including biochemical, histological and behavioral analysis. The investigation of the fucosidosis storage material as well as of neurological alterations of the mouse model is of particular interest, as the latter are the leading symptoms in human fucosidosis.

A second objective of this study is the establishment of an expression system for human α-L-fucosidase in CHO-K1 cells. Therefore, CHO-K1 cells will be transfected with an expression plasmid encoding an untagged as well as a His_6-tagged human α-L-fucosidase, respectively. The cultivation of stable transfected cells in an adherent culture system is supposed to be sufficient for initial experiments, but also an adaption of the cells to suspension conditions is intended. A suspension culture might enable a more sufficient large-scale production of the

recombinant enzyme under industrial conditions. Moreover, the establishment of a purification strategy for the untagged and the His_6-tagged human α-L-fucosidase is aimed, respectively.

The ultimate goal of this study is an enzyme replacement therapy of the fucosidosis mouse model by intravenous application of purified human α-L-fucosidase. The benefits of this therapeutic approach will be analyzed particularly with regard to the storage material and a reduction of the lysosomal storage is expected which might also improve the phenotypic disease severity.

At last, the generation of an α-L-fucosidase-specific antibody is intended, as no antibody is currently commercial available. Therefore, *Fuca1*$^{(-/-)}$ mice will be immunized by ballistic injection of coated gold particles carrying an expression plasmid for murine α-L-fucosidase. The resulting B-lymphocytes will be fused with myeloma cells in order to establish hybridoma cell lines secreting α-L-fucosidase-specific monoclonal antibodies. The specificity of the antibodies has to be analyzed against the recombinant human enzyme and against genuine murine α-L-fucosidase by Western blotting and immunofluorescence studies.

2 Materials

2.1 Laboratory equipment

Item	Manufacturer
ÄKTA Ettan LC system	GE Healthcare
ÄKTA Explorer system	GE Healthcare
Autoclave, Laboklav	SHP Steriltechnik
Charge Coupled Device (CCD)-Kamera	Fuji Film
with Luminescent Image Analyzer LAS 3000	Fuji Film
Cell counter Cedex XS	Innovatis
Centrifuge, Eppendorf 5417 R	Eppendorf
Centrifuge, Eppendorf 5810 R	Eppendorf
Centrifuge, MIKRO 200R	Hettich Zentrifugen
Centrifuge, Optima™ L-80 Ultracentrifuge	Beckmann Coulter
with rotor Sorvall® T-1270	
with rotor Sorvall® TLA-55	
Centrifuge, Sorvall® ULTRA Pro 80	Thermo Scientific
with rotor Sorvall® T-880	
with rotor Sorvall® TH-641	
Centrifuge, Sorvall® RC5B PLUS	Thermo Scientific
with rotor Sorvall® GS-3	
Electrophoresis chamber for agarose gels, custom-made	Bielefeld University
Electrophoresis chamber for polyacrylamide gels, custom-made	Bielefeld University
Electrophoresis chamber for Western blots, custom-made	Bielefeld University
Elektrophoresis Power Supply EPS200	Pharmacia Biotech
Freeze dryer, Christ alpha 2-4 LSC with SpeedVac RVC 2-18	Christ
Homogenizer Potter S	B.Braun
Ice machine	Ziegra

Item	Manufacturer
Incubator for bacterial cultures	Heraeus
Incubator for cell cultures, HERAcell	Heraeus
Incubator shaker Inova 4300	New Brunswick Scientific
Microplate reader infite M200	Tecan
Microscope, confocal, LSM700	Zeiss
Microscope, Leica DMIL	Leica
Microscope, Leica DM IRB with DC 300F camera	Leica
Microscope, epi-fluorescence, Leica DM5000 B with DFC350 FX camera	Leica
Microtome SM 2000R	Leica
Microwave	Siemens
NanoDrop ND-1000	PeqLab
pH meter, SevenMulti	Mettler Toledo
Pipetboy, pipetus	Hirschmann Laborgeräte
Pipettes	Gilson
Rocking platform	VWR
Rotator, SB3	Stuart
Sonifier, Model 450	Branson
Sonifier, wather bath	Bandelin-Sonorex
Step One Plus Real- Time PCR cycler	Applied Biosystems
Sterile laminar flow workbench, HERAsafe	Heraeus
Thermocycler PTC-200	MJ Research
Thermomixer, Eppendorf 5417	Eppendorf
TLC tanks, custom-made	Bielefeld University
Transilluminator	PeqLab
ULTRA-TURRAX	IKA
Vortex-Genie 2	Scientific Industries
Water filtration system, Milli-Q	Millipore
Water bath	Memmert

2.2 Laboratory material

Item	Manufacturer
10 ml (Mobicol) Columns with Bayonet Joint Lid	Mo Bi Tec
96 well microtiter plates, polystyrene, flat bottom, transparent	Greiner Bio-One
96 well microtiter plates, Microlon, flat bottom, black	Greiner Bio-One
Amicon® Ultra-4 Centrifugal Filter, 10,000 NMWL, 4 ml	Millipore
Butterfly needle, Multifly® Set 21G tubing 8”	Sarstedt
Cell counting chamber, Cedex XS Smart Slide	Innovartis
Cell culture cryotubes	Sarstedt
Cell culture flasks, T25 and T75 with cap filters	Nunc
Cell culture plates, 4, 6, 12 and 24 wells	Nunc
Cell culture plates, 6, 10 and 15 cm	Nunc
Cell scraper	Sarstedt
CNBr-activated sepharose beads	GE Healthcare
ConA Sepharose™ 4B	GE Healthcare
Corning® shake flask 125 ml	Corning
Cover slips 18 x 18 mm	Marienfeld
Dialysis tubing, MWCO 14 kDa	Roth
Glass beads, 3 mm diameter	Roth
Glass rings, for cell culture clone isolation, custom-made	Bielefeld University
HisTrap HP 1 ml column	GE Healthcare
HiTrap DEAE FF 1 ml	GE Healthcare
HiTrap NHS-activated HP 1 ml column	GE Healthcare
HiTrap SP HP 1 ml column	GE Healthcare
Mouse restrainer	Sigma
Object holder 76 x 26 x 1 mm	Marienfeld
Roti-PVDF Membran	Roth
Sep-Pak® Vac 6cc (1 g) C18 cartridges	Waters
Silica gel F60 plates	Merck
Superdex 200 10/30 GL column	GE Healthcare
Syringe filters, Filtropur S 0.2 μm	Sarstedt
Syringe for intravenous injections, BD Micro-Fine® + Demi, 30G x 8 mm	BD Medical
Whatman filter paper for Western blots	GE Healthcare

2.3 Chemicals and reagents

All general chemicals were obtained in analytical quality (p.A.) from Invitrogen, Merck, Sigma or Roth.

Item	Manufacturer
Agarose Standard	Roth
Ammonium persulfate	Merck
Ampicillin sodium salt	Roth
BSA, Albumin Standard 2 mg/ml	Thermo Scientific
BSA, Albumin fraction V	Roth
Coomassie Brilliant Blue G250	Serva
Corning® PF medium	Corning
Cytochrom C from horse heart	Sigma
Deoxynucleoside triphosphates dATP, dTTP, dCTP and dGTP	Roche
Dabco	Roth
DAPI	Sigma
Diethylpyrocarbonat (DEPC)	Roth
Dulbecco's modified Eagle medium (DMEM) dry powder	Invitrogen
DNA markers, 100 bp and 1 kb DNA ladders	New England Biolabs
DMSO	Invitrogen
Escherichia coli DH5α	Invitrogen
Ethidium bromide, p.A., 1 % solution	Roth
Fetal calf serum (FCS)	Lonza
Filipin III from *Streptomyces filipinensis*	Sigma
L-fucose	Roth
G418	Calbiochem
Gel Filtration Calibration Kit HMW	GE Healthcare
β-glycerophosphate disodium salt hydrate	Sigma
Glucose-6-phosphate disodium salt hydrate	Sigma
L-Glutamin, 200 mM	Lonza
Glutaraldehyde 25 %	Roth
Goat-serum	Gibco, Invitrogen
Hybrido DIF 1000	Biochrom
Hydrogen peroxide	Sigma
Hygromycin	PAA

Item	Manufacturer
Mannose-6-phosphate sodium salt	Carbosynth
4-methylumbelliferone	Sigma
4-methylumbelliferyl-α-L-fucopyranoside	Carbosynth
Milk powder, non fat	TSI
Mitomycin C	Sigma
Mixed-bed ion exchange resin (AG 501-X8, 20 - 50 mesh)	BioRad
Mowiol	Roth
N-(ε-aminocaproyl)-β-L-fucopyranosylamine	Carbosynth
para-nitrophenyl-α-D-mannopyranoside	Sigma
para-nitrophenyl-α-L-fucopyranoside	Roth
para-nitrophenyl-α-*N*-acetyl-β-D-glucosaminide	Roth
Nuclear Fast Red	Roth
OptiMEM medium	Gibco, Invitrogen
Orcinol monohydrate from Lichens	Sigma
para-formaldehyde	Roth
PEI MW 40 000	Polyscience Europe
Penicillin/Streptomycin, 10 U each	Lonza
Percoll	Amersham Bioscience
Poly-L-lysine	Sigma
Protein marker, Precision Plus Protein Standards All Blue	BioRad
Rotiphorese® Gel 30 (30 % acrylamide and 0.8 % bis-acrylamide (37.5 : 1))	Roth
Saponin from Quillaja Bark	AppliChem
Sodium dodecyl sulfate (SDS), research grade	Roth
Sodium deoxycholate	Serva
Sudan Black B	Serva
Ponceau S	Merck
SuperSignal West Femto Chemiluminescent Substrate	Pierce
SuperSignal West Pico Chemiluminescent Substrate	Pierce
Trichloro acetic acid	Sigma
TEMED	Roth
TheraPEAK™ (FGM-CD) medium	Lonza
Trizol reagent	Invitrogen
Tyloxapol (Triton WR-1339), BioXtra	Sigma
Trypan blue (0.4 %)	Sigma

2.4 Kits

Kit	Supplier
DC Protein Assay Kit	BioRad
High Pure PCR Product Purification Kit	Roche
HRP substrate Kit	VectorLabs
iScript cDNA Synthesis Kit	BioRad
KAPA HIFI Hot Start Ready Mix	PeqLab
KAPA Mouse Genotyping Hot Start Kit	PeqLab
KAPA SYBR Fast Universal Kit	PeqLab
QIAGEN Plasmid Midi Kit	Quiagen
QIAprep Spin Miniprep Kit	Quiagen
RNeasy Midi Kit	Quiagen

2.5 Enzymes

Enzyme	Supplier
Antarctic Phosphatase, 5 000 U/ml	New England Biolabs
BIOTAQ DNA Polymerase	Bioline
DNAse I	Roche
*Dpn*I restriction endonuclease, 20 000 U/ml	New England Biolabs
EndoH	Roche
*Nhe*I-HF restriction endonuclease, 20 000 U/ml	New England Biolabs
*Not*I-HF restriction endonuclease, 20 000 U/ml	New England Biolabs
PfuUltra II Fusion HS DNA Polymerase	Agilent Technolgies
PNGase F	Roche
Proteinase K, $\geq$ 30 U/mg	Roth
T4 DNA Ligase 400 000 mU/ml	New England Biolabs
TrypLE^{TM} Express	Gibco, Invitrogen
Trypsin-EDTA	Gibco, Invitrogen
*Xho*I restriction endonuclease, 20 000 U/ml	New England Biolabs

2.6 Antibodies and lectins

If not stated otherwise, all primary antibodies were of IgG isotype.

Primary antibody	Species	Dilution WB	Dilution IF	Supplier
α-Aquaporin2	goat	–	1 : 200	kind gift from Prof. Schmidt-Ott, Max-Delbrück-Center for Molecular Medicine, Berlin, Germany
α-Calbindin	mouse	–	1 : 500	Sigma
α-mCD68 (FA-11)	rat	–	1 : 500	AbD Serotec
α-mCtsD (KIIS9)	rabbit	1 : 1500	1 : 100	internal available, Braulke et al. (1987)
α-F4/80	rat	–	1 : 100	internal available, Austyn and Gordon (1981)
α-Fuca1 (A112/A180)	mouse	1 : 1000	1 : 500	generated during this thesis in cooperation with Prof. Koch-Nolte, University Medical Center Hamburg-Eppendorf, Germany
α-GAPDH (FL-335)	rabbit	1 : 500	–	R&D Systems
α-GFAP (GA5)	mouse	1 : 2000	1 : 500	Sigma
α-GM2 (IgM isotype)	mouse	–	1 : 5	kind gift from Prof. Dobrenis (Albert Einstein College of Medicine, New York, USA)
α-mHSP70	mouse	1 : 1000	–	kind gift from Prof. Fischer von Mollard (Bielefeld University, Germany)
α-Iba1	rabbit	–	1 : 500	GeneTex
α-mLamp1 (1D4B)	rat	1 : 250	1 : 250	Santa Cruz
α-MBP	rat	1 : 1000	1 : 500	Millipore
α-mNeuN (A60)	mouse	1 : 2000	1 : 1000	Millipore
α-Plbd2 (G9)	rabbit	1 : 500	1 : 50	internal available, Deuschl et al. (2006)
α-RGS-His_6	mouse	1 : 3000	1 : 100	Quiagen

Lectin	Dilution WB	Dilution IF	Supplier
biotinylated *Aleuria aurentia* lectin	0.5 µg/ml	5 µg/ml	VectorLabs
biotinylated *Lens culinaris* lectin	5 µg/ml	5 µg/ml	VectorLabs
Secondary antibody WB	**Species**	**Dilution**	**Supplier**
α-mouse IgG-HRP	goat	1 : 5000	Invitrogen
α-rabbit IgG-HRP	goat	1 : 5000	Dianova
α-rat IgG-HRP	goat	1 : 5000	Dianova
Streptavidin-HRP	–	0.25 µg/ml	VectorLabs
Secondary antibody IF			
α-goat IgG-Alexa Flour® 555	donkey	1 : 500	Invitrogen
α-mouse IgG-Alexa Flour® 488	goat	1 : 2000	Invitrogen
α-mouse IgM-Alexa Flour® 488	goat	1 : 2000	Invitrogen
α-mouse IgM-HRP	goat	1 : 2000	Dianova
α-rabbit IgG-Alexa Flour® 488	goat	1 : 2000	Invitrogen
α-rat IgG-Alexa Flour® 647	donkey	1 : 2000	Dianova
Streptavidin-DyeLight® 594	–	5 µg/ml	VectorLabs

2.7 Oligonucleotide primers

2.7.1 Primers for cloning of human and murine α-L-fucosidase cDNA

Primer	T_M/°C	Sequence 5'→3'
mFuca1 fw NheI	61	TTCCGCTAGCTGGGATGCTGCTGCTGCTG
mFuca1 rev NotI		TTCCGCGGCCGCGTCAGTTCACCTTTGTCAGCTTCAG
hFuca1 fw NheI	62	ACGCTAGCACCATGCGGGCTCCGGGGATGAGGTCGC GGCCGGCGGGTCC
hFuca1 rev XhoI		CCTCGAGGTTACTTCACTCCTGTCAGCT

Primer	T_M/°C	Sequence 5'→3'
hFuca1 fw NheI	60	ACGCTAGCACCATGCGGGCTCCGGGGATGAGGTCGC GGCCGGCGGGTCC
hFuca1 rev His_6 XhoI		GTACTCGAGGTATCATCCGTGATGGTGATGGTGATGC GATCCTCTTCCCTTCACTCCTGTCAGCTT

2.7.2 Colony PCR primers

Primer	T_M/°C	Sequence 5'→3'
T7 (fw)	55	TAATACGACTCACTATAGGG
Bgh (rev)		CCTCGACTGTGCCTTCTA

2.7.3 Primers for site-directed mutagenesis

Primer	T_M/°C	Sequence 5'→3'
hFuca1-D230N (fw)	57	GATCTGGTCT**A**ATGGGGAGTGG
hFuca1-D230N (rev)		CCACTCCCCA**T**TAGACCAGATC
hFuca1-E294Q (fw)	62	TCACAAGTGG**C**AGATGTGCAC
hFuca1-E294Q (rev)		GTGCACATCT**G**CCACTTGTGA

2.7.4 Primers for *Fuca1* gene knock-out generation and validation

Primer	T_M/°C	Sequence 5'→3'
E1 (fw)	65	CCAAGTTCGGGGTGTTCGTGCAC
E1 (rev)		CCTGAAAGAGTTCGGCCCACTG
F4 (fw)	58	TTTTCCCACTGATCCCTAACGA
AK31-as (rev)		CCTGCGTGCAATCCATCTTG
F1 (fw)	63	GACTGGCAGAGCTTGGACTC
R2 (rev)		AGCAGTCTGGCTTGTTACTTCC

Primer	T_M/°C	Sequence 5'→3'
AK31 (fw)	54	CAAGATGGATTGCACGCAGG
R1 (rev)		GTGTGTTGCCCTCTTTGGTT
F4 (fw)	58	TTTTCCCACTGATCCCTAACGA
R3 (rev)		CTCGTCTTTAGCGTCCTTCC

2.7.5 Primers for routine mouse genotyping

Primer	T_M/°C	Sequence 5'→3'
F2 (fw)		GGTTCGATGAGGCCAAGTTC
AK30-R (fw)	62	CGGCTGCATACGCTTGATCCG
R3 (rev)		CTCGTCTTTAGCGTCCTTCC

2.7.6 Real-Time primers

Target gene	Primer fw 5'→3'	Primer rev 5'→3'
CD68	TGGATTCAAACAGGACCTACATC	TGAATGTCCACTGTGCTGC
CtsB	CTCTTGTTGGGCATTTGGG	GTAGACTCCACCTGAAACCA
Fuca1	TGCGGAAGAGGAACATACG	TGTCAGGACACTCCCACTC
Fuca2	TGTATAATGAAAGCCCAGTTCGG	GTTTCCACAAGTTTCTTCACCAAC
Gapdh	GCAGTGCCAGCCTCGTCCC	CAGGCGCCCAATACGGCCA
GFAP	AAGGTTGAATCGCTGGAGGA	GCTGTGAGGTCTGGCTTGG
Glb1 (βGal)	TGCTCTGAGAAAGTTCAAGAC	GTTGTTCGGTACAGCACATA
HexB	TTTCGGGACTTTCACCATC	GATAAGGGAAAGACTGGTCG
Iba1	GGATCAACAAGCAATTCCTCG	AACTCCATGTACTTCACCTTGA
Lamp1	CAGCATCTCCAACCATTCAC	CACTCTTCCACAGACCCAAA
Man2B1 (αMan)	TATTACGGCATCCTGAGTGA	ACATAGATGAAGCGACGGG
Manba (βMan)	TGGGATAATGGTGTGGCAG	GATGATGGAGGGGTGAGATT
MBP	GTACAAGGACTCACACACGA	CTTGGGATGGAGGTGGTGT
Plp1	GCTGAGTTCCAAATGACCTTCC	TGAAGGTGAGCAGGGAAACT

2.8 Plasmids

Vector maps are attached in the appendix.

Plasmid	Size	Resistance	
pcDNA3.1Hygro(+)	5597 bp	ampicillin/ hygromycin	
pcDNA3.1Hygro(+)hFuca	6918 bp	ampicillin/ hygromycin	expression of human α-L-fucosidase
pcDNA3.1Hygro(+)hFuca-His_6	6953 bp	ampicillin/ hygromycin	expression of His_6-tagged human α-L-fucosidase
pcDNA3.1Hygro(+)hFuca-His_6-D230N	6953 bp	ampicillin/ hygromycin	expression of His_6-tagged human α-L-fucosidase carrying a mutation at position 230 (aspartate $\rightarrow$ asparagine)
pcDNA3.1Hygro(+)hFuca-His_6-E294Q	6953 bp	ampicillin/ hygromycin	expression of His_6-tagged human α-L-fucosidase carrying a mutation at position 294 (glutamate $\rightarrow$ glutamine)
pcDNA3.1Hygro(+)hFuca-His_6-D230N-E294Q	6953 bp	ampicillin/ hygromycin	expression of His_6-tagged human α-L-fucosidase carrying two mutations at positions 230 and 294 (enzymatically inactive fucosidase)
pMSSVLT	5.4 kb	ampicillin/ neomycin	expression of the SV40-large T-antigen (for immortalization of mouse embryonic fibroblasts)

2.9 Buffers, solutions and media

Buffer, solution, medium	Composition
Coomassie-staining solution	0.2 % (w/v) Coomassie Brilliant Blue G250 45 % (v/v) ethanol 10 % acetic acid
DEPC-H_2O	2 ml DEPC diluted in 1 L H_2O solution is stirred over night and autoclaved

Buffer, solution, medium	Composition
DMEM (Dulbecco's modified Eagle medium)	13.38 g/L DMEM dry powder 3.4 g/L $NaHCO_3$ 8 ml/L 1 M HCl 0.1 g/L phenol red, adjusted to pH 7.4 sterile filtered, stored at 4 °C
DMEM cryo medium	DMEM standard medium + 10 % DMSO, sterile filtered
DMEM standard medium	DMEM including 1 % (v/v) penicillin/streptomycin (100 x solution) 2 mM L-glutamine solution 10 % (v/v) fetal calf serum (FCS)
DNA-loading dye	0.15 % (w/v) bromophenol blue 0.15 % (w/v) xylene cyanol 40 % (w/v) sucrose in 1 x TAE
HisTrap binding buffer	20 mM Tris-HCl, adjusted to pH 7.4 500 mM NaCl 50 mM imidazole
HisTrap elution buffer	20 mM Tris-HCl, adjusted to pH 7.4 500 mM NaCl 500 mM imidazole
Laemmli buffer (4 x)	320 mM Tris/HCl, pH 6.8 8 % (w/v) SDS 40 % (v/v) glycerol 0.04 % (w/v) bromophenol blue 2 % (v/v) β-mercaptoethanol
Luria-Bertani (LB) medium	1 % (w/v) peptone 0.5 % (w/v) yeast extract 0.5 % (w/v) NaCl, adjusted to pH 7.4 autoclaved for 20 min at 121 °C, antibiotics were added at temperatures < 50 °C

Buffer, solution, medium	**Composition**
LB agar	LB medium 1.2 % (w/v) agar-agar autoclaved for 20 min at 121 °C, antibiotics were added at temperatures < 50 °C
PB Buffer (pH 7.4)	19 ml 0.2 M NaH_2PO_4 81 ml 0.2 M Na_2HPO_4 100 ml dH_2O
10 x PBS	1.4 M NaCl 27 mM KCl 100 mM Na_2HPO_4 18 mM KH_2PO_4
Mowiol/Dabco	8 g Mowiol 20 ml 0.2 M Tris-HCl, adjusted to pH 8.5 20 ml glycerin 2.5 % Dabco
SCX binding buffer	50 mM NaOAc, adjusted to pH 5.0
SCX elution buffer	50 mM NaOAc, adjusted to pH 5.0 1 M NaCl
SDS-PAGE running buffer (10 x)	1.92 M glycine 0.5 M Tris base 1 % (w/v) SDS
SOC medium	0.5 % (w/v) yeast extract 2 % (w/v) tryptone 10 mM NaCl 2.5 mM KCl 10 mM $MgSO_4$ 2 mM glucose, adjusted to 7.4
10 x TAE	2 M Tris 50 mM EDTA, adjusted to pH 8.0 with acetic acid
10 x TBS	100 mM Tris-HCl 1.5 M NaCl, adjusted to pH 7.4

Buffer, solution, medium	Composition
TBS-T	0.1 % Tween-20 (v/v) in 1 x TBS
Western blot anode buffer	75 mM Tris-HCl, adjusted to pH 7.5 20 % (v/v) methanol
Western blot cathode buffer	40 mM 2-aminohexanoic acid 25 mM Tris -HCl, adjusted to pH 9.0 20 % (v/v) methanol

2.10 Mammalian cell lines

Cell line	Origin
CHO-K1	Chinese hamster ovary cells
CHO-K1 hFuca #C1/A5	CHO-K1 cells stably transfected with pcDNA3.1Hygro(+)hFuca for overexpression of human α-L-fucosidase
CHO-K1 hFuca-His_6 #C2/C1	CHO-K1 cells stably transfected with pcDNA3.1Hygro(+)hFuca-His_6 for overexpression of human His_6-tagged α-L-fucosidase
Mouse embryonic fibroblasts (MEFs, wildtype or *Fuca1*$^{(-/-)}$)	embryonic fibroblasts derived from mouse embryos (wildtype or *Fuca1*$^{(-/-)}$) at embryonic day E12.5
MEFs MLII	*GNPTAB*$^{(-/-)}$; mucolipidosis II
Neu2A	murine neuroblastoma cell line

2.11 Software

Software	Supplier/website
AIDA (advanced image data analyzer) Version 4.06	Fujifilm
i-control	Tecan
Image J 1.45s	National Institutes of Health
Image Reader LAS 300	Fujifilm
Leica application suite 1.8.0	Leica

Software	Supplier/website
NetSurfP prediction program version 1.1	Petersen et al. 2009
Oligo Analyzer 3.1 online tool	IDT
Primer3web online tool version 4.0.0	Untergasser et al. 2012
UNICORN 5.0	GE Healthcare
Zen	Zeiss

3 Methods

3.1 Molecular biological methods

3.1.1 Primer design

In order to clone the human α-L-fucosidase (untagged as well as *C*-terminal His_6-tagged) and the murine α-L-fucosidase (untagged) into the pcDNA3.1Hygro(+) plasmid, their cDNA sequences were derived from National Center for Biotechnology Information (NCBI; http:// www.ncbi.nlm.nih. gov) and used to design specific primer pairs. The forward primer started right at the beginning of the ATG-translation start codon and contained a Kozak consensus sequence as well as a 5' overhanging restriction site. The reverse primer ended either right before the translational stop codon and contained an additional glycine residue followed by a RGS-His_6-tag, a second glycine residue, a translational stop codon and a 5' overhanging restriction site (His_6-tagged enzyme) or ended right after the translational stop codon and contained only a 5' overhanging restriction site (untagged enzyme).

Primer pairs for Real-Time PCR analysis (section 3.1.6.5) were designed exon-spanning to receive PCR products with a length of 100 - 250 bp.

The Primer3web online tool (version 4.0.0; Untergasser et al. 2012; http://primer3.ut.ee) was used to design primer pairs for genotyping *Fuca1*$^{(-/-)}$ mice (section 3.1.6.4). The genomic sequence of the murine α-L-fucosidase gene was obtained from the UCSC Genome Browser (https://genome.ucsc.edu).

All primers were analyzed with respect to a sufficient GC-content, minimal hairpin structures, self- and hetero-dimers using the Oligo Analyzer 3.1 online tool from IDT (http://eu.idtdna. com/calc/analyzer). The specificity as well as the optimal melting temperature of each primer pair was determined using the Primer-BLAST online tool from NCBI.

3.1.2 Isolation and purification of RNA

RNA was purified either from mouse tissues or from MEF cells. RNA from mouse tissues was further transcribed into cDNA and used for cloning approaches or Real-Time PCR analysis, whereas RNA from MEF cells was used to verify a successful transfection of these cells on transcript level.

3.1.2.1 Isolation of RNA from mouse tissues

Mice were sacrificed by cervical dislocation and mouse tissues were dissected and either flash frozen in liquid N_2 or immediately homogenized using an ULTRA-TURRAX (IKA). RNA was isolated from approximately 100 - 150 mg fresh weight tissue using the RNeasy Midi Kit (Quiagen). 4 ml Buffer RLT containing 10 μl/ml β-mercaptoethanol were added to the fresh tissue and homogenized for approximately 15 sec. The further isolation steps were performed according to the manufacturer's instructions including the digestion of DNA directly on the column. The RNA was eluted using 100 μl RNase-free water. The concentration was measured using a NanoDrop ND-1000 spectrophotometer (PeqLab) and the RNA was stored at -80 °C.

3.1.2.2 Isolation of total RNA from MEFs

MEF cells were transfected (section 3.3.3.1) at 80 % confluence (10 cm dish) and further cultivated for 48 h. The cells were harvested by trypsination and pelleted by centrifugation at 250 x g for 3 min. The cell pellet was washed with PBS, divided into two equal amounts and again centrifuged at 250 x g for 3 min. The supernatant was discarded. Half of the cells was further used for RNA isolation (see below), whereas the other half was lysed in order to obtain cell homogenates (section 3.2.2).

The cell pellet was resuspended in 2 ml Trizol. 400 μl chloroform were added, the sample was rigorously shaken for 15 sec and incubated at room temperature for 5 min. The sample was centrifuged at 12 000 x g for 15 min at 4 °C, subsequently. The aqueous phase was transferred into a new tube and 1 ml isopropanol was added. The sample was rigorously mixed, incubated at -20 °C for 60 min and centrifuged at 12 000 x g for 30 min at 4 °C. The supernatant was discarded and the pellet was washed with 70 % ethanol (in DEPC water, section 2.9). Again, the sample was centrifuged at 12 000 x g for 10 min at 4 °C. The supernatant was discarded and the pellet was dried at 37 °C. The RNA pellet was subsequently resuspended in 50 μl

DEPC water (section 2.9), the RNA concentration was measured using a NanoDrop ND-1000 spectrophotometer (PeqLab) and the RNA was stored at -80 °C.

3.1.3 Northern blot

RNA was isolated from different mouse tissues as described in section 3.1.2.1. The abundance of the *Fuca1* mRNA transcript was analyzed using a Northern blot. Agarose gelelectrophoresis of RNA samples, Northern blotting, radioactive labeling of the DNA probe as well as the hybridization and processing of the blot was performed by Prof. Lübke (Bielefeld University, Germany). Briefly, 10 μg RNA were applied to RNA-agarose gelelectrophoresis (denaturating in the presence of formaldehyde). The separated RNA was subsequently blotted onto a positively-charged membrane by capillary forces and immobilized using UV-irradiation. In parallel, a radioactive labeled DNA probe was generated. Double-stranded DNA was amplified from cDNA of *Fuca1* and *Gapdh* (as loading control). The probes were labeled by random priming using P^{32}-αdCTP. The Northern Blot was incubated with a hybridization mixture containing the *Fuca1* DNA probe, was washed and developed by phosphor imaging. Then, the blot was stripped and developed using the *Gapdh* DNA probe.

3.1.4 cDNA synthesis

Freshly isolated RNA (section 3.1.2) was used for cDNA synthesis according to the iScript cDNA Synthesis Kit (BioRad). 1 μg RNA was added to 4 μl of 5 x iScript reaction mix and 1 μl of iScript reverse transcriptase. The reaction was filled up to 20 μl with nuclease-free water. The samples were incubated for 5 min at 37 °C, following by 30 min at 42 °C and 5 min at 85 °C. The cDNA was stored at -20 °C.

3.1.5 Isolation of genomic DNA from mouse tissues or cells

In order to identify individual mice, they were numbered consecutively by piercing their ears. The tissue material of the ear holes was collected and genomic DNA was extracted in order to genotype the mice using the KAPA Mouse Genotyping Hot Start Kit (PeqLab). 88 μl dH_2O, 10 μl extraction buffer as well as 2 μl of extraction enzyme were added to the tissue pieces and were rigorously shaken for 20 min at 75 °C. Afterwards, the sample was incubated for 5 min at 95 °C and spun down. 0.5 μl of the supernatant was used in the genotyping PCR (section 3.1.6.4).

Alternatively, genomic DNA was extracted from confluent MEF cells. Therefore, the cells were harvested by trypsination and pelleted by centrifugation (3 min at 250 x g). The cell pellet was washed with PBS, centrifuged again and resuspended in extraction buffer. The genomic DNA was extracted as described above.

3.1.6 Polymerase chain reaction

DNA was amplified during polymerase chain reactions (PCRs) using specific primer pairs. The reactions were used to amplify cDNAs for further cloning strategies, to control the integration of inserts after ligation and transformation of chemically competent bacteria, to determine the genotype of mice as well as to analyze the expression of certain mRNA targets.

3.1.6.1 Add-on PCR

An add-on PCR system was used to amplify the cDNA of human and murine α-L-fucosidase. In case of the human enzyme, a *C*-terminal RGS-His_6-tag was added simultaneously. The reactions were prepared as shown in table 3.1 and incubated in a thermocycler according to the protocol shown in table 3.2. In order to minimize possible PCR-derived mutations, a proof-reading polymerase was used. 30 μl of the reaction batch were mixed with 6 μl of 6 x DNA loading dye (section 2.9) and loaded on a 1 % agarose gel (section 3.1.7). The correct size of the PCR product was checked and the band was cut out from gel, purified (section 3.1.8) and used for further cloning steps.

Table 3.1: Setup for add-on PCR

	Component	Volume
	PfuUltra II fusion HS DNA polymerase	1 μl
	10x PfuUltra II reaction buffer	5 μl
	Forward primer, 10 μM	1 μl
	Reverse primer, 10 μM	1 μl
	dNTPs, 10 mM each	0.5 μl
	DNA (pcDNA3.1Hygro(+)hFuca)	0.5 μl
or	murine cDNA	0.5 μl
	dH_2O	41 μl
		50 μl

Table 3.2: Temperature program for add-on PCR

	Temperature	Time	Cycles
Initial denaturation	95 °C	3 min	1
Denaturation	95 °C	15 sec	35
Annealing	optimal melting temperature see section 2.7.1	15 sec	
Amplification	72 °C	2 min	
Final amplification	72 °C	3 min	1
Cooling	4 °C	∞	1

3.1.6.2 Colony PCR

After transformation of chemically competent bacteria (section 3.1.14) colonies were received and screened for the cloned cDNA sequence using a colony PCR. The colonies were picked with a pipette tip and resuspended in 20 μl dH_2O. 1 μl of this solution was used as template. Amplification was performed using sequencing primer flanking the multiple cloning site of the pcDNA3.1Hygro(+) plasmid. The reactions were prepared as shown in table 3.3 and incubated in a thermocycler according to the protocol shown in table 3.4. Afterwards 5 μl of the amplicon were mixed with 1 μl 6 x DNA loading dye (section 2.9) and loaded on a 1 % agarose gel (section 3.1.7) in order to control the correct size of the PCR product.

Table 3.3: Setup for colony PCR

Component	Volume
BIOTAQ^{TM} DNA polymerase	0.2 μl
10x NH_4 reaction buffer	2 μl
$MgCl_2$, 50 mM	0.5 μl
Forward primer (T7), 10 μM	0.5 μl
Reverse primer (Bgh), 10 μM	0.5 μl
dNTPs, 10 mM each	0.5 μl
Template	1 μl
dH_2O	14.8 μl
	20 μl

Table 3.4: Temperature program for colony PCR

	Temperature	Time	Cycles
Initial denaturation	95 °C	3 min	1
Denaturation	95 °C	15 sec	35
Annealing	55 °C	15 sec	
Amplification	72 °C	3 min	
Final amplification	72 °C	10 min	1
Cooling	4 °C	∞	1

3.1.6.3 Validation of the *Fuca1* knock-out allele

In order to validate the correct integration of the bacterial *npt I* gene into Exon 1 of the *Fuca1* gene, the 5' homologous recombination site was amplified from genomic mouse DNA (section 3.1.5). The forward primer was located in the promoter region of the gene, whereas the reverse primer was located within Exon 1 (after the insertion site of the neomycin-cassette). A wildtype PCR product of 4108 bp and a knock-out PCR product of 5287 bp was received. The PCR reactions were prepared as shown in table 3.5 and incubated in a thermocycler according to the protocol shown in table 3.6. Afterwards 5 μl of the amplicon were mixed with 1 μl 6 x DNA loading dye (section 2.9) and loaded on a 1 % agarose gel (section 3.1.7) and the DNA was separated according to their size. The PCR products were further isolated from the gel (section 3.1.8) and analyzed by sequencing (section 3.1.17).

Table 3.5: PCR setup for validation of the *Fuca1* knock-out allele

Component	Volume
KAPA HIFI Hot Start Ready Mix	12.5 μl
Forward primer (F4), 10 μM Reverse primer (R3), 10 μM	0.75 μl
DMSO	1.25 μl
Template	100 ng
dH_2O	x μl
	25 μl

Table 3.6: PCR temperature program for validation of the *Fuca1* knock-out allele

	Temperature	Time	Cycles
Initial denaturation	95 °C	5 min	1
Denaturation	98 °C	20 sec	
Annealing	58 °C	15 sec	35
Amplification	72 °C	5 min	
Final Amplification	72 °C	5 min	1
Cooling	4 °C	∞	1

3.1.6.4 PCR for routine mouse genotyping

Genomic DNA was extracted from tissue material received during mouse ear piercing (section 3.1.5) and was applied as template for mouse genotyping. A multiplex PCR approach was established using the KAPA HIFI Hot Start Ready Mix Kit (PeqLab). The forward primer was located at the beginning of Exon 1 of the *Fuca1* gene (before the insertion site of the neomycin-cassette). One reverse primer was located at the end of Exon 1 (after the insertion site of the neomycin-cassette), thereby producing a PCR product of 350 bp in case of a wildtype gene. In contrast, the second reverse primer was located within the neomycin casette and enabled a PCR product of 735 bp in case of a knock-out gene. Heterozygous mice gave rise to both PCR products. The PCR reactions were prepared as shown in table 3.7 and incubated in a thermocycler according to the protocol shown in table 3.8. Afterwards, 5 μl of the amplicon were mixed with 1 μl 6 x DNA loading dye (section 2.9), loaded on a 1 % agarose gel (section 3.1.7) and the DNA was separated according to their size.

Table 3.7: Genotyping PCR setup

Component	Volume
KAPA HIFI Hot Start Ready Mix	6.25 μl
Forward primer (F2), 10 μM	
Reverse primer (R3), 10 μM	0.185 μl
Reverse primer (AK30-R), 10 μM	
DMSO	0.625 μl
Template	0.5 μl
dH_2O	4.57 μl
	12.5 μl

Table 3.8: Genotyping PCR temperature program

	Temperature	Time	Cycles
Initial denaturation	95 °C	2 min	1
Denaturation	98 °C	20 sec	
Annealing	62 °C	15 sec	35
Amplification	72 °C	30 sec	
Final Amplification	72 °C	5 min	1
Cooling	4 °C	∞	1

3.1.6.5 Real-Time PCR

The differential mRNA expression of selected genes in tissues of *Fuca1*$^{(-/-)}$ mice versus wiltype tissues was monitored using a Real-Time PCR approach. After isolation of mRNA (section 3.1.2.1), cDNA was synthesized (section3.1.4). The Real-Time PCR reactions were prepared in a 96-well plate using the KAPA SYBR Fast Universal Kit (PeqLab) as shown in table 3.9 and incubated in a Step One Plus Real-Time PCR cycler (Applied Biosystems) according to the protocol shown in table 3.10. Each reaction was prepared as triplicates. A no-template-control (NTC) was done for each primer pair in duplicates as internal quality control using water instead of cDNA. Primer pairs were designed as stated in section 3.1.1.

Table 3.9: Real-Time PCR setup

Component	Volume
KAPA Master Mix (2x)	6 µl
KAPA Rox	0.25 µl
Primer mix (forward + reverse), each 10 µM	2 µl
cDNA	2 µl
dH_2O	1.75 µl
	12.0 µl

Table 3.10: Real-Time PCR temperature program

	Temperature	Time	Cycles
Initial denaturation	95 °C	20 sec	1
Denaturation	95 °C	3 sec	35
Annealing and amplification	60 °C	30 sec	
Denaturation	95 °C	15 sec	
Annealing	60 °C	1 min	melting curve
Heating to 95 °C	0.3 °C every 15 sec	30 min	
Cooling	4 °C	∞	1

Amplification of the target gene was recorded in real time based on the increase in fluorescence of the SYBR Green intercalating dye. The Rox reference dye was used for internal normalization to compensate slight variations in SYBR Green fluorescence detection due to minimal differences in reaction volume and position of the wells. As the PCR reactions reached a plateau phase during the late amplification cycles, the early phase of the reaction was used for quantification. The C_P value (crossing point) was determined using the Step One Plus Real-Time PCR cycler software (Applied Biosystems) and is defined as the cycle at which the fluorescence rises substantially above the background. The C_P value is directly linked to the amount of template cDNA present in the reaction mix. Following the mathematical model from Pfaffl (2001), the relative fold change (R) in mRNA expression can be calculated as shown in equation 3.1.

$$R = 2^{-\Delta\Delta C_P} \tag{3.1}$$

$$\Delta\Delta C_P = \Delta C_{P(\text{knock-out})} - \Delta C_{P(\text{wildtype})}$$

$$\Delta C_P = C_{P(\text{target gene})} - C_{P(\text{Gapdh})}$$

R values greater than 1 indicate an elevated mRNA expression of the target gene in the *Fuca1*$^{(-/-)}$ tissue compared to the wildtype tissue, whereas values less than 1 represent a decreased expression.

The specificity of the Real-Time PCR reactions was shown by a melting curve. The amplicons were annealed followed by a gradually temperature increase up to 95 °C. The denaturation of

the PCR product occurred at a temperature specific to each amplicon leading to a decrease in SYBR Green fluorescence. Homogeneous PCR products resulted in a single peak, whereas multiple peaks were obtained in case of additional unspecific PCR products. The amplicons were also analyzed by agarose gel electrophoresis (section 3.1.7) and only data from homogeneous amplicons were evaluated.

3.1.7 Agarose gel electrophoresis

In order to determine the size of DNA fragments, an agarose gel electrophoresis was used. 1 % Agarose (w/v) was dissolved in TAE buffer (section 2.9) using a microwave oven and ethidium bromide was added to a final concentration of 1 μl/ml. The gel was poured into gel chambers and sample pockets were formed by an appropriate comb. The hardened gel was covered with TAE and the DNA samples were mixed with 6 x loading dye (section 2.9) and loaded into the pockets. For size determination a 100 bp or 1 kb DNA ladder was also loaded. Electrophoresis was performed at a constant voltage of 90 V for 45 - 60 min. Afterwards the DNA bands were visualized by UV light (312 nm) on a transilluminator (Peqlab) and photographed for documentation.

3.1.8 Purification of DNA from agarose gels

For cloning strategies a 50 μl PCR setup (section 3.1.6.1) was performed. 30 μl of amplicon were mixed with 6 μl 6 x DNA loading dye (section 2.9). The DNA samples were separated according to their size by agarose gel electrophoresis (section 3.1.7). The DNA bands were documented and cut out with a scalpel. The DNA was purified using the High Pure PCR Product Purification Kit (Roche) according to the manufacturer's instructions. The DNA was eluted from the purification column with 50 μl dH_2O.

3.1.9 Restriction digest

Restriction endonucleases were used either to control a ligated plasmid DNA or to digest and prepare DNA for ligation and cloning purposes.

3.1.9.1 Analytical restriction

After a successful ligation approach the purified plasmid DNA (section 3.1.16) was checked for correct insert integration. 1 µg plasmid DNA was treated with 0.2 µl of specific restriction enzymes flanking the insert sequence. The DNA was dissolved in the buffer recommended by the manufacturer using a total reaction volume of 20 µl. The samples were incubated for 1 h at 37 °C and separated according to their size by agarose gel electrophoresis (section 3.1.7).

3.1.9.2 Quantitative restriction

For cloning approaches, the cDNA of murine or human α-L-fucosidase was amplified by PCR in order to add additional restriction sites (section 3.1.6.1) and was purified from an agarose gel (section 3.1.8). The DNA insert as well as the target plasmid were digested with the same restriction endonucleases. NheI and XhoI were used to clone the human α-L-fucosidase into the pcDNA3.1Hygro(+) vector. NheI and NotI were used for the murine enzyme. 43 µl of insert DNA and 2 µg of plasmid DNA were digested with 1 µl of each restriction enzyme. 5 µl of buffer recommended by the manufacturer were added and the samples were filled up to a final volume of 50 µl. The reactions were incubated for 2 h at 37 °C.

3.1.10 Dephosphorylation of DNA fragments

In order to prevent re-alignment of the plasmid backbone during ligation (section 3.1.11), the plasmid DNA had to be dephosphorylated after enzyme restriction (section 3.1.9.2). 1 µl of Antarctic Phosphatase and 6 µl of Antarctic Phosphatase buffer were added to the entire restriction sample (50 µl) and incubated for 15 min at 37 °C. The Antarctic Phosphatase was inactivated by incubation at 65 °C for 5 min.

3.1.11 Ligation

Prior to ligation, the DNA insert and plasmid backbone were purified using the High Pure PCR Product Purification Kit (Roche) according to the manufacturer's instructions. The DNA was eluted with 50 µl dH_2O and quantified using a NanoDrop ND-1000 spectrophotometer (PeqLab). 50 ng plasmid DNA were ligated with insert DNA in a molar ration of 1 : 5 (plasmid : insert). The reaction was filled up with dH_2O to a volume of 17 µl, was incubated at 65 °C for 5 min in order to destroy secondary structures and then immediately placed on ice.

2 µl ligation buffer and 1 µl T4-ligase were added and the ligation was performed at 4 °C over night.

3.1.12 Site-directed mutagenesis

The catalytic activity of the human α-L-fucosidase is carried out by an aspartate residue (D230) and a glutamate residue (E294) (Liu et al. 2009; there referred to as D225 and E289). An inactive variant of the enzyme was generated by site-directed mutagenesis, thereby replacing the aspartate by an asparagine (D230N) and the glutamate by a glutamine residue (E294Q). These mutations required only a single base exchange (appendix A.4). Complementary primers were designed that contained the desired mutation and flanked the site of mutation by approximately 10 nucleotides in each direction. The whole vector containing the wildtype α-L-fucosidase cDNA sequence (pcDNA3.1Hygro(+)hFuca or pcDNA3.1Hygro(+)hFuca-His_6) was amplified by PCR. The samples were prepared as shown in table 3.11 and incubated according to table 3.12. In order to minimize possible PCR-derived mutations, a proof-reading polymerase was used. In a first approach both single mutations were introduced separately following the protocol described below and were then applied to a second mutagenesis step to obtain the cDNA sequence of the human α-L-fucosidase carrying both mutations.

Following PCR, 40 µl of the amplicon were added to 4.5 µl of DpnI Buffer and 1 µl of DpnI restriction enzyme and incubated for 4 h at 37 °C in order to digest the template plasmid that was purified from *E. coli* and therefore contained DAM-methylated sites. DpnI specifically recognizes and digests this methylation pattern. The newly synthesized plasmid containing

Table 3.11: PCR setup for site-directed mutagenesis

Component	Volume
PfuUltra II fusion HS DNA polymerase	0.5 µl
10x PfuUltra II reaction buffer	5 µl
Forward primer, 10 µM	1.5 µl
Reverse primer, 10 µM	1.5 µl
dNTPs, 10 mM each	1 µl
DNA	1 µg
dH_2O	39.5 µl
	50 µl

Table 3.12: PCR temperature program for site-directed mutagenesis

	Temperature	Time	Cycles
Initial denaturation	95 °C	3 min	1
Denaturation	95 °C	30 sec	
Annealing	optimal melting temperature see section 2.7.3 °C	30 sec	35
Amplification	72 °C	5 min	
Final Amplification	72 °C	10 min	1
Cooling	4 °C	∞	1

the desired mutation is not DAM-methylated and thus it is not recognized by DpnI. After the digest, 5 µl of the sample were added to 1 µl of 6 x DNA loading buffer (section 2.9) and analyzed on a 1 % agarose gel (section 3.1.7). Thereby the sample was checked for a sufficient amount of synthesized DNA as well as for its correct size. 2 µl of the sample were transformed into chemically competent cells and plated on LB plates containing 100 µg/ml ampicillin (section 3.1.14).

3.1.13 Preparation of chemically competent bacteria

Chemically competent *E. coli* bacteria (DH5α) were generated according to the $CaCl_2$ method (Sambrook and Russel 2001). A 250 ml culture was inoculated with a fresh overnight culture of the DH5α strain to a final OD_{600} of 0.5 (37 °C, 200 rpm). The cells were chilled on ice for 10 min and harvested at 4 000 x g for 10 min at 4 °C. The supernatant was discarded and the cell pellet was resuspended in 65 ml ice-cold 100 mM $MgCl_2$. The culture was kept on ice for 5 min and centrifuged again. The cell pellet was resuspended in 13 ml ice-cold 100 mM $CaCl_2$ and kept on ice for 20 min. Again, the cells were pelleted at 4 000 x g for 10 min at 4 °C. The supernatant was discarded and the cell pellet was resuspended in 2.6 ml of ice-cold 85 mM $CaCl_2$ containing 15 % glycerol (v/v). 50 µl aliquots were flash frozen in liquid N_2 and stored at -80 °C.

3.1.14 Transformation of chemically competent bacteria

Chemically competent *E. coli* were transformed with plasmid DNA or ligated DNA samples (section 3.1.16 and 3.1.11) according to the heat shock method (Sambrook and Russel 2001).

Therefore 50 µl of chemically competent DH5α were thawed on ice. 2 µl of DNA were added and mixed by gently stirring with the pipette tip. After incubation for 30 min on ice the heat shock was performed at 42 °C for 30 sec. Then the cells were incubated on ice for 2 min and 250 µl of pre-warmed SOC medium (section 2.9) were added. The cells were shaken at 200 rpm for 1 h at 37 °C. Finally the cell suspension was plated on pre-warmed LB agar plates (section 2.9) containing 100 µg/ml ampicillin as selection marker. The plates were incubated upside-down at 37 °C over night.

3.1.15 Glycerol cultures of bacteria

Glycerol cultures of respective *E. coli* clones were used for long term storage (Sambrook and Russel 2001). 2 ml over night culture were pelleted at 10 000 x g for 1 min. 1.6 ml of the supernatant were discarded. The bacterial cell pellet was resuspended in the remaining 0.4 ml and 100 µl of 87 % glycerol (sterile) were added to receive a final glycerol concentration of 17 % (v/v). The cultures were immediately stored at -80 °C.

3.1.16 Purification of plasmid DNA

Plasmid DNA was purified from overnight cultures of respective *E. coli* clones received after transformation (section 3.1.14). An analytical preparation was performed to control the sequence of cloned plasmids by further sequencing (section 3.1.17). A quantitative preparation was used to receive a higher concentration and purity of plasmid DNA for further transfection approaches (section 3.3.3). DNA concentrations were measured using a NanoDrop ND-1000 spectrophotometer (PeqLab).

3.1.16.1 Analytical preparation

The respective *E. coli* clones were inoculated in 6 ml LB medium (section 2.9) containing 100 µg/ml ampicillin and cultivated over night at 37 °C and 250 rpm. The cells were pelleted stepwise in a 2 ml tube at 8 000 x g. Plasmid DNA was isolated using the QIAprep Spin Miniprep Kit (Quiagen) according to the manufacturer's instructions. The DNA was eluted using 50 µl dH_2O and stored at -20 °C.

3.1.16.2 Quantitative preparation

The respective *E. coli* clones were inoculated in 200 ml LB medium (section 2.9) containing 100 μg/ml ampicillin and cultivated at 37 °C and 250 rpm over night. 100 ml of over night culture were used for DNA purification. The cells were pelleted stepwise in a 50 ml tube at 8 000 x g. Plasmid DNA was isolated using the QIAGEN Plasmid Midi Kit (Quiagen) according to the manufacturer's instructions. Finally the DNA pellet was resuspended in 100 μl dH_2O and stored at -20 °C.

3.1.17 Sequencing

Cloned and purified plasmid DNA (section 3.1.16) was sequenced in order to exclude mutations and PCR-derived errors. Therefore specific primer pairs framing the multiple cloning site of the pcDNA3.1Hygro(+) plasmid were used (section 2.7.2). The insert was sequenced by the sequencing core facility (CeBiTec, Bielefeld, Germany) on Applied Biosystems Abi Prism 377, 3100 and 3730 sequencers using BigDye-terminator v3.1 chemistry. Premixed reagents were purchased from Applied Biosystems. The plasmid sequences are attached in the appendices A.1 and A.3.

3.2 Biochemical methods

3.2.1 Isolation of lysosome-enriched fractions

3.2.1.1 Isolation of tritosomes from mouse liver

Mouse liver lysosomes were enriched according to the method described Leighton et al. (1968). Usually, lysosomes exhibit the same density as mitochondria thereby challenging a proper separation of the organelles by a conventional centrifugation using density gradients. However, the density of lysosomes can be decreased by the use of tyloxapol (Triton WR-1339) that inhibits the lipoprotein lipase (Hayashi et al. 1981) resulting in an increased amount of LDL-particles in the mouse serum, which are further transported to the liver lysosomes for degradation. Due to the increased lipid content, the density of liver lysosomes is decreased and they are further referred to as tritosomes. Tritosomes are isolated by differential centrifugation of organelles followed by a discontinuous sucrose gradient. All work was done at 4 °C.

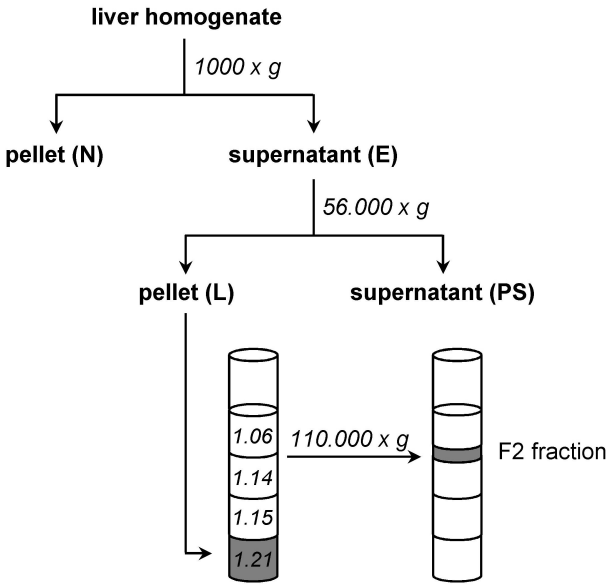

Figure 3.1: Isolation of lysosome-enriched fractions from mouse liver
Schematic outline of the isolation of lysosome-enriched fractions from mouse liver.

Mice were peritoneally injected with 4 μl of 17 % tyloxapol (in 0.9 % NaCl) per 1 g body weight 3 - 4 days prior to tritosome isolation. The animals were sacrificed by cervical dislocation. The liver was dissected and homogenized in 5 ml of 0.25 M sucrose by 1 stroke in a Potter S homogenizer (B. Braun; pestle speed: 1 500 rpm). The homogenate was centrifuge at 1 000 x g for 10 min (figure 3.1). The pellet was resuspended in 3.5 ml 0.25 M sucrose, homogenized by 1 stroke in a Potter S homogenizer and again centrifuged. The pellet contained cell debris, nuclei and intact cells and was referred to as pellet N. Both supernatants were combined (supernatant E) and centrifuged at 56 000 x g for 7 min (Sorvall® ULTRA Pro 80 centrifuge, Thermo Scientific, rotor T-880). The pellet was carefully resuspended in 8.5 ml of 0.25 M sucrose and again centrifuged. Both supernatant were combined and contained microsomes and cytosolic proteins (supernatant PS). The pellet L contained lysosomes and mitochondria and was further applied to a discontinuous sucrose gradient. The pellet was carefully resuspended in 2.5 ml of sucrose (density of $\rho = 1.21$), homogenized by 1 stroke in a Potter S homogenizer (pestle speed: 200 rpm) and transferred into a centrifugation-tube. The sample was carefully overlaid with 2.25 ml of sucrose ($\rho = 1.15$) followed by 2.25 ml of sucrose ($\rho = 1.14$) and finally 1 ml of sucrose ($\rho = 1.06$). The sample was centrifuged at 111 000 x g for 150 min in a swing-out rotor (Sorvall® ULTRA Pro 80 centrifuge, Thermo Scientific, rotor TH-641). During centrifugation the tritosomes were concentrated at the interphase between

the sucrose densities 1.06 and 1.14 forming a brownish layer (F2 fraction: ~1 ml), that was carefully transferred into a new tube.

For some purposes it was necessary to further concentrate the tritosomes or to enable a quick buffer exchange without dialysis. As the tritosomes were still intact after isolation they could be pelleted at 100 000 x g for 40 min (Optima^{TM} L-80 Ultracentrifuge, Beckmann Coulter, rotor TLA-55) and were resuspended in a smaller volume (e. g. 100 μl) of buffer of choice.

The tritosomes were stored at -20 °C until usage. Lysis was performed by addition of 0.5 % Triton X-100 (v/v) and sonification at 4 °C using a sonifier 450 (Branson; 3 x 20 sec pulses, 40 % intensity). After incubation on ice for 30 min insoluble particles were pelleted at 18 000 x g for 15 min and the supernatant was further subjected to activity measurements (section 3.2.6), Western blot analysis (section 3.2.5) or gel filtration studies (section 3.2.10).

3.2.1.2 Isolation of lysosome-enriched fractions from mouse brain

Lysosome-enriched fractions from brain were isolated as described by Caimi et al. (1989) by differential centrifugation followed by a continuous Percoll gradient. All work was done at 4 °C.

Mice were sacrificed by cervical dislocation. The whole brain was dissected and homogenized in 4 ml SED buffer (0.32 M sucrose containing 1 mM EDTA) by 5 strokes in a Potter S homogenizer (B. Braun; pestle speed: 500 rpm). The homogenate was cleared by centrifugation at 1 000 x g for 10 min (figure 3.2). The pellet was resuspended in 3 ml SED buffer and again centrifuged. The pellet contained cell debris, nuclei and intact cells. Both supernatants were combined and intact organelles were pelleted at 17 500 x g for 1 h (Optima^{TM} L-80 Ultracentrifuge, Beckmann Coulter, rotor T-1270). The supernatant containing cytosolic proteins and microsomes was removed. The pellet was resuspended in 1 ml SED buffer. Percoll was made isocratic by adding 9 ml Percoll to 1 ml 2.5 M sucrose containing 10 mM EDTA (100 % Percoll) and diluted to 27 % (v/v) with SED buffer. The resuspended organelles (1 ml) were layered over 9 ml of 27 % Percoll solution and centrifuged for 90 min at 20 000 x g (Optima^{TM} L-80 Ultracentrifuge, Beckmann Coulter, rotor T-1270). The gradient was collected from top to bottom in eight fractions of 1 ml volume and four fractions of 0.5 ml volume. 0.1 % Triton X-100 (v/v) was added and the organelles were lysed by sonification at 4°C using a sonifier 450 (Branson; 3 x 20 sec pulses, 40 % intensity). The lysosome-enriched fraction

was identified by determining the specific β-hexosaminidase activity (section 3.2.7). The α-L-fucosidase activity (section 3.2.6) as well as the protein concentration (section 3.2.3) was further determined.

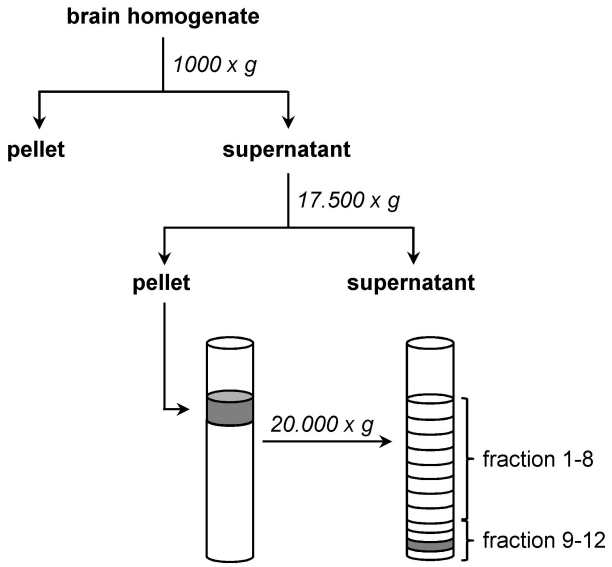

Figure 3.2: Isolation of lysosome-enriched fractions from mouse brain
Schematic outline of the isolation of lysosome-enriched fractions from mouse brain.

3.2.2 Preparation of tissue and cell homogenates

For the preparation of tissue homogenates, mice were sacrificed by cervical dislocation. Mouse organs were either directly used or frozen in liquid nitrogen and stored at -80 °C until usage. Approximately 150 mg of tissue (fresh weight) were homogenized in the 20 x volume of TBS containing 0.5 % Triton X-100 as well as protease inhibitors by 6 strokes in a Potter S homogenizer (B. Braun; pestle speed: 1 500 rpm). The resulting samples were lysed by sonification at 4°C using a sonifier 450 (Branson; 3 x 20 sec pulses, 40 % intensity).

Cell lysates were produced by pelleting trypsinized cells at 200 x g for 3 min. The cell pellet was washed once with 1 x PBS and centrifuged again. The supernatant was discarded and the cell pellet stored at -20 °C. For cell lysis, 100 μl (large cell pellets) or 50 μl (small cell pellets) of TBS containing 0.1 % Triton X-100 as well as protease inhibitors were added. The cells were sonified at 4 °C using a sonifier 450 (Branson; 3 x 20 sec pulses, 40 % intensity).

After sonification the tissue or cell homogenates were placed on ice for 30 min, were rigorously shaken and centrifuged at 18 000 x g for 15 min at 4 °C. 10 µl were used for determination of protein concentrations (1 : 10 diluted; section 3.2.3).

3.2.3 Determination of protein concentration

Protein concentrations of distinct samples (e. g. cell and tissue homogenates (section 3.2.2) or lysosome-enriched fractions (section 3.2.1)) were determined using the *DC* Protein Assay Kit (BioRad). The assay is based on a method described by Lowry et al. (1951). The first step is a Biuret reaction including a complex formation between peptide bonds and Cu(II) ions. In a second step, Cu(II) is reduced to Cu(I), which in turn reduces the yellow folin reagent to molybdenum blue. The blue dye can be quantified by measuring the absorbance at 750 nm.

Usually, 10 µl of tissue and cell homogenates (1 : 10 diluted) or 5 µl of lysosome-enriched (undiluted) were used. The samples were added to dH_2O in a 96-well microtiter plate (final volume of 100 µl). 1 ml of Reagent A was mixed with 20 µl of Reagent S and 25 µl of the mixture were applied to each sample. Then 200 µl of Reagent B were added. The reactions were incubated for 15 min at room temperature and their absorbencies were measured at 750 nm using the Infinite 200 microplate reader (Tecan). Blank values were taken from samples using a appropriate amount of dH_2O instead of sample. The protein concentration was determined from a reference curve using different amounts of bovine serum albumin (BSA; 0 - 16 µg). All measurements were done as duplicates.

3.2.4 SDS polyacrylamide gel electrophoresis

Proteins were separated according to their size by sodium dodecyl sulfate polyacrylamide gel electrophoresis (SDS - PAGE). Therefore gels were polymerized between glass plates using spacers according to table 3.13 and sample wells were formed by an appropriate comb. Samples from tissue and cell homogenates (section 3.2.2), lysosome-enriched fractions (section 3.2.1) or α-L-fucosidase purification fractions (section 3.2.8) were mixed with an appropriate volume of 4 x Laemmli buffer (section 2.9), denatured for 5 min at 95 °C and loaded onto the gel. For electrophoresis, gels were placed in SDS running buffer (section 2.9) at a constant current of 20 - 40 mA. Afterwards the proteins were either blotted onto PVDF membranes (Western blotting, section 3.2.5) or were stained (coomassie or silver stainings, section 3.2.4.1).

Table 3.13: Preparation of separating and stacking gels for SDS - PAGE

	separating gel		**stacking gel**
Acrylamide concentration	10 %	15 %	5 %
dH_2O	12.6 ml	7.70 ml	6.10 ml
Rotiphorese® Gel 30 (30 % acrylamide and 0.8 % bis-acrylamide (37.5 : 1))	9.80 ml	14.7 ml	1.30 ml
1.5 M Tris, pH 8.8	7.50 ml	7.50 ml	–
0.5 M Tris, pH 6.8	–	–	2.50 ml
TEMED	25 μl	25 μl	10 μl
10 % APS solution	250 μl	250 μl	100 μl
Total volume	30 ml		10 ml

3.2.4.1 Coomassie and silver staining

The purity of fractions received during α-L-fucosidase purification (section 3.2.8) was analyzed on a SDS-PAGE by coomassie or silver staining. After gelelectrophoresis, the proteins were fixed and stained with coomassie by incubating the gel in coomassie staining solution (section 2.9) over night with gentle agitation. The background of the gel was destained at the next day using 50 % methanol. The gel was washed intensively with dH_2O and documented using a CCD-camera (Fuji-Film).

If the concentration of the analyzed proteins was too low, the coomassie staining produced only slightly visible protein bands. A silver staining was performed to improve the detection. Silver ions (Ag^{2+}) attach at negatively charged amino acids. They can be reduced to elemental silver by addition of formaldehyde resulting in a staining of the proteins. The gel was sensitized by gentle shaking in 0.02 % sodium thiosulfate solution (w/v in dH_2O) for 1 min. Then the gel was washed three times with dH_2O for 20 sec and stained with 0.2 % silver nitrate solution (w/v in dH_2O) containing 0.05 % formaldehyde for 20 min at 4 °C under gentle agitation. Again, the gel was washed for three times with dH_2O for 20 sec and transferred into a clean dish. For development the gel was incubated in 3 % sodium carbonate solution (w/v in dH_2O) containing 0.05 % formaldehyde under gentle agitation. The reaction was stopped by washing the gel in dH_2O for 20 sec followed by an incubation in 5 % acetic acid (in dH_2O). The gel was documented using a CCD-camera (Fuji-Film).

3.2.5 Semi-dry Western blotting

After SDS-PAGE (section 3.2.4) proteins were transferred onto a PVDF-membrane in order to enable a specific protein detection using antibodies. Two layers of Whatman paper as well as the gel were equilibrated in cathode buffer (section 2.9) and arranged on the cathode site of the blotting equipment. The PVDF-membrane was activated for 30 sec in methanol and afterwards also equilibrated in cathode buffer. The membrane was applied to the blotting aperture and covered by another two layer of Whatman paper equilibrated in anode buffer (section 2.9). The proteins were transferred at a constant current of 1 mA/cm^2 for 80 min.

After the protein transfer, the membrane was blocked for 1 h using 5 % milk powder in TBS-T (section 2.9). The primary antibody was applied in TBS-T containing 5 % milk powder and incubated overnight with gentle agitation. The membrane was subsequently washed 4 times for 10 min with TBS-T before the secondary antibody was applied in TBS-T containing 5 % milk powder for 1 h at room temperature. Again the membrane was washed 4 times with TBS-T. The secondary antibody is conjugated to horseradish peroxidase (HRP) and the proteins were detected by enhanced chemiluminescence (ECL) signals. 1 ml luminol reagent was mixed with 1 ml peroxide solution (SuperSignal West Pico Chemiluminescent Substrate, Pierce). The solution was applied to the membrane that was then covered with a transparent sheet. The horseradish peroxidase converts luminol in the presence of H_2O_2 to 3-aminophthalate which is produced in an excited state. Light is emitted during the transition to the basic state. The emitted light signals were detected by a LAS 3000 luminescent image analyzer (Fuji-Film). If the detected signal were only weak, 40 μl of enhancer solutions A and B (SuperSignal West Femto Chemiluminescent Substrate, Pierce), respectively, were added in order to increase the ECL signals.

3.2.5.1 Stripping of Western blot membranes

Western Blot membranes were developed with a specific primary and secondary antibody (section 3.2.5). In order to enable further detections using other specific antibodies, the membrane was incubated in 1 M NaOH for 2 min at room temperature under gentle agitation. Afterwards the membrane was intensively washed with dH_2O followed by 4 washing steps with TBS-T (section 2.9) for 10 min. Then 5 % milk powder was applied for 1 h to block unspecific interactions. The further protein detection was performed as described above.

3.2.5.2 Ponceau S staining

Ponceasu S staining was used as loading control on Western blots. The staining solution (section 2.9) was added to the blot after stripping the membrane (section 3.2.5.1). Protein bands were visible within 1 - 2 min. The background of the blot was destained by incubation in dH_2O under gentle agitation. The staining was documented using a CCD-camera (Fuji-Film).

3.2.6 Determination of α-L-fucosidase activity

The α-L-fucosidase activity was measured using artificial pseudosubstrates. The enzyme converts 4-methylumbelliferyl-α-L-fucopyranoside (4-MUF; tissue and cell homogenates, lysosome-enriched fractions) to the fluorogenic product 4-methylumbelliferone (4-MU) thereby enabling a very sensitive detection of fucosidase activity. For activity measurements of purified recombinant enzyme it was sufficient to use the less sensitive substrate *para*-nitrophenyl-α-L-fucopyranoside (pNPF) that is converted to the chromogenic product *para*-nitrophenol (pNP). All measurements were done in duplicates. The background was determined by analyzing a substrate black value (addition of water instead of enzyme/sample) as well as an enzyme black value of each sample (addition of activity buffer without substrate). Reactions were prepared as stated below.

Regarding 4-MUF activity measurements, tissue homogenates (10 μl) or lysosome-enriched fractions (5 μl for liver or 25 μl for brain) were incubated with 150 μl of 0.75 mM 4-MUF in 0.1 M sodium citrate pH 5.5 including 0.2 % BSA and 0.04 % sodium azide for 16 h (tissue homogenates) or 6 h (liver lysosomes) or 4 h (brain lysosomes) at 37 °C and stopped by the addition of 150 μl of 1 M sodium carbonate (pH 10.4). The amount of liberated 4-MU was determined by fluorescence measurements (excitation: 360 nm; emission: 465 nm) using the Infinite 200 microplate reader (Tecan) and was calculated using a reference curve (0 – 10 nmol of 4-MU). The α-L-fucosidase activity was calculated as stated in equation 3.2. If necessary, tissue homogenates were diluted 1 : 10 - 1 : 100 to reach a linear range. For analysis of α-L-fucosidase pH dependency, McIlvaine's buffer (McIlvaine 1921) was used instead of 0.1 M sodium citrate and adjusted to the stated pH values.

$$Activity\ [mU/ml] = \frac{liberated\ 4{-}MU\ [nmol]}{V_{sample\ volume}\ [ml] \cdot t\ [min]} \cdot F \tag{3.2}$$

t = incubation time
F = dilution factor

In case of pNPF activity measurements, up to 50 μl of the fractions received during α-L-fucosidase purification (section 3.2.8) were filled up with dH_2O to a final volume of 100 μl and were added to 100 μl of 2 mM pNPF in 0.1 M sodium citrate pH 5.5 including 0.2 % BSA and 0.04 % sodium azide. The reaction was incubated for 1 h at 37 °C and stopped by the addition of 1 ml of 0.4 M glycine in NaOH (pH 10.4). The amount of liberated pNP was determined in a 96-well plate (in 300 μl) by measuring the absorbence at 405 nm using the Infinite 200 microplate reader (Tecan). The fucosidase activity was calculated according to the Lambert-Beer law (A = e * c * d) as stated in equation 3.3. Purified fractions containing a high amount of recombinant enzyme had to be diluted up to 1 : 1000 to reach a linear range (absorbance value < 1).

$$Activity\ [mU/ml] = \frac{\Delta E \cdot 10^6}{\varepsilon\ [\frac{L}{mol \cdot cm}] \cdot d\ [cm] \cdot t\ [min]} \cdot \frac{V_{assay\ volume}\ [\mu l]}{V_{sample\ volume}\ [\mu l]} \cdot F \tag{3.3}$$

$\Delta E = E_{sample} - E_{enzyme\ blank} - E_{substrate\ blank}$
$\varepsilon_{450\,nm}$ = molar extinction coefficent (18 500 L mol^{-1} cm^{-1})
d = layer thickness (300 μl = 0.85 cm)
t = incubation time (1 h)
$V_{assay\ volume}$ = volume after reaction stop (1200 μl)
F = dilution factor

3.2.7 Activity assays of other lysosomal glycosidases

The activities of lysosomal glycosidases (β-hexosaminidase and α-mannosidase) were measured in mouse tissue homogenates using artificial pseudosubstrates (*para*-nitrophenyl-*N*-acetyl-β-D-glucosaminide and *para*-nitrophenyl-α-D-mannopyranoside, respectively). The substrates were converted to *para*-nitrophenol (pNP) and the amount of liberated pNP was measured at 405 nm using the Infinite 200 microplate reader (Tecan). The molar extinction

coefficient of pNP at 405 nm accounts to $\varepsilon_{405} = 18\,500\,M^{-1}cm^{-1}$. The light path length in a 96-well microtiter plate with 300 μl volume is 0.85 cm (d = 0.85 cm). All measurements were done in duplicates. The background was determined by analyzing a substrate black value (addition of water instead of enzyme/sample) as well as a enzyme black value of each sample (addition of activity buffer without substrate). Reactions were prepared as stated below.

For α-mannosidase, up to 100 μl of tissue homogenates were used and added to 50 μl of 2 x activity buffer (0.2 M sodium citrate pH 4.2 including 0.4 % BSA and 0.08 % sodium azide) and 50 μl substrate (10 mM in dH_2O). The reactions were filled up with dH_2O to a final volume of 200 μl and were incubated at 37 °C for 16 h (visceral tissues) or 6 days (brain). The reactions were stopped by adding 1 ml of 0.4 M glycine in NaOH (pH 10.4). The absorbance of liberated pNP was measured in a microtiter plate using 300 μl of the reactions.

Regarding the β-hexosaminidase activity, the tissue homogenates had to be diluted 1 : 5 - 1 : 20. 10 μl were added to 100 μl of substrate (10 mM in 0.1 M sodium citrate pH 4.6 including 0.2 % BSA and 0.04 % sodium azide). The reactions were filled up with dH_2O to a final volume of 200 μl and were incubated at 37 °C for 2h. The reactions were stopped by adding 1 ml of 0.4 M glycine in NaOH (pH 10.4). The absorbance of liberated pNP was measured in a microtiter plate using 300 μl of the reactions. The β-hexosaminidase activity of enriched brain lysosomes was determined using up to 25 μl of percoll fractions. The reactions were prepared as described above and incubated for 30 min at 37 °C.

3.2.8 Purification of His_6-tagged α-L-fucosidase

The His_6-tagged human α-L-fucosidase was produced using a stable transfected CHO-K1 cell line (#C2 / C1). The cells were grown adherently (section 3.3.4.1), the conditioned medium was applied to an ammonium sulfate precipitation and the enzyme was subsequently purified by a Ni^{2+}-affinity chromatography followed by a strong cation exchange chromatography (SCX) as described below. All steps were carried out at 4 °C.

3.2.8.1 Ammonium sulfate precipitation

Conditioned medium from the cell line CHO-K1-hFuca-His_6 #C1 / C2 was harvested every two days (section 3.3.4.1) and immediately centrifuged at 8 000 x g for 30 min at 4 °C in order to remove death cells. 50 % $(NH_4)_2SO_4$ (w/v) were added and rigorously stirred for 1 h at

room temperature. The solution was subsequently stirred over night at 4 °C and stored at 4 °C for one week at the most.

3.2.8.2 Ni^{2+}-affinity chromatography

Approximately 1 L of conditioned medium was used for enzyme purification and precipitated as described above. The precipitate was centrifuged at 8 000 x g for 30 min at 4 °C and the protein pellet was resuspended in a minimal volume of HisTrap binding buffer (approximately 20 ml; including 50 mM imidazole; section 2.9) and dialyzed overnight at 4 °C with gentle stirring in a dialysis tube (MWCO 14 000) against 5 L of HisTrap binding buffer. The dialysate was harvested and centrifuged at 18 000 x g for 30 min at 4 °C and was transferred into a new tube for three times. Afterwards it was filtrated using 0.22 μm syringe filters.

A Ni^{2+}-affinity chromatography was performed using the ÄKTA Explorer system (GE Healthcare). A 1 ml HisTrap HP column (GE Healthcare) was equilibrated with 5 CV of HisTrap binding buffer, washed with 5 CV of HisTrap elution buffer and was re-equilibrated with 5 CV of HisTrap binding buffer. A constant flow of 1 ml/min was used during the whole purification protocol. The clarified sample was loaded using a 50 ml Superloop. The loop was emptied with a distinct volume of HisTrap binding buffer that corresponded to the amount of loaded sample. Afterwards the column was washed with 10 ml of binding buffer. The elution was performed in a one-step procedure by applying 100 % of HisTrap elution buffer (500 mM imidazole) for 15 ml, collecting 15 fraction of 1 ml each. The α-L-fucosidase activity was measured in each fraction (section 3.2.6). Usually fractions 2 - 5 contained the highest amount of enzyme and were pooled for further purification.

In order to apply a second purification step, the pooled fractions were immediately diluted 1 : 10 in SCX binding buffer (section 2.9) and were subsequently applied to the SCX as described below.

3.2.8.3 Strong cation exchange chromatography (SCX)

As a second purification step, a strong cation exchange chromatography (SCX) was performed using a 1 ml HiTrap SP HP column (GE Healthcare) connected to the ÄKTA Explorer system (GE Healthcare). A constant flow of 1 ml/min was used during the whole purification protocol. The column was equilibrated with 5 CV of SCX binding buffer (section 2.9), washed with 5 CV of SCX elution buffer and again was re-equilibrated with 5 CV of binding buffer. The

sample was loaded using a 50 ml Superloop. The loop was emptied with approximately 40 ml of SCX binding buffer and afterwards the column was washed with 10 ml of binding buffer. The further washing procedure was performed using a segmented protocol. In a first step, a linear gradient from 0 % to 40 % (400 mM NaCl) of SCX elution buffer over a length of 5 ml was used. The column was further washed with 40 % SCX elution buffer for 10 ml. The elution of the enzyme was performed in one step by applying 100 % (1 M NaCl) of SCX elution buffer for 15 ml. Fractions of 1 ml volume were collected and the α-L-fucosidase activity was measured in each sample (section 3.2.6). Usually, fractions 17 - 19 contained the highest amount of enzyme and were pooled and re-buffer into PBS as described below.

3.2.8.4 Buffer exchange via centricon

During SCX, the enzyme was eluted in an acidic buffer containing a high amount of NaCl and had to be re-buffered into PBS prior to intravenous injection into *Fuca*$^{(-/-)}$ mice (section 3.7.3). The pooled sample (~ 3 ml) was given into an Amicon® Ultra-4 Centrifugal Filter (10,000 NMWL, for volumes up to 4 ml; Millipore) hereinafter referred to as centricon. The sample was concentrated to 500 μl by centrifugation at 4000 x g at 4 °C in a swing-out rotor (for approximately 30 min). 3.5 ml of PBS were added and the sample was again concentrated to 500 μl by centrifugation (for approximately 45 min). This step was repeated. The final sample was flash-frozen in liquid nitrogen and the enzyme was stored at -80 °C.

3.2.9 Purification of the untagged α-L-fucosidase

3.2.9.1 Fucose-affinity chromatography

Fucose-affinity chromatography was carried out using a self-made affinity matrix. *N*-(ε-aminocaproyl)-β-L-fucopyranosylamine (hereinafter referred to as ligand) was coupled on CNBr-activated sepharose beads (GE Healthcare) or on a HiTrap NHS-activated HP column (GE Healthcare), respectively. Initially, the affinity matrices were tested separately, while the matrices were pooled in further experiments.

5 mg of the ligand were resuspended in 300 μl H_2O and were coupled to CNBr-activated sepharose beads according to the manufacturer's instructions. 150 μl of the ligand were diluted in 5 ml of coupling buffer (0.1 M $NaHCO_3$, 0.5 M NaCl, pH 8.3). 1 g of CNBr-activated sepharose beads was washed with 1 mM HCl and was transferred into a Mobicol column (MoBiTec). The beads were incubated with the coupling solution over night at 4 °C by rotation

and the affinity column was subsequently washed with 20 ml coupling buffer. In order to block non-coupled reactive groups, the column was washed with buffers with alternating pH values (0.1 M NaOAc pH 4.0 containing 0.5 M NaCl; 0.1 M Tris pH 8.0 containing 0.5 M NaCl) for three times and was stored in 20 % ethanol at 4 °C.

2.5 mg of the ligand were resuspended in 1 ml coupling buffer (0.1 M $NaHCO_3$, 0.5 M NaCl, pH 8.3). The NHS-activated column was washed with 2 ml of 1 mM HCl for three times using a syringe and the ligand was incubated on the column for 30 min at room temperature. The affinity column was subsequently washed with 3 ml coupling buffer followed by three washing steps using buffers with alternating alternating pH values (0.1 M NaOAc pH 4.0 containing 0.5 M NaCl; 0.1 M Tris pH 8.0 containing 0.5 M NaCl). The column was stored in 20 mM Tris pH 7.4 containing 20 % ethanol at 4 °C.

Both affinity matrices were pooled and transferred into a Mobicol column. The α-L-fucosidase purification was carried out at 4 °C by gravity flow. The untagged enzyme was produced using adherently grown CHO-K1 cells (clone # C1 / A5, section 3.3.4.1). The conditioned medium was precipitated using ammonium sulfate (section 3.2.8.1). The precipitate was centrifuged at 8 000 x g for 30 min at 4 °C and the protein pellet was resuspended in a minimal volume of binding buffer (50 mM NaOAc, 500 mM NaCl, pH 5.0). The sample was incubated on the affinity matrix for 2 h at 4 °C by rotation. The flow trough was collected and the column was washed with 10 ml binding buffer. Elution was performed using 15 ml of 50 mM NaOAc, 500 mM NaCl, 100 mM L-fucose, pH 5.0 and 1 ml fractions were collected. The α-L-fucosidase activity (section 3.2.6) was measured in load, flow trough and washing fractions, while the elution fractions were analyzed by SDS-PAGE and subsequent silver-staining (section 3.2.4 and 3.2.4.1) and / or Western blotting (section 3.2.5).

3.2.9.2 Concanavalin A-chromatography

1 ml Concanavalin A (ConA)-beads were transferred into a Mobicol column and equilibrated with binding buffer (20 mM Tris, 500 mM NaCl, 1 mM $CaCl_2$, 1 mM $MnCl_2$, pH 7.4). The purification of the untagged α-L-fucosidase was carried out at 4 °C by gravity flow as described in section 3.2.9.1. 50 mM NaOAc, 500 mM NaCl, 1 M α-D-methylglucoside, pH 4.5 was used as elution buffer. The α-L-fucosidase activity (section 3.2.6) was subsequently measured in each fraction.

3.2.9.3 Ion exchange and Ni^{2+}-affinity chromatography

The untagged α-L-fucosidase was produced using adherently grown CHO-K1 cells (clone # C1 / A5, section 3.3.4.1). The conditioned medium was precipitated using ammonium sulfate (section 3.2.8.1). The precipitate was centrifuged at 8 000 x g for 30 min at 4 °C and the protein pellet was resuspended in a minimal volume of binding buffer. The sample was clarified by centrifugation for three times at 18 000 x g for 30 min at 4 °C and subsequent filtration using 0.22 μm syringe filters. The α-L-fucosidase was purified either by a strong cation exchange chromatography (HiTrap SP HP 1 ml column, GE Healthcare), a weak anion exchange chromatography (HiTrap DEAE FF 1 ml column, GE Healthcare) or a Ni^{2+}-affinity chromatography (HisTrap HP 1 ml cloumn, GE Healthcare). The columns were connected to the ÄKTA Explorer system (GE Healthcare) and were washed with 5 ml binding buffer, followed by 5 ml elution buffer and were re-equilibrated with 5 ml binding buffer. The clarified sample was loaded using a 5 ml sample loop and the column was subsequently was with 10 ml binding buffer. Elution was performed using an linear elution gradient from 0 % - 100 % elution buffer over 15 ml followed by a washing step using 100 % elution buffer over 5 ml. Fractions of 1 ml were collected and analyzed for α-L-fucosidase activity (section 3.2.6). The purity of the enzyme was determined by SDS-PAGE (section 3.2.4) and subsequent silver-staining (section 3.2.4.1).

HiTrap SP HP binding buffer	50 mM NaOAc pH 4.0 or 4.5 or 5.0 or 7.4
HiTrap SP HP elution buffer	50 mM NaOAc, 1 M NaCl pH 4.0 or 4.5 or 5.0 or 7.4
HiTrap DEAE FF binding buffer	10 mM Tris pH 4.6 or 8.0
HiTrap DEAE FF elution buffer	10 mM Tris, 1 M NaCl pH 4.6 or 8.0
HisTrap HP binding buffer	10 mM Tris, 500 mM NaCl pH 7.4
HisTrap HP elution buffer	10 mM Tris, 500 mM NaCl, 500 mM imidazole pH 7.4

3.2.10 Size-exclusion chromatography

A possible oligomerization of the α-L-fucosidase was analyzed by size exclusion chromatography. The native murine as well as the recombinant human enzyme (untagged and His_6-tagged) were analyzed at different pH values. With respect to the murine α-L-fucosidase, freshly isolated tritosomes were pelleted (section 3.2.1.1), resuspended in 100 μl PBS pH 7.4

or McIlvaine's buffer pH 4.6 (McIlvaine 1921) supplemented with 140 mM NaCl and were lysed by sonification. The sample was loaded using a 100 μl loop. The human His_6-tagged enzyme was purified by a Ni^{2+}-affinity chromatography followed by an strong cation exchange chromatography (section 3.2.8.2 and 3.2.8.3) whereas the untagged enzyme was purified by SCX only (section 3.2.9.3). The fractions containing the highest α-L-fucosidase activity were dialyzed over night against PBS pH 7.4 or McIlvaine's buffer pH 4.6 supplemented with 140 mM NaCl. 100 μl sample were loaded on a Supderdex 200 10/300 GL column (GE Healthcare) connected to the Äkta Ettan LC system (GE Healthcare) at a constant flow rate of 0.3 ml/min. Fractions of 250 μl volume were collected. The α-L-fucosidase was detected by activity measurements (section 3.2.6). As an internal control the oligomerization of the β-hexosaminidase as well as the Plbd2 was analyzed using the fractions received during analysis of tritosomes. β-hexosaminidase was detected by activity measurements (section 3.2.7) whereas Plbd2 oligomerization was detected by Western blotting (section 3.2.5).

Prior to the sample runs, identical standard runs in PBS as well as in McIlvaine's buffer pH 4.6 supplemented with 140 mM NaCl were performed. Thyroglobulin (669 kDA), ferritin (440 kDa), bovine serum albumin (65 kDa), ovalbumin (45 kDa) and cytochrom C (12.5 kDa) were applied and detected by measuring the UV absorbance. The corresponding calibration curve was used to determine the molecular weight of the α-L-fucosidase.

3.2.11 Affinity chromatography using a mannose-6-phosphate receptor (MPR) matrix

A mannose-6-phosphate receptor (MPR) matrix was used to quantify the amount of mannose-6-phosphorylation on purified His_6-tagged α-L-fucosidase (section 3.2.8). 20 μg of the enzyme were diluted in 1 ml of MPR-binding buffer and loaded over night at 4 °C on an Affigel-10-based-affinity matrix (Bio-Rad) to which a 1 : 1 mixture of MPR46 : MPR300 (2.5 mg/ml; purified from goat) was immobilized (Braulke et al. 1990; kind gift of Siva Kumar, Hyderabad, India). Prior to sample loading the column was equilibrated using 10 ml of binding buffer. All steps were carried out by gravity flow using pre-cooled buffers. The flow through was collected and the column was washed with 8 ml of binding buffer followed by 6 ml of washing buffer. The enzyme was eluted using 10 ml of elution buffer. Finally the column was washed with 5 ml of acidic elution buffer and subsequently stored at 4 °C in 20 % ethanol. The α-L-fucosidase activity was measured using pNPF as substrate and 50 μl of each fraction (section

MPR binding buffer	50 mM imidazole-HCl, pH 6.5 0.15 M NaCl 5 mM sodium β-glycerophosphate 10 mM $MgCl_2$ 2 mM EDTA 0.05 % Triton X-100 0.02 % sodium azide
MPR washing buffer	MPR binding buffer + 5 mM glucose-6-phosphate
MPR elution buffer	MPR binding buffer + 5 mM mannose-6-phosphate
acidic elution buffer	0.1 M sodium acetate, pH 4,5 1 M NaCl 0.05 % Triton X-100 0.02 % sodium azide

3.2.6). Moreover 1/20th of each fraction was pelleted by TCA-precipitation and analyzed by Western blotting (section 3.2.12).

3.2.12 TCA-precipitation

TCA-precipitation was used to pellet low-concentrated protein samples. In order to reach the critical protein concentration for precipitation, cytochrom C (10 mg/ml in dH_2O) was added to a final concentration of 1 mg/ml. 0.02% sodium deoxycholate was added and the samples were mixed and incubated on ice for 30 min. Afterwards 15 % (v/v) trichloroacetic acid was added and the samples were mixed and incubated over night at 4 °C. At the next day, the samples were centrifuged at 4 °C for 10 min at 15 000 x g. The supernatant was discarded and the protein pellet resuspended in 1 ml of ice-cold acetone. The samples were vigorously mixed, incubated at room temperature for 5 min and again centrifuged. This step was repeated. Finally the dried protein pellet was resuspended in 50 μl of 2 x Laemmli buffer (section 2.9) by incubation at 37 °C for 30 min and was then denatured at 95 °C for 5 min. The samples were further analyzed by Western blotting (section 3.2.5).

3.3 Cell culture methods

3.3.1 General cell culture conditions in the presence of 10 % FCS

Usually, cell lines were grown adherently in sterile cell culture flasks in DMEM standard medium containing 10 % FCS (section 2.9) at 37 °C, 5 % CO_2 and 99 % humidity. After 2 - 3 days the cells had reached confluence and had to be passaged. The culture medium was discarded, the cells washed once with PBS and treated with 1.5 ml or 0.5 ml trypsin-EDTA (in case of a T75 or a T25 flask, respectively). After a few minutes it was verified microscopically that the cells had detached from the surface. 8.5 ml or 4.5 ml of DMEM standard medium were added and the cells were resuspended by pipetting. The cultures were split in a ration of 1 : 2 to 1 : 10 depending on the desired cell density. The cell culture flask was filled up with DMEM standard medium to 10 ml or 3 ml in case of a T75 or a T25 flask, respectively.

3.3.2 Cryo-conservation and thawing

For cryo-conservation, the cells were grown to confluence in a T75 flask. They were trypsinized as described above and pelleted by centrifugation at 250 x g for 3 min. The supernatant was discarded and the cells were resuspended in a suitable volume of cryo-conservation medium (section 2.9). They were frozen in 1 ml aliquots in cryotubes overnight at -80 °C. For long term storage the cultures were transferred to -150 °C.

Frozen cells were thawed in a water bath at 37 °C and immediately transferred into 10 ml of culture medium (usually DMEM standard medium containing 10 % FCS). The cells were pelleted at 250 x g for 3 min and the supernatant was discarded to remove DMSO from the cryo-conservation medium. The cells were resuspended in 3 ml of culture medium and transferred to a T25 cell culture flask.

3.3.3 Transfection

Transfections were performed using Polyethylenimine (PEI) as transfection reagent. PEI is a highly branched polymer and contains positively charged amino groups on its surface that interact with the negatively charged DNA. The PEI-DNA complex is endocytosed by the cells and enters the cytoplasm. During cell divisions the DNA can be incorporated into the nucleus and can be randomly integrated into the host cell genome (stable transfection). Otherwise the

transfected DNA gets lost within a few cell cycles (transient transfection). For transfection, cells were grown to 70 - 80 % confluence. The transfection mixture was prepared using serum-free OptiMEM medium, to avoid interactions of FCS during DNA-PEI complex formation. The transfection mixture was incubated for 15 min at room temperature. Meanwhile the cell culture medium of the cells was exchanged. The transfection mixture was added to the cells, incubated for 5h under standard cell culture conditions (section 3.3.1) and the cell culture medium was subsequently exchanged to reduce toxicity of the PEI reagent.

3.3.3.1 Transient transfection

Transient transfections promote high expression rates of the transfected gene. However, cells, that have stably integrated the desired DNA sequence are not selected. For transient transfections, cells were usually seeded in a 6 cm cell culture dish. The transfection mixture was prepared by adding 1 μg DNA and 3 μl PEI solution to 100 μl OptiMEM medium. The cells were harvested after 24 - 72 h and cell homogenates were prepared as described in section 3.2.2.

For immunofluorescence, cells were seeded on PLL-coated cover slips (section 3.4.1) in 24-well plates and transfected using 0.5 μg DNA and 1.5 μl PEI solution (in 100 μl OptiMEM medium). Immunofluorescence staining (section 3.4.2) was performed after 24 h - 48 h.

3.3.3.2 Stable transfection and isolation of single cell clones

CHO-K1 cells were stable transfected with an expression plasmid carrying either the coding sequence for the human His_6-tagged α-L-fucosidase or the human untagged enzyme (pcDNA3.1Hygro(+)hFuca-His_6 or pcDNA3.1Hygro(+)hFuca). Cells were grown to 70 - 80 % confluence in a 6-well plate. 5 μg of the respective plasmid were added to 15 μl PEI solution and 100 μl OptiMEM medium. After 24 h, the cells were trypsinized and 1/5 of the cells was seeded on a 10 cm cell culture dish in DMEM standard medium (section 2.9) supplemented with 100 μg/ml hygromycin to select stable transfected cells. At the next day the hygromycin concentration was raised to 800 μg/ml (selective growth medium). All untransfected cells died within a few days, whereas the transfected cells survived. Single cell clones were visible within 2 - 3 weeks and trypsinized using cloning rings. The cell clones were seeded in 24-well plates and grown to confluence in selective growth medium. Then the cells were treated with FCS-free DMEM to promote secretion of the fucosidase. The cell culture supernatant

was harvested after 24 h and the cells were further grown in selective growth medium. The supernatant was used to measure the α-L-fucosidase activity (section 3.2.6). The cell clone possessing the highest enzyme production capacity was further expanded and then subjected to a limited dilution assay. Therefore the cells were trypsinized, the cell number was determined and the cells were seeded with a concentration of 0.5 cells/well in several 96-well plates using selective growth medium. Due to this cell concentration, it was ensured, that one cell at a maximum was seeded per well. Single cell clones were grown to confluence after approximately 3 weeks and were further expanded in 24-well plates. As described above, the α-L-fucosidase activity was measured in the cell culture supernatant. The cell clones possessing the highest enzyme production capacity was further expanded using DMEM standard medium and used for enzyme production (section 3.3.4).

3.3.4 Cell culture conditions for protein production

Stable transfected CHO-K1 cells (section 3.3.3.2) were used for production of recombinant human α-L-fucosidase (either untagged or His_6-tagged). Conditions for maximal enzyme secretion were initially established for adherent cells. Later, cells were also adapted to FCS-free suspension conditions.

3.3.4.1 Adherent culture conditions in the presence of 0.5 % FCS

The α-L-fucosidase was produced in the presence of 0.5 % FCS. Cells were adherently grown on 16 cm cell culture dishes (usually 25 - 30 dishes were used for one production cycle) using DMEM standard medium (section 2.9) supplemented with 10 % FCS. After reaching confluence, cells were thoroughly washed with PBS for two times and then cultivated using DMEM standard medium supplemented with 0.5 % FCS. The diminished FCS concentration inhibited further cell divisions and promoted enzyme production and secretion. However, a cultivation in FCS-free DMEM was not possible, as the cells died within a few days. 20 ml of production medium was added to each 16 cm dish and the cell culture supernatant was harvested every second day for four times. A further cultivation was not efficient as the α-L-fucosidase production decreased massively after the fourth harvest. The supernatant was further processed as described in section 3.2.8 and used for α-L-fucosidase purification. Usually the supernatants of the first and second as well as of the third and fourth harvest were combined, respectively (approximately 1 L) and purified immediately.

3.3.4.2 Conditions for serum-free suspension culture

A cultivation under serum-free suspension conditions is often favorable, because the FCS as a contaminant is removed and eases protein purification. Moreover the cells often reach a higher protein production capacity under serum-free culture conditions.

Stably transfected CHO-K1 cells were usually grown adherently in DMEM standard medium containing 10 % FCS. During adaption to serum-free conditions, the standard medium was mixed with serum-free Corning® PF medium (Corning). Culture conditions of 36.5°C, 6 % CO_2 and 99 % humidity were chosen. Initially, a concentration of 25 % serum-free medium was used and then raised to 50 %, 75 %, 90 % and finally 100 % of Corning® PF medium was used. The cells were grown under each condition for a minimum of two passages. Starting with 75 % of serum-free medium, the cells were detached from the culture flask using the TrypLE reagent instead of trypsin-EDTA, as the diminished amount of FCS was not sufficient to inhibit trypsin. After two passages in 100 % Corning® PF medium, the cells detached automatically from the cell culture flask and started to grow as spheres in suspension. They were harvested by centrifugation at 250 x g for 3 min and were separated by resuspension in TrypLE reagent and incubation at 37 °C. Afterwards, the cells were resuspended in PBS, pelleted by centrifugation at 250 x g for 3 min and finally resuspended in Corning® PF medium. The cell number was measured (section 3.3.7) and adjusted to 5 x 10^5 viable cells/ml. The cells were grown as 30 ml culture in Corning® shake flasks at 36.5 °C, 6 % CO_2, 99 % humidity and 125 rpm. After two weeks of adaption, the starting cell culture concentration was decreased to 3 x 10^5 viable cells/ml. A density of 3 - 4 x 10^6 viable cells/ml was reached after 4 - 5 days and a subculturing was performed by dilution of an appropriate amount of cells.

3.3.5 Primary mouse embryonic fibroblasts (MEFs)

3.3.5.1 Isolation of MEFs

Primary mouse embryonic fibroblasts (MEFs) were isolated from mouse embryos obtained from matings of heterozygous *Fuca1*$^{+/-}$ mice. Hence, wildtype, *Fuca1*$^{+/-}$ and *Fuca1*$^{-/-}$ embryos were obtained. MEFs were isolated at embryonic day 12.5. The embryos were washed with PBS. The visceral tissues were removed and the head was dissected and used for genotyping (section 3.1.6.4; heterozygous cultures were discarded immediately after genotyping). The remaining embryonic tissue was transferred into a 2 ml tube, covered with 0.5 ml trypsin-EDTA and cut into small pieces. The tissue was transferred into a sterile Erlenmeyer flask

containing two layers of glass beads (3 mm diameter) and was dissociated by incubation for 15 min at 37 °C meanwhile shaking every 5 min. Afterwards the tissue was resuspended by adding 5 ml of DMEM standard medium containing 10 % FCS (section 2.9). The cells were dissociated by pipetting with a Pasteur pipette, transferred into a 15 ml tube and centrifuged at 250 x g for 3 min. The supernatant was discarded and the cells were resuspended in 5 ml of DMEM standard medium containing 10 % FCS and grown in a T25 cell culture flask. On the following day the medium was changed to remove dead cells. Approximately after two days the cells had grown to confluence and were trypsinized and splitted (passage 1). A part of the cells was collected as backup by cryo-conservation (section 3.3.2). Usually at passage 2 the cells were transfected for further immortalization as described below.

3.3.5.2 Immortalization of MEFs

Wildtype and *Fuca1*$^{-/-}$ MEFs were immortalized by transfecting the pMSSVLT plasmid carrying the CDS of the SV40 large T-antigen as well as a neomycin resistance cassette. MEFs were grown to 80 % confluence in a T25 cell culture flask (usually at passage 2). 5 μg of the pMSSVLT plasmid were added to 100 μl OptiMEM medium and mixed with 15 μl PEI. The sample was incubated for 15 min at room temperature. Meanwhile the cell culture medium of the MEFs was exchanged. The transfection mixture was added to the cells, incubated for 5 h under standard cell culture conditions (section 3.3.1) and afterwards the cell culture medium was exchanged. Transfected cells were selected after 24 h by adding G418 (500 μg/μl) to the medium.

Due to selection with G418 untransfected wildtype cells died within a few days. Transfected cell clones were visible after 2 - 3 weeks. Cells were trypsinized and mixed cell clones were established. The wildtype MEF cell lines were intensively passaged every 2 - 3 days for up to 6 weeks to promote selection of rapidly dividing (immortalized) cells. An increase in proliferation rate was observed over time.

Selection of transfected *Fuca1*$^{-/-}$ cells was not possible using G418 as all *Fuca1*$^{-/-}$ cells already contained a neomycin resistance cassette that was integrated into exon 1 of the *Fuca1* gene to disrupt its open reading frame (section 4.1.1). However, transfected cells were enriched by intensive passaging of the *Fuca1*$^{-/-}$ cultures using selection medium. Approximately after passage 5 - 8, a massive decrease in proliferation rate was observed as all untransfected cells reached the Hayflick limit and entered a cell cycle arrest. Further passages were not necessary

until cell clones of transfected *Fuca1*$^{-/-}$ cells were visible after several weeks. Of note, the immortalization of the *Fuca1*$^{-/-}$ MEFs could have also occurred spontaneously rather than by transfection. As described for the wildtype cell lines, mixed cell clones were established and immortalized *Fuca1*$^{-/-}$ cells were further selected by intensive passaging for up to 6 weeks. Again, an increase in proliferation rate was observed over time.

3.3.6 Endocytosis

For endocytosis experiments, wildtype and *Fuca1*$^{-/-}$ MEFs were grown to 80 % confluence in 6 cm cell culture dish. The cell culture medium was discarded and the cells were washed with PBS for two times. The cells were subsequently cultured in 1.5 ml of DMEM containing 0.1 % BSA. After 1 h, purified recombinant His_6-tagged α-L-fucosidase was added (20 μg/ml) and incubated for 5 h under standard cell culture conditions (section -3.3.1). Finally the cells were harvested by trypsination, cell lysates were prepared (section 3.2.2) and the α-L-fucosidase activity was determined (section 3.2.6). Of note, a thorough trypsination was mandatory, as the recombinant enzyme sticked tightly to the surface of the cells. Hence, the cell surface proteins had to be thoroughly digested with trypsin, as false positive results were obtained, when the cells were harvested by scraping.

3.3.7 Determination of cell numbers

For determination of cell numbers, an aliquot of trypsinized cells or an aliquot of cells cultivated under suspension conditions was used. 20 μl of the cell suspension were mixed with 20 μl of trypan blue solution (1 : 4 diluted in PBS) and 10 μl were added into a cell counting chamber (Innovartis). Cell number was measured in duplicates using the cell counter Cedex XS (Innovartis).

3.4 Cell biological methods

3.4.1 Coating of cover slips with poly-L-lysine

For immunofluorescence stainings, mammalian cells were seeded on cover slips, that were coated with Poly-L-lysine (PLL). The cover slips were treated with acetone for 30 min and washed thoroughly with dH_2O for three times. 0.01 % PLL (w/v) was added and incubated

over night at 4 °C. Again the cover slips were washed with dH_2O for three times, dried for 2 h in a sterile air flow and were sterilized with UV-light for 10 min. Coated cover slips were stored at room temperature until usage.

3.4.2 Immunofluorescence staining of mammalian cells

For immunofluorescence staining, mammalian cells were seeded on PLL-coated cover slips (section 3.4.1) in 24-well plates. After attachment, cells were either transfected and grown for 24 h - 48 h (section 3.3.3.1) or were directly processed. Fixation was performed either by using 4 % *para*-formaldehyde (PFA) or by using methanol. All steps were performed in 24-well plates, except for the antibody and DAPI stainings. Therefore, the cover slips were incubated up-side down in a 50 μl drop of staining solution in a wet chamber.

Regarding PFA-fixation, cells were washed three times with PBS and incubated for 20 min in 4 % PFA-solution (in PBS). Afterwards the cells were washed again with PBS for three times and permeabilized for 5 min with 0.2 % saponin (in PBS; S-PBS). Autofluorescence was quenched by incubation in 0.12 % glycine (in S-PBS) for 10 min. The cells were washed with S-PBS and blocked for 30 min in 10 % FCS (in S-PBS) and were further applied to antibody staining as described below.

For methanol fixation, cells were washed with PBS for three times and incubated with cold methanol for 10 min at -20 °C. For re-hydration the cells were thoroughly washed with PBS for three times. An additional permeabilization step was not necessary, as methanol automatically permeabilized the cells. A blocking step was performed by incubation for 30 min in 1 % BSA (in PBS). The cells were further applied to the antibody staining as described below.

After blocking of unspecific binding sites, the cells were incubated over night with the primary antibody in 1 % goat-serum (in S-PBS) at 4 °C. At the next day, the cells were washed with S-PBS for four times and incubated with the Alexa Fluor®-coupled secondary antibody (1 : 2000 in 1 % goat-serum in S-PBS) for 2 h at room temperature. Again, the cells were washed for four times in S-PBS followed by two washing steps in dH_2O. Cell nuclei were stained in DAPI solution (1 : 1000 in S-PBS; DAPI stock: 1 mg/ml) for 20 sec. Afterwards the cover slips were shortly dipped in dH_2O and mounted in Mowiol/Dabco on an object holder. The mounting solution was allowed to dry over night at room temperature and the immunofluorescence staining was documented using a confocal laser-scanning microscope (LSM700, Zeiss).

3.5 Histological methods

3.5.1 Generation of tissue sections

All histological stainings were performed using 35 µm-thick free-floating tissue sections. Therefore, mouse organs were actively perfused with 4 % *para*-formaldehyde (section 3.7.2) and placed on the organ holder of an SM 2000R microtome (Leica). The microtome was cooled down with dry ice. Organs were frozen on a layer of 5 % sucrose (in PB-buffer) and embedded using 30 % sucrose (in PB-buffer). The organs were cut into 35 µm-thick sections and transferred into 24-well plates with an brush. The tissue sections were stored at 4 °C in PB-buffer containing 0.02 % sodium azide.

3.5.2 Immunofluorescence staining of tissue sections

Free-floating tissue sections (section 3.5.1) were transferred into 24-well plates using a brush and washed three times with PB-buffer to remove sodium azide. Permeabilization of the sections and blocking of unspecific binding sites was performed by incubation in PB-buffer containing 0.5 % Triton X-100 as well as 4 % goat serum (blocking solution) for 2 h at room temperature. Then the tissue sections were treated with primary antibody diluted in blocking solution over night at 4 °C. At the next day, the sections were washed three times with PB-buffer containing 0.25 % Triton X-100 (washing solution) and incubated with Alexa Fluor®-coupled secondary antibody (1 : 2000 in washing solution) for 2 h at room temperature. The sections were washed once. Cell nuclei were stained for 10 min in DAPI solution (1 : 1000 in washing solution; DAPI stock: 1 mg/ml). The sections were washed once again in PB buffer without Triton X-100 and then transferred onto object holders using a brush. The sections were mounted with Mowiol/Dabco and the mounting solution was allowed to dry over night at room temperature. The immunofluorescence staining was documented using a confocal laser-scanning microscope (LSM700, Zeiss).

Lectins are complex carbohydrate-binding proteins. They exhibit a high specificity for certain sugar moieties but possess no intrinsic enzyme activity. Biotinylated lectins were used in histological analyses and detected using Alexa Flour®-coupled streptavidin. Unfortunately, a co-staining with other antibodies (e. g. Lamp1 for lysosomes) was not possible, due to incompatible blocking steps during the staining protocol. However, an α-aquaporin2 antibody could be applied and was used as a marker for renal collecting ducts. For immunofluorescence

stainings using lectins (Aleuria aurentia and Lens culinaris) all blocking steps were performed using 1 % BSA instead of 4 % goat serum. The lectins were detected using Dye-Light® 594-coupled streptavidin.

3.5.3 Staining of unesterified cholesterol using filipin

Filipin staining was performed on free floating sections (section 3.5.1). Sections were permeabilized, blocked and autofluorescence was quenched with 1 % BSA, 0.15 % glycine and 0.02 % saponin in PBS for 1.5 h (washing solution). Filipin was resuspended as 0.1 % stock-solution in 10 % DMSO in PB buffer. Unesterified cholesterol was stained by applying 0.005 % Filipin (diluted in PBS) for 30 min. The sections were washed for three times with washing solution, followed by three washes with PBS and were finally mounted with Mowiol/ Dabco and were analyzed with a Leica DM5000B epi-fluorescence microscope (excitation filter BP340-380; dichromatic mirror 400; suppression filter LP425).

3.5.4 Staining of lipids using sudan black

1 g Sudan Black B was resuspended in 100 ml 70 % ethanol by boiling. The solution was immediately used after cooling down and filtration. The staining was performed on free floating sections (section 3.5.1). The sections were treated with 50 % ethanol for 10 min, covered with the Sudan Black B solution for 5 min and washed three times with 70 % ethanol. Sections were incubated in dH_2O for 10 min and counterstained with Nuclear Fast Red for 5 min and finally washed three times with dH_2O. The sections were mounted with Mowiol and documented with a Leica DM IRB microscope.

3.5.5 Light and transmission electron microscopy (TEM)

Histological analysis of mouse organs by light and transmission electron microscopy (TEM) was done by Prof. Dr. Renate Lüllmann-Rauch (University of Kiel, Germany). Briefly, mice were perfused with glutaraldehyde (section 3.7.2) and tissue blocks were post-fixed with 2 % osmium tetroxide and embedded in araldite. Semithin sections were stained with toluidine blue. Ultrathin sections were processed with uranyl acetate and lead citrate and analyzed with a Zeiss EM 900 electron microscope (Zeiss).

3.6 Glycobiological methods

3.6.1 Isolation of neutral oligosaccharides

Neutral oligosaccharides were isolated from mouse tissues according to the method described by Stinchi et al. (1999). 100 mg tissue (fresh weight) were homogenized in the 20 x volume of dH_2O using an ULTRA-TURRAX (IKA) and were lysed by sonification at 4 °C using a sonifier 450 (Branson; 3 x 20 sec pulses, 40 % intensity). 2.6 ml methanol were added per 600 µl tissue homogenate, were rigorously mixed and centrifuged at 3650 x g for 10 min at 4 °C. The pellet was resuspended in 1.3 ml of 80 % methanol per 600 µl tissue homogenate, was mixed and again centrifuged. Both supernatants were combined and 910 µl chloroform were added per 600 µl tissue homogenate, mixed and centrifuged at 2000 x g for 5 min at 4 °C. The supernatant was mixed with 2.72 ml dH_2O per 600 µl tissue homogenate and centrifuged at 3650 x g for 10 min at 4 °C. The water-soluble fraction was collected and incubated with 250 mg of a mixed-bed ion exchange resin (AG 501-X8, 20-50 mesh) over night at 4 °C. The unbound material was lyophilized and resuspended in 1 µl dH_2O per 1 mg tissue (fresh weight).

3.6.2 *In-vitro* digest of fucosidosis storage material

Neutral oligosaccharides were isolated from mouse tissues as described in section 3.6.1. 20 µl (according to 20 mg of fresh weight tissue) were treated with 100 mU of purified His_6-tagged α-L-fucosidase (section 3.2.8). 100 µl of activity buffer (0.1 M sodium citrate pH 5.5 including 0.2 % BSA and 0.04 % sodium azide) were added and the reactions were filled up with dH_2O to a final volume of 200 µl. As internal control, reactions were prepared adding activity buffer instead of enzyme. All reactions were performed as triplicates and incubated at 37 °C for 3 days. The proteins were precipitated by incubation at 95 °C for 5 min and centrifugation at 18 000 x g for 15 min. The supernatant was desalted by incubation with 50 mg of a mixed-bed ion exchange resin (AG 501-X8, 20-50 mesh) over night at 4 °C. The unbound material was lyophilized and resuspended in 20 µl dH_2O.

3.6.3 Isolation of lipids

Lipids were isolated from mouse tissues according to the method described by Kyrklund (1987). 150 mg tissue (fresh weight) were homogenized in the 13.33 x volume of methanol

(2 ml) using an ULTRA-TURRAX (IKA). 1 ml chloroform was added, mixed and incubated at room temperature for 15 min. The samples were centrifuged at 1000 x g for 10 min at 4 °C and the pellet was resuspended in 2 ml methanol. Again, 1 ml chloroform was added, mixed and incubated at room temperature for 15 min. The samples were centrifuged and both supernatants were combined.

The isolated lipids were desalted using Sep-Pak® Vac 6cc (1g) C18 cartidges (Waters) and were separated into two fraction by a sequentional elution procedure. Fraction I contained gangliosides, acidic phospholipids and sulfatides whereas fraction II contained neutral phospholipids. The columns were washed with 6 ml chloroform : mehtanol (1 : 2) followed by 3 ml methanol. 6 ml isolated lipids were added to 8 ml methanol : dH_2O (1 : 1) and applied to the column. The flow through was collected and 8 ml methanol : 0.9 % NaCl (1 : 1) were added and applied to the same column. This step was repeated. The final flow through was discarded and the column washed with 2 ml dH_2O to remove contaminating salts. Fraction I was eluted using 8 ml methanol : dH_2O (12 : 1) whereas fraction II was eluted using 8 ml chloroform : methanol (1 : 2). The column was washed with 5 ml methanol, equilibrated with 8 ml chloroform : methanol : 0.1 M KCl (3 : 48 : 47) and stored at room temperature. The lipid-containing fractions were lyophilized and resuspended in 1 μl methanol per 1 mg tissue (fresh weight).

3.6.4 Thin-layer chromatography (TLC)

Isolated neutral oligosaccharides (section 3.6.1) or lipids (section 3.6.3) were separated by thin-layer chromatography (TLC) on silica gel F60 plates (20 x 20; Merck). Prior to sample application, the plates were heated at 120 °C for 15 min. The samples were spotted semi-automated on the plates using the Linomat 5 application system (Camag) and a Hamilton syringe. For analytical TLCs, material corresponding to 10 mg of mouse tissues was loaded whereas material corresponding up to 25 mg of mouse tissue was loaded for preparative TLCs. The plates were dried for 1 h at room temperature and developed in running buffer (table 3.14) in a saturated atmosphere in TLC tanks for 16 h (neutral oligosaccharides), 1.75 h (lipids, fraction I) or 1 h (lipids, fraction II). The plates were dried for 1 h at room temperature and 5 min at 120 °C and were sprayed with staining solution (table 3.14). The plates were heated at 120 °C for approximately 5 min until the desired staining intensity was reached. The staining was documented using a CCD-camera (Fuji-Film).

Table 3.14: TLC running buffers and staining solutions

running buffer for neutral oligosaccharides	acetic acid : dH_2O (75 : 25)
running buffer for lipids (fraction I)	chloroform : methanol : 0.25 % CaCl (60 : 35 : 8)
staining solution for neutral oligosaccharides and lipids (fraction I)	0.2 % orcinol in 20 % H_2SO_4 in dH_2O
running buffer for lipids (fraction II)	chloroform : methanol : dH_2O (65 : 25 : 4)
staining solution for lipids (fraction II)	20 % H_2SO_4 in dH_2O

3.6.5 Identification of fucosidosis storage material by mass spectrometry

Neutral oligosaccharides were separated on a preparative TLC. The TLC was done as duplicate (section 3.6.4). One TLC plate was stained for carbohydrates. The retention-values of single glycocompounds were measured and the corresponding material was scraped off from the second undeveloped plate. The compounds were dissolved from the silica material by adding 100 μl dH_2O and incubation for 30 min at room temperature and were analyzed by HPLC-MS by Dr. Hans Christian Beck (Odense University Hospital, Denmark). Urine material was directly analyzed by HPLC-MS. Briefly, the samples were centrifuged at 14 000 x g for 20 min and 10 μl extract were mixed with 10 μl of a 0.01 nmol/μl maltotriose internal standard. The mixture was dried in an Eppendorf Concentrator and re-dissolved in 10 μl derivatization buffer (64 mg/ml sodium-cyanoborohydride and 41 mg/ml 2-aminobenzamide dissolved in a mixture of dimethylsulfoxide and acetic acid (v/v 7 : 3)) and incubated for 3 h at 70 °C followed by evaporation to dryness. After drying, the samples were re-dissolved in 50 μl acetonitrile/0.1 % TFA and were analyzed by hydrophilic interaction chromatography (HILIC) using a Dionex Ultimate 3000 HPLC system coupled to a Q-Exactive Orbitrap mass spectrometer (Thermo Scientific).

The oligosaccharides were separated on a 100 mm x 100 μm ID column packed with TSK-gel Amide-80 column material (Tosoh Bioscience LLC, PA, USA) by a 5 min gradient from 95 % to 86 % organic solvent (100 % ACN/0.1 % TFA) followed by a 30 min gradient from 86 % to 70 % organic solvent at a 900 nl/min flow.

The 2-AB-derivatized internal standard and the storage material of unknown structure were quantified by correlating the peak area obtained from 2-AB-derivatized internal standard (2-AB-maltodextrose; m/z 625.24) with peak areas of the detected species of unknown concen-

trations. The identities of the unknown storage material were based on molecular weights and fragmentation patterns as determined by electrospray ionization tandem mass spectrometry.

3.6.6 PNGase F digest

The glycosylation pattern of the recombinant His_6-tagged α-L-fucosidase was determined by PNGase F and EndoH digest. 10 μl (approximately 80 μg) of the purified enzyme were used and 10 μl H_2O, 5 μl 2 % SDS and 5 μl 1 M β-mercaptoethanol were added and the sample was denatured for 5 min at 95 °C. Afterwards, 5 μl 1 M Tris-HCl, 100 mM EDTA pH 8.0 in case of PNGase F or 100 mM NaOAc pH 5.5 were added as well as 5 μl 10 mM PMSF, 5 μl 10 % Triton X-100 and 2 μl PNGase F or 2 μl EndoH. The reactions were incubated at 37 °C over night and were further processed for SDS-PAGE (section 3.2.4) and were analyzed by Western blotting (section 3.2.5).

3.7 Animal handling

3.7.1 Mouse housing

Mice were housed in the central animal facility of the Bielefeld University (Germany) under standard and sterile housing conditions. Animals were allowed to eat and drink *ad libidtum*.

3.7.2 Perfusion

Mice were narcotized using 0.65 mg ketamine per 10 g body weight for analgesia and 0.13 mg xylazin and 0.02 mg acepromazin per 10 g body weight for narcosis. After approximately ten minutes the animals were free of pain reactions. The thorax was opened using scissors and a butterfly needle was introduced into the left ventricle of the heart. PB-buffer including 1 % procaine (washing solution) was injected with a flow rate of 10 ml/min using a peristaltic pump. Directly after starting the perfusion, the right ventricle of the heart was cut open. After injecting 50 ml of washing solution, the mouse tissues were fixed with 50 mL 4 % (w/v) *para*-formaldehyde or 6 % glutaraldehyde (v/v) in PB-buffer including 1 % procaine (perfusion solution). The PFA-fixed tissues (liver, kidney, spleen and brain) were dissected, subsequently treated with perfusion solution for 24 h and then stored at 4 °C in 30 % (w/v) sucrose in PB-buffer. The tissues were further cut into free-floating sections (section 3.5.1). Glutaraldehyde-

fixed animals were transferred into a 50 ml falcon, stored in perfusion solution and shipped to the University of Kiel (Germany) for further light and electron microscopic analysis (section 3.5.5) by Prof. Dr. Renate Lüllmann-Rauch.

3.7.3 Intravenous injection

Purified His_6-tagged α-L-fucosidase (section 3.2.8) or PBS (as control) was injected intravenously into the tail vein of mice. The animals were fixed using a mouse restrainer and the tail was pre-warmed in warm water to enhance visibility of the tail vein. 250 mU of pre-warmed enzyme per 1 g body weight (according to approximately 200 μl) were injected.

4 Results

4.1 Generation and characterization of a constitutive fucosidosis mouse model

4.1.1 Generation of *Fuca1*$^{(-/-)}$ mice

α-L-Fucosidase knock-out mice (*Fuca1*$^{(-/-)}$) were generated by a gene targeting strategy. A 6-kb fragment of the murine *Fuca1* gene including exon 1 and exon 2 was amplified from genomic DNA (primer pair E1fw / E1rev, section 2.7.4) and was cloned into the pKO Scrambler V901-DT vector (figure 4.1 A). This vector included a diphtheria toxin A (DTA)-coding sequence, which was further used as a negative selection marker. The neomycin phosphotransferase gene (nptI) was inserted into exon 1 of the *Fuca1* gene using AfeI restriction sites and the knock-out construct was electroporated into murine embryonic stem cells (D3 / 129S2 / SvPas). Geneticin (G418)-resistant ES cell clones were screened for homologous recombination events by PCR. The 5'-homologous recombination site was validated using the primer pair F4/AK31as and the 3'-homologous recombination site was identified in a nested PCR approach using the primer pairs F1/R2 and AK31/R1. Two ES cell clones carrying the *Fuca1*$^{(-/-)}$ allele were identified and ES cells (clone #39) were microinjected into blastocysts (strain C57BL/6) which were then implanted into pseudo-pregnant mice. The resulting chimeric mice were crossed with C57BL/6 mice and germline transmission was validated as described in section 4.1.2. The heterozygous offspring was intercrossed to obtain homozygous mice with a mixed genetic background (C57BL/6 & 129S2/SvPas).

Cloning of the *Fuca1*$^{(-/-)}$ construct as well as ES cell electroporation and screening was done by Prof. Lübke (Bielefeld University, Germany). Blastocyst injection was performed by Dr. Hermans-Borgmeyer (Center for Molecular Neurobiology Hamburg, Germany).

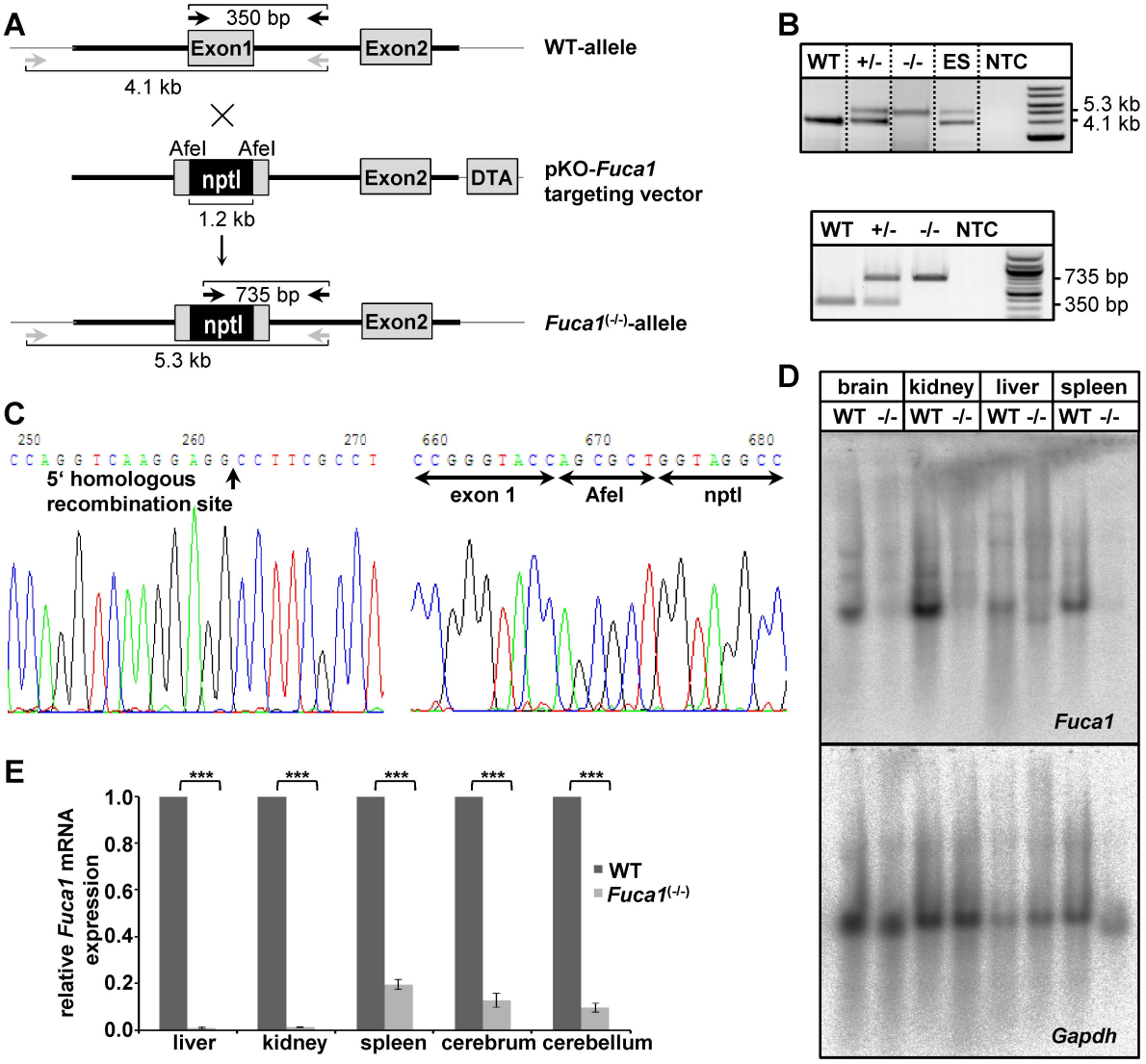

Figure 4.1: Validation of the *Fuca1* gene knock-out on genomic and transcript level
(**A**) *Fuca1*$^{(-/-)}$ mice were generated by a gene targeting strategy. The wildtype allele, the *Fuca1*-targeting vector as well as the *Fuca1*$^{(-/-)}$ allele are shown schematically. Primer pairs used for knock-out validation and mouse genotyping are marked by arrows. nptI = neomycin phosphotransferase gene; DTA = diphtheria toxin A-coding sequence (**B**) Ethidium bromide-stained agarose gel of PCR products from *Fuca1* knock-out validation (upper panel, primer pair F4/R3) and routine genotyping (lower panel, primer pairs F2/AK30-R/R3). ES = ES cell clone #39 (used for blastocyst injection); NTC = no template control. (**C**) Validation of the 5' homologous recombination site as well as the integration site of the neomycin phosphotransferase gene (*nptI*) was done by sequencing a PCR product of the *Fuca1*$^{(-/-)}$ allele shown in (B, upper panel). (**D**) The *Fuca1* mRNA expression was analyzed in several tissues of *Fuca1*$^{(-/-)}$ mice (3-month-old) using a Northern blot. Results were kindly provided by Prof. Lübke (Bielefeld University, Germany). (**E**) The *Fuca1* transcript expression was monitored by Real-Time PCR on cDNA from several wildtype and *Fuca1*$^{(-/-)}$ tissues (5-month-old mice). Gapdh was used for normalization. ***$p < 0.0005$

4.1.2 Validation of the *Fuca1* gene knock-out

The *Fuca1* gene knock-out was validated on mouse genomic DNA by PCR amplification resulting in a 4.1-kb fragment for the wildtype allele and a 5.1-kb fragment for the *Fuca1*$^{(-/-)}$ allele (figure 4.1 A and B, upper panel). The homologous recombination was confirmed by subsequent sequencing of the PCR products (figure 4.1 C). Routine genotyping was carried out using a multiplex PCR approach resulting in a 350-bp fragment for the wildtype allele and a 735-bp fragment for the *Fuca1*$^{(-/-)}$ allele (figure 4.1 A and B, lower panel).

On transcript level, a Northern blot revealed a markedly decreased expression of *Fuca1* transcript in several tissues of the *Fuca1*$^{(-/-)}$ mice (figure 4.1 D; results were kindly provided by Prof. Lübke, Bielefeld University, Germany). A detailed analysis using Real-Time PCR showed that the *Fuca1* transcript expression was reduced by approximately 99 % in *Fuca1*$^{(-/-)}$ liver and kidney (figure 4.1 E). A significant reduction of *Fuca1* transcript by 80 %, 88 % and 90 % was detected in spleen, cerebrum and cerebellum, respectively.

In order to exclude, that the residual *Fuca1* transcript translates into functional protein, α-L-fucosidase activity was measured at pH 5.5 in several tissue homogenates and was found to be completely absent in all *Fuca1*$^{(-/-)}$ tissues (figure 4.2 A). Moreover, lysosome-enriched fractions from liver were analyzed and no α-L-fucosidase activity was measured in *Fuca1*$^{(-/-)}$ lysosomes at pH 5.5 (figure 4.2 B). In addition, brain lysosomes were isolated on a self-forming Percoll gradient (figure 4.2 C and D) and fractions were analyzed for protein content, α-L-fucosidase and β-hexosaminidase activity, respectively. In wildtype, the lysosomal enzymes showed the highest activity in fraction 3 and 11, of which fraction 11 displayed the highest specific activity for lysosomal enzymes. In contrast, *Fuca1*$^{(-/-)}$ brain did not show α-L-fucosidase activity in any Percoll gradient fraction, but also displayed the highest specific activity for β-hexosaminidase in fraction 11.

Besides the lysosomal α-L-fucosidase encoded by the *Fuca1* gene, the *Fuca2* gene encodes another putative fucosidase that was termed as plasma α-L-fucosidase. In order to exclude, that this second fucosidase might affect the *Fuca1* gene knock-out, kidney homogenates of wildtype, *Fuca1*$^{(+/-)}$ and *Fuca1*$^{(-/-)}$ mice were analyzed at different pH values ranging from pH 4.0 to 8.0 (figure 4.2 E). No α-L-fucosidase activity was measured in *Fuca1*$^{(-/-)}$ kidney. Moreover, lysosome-enriched fractions from *Fuca1*$^{(-/-)}$ liver did not show α-L-fucosidase activity at pH 7.5 (figure 4.2 B), thus excluding α-L-fucosidase 2 as a source of residual activity.

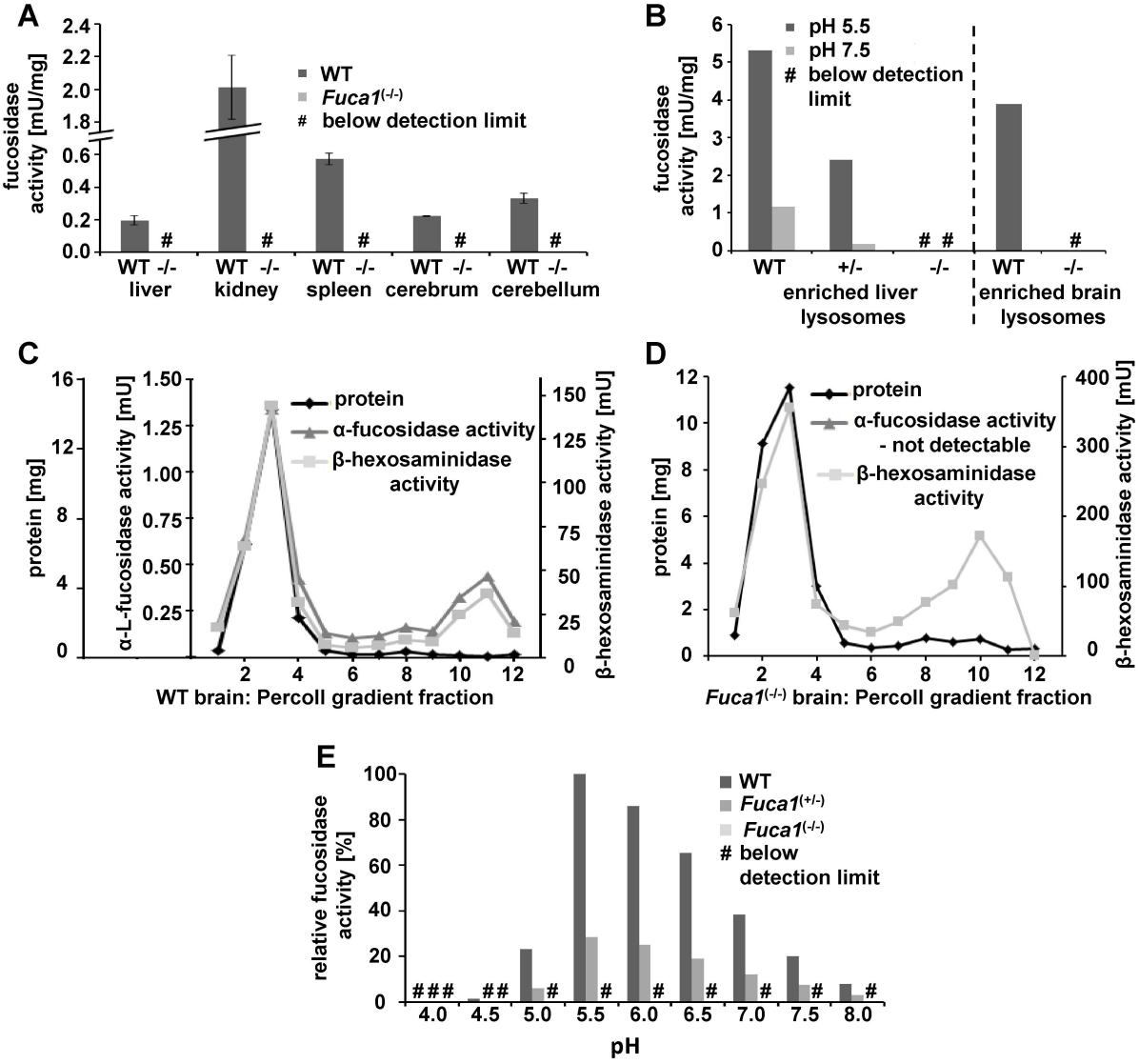

Figure 4.2: Validation of the *Fuca1* gene knock-out on enzyme level
(**A**) Specific α-L-fucosidase activity was measured at pH 5.5 in several tissue homogenates of 5-month-old mice. No α-L-fucosidase activity was detected in *Fuca1*$^{(-/-)}$ tissues. (**B**) Specific α-L-fucosidase activity was determined in isolated liver lysosomes of wildtype, *Fuca1*$^{(+/-)}$ and *Fuca1*$^{(-/-)}$ mice at pH 5.5 and 7.5, respectively. Brain lysosomes from wildtype and *Fuca1*$^{(-/-)}$ mice were analyzed at pH 5.5. No α-L-fucosidase activity was detected in lysosomes from *Fuca1*$^{(-/-)}$ mice. (**C** and **D**) Lysosome-enriched fractions were isolated from brains of 5-month-old animals using a self-forming Percoll gradient. 1 ml-fractions (F1-8) or 0.5 ml-fractions (F9-12) were collected and analyzed for protein content as well as β-hexosaminidase activity and α-L-fucosidase activity, respectively. In wildtype, the lysosomal enzymes showed the highest specific activity in fraction 11. No α-L-fucosidase activity was detected in any of the fractions from brain of *Fuca1*$^{(-/-)}$ mice whereas highest specific activity for β-hexosaminidase was also measured in fraction 11. (**E**) Specific α-L-fucosidase activity was measured in kidney homogenates of 3-month-old mice at different pH values. No α-L-fucosidase activity was detected in *Fuca1*$^{(-/-)}$ kidney.

In summary, the *Fuca1* gene knock-out was verified on genomic, transcript and enzyme level confirming the use of the α-L-fucosidase knock-out mice as a valid model for fucosidosis.

4.1.3 Breeding of *Fuca1*$^{(-/-)}$ mice

A *Fuca1*$^{(-/-)}$ mouse strain exhibiting a mixed genetic background (C57BL/6 & 129S2/SvPas) was established by inbreeding. These *Fuca1*$^{(-/-)}$ mice were used for all analyses reported in this work. In parallel, the mouse model was crossed back into C57BL/6 over a minimum of ten generations to reach 99.9 % C57BL/6 genetic background, but the back crossing has not yet finished.

Nearly 700 mice of the inbreeding strain were born until now, of which 49.7 % were male and 50.3 % were female. The average litter size was 7.1$\pm$2.3. 27.6 % wildtype, 51.9 % *Fuca1*$^{(+/-)}$ and 20.5 % *Fuca1*$^{(-/-)}$ animals were obtained. These data match with the expected Mendelian law, although a slightly reduced outcome of *Fuca1*$^{(-/-)}$ animals was recorded. It can be assumed, that the *Fuca1* gene knock-out has no influence on the distribution between the sexes and the embryonic development of the mice.

4.1.4 Regulation of other lysosomal proteins

Changes in the lysosomal proteome are characteristic for LSDs (van Hoof and Hers 1968a, Sandhoff et al. 1971) and were also analyzed in the fucosidosis mouse model. Real-Time PCR analyses of cDNA from cerebrum revealed a significantly increased transcription of all analyzed lysosomal genes in *Fuca1*$^{(-/-)}$ mice (figure 4.3 A). Interestingly, the transcription of these genes seemed to be regulated in a tissue-specific manner, as the mRNA levels were nearly unaffected in the kidney with exception of the genes for β-hexosaminidase, α-mannosidase and α-L-fucosidase 2, which were all significantly down-regulated (figure 4.3 B).

The α-L-fucosidase 2 (*Fuca2*) transcript was found to be threefold elevated in *Fuca1*-deficient cerebrum (figure 4.3 A), but was decreased by 50 % in the kidney (figure 4.3 B). As already stated in section 4.1.2, no residual α-L-fucosidase activity could be detected in tissue homogenates and lysosome-enriched fractions whatever pH value was used. It remains unknown whether *Fuca2* is translated or under what conditions the enzyme possesses activity *in vivo*.

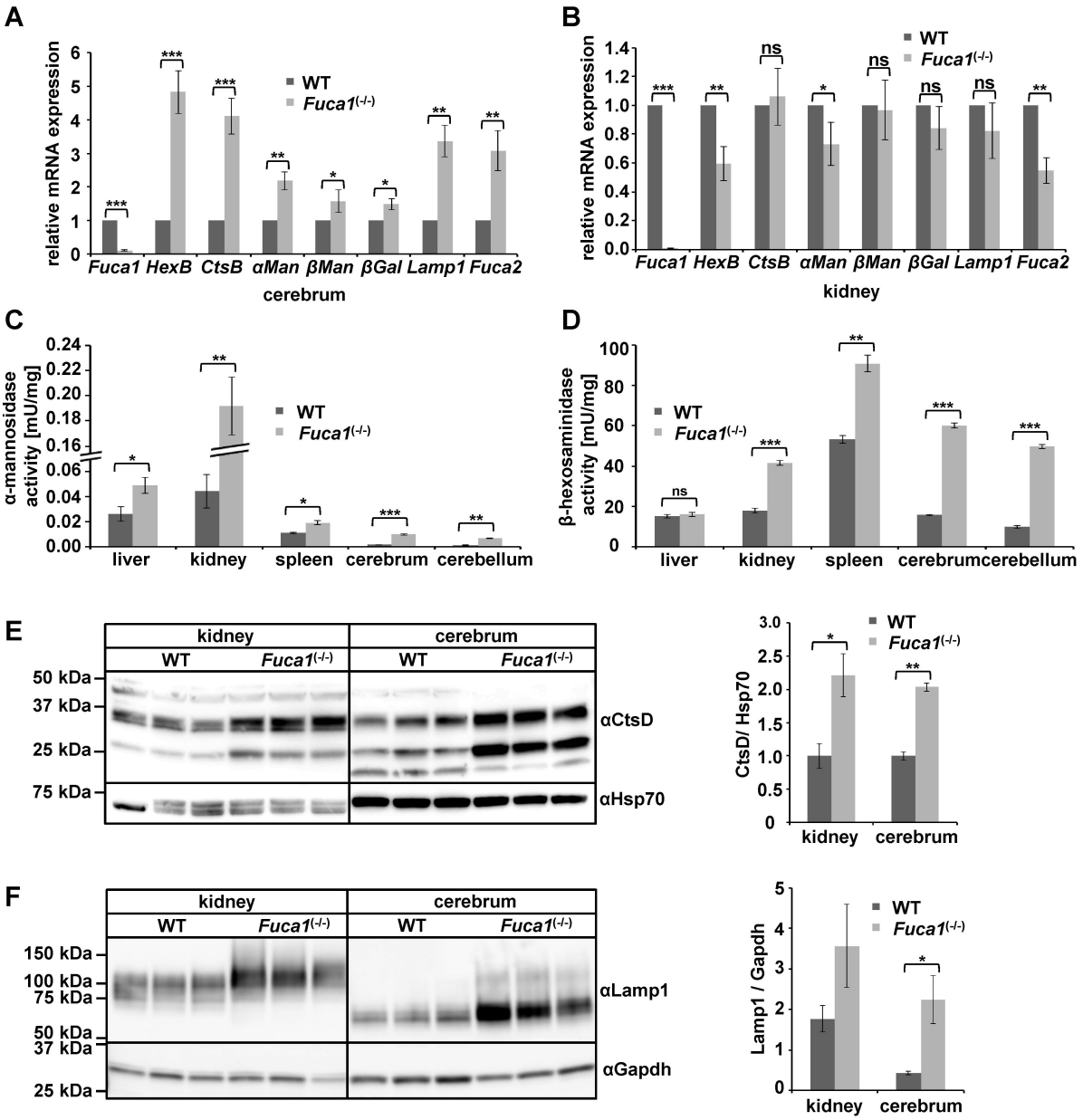

Figure 4.3: Regulation of lysosomal proteins in *Fuca1*$^{(-/-)}$ mice

(**A** and **B**) The expression of lysosomal hydrolases as well as of the lysosomal marker Lamp1 and the α-L-fucosidase 2 were analyzed by Real-Time PCR on cDNA from cerebrum and kidney of 5-month-old wildtype and *Fuca1*$^{(-/-)}$ mice. (**C** and **D**) Enzyme activities for α-mannosidase and β-hexosaminidase were measured in several tissue homogenates of 5-month-old animals, respectively. (**E** and **F**) Cathepsin D and Lamp1 were analyzed by immunoblotting of tissue homogenates from kidney and cerebrum of 5-month-old animals. An organ-specific glycosylation of Lamp1 was seen resulting in different molecular weights. Hsp70 or Gapdh was used for normalization. *$p < 0.05$, **$p < 0.005$, ***$p < 0.0005$, ns = not significant

Besides the transcriptional level, activities of lysosomal enzymes were measured in tissue homogenates and the α-mannosidase activity was shown to be two- to sixfold elevated in all analyzed *Fuca1*$^{(-/-)}$ organs (figure 4.3 C). The activity of the β-hexosaminidase showed a more tissue-specific regulation. A two- to threefold increase was detected in kidney, spleen, cerebrum and cerebellum, whereas the activity of the liver was unaffected by the *Fuca1* gene knock-out (figure 4.3 D). Remarkably, the mRNA levels of both genes were significantly down-regulated in the *Fuca1*$^{(-/-)}$ kidney, whereas on enzyme level an increased activity was detected, indicating an enhanced stability of both enzymes.

The amount of cathepsin D protein was analyzed by immunoblotting and was found to be twofold elevated in *Fuca1*$^{(-/-)}$ kidney and cerebrum (figure 4.3 E). Also the amount of Lamp1 (lysosome-associated membrane protein 1) was fivefold increased in the cerebrum, whereas there was only a slight trend towards an enhanced Lamp1 expression in the kidney (figure 4.3 F). An increased amount of Lamp1 protein can be used as a marker for LSDs, as its expression is often upregulated due to the general enlargement of the endosomal-lysosomal compartment (Meikle et al. 1997). In summary, the altered regulation of several lysosomal proteins indicated the formation of a LSD-like phenotype in the *Fuca1*$^{(-/-)}$ mice.

4.1.5 Macroscopic observations

Fuca1$^{(-/-)}$ mice were viable and fertile, showed a normal growth and weight gain and were indistinguishable from their wildtype littermates until the age of approximately 6 months. At older ages, the *Fuca1*$^{(-/-)}$ mice suffered from a worsening tremor and ataxia. Progressive problems in movement and coordination were observed resulting in an abnormal posture of the hind legs (figure 4.4 A and B). Moreover, the animals became progressively hypoactive.

During autopsy, the cerebrum of *Fuca1*$^{(-/-)}$ mice appeared reduced in size, whereas the cerebellum seemed to be swollen (figure 4.4 D and E). In this regard, the superior/ inferior colliculus (part of the midbrain; figure 4.4 D and E, marked by arrows) was markedly enlarged in comparison to wildtype brain. The altered macroscopic appearance of the *Fuca1*$^{(-/-)}$ brains suggested a neurological phenotype, which was verified later by histological and behavioral analyses (sections 4.1.9 and 4.1.10). At 8 months of age, male *Fuca1*$^{(-/-)}$ mice displayed a tremendously enlarged bladder with an overall urinary volume of ~ 3 ml (figure 4.4 C), whereas only a few female animals were affected. Due to animal welfare, *Fuca1*$^{(-/-)}$ mice had to be euthanized at 9 - 11 months of age.

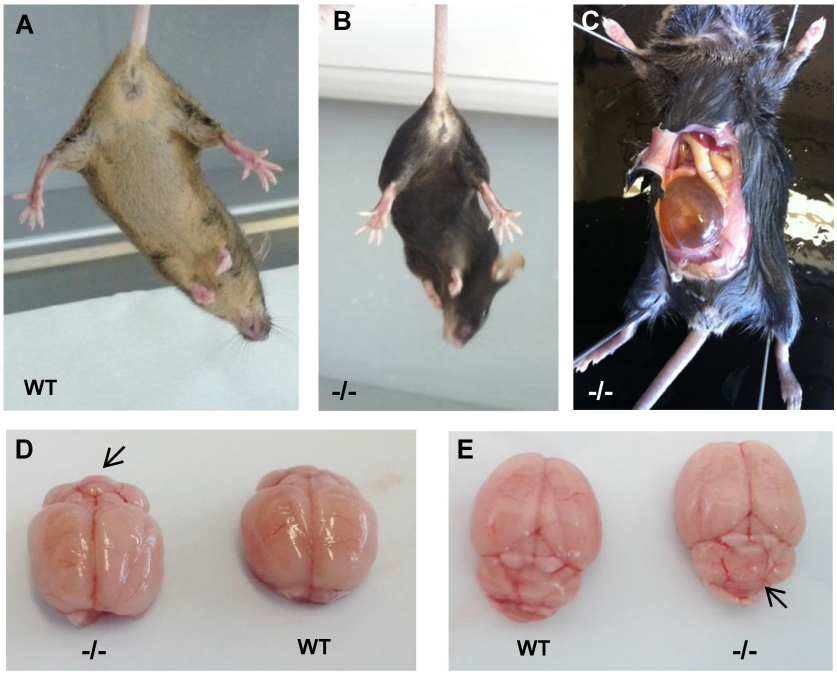

Figure 4.4: Macroscopic observations of *Fuca1*$^{(-/-)}$ mice
11-month-old wildtype (**A**) and *Fuca1*$^{(-/-)}$ (**B**) mice are shown. The mice were lifted at their tails. Thus, they spread their hind legs to keep balance. The *Fuca1*$^{(-/-)}$ mouse showed an abnormal posture of the hind legs that might be due to problems in movement and coordination. (**C**) A 9-month-old male *Fuca1*$^{(-/-)}$ mouse is shown that displayed a massively enlarged bladder. (**D** and **E**) The brain of a 10.5-month-old wildtype and a *Fuca1*$^{(-/-)}$ mouse is shown. The heavily enlarged superior/inferior colliculus is marked by arrows.

4.1.6 Storage pathology of visceral organs

Several visceral organs of wildtype and *Fuca1*$^{(-/-)}$ mice from 5 to 9 months of age were investigated in detail by light and, if needed, also by transmission electron microscopy (TEM). These analyses were performed by Prof. Lüllmann-Rauch (University of Kiel, Germany). Cytoplasmic storage vacuoles were found in almost all investigated organs of the *Fuca1*$^{(-/-)}$ mice. These membrane-enclosed vacuoles appeared mainly translucent indicating water-soluble compounds as the major storage material accumulating in murine fucosidosis. In most cases, light microscopy of semi-thin sections was sufficient to visualize the storage phenotype. Only in a few cases, e. g. hepatocytes of the liver and cells of the renal proximal convoluted tubule, TEM was necessary to detect storage material containing more heterogeneous material of moderate electron density. Moreover, selected visceral organs were analyzed

by immunofluorescence staining using a Lamp1 (lysosome-associated membrane protein 1)-specific antibody. Lamp1 is commonly used as a lysosomal marker and its expression is massively increased in several LSDs (Meikle et al. 1997) due to the overall enlargement of the endosomal-lysosomal compartment.

In the liver of *Fuca1*$^{(-/-)}$ mice, numerous large storage vacuoles were detected in Kupffer cells and sinusoidal endothelial cells (figure 4.5 B and C), while TEM was necessary to detect storage vacuoles in the hepatocytes which were loacated near the bile canaliculus and contained heterogenous material of moderate electron density (figure 4.5 D). Using immunostainings, a massive increase in Lamp1 protein became obvious in the *Fuca1*$^{(-/-)}$ liver (figure 4.6 A) indicating an enlarged endosomal-lysosomal compartment. A detailed analysis showed numerous vacuolated cells that were not found in the wildtype liver. By comparison with light microscopy data, these vacuolated cells were identified as Kupffer cells. Further analysis was performed by co-staining with the macrophage-specific marker F4/80. Due to technical reasons, cathepsin D instead of Lamp1 was used as lysosomal marker. These co-stainings confirmed that the Kupffer cells contained numerous storage vacuoles (figure 4.6 B) which were not present in the wildtype tissue.

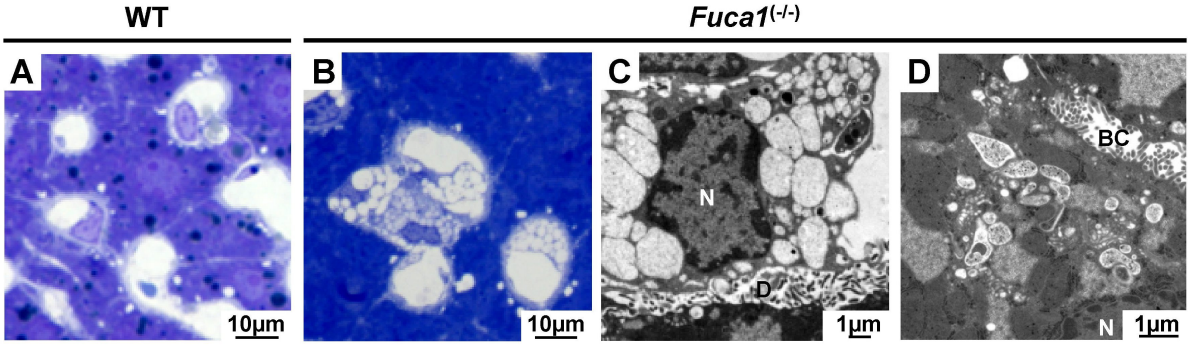

Figure 4.5: Storage pathology of the liver
The liver of 5-month-old wildtype and *Fuca1*$^{(-/-)}$ mice was analyzed by light (**A** and **B**) or transmission electron microscopy (TEM; **C** and **D**) in cooperation with Prof. Lüllmann-Rauch (University of Kiel, Germany). (**B**) Storage vacuoles were found in sinusoidal endothelial cells and Kupffer cells of the *Fuca1*$^{(-/-)}$ liver. (**C**) A Kupffer cell in higher magnification. D: space of Disse. (**D**) Using TEM, storage vacuoles were detected in hepatocytes (9-month-old mice) containing heterogeneous material of moderate electron density. N: nucleus, BC: bile canaliculus.

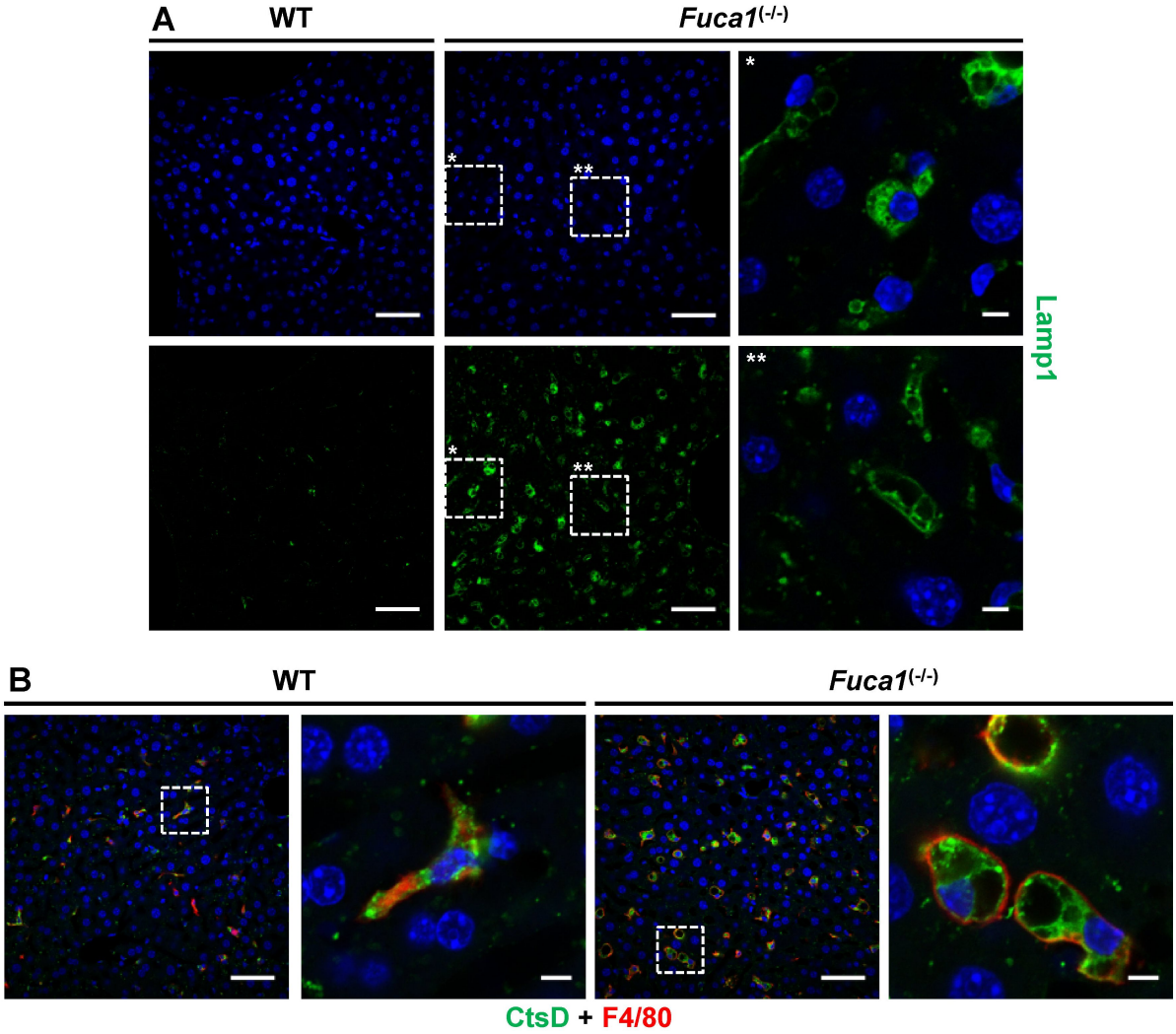

Figure 4.6: The endosomal-lysosomal compartment of the liver is enlarged in *Fuca1*$^{(-/-)}$ mice
(**A**) Semi-thin sections of the liver of 5-month-old wildtype and *Fuca1*$^{(-/-)}$ mice were stained with a Lamp1-specific antibody or (**B**) were co-staining using a cathepsin D-specific and an α-F4/80 antibody. Cell nuclei were stained with DAPI (blue). Bars correspondent to 50 μm (low magnification) or 5 μm (high magnification).

In the kidney of the *Fuca1*$^{(-/-)}$ mice, the renal cortex was moderately affected. Translucent storage vacuoles were found in the glomerular podocytes (figure 4.7 B, marked by arrows) and in the glomerular mesangium cells, while the proximal convoluted tubules contained storage material of moderate electron density (figure 4.7 C). The distal convoluted tubules as well as the intermediate tubules (Henle's loop), the distal straight tubules (thick ascending limp of Henle's loop) and the distal convoluted tubules were unaffected (data not shown). The collect-

ing ducts of the outer and inner medulla showed a severe storage phenotype, that worsened towards the inner medulla. The intercalated cells contained numerous foam-like vacuoles (figure 4.7 E) and particularly in the inner medulla, intercalated cells composed of a single giant storage vacuole were found (figure 4.7 E, inset). The principal cells appeared inconspicuous at the light microscopic level, but storage vacuoles containing moderate electron-dense material were detected by TEM (figure 4.7 F). Immunofluorescence stainings using a Lamp1-specific antibody revealed a moderately enlarged endosomal-lysosomal compartment in the renal cortex and medulla (figure 4.8). Highly vacuolated cells were found in the renal inner medulla of the *Fuca1*$^{(-/-)}$ kidney but not in the wildtype tissue. After comparison with light microscopic analysis, these cells were identified as intercalated cells of the renal collecting duct. Similarly to the light microscopic data, these cells contained mainly small foam-like vacuoles.

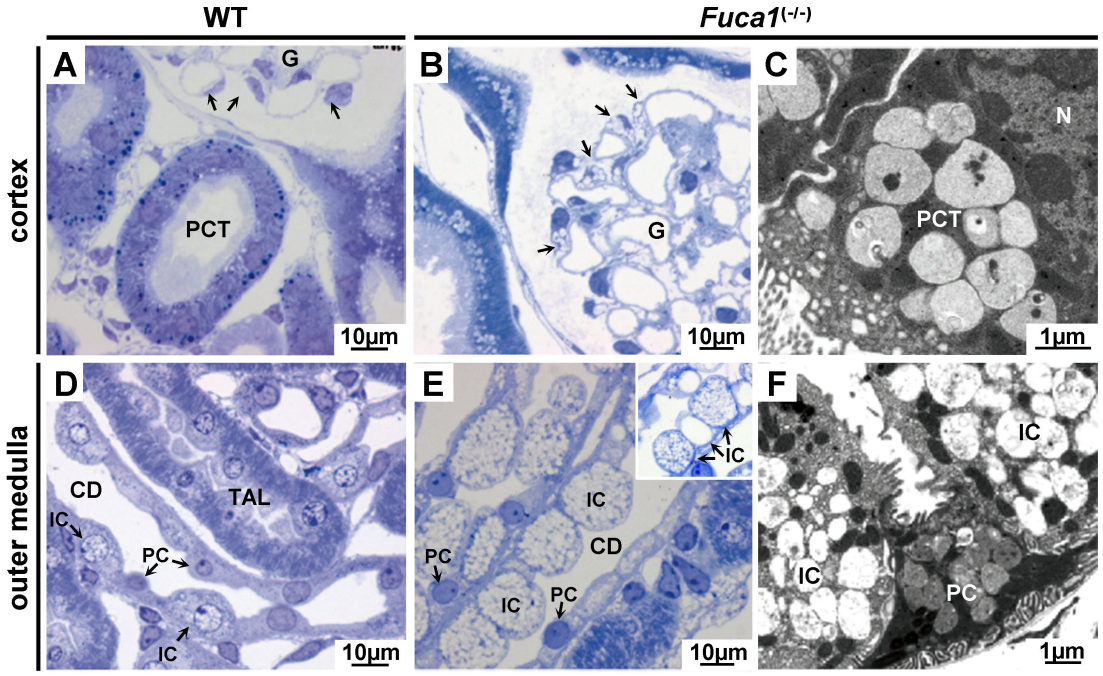

Figure 4.7: Storage pathology of the kidney
The kidney of 5-month-old wildtype and *Fuca1*$^{(-/-)}$ mice was analyzed by light (**A**, **B**, **D** and **E**) or transmission electron microscopy (TEM; **C** and **F**) in cooperation with Prof. Lüllmann-Rauch (University of Kiel, Germany). (**B**) In the *Fuca1*$^{(-/-)}$ cortex, storage vacuoles were found in podocytes (marked by arrows). (**C**) Using TEM, storage vacuoles were also detected in the proximal convoluted tubules (PCT). G: glomerulus, N: nucleus. In the outer medulla (**D**–**F**) the collecting ducts (CD) are composed of intercalated cells (IC) and principal cells (PC). (**E**) The *Fuca1*$^{(-/-)}$ ICs were vacuolated. (**E** inset) *Fuca1*$^{(-/-)}$ ICs of the inner medulla. (**F**) Using TEM, storage vacuoles were detected in the PCs. TAL: thick ascending limb of the Henle's loop.

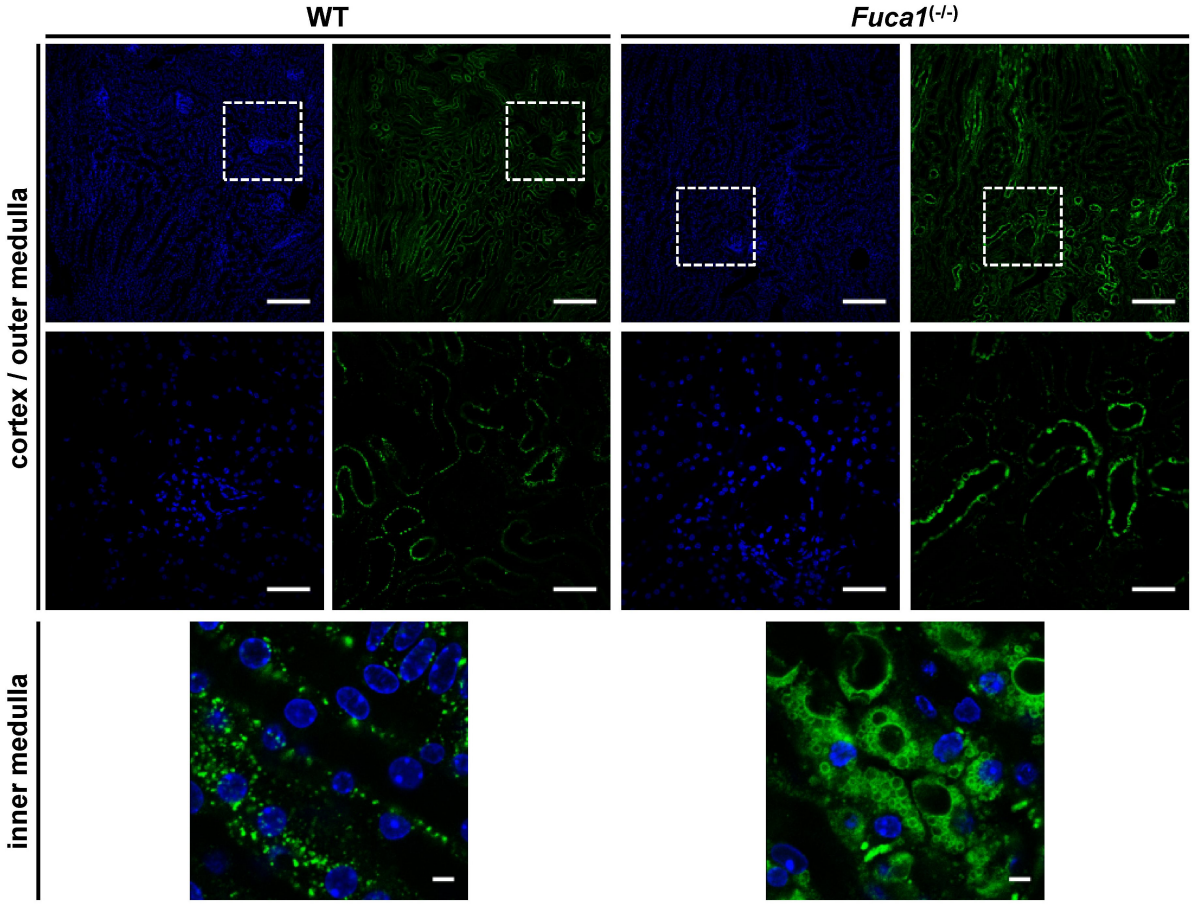

Figure 4.8: The endosomal-lysosomal compartment of the kidney is enlarged in *Fuca1*$^{(-/-)}$ mice
Semi-thin sections of the kidney of 5-month-old wildtype and *Fuca1*$^{(-/-)}$ mice were stained with a Lamp1-specific antibody. Cell nuclei were stained with DAPI (blue). Bars correspondent to 50 μm (low magnification) or 5 μm (high magnification).

In the *Fuca1*$^{(-/-)}$ spleen, a moderate storage phenotype and translucent storage vacuoles were found, which affected lymphocytes, reticulum cells, sinusoidal endothelial cells (figure 4.9 A) as well as trabecular fibroblasts (data not shown). A moderately enlarged endosomal-lysosomal compartment was also detected by immunofluorescence staining using a Lamp1-specific antibody (figure 4.9 B).

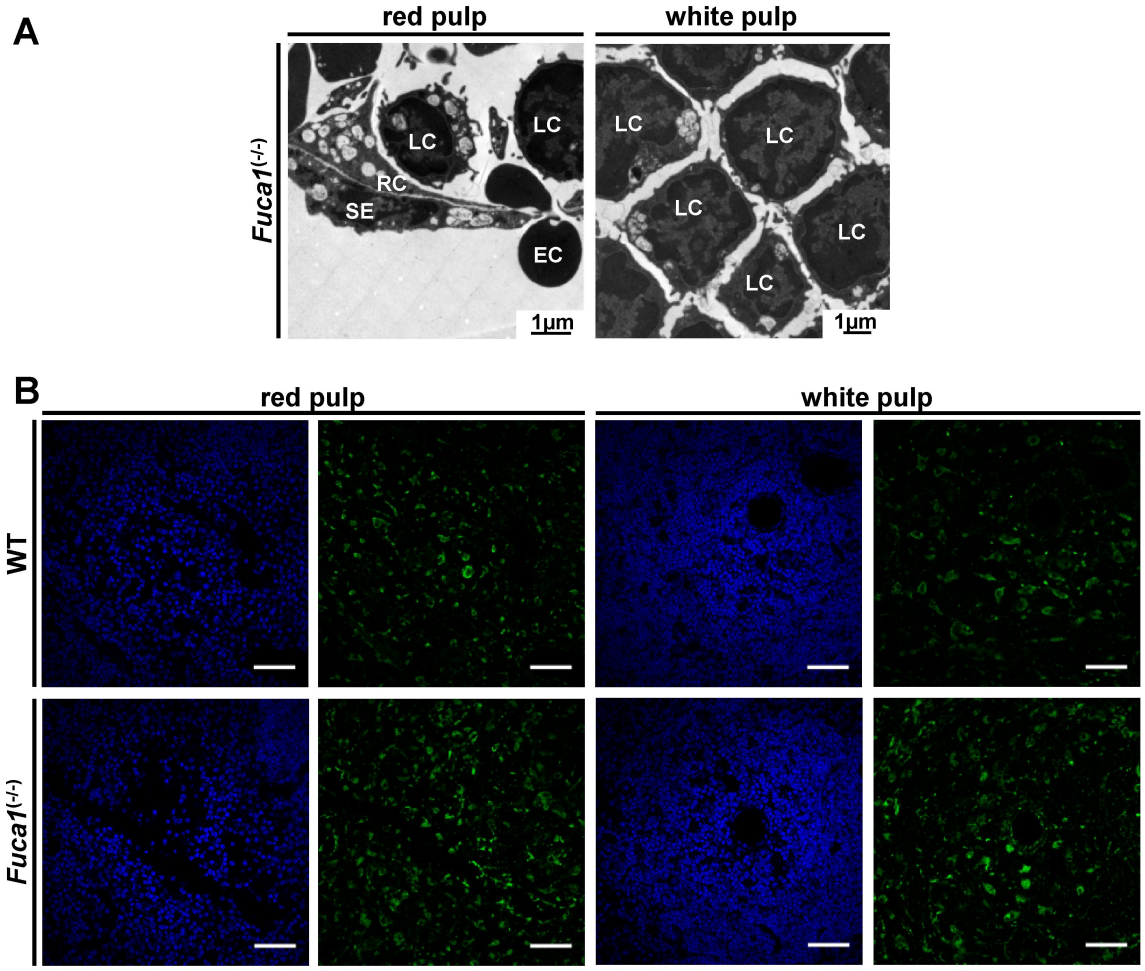

Figure 4.9: Storage pathology of the spleen
(**A**) The spleen of 5-month-old mice was analyzed by transmission electron microscopy (TEM) in cooperation with Prof. Lüllmann-Rauch (University of Kiel, Germany). The red pulp (left panel) and the white pulp (right panel) of a *Fuca1*$^{(-/-)}$ mouse are shown. LC: lymphocytes, RS: reticulum cells, SE: sinusoidal endothelial cells, EC: erythrocyte. (**B**) Semi-thin sections of the spleen of 5-month-old wildtype and *Fuca1*$^{(-/-)}$ mice were stained with an Lamp1-specific antibody. Cell nuclei were stained with DAPI (blue). Bars correspondent to 50 μm.

Besides liver, kidney and spleen, several other visceral organs were investigated regarding their storage pathology. The urinary bladder of *Fuca1*$^{(-/-)}$ mice was severely affected and particularly the superficial umbrellar cells were filled with numerous foam-like vacuoles (figure 4.10 B). Some large storage vacuoles containing heterogeneous material of moderate electron density were detected in the *Fuca1*$^{(-/-)}$ gall bladder (figure 4.10 D), whereas the acinus cells of the exocrine pancreas were less affected (data not shown).

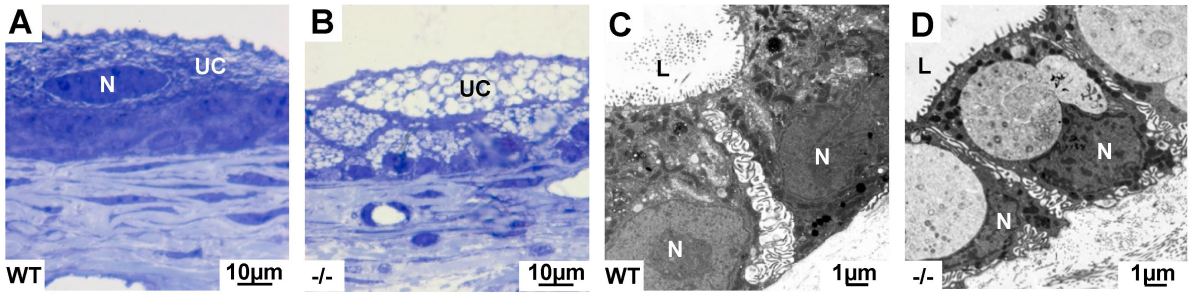

Figure 4.10: Storage pathology of the urinary bladder and gall bladder
The urinary bladder of 9-month-old wildtype and *Fuca1*$^{(-/-)}$ mice was analyzed by light microscopy (**A** and **B**). UC: umbrella cells. (**C** and **D**) The gall bladder of 5-month-old mice was analyzed by transmission electron microscopy (TEM). N: nucleus. Results were kindly provided by Prof. Lüllmann-Rauch (University of Kiel, Germany).

In summary, nearly all investigated visceral organs of *Fuca1*-deficient mice were affected from storage pathology, but the number, size as well as the nature of the accumulating material differed in a cell type-specific manner. Remarkably, some organs and cell types were unaffected from storage pathology, e. g. the renal intermediate tubules, bone cells, skeletal muscle and heart muscle.

4.1.7 Fucosylated glycoasparagines accumulate in fucosidosis

4.1.7.1 Analysis of storage material by TLC

The histological analysis of the fucosidosis mouse model revealed high amounts of storage vacuoles in many organs. In order to identify the accumulating material, neutral oligosaccharides were extracted from different tissues of wildtype and *Fuca1*$^{(-/-)}$ mice. Using thin-layer chromatography (TLC), high amounts of different glycocompounds were detected in the *Fuca1*$^{(-/-)}$ tissues (figure 4.11 A). As the TLC alone does not allow the identification of the storage material, TLC-separated material was scraped off the plates and further characterized by HPLC-MS/MS (performed by Dr. Beck, Odense University Hospital, Denmark). Material from single bands of the *Fuca1*$^{(-/-)}$ kidney and cerebrum as well as comparable TLC areas from wildtype tissues were analyzed. As expected, no glycoconjungates were detected in samples derived from wildtype tissues. However, the core-fucosylated glycoasparagine Asn-GlcNAc-Fuc (m/z 482.20 $[M+H]^+$) was identified in TLC material from *Fuca1*$^{(-/-)}$ tissues. In addition, the core-fucosylated asparaginyl-linked pentasaccharide Asn-GlcNAc-(Fuc)-GlcNAc-Man-Man (m/z 1009.39 $[M+H]^+$) was detected and another prominent band contained ma-

terial of m/z 1177.47, which would fit to a heptasaccharide composed of five hexoses, one *N*-acetyl-glucosamine and one fucose residue.

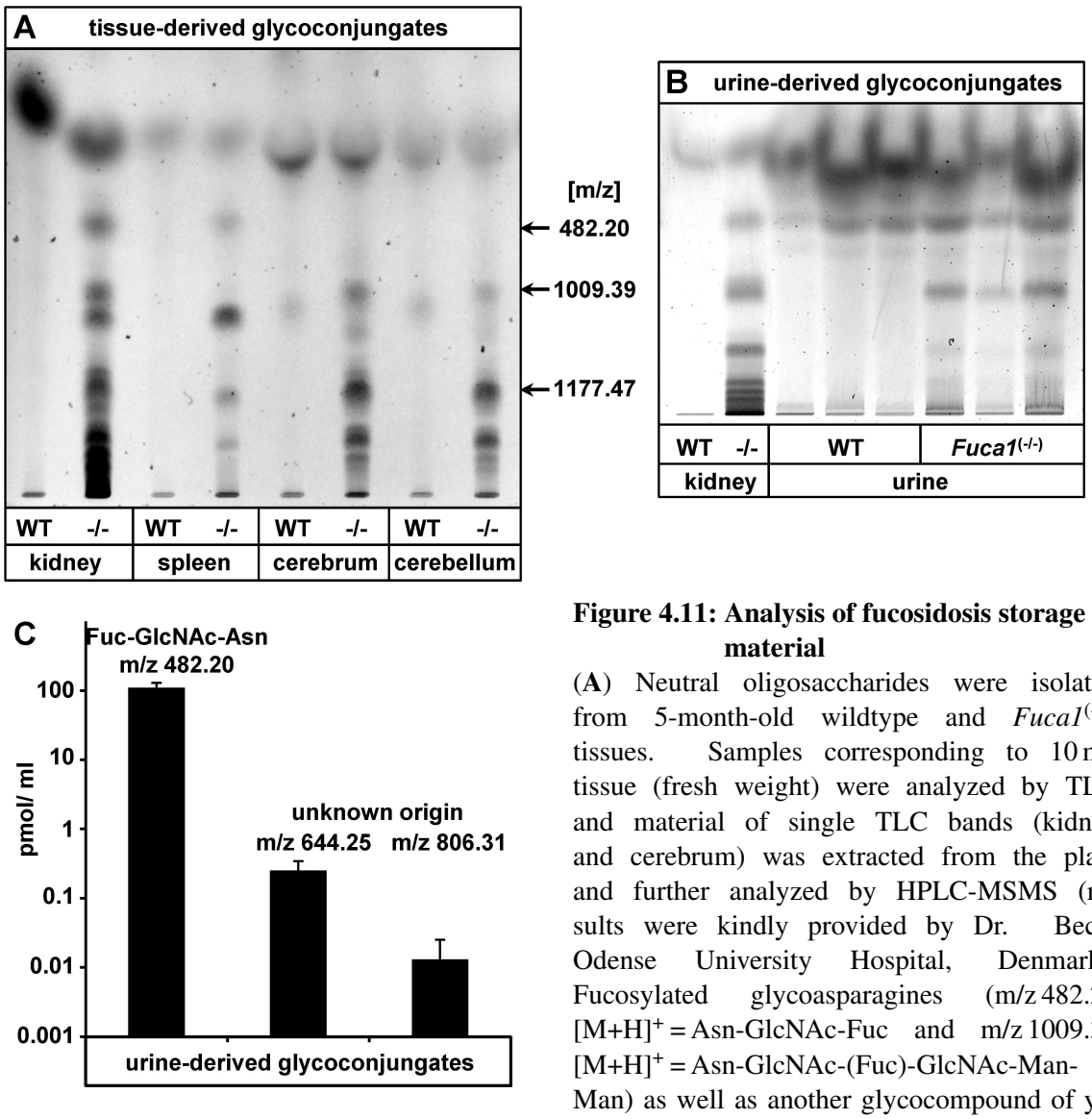

Figure 4.11: Analysis of fucosidosis storage material

(**A**) Neutral oligosaccharides were isolated from 5-month-old wildtype and *Fuca1*$^{(-/-)}$ tissues. Samples corresponding to 10 mg tissue (fresh weight) were analyzed by TLC and material of single TLC bands (kidney and cerebrum) was extracted from the plate and further analyzed by HPLC-MSMS (results were kindly provided by Dr. Beck, Odense University Hospital, Denmark). Fucosylated glycoasparagines (m/z 482.20 $[M+H]^+$ = Asn-GlcNAc-Fuc and m/z 1009.39 $[M+H]^+$ = Asn-GlcNAc-(Fuc)-GlcNAc-Man-Man) as well as another glycocompound of yet unknown origin were identified. (**B**) Spot urine of 5-month-old wildtype and *Fuca1*$^{(-/-)}$ mice was collected, desalted and 10 μl were directly analyzed by TLC. Neutral oligosaccharides isolated from kidney were loaded as control. (**C**) Spot urine of 9-month-old wildtype and *Fuca1*$^{(-/-)}$ mice was collected and directly analyzed by HPLC-MS. Results were kindly provided by Dr. Beck (Odense University Hospital, Denmark). The core-fucosylated glycoasparagine Asn-GlcNAc-Fuc as well as other glycocompounds of yet unknown origin were detected in *Fuca1*$^{(-/-)}$, but not in wildtype samples.

A clinical hallmark of fucosidosis is the excretion of storage material with the urine of human patients, where the core-fucosylated glycoasparagine Asn-GlcNAc-Fuc (Michalski and Klein 1999) was found as prominent glycocompound. Hence, spot urine from wildtype and *Fuca1*$^{(-/-)}$ mice was collected and analyzed by TLC. Several glycocompounds were exclusively found in the *Fuca1*$^{(-/-)}$ samples and exhibit comparable retention values to storage material of the *Fuca1*$^{(-/-)}$ kidney (figure 4.11 B). In order to identify these storage materials, spot urine was directly analyzed by HPLC-MS. As expected, the core-fucosylated glycoasparagine Asn-GlcNAc-Fuc was detected as the far most abundant glycocompound in the *Fuca1*$^{(-/-)}$ samples (figure 4.11 C) and was absent in the wildtype. Also other compounds of so far unknown origin (m/z 644.25 $[M+H]^+$ and m/z 806.30 $[M+H]^+$) were identified albeit to a much lesser extend. However, the masses of both compounds did not fit with masses of *N*-linked oligosaccharides of commonly known structures. These results indicate that a mixture of undigested fucosylated glycocompounds is accumulating in *Fuca1*$^{(-/-)}$ mice and that the storage material is also partially excreted with the urine.

4.1.7.2 Analysis of storage material using *Aleuria aurentia* lectin

In order to detect the fucosidosis storage material in tissue section of *Fuca1*$^{(-/-)}$ mice, the *Aleuria aurentia* lectin was used for immunofluorescence stainings. The lectin binds specifically to fucose residues linked α1-6 to *N*-acetylglucosamine, the so-called core structure of complex *N*-glycans.

In the liver, an *Aleuria aurentia*-specific staining of the sinusoid walls (most likely endothelial cells) was detected, whereas hepatocytes remained unstained (figure 4.12 A). A detailed analysis of the *Fuca1*$^{(-/-)}$ tissue revealed another cell type with a vacuolated micro-architecture that was not found in the wildtype liver (figure 4.12 A, marked by arrow). After comparison with light microscopic data (figure 4.5 B), these cells were identified as Kupffer cells. Remarkably, only the membranes of the storage vacuoles were stained, whereas their lumen remained unstained, which was explained by the water-soluble properties of the fucosylated storage material. It is very likely, that most of the stored glycocompounds were washed out during the staining procedure. Comparably, translucent storage vacuoles were already detected during light microscopic analysis (section 4.1.6).

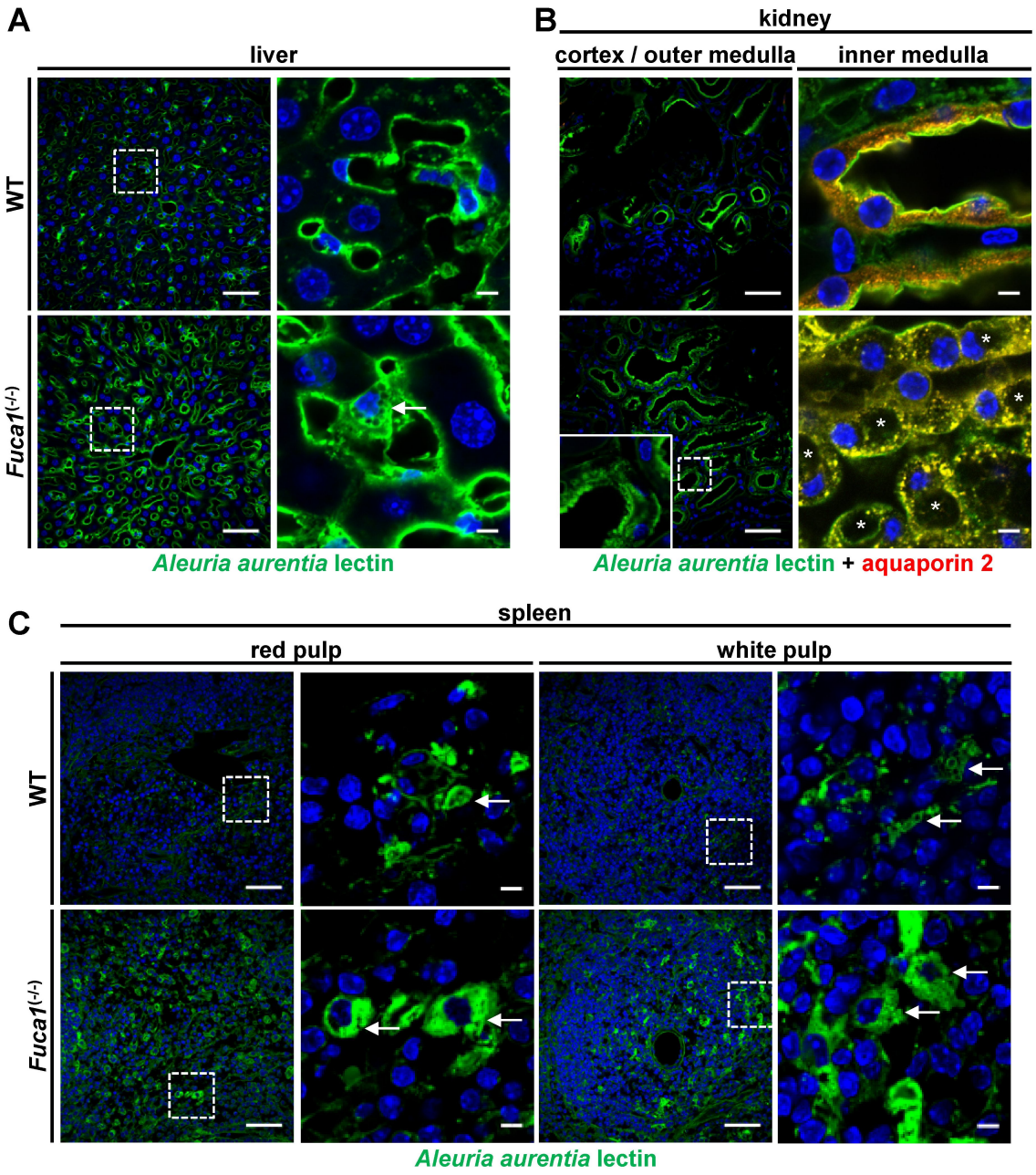

Figure 4.12: *Aleuria aurentia* lectin staining of visceral tissues
Semi-thin sections of liver (**A**), kidney (**B**) and spleen (**C**) of 5-month-old wildtype and *Fuca1*$^{(-/-)}$ mice were stained with *Aleuria aurentia* lectin. Bars correspondent to 50 μm (low magnification) or 5 μm (high magnification). Arrows indicate vacuolated cells. Stars indicate giant storage vacuoles in the renal collecting ducts.

In the spleen, *Aleuria aurentia* lectin stained single cells that were homogeneously distributed throughout the red and white pulp (figure 4.12 C). Detailed analysis revealed that most of these cells were vacuolated in both, wildtype and *Fuca1*$^{(-/-)}$ spleen (figure 4.12 C, marked by

arrows) and could represent macrophages. Again, only the membranes of the vacuoles were stained and the *Fuca1*$^{(-/-)}$ spleen exhibited a higher staining intensity.

In the renal cortex and outer medulla the apical cell pole of many tubules was stained in both genotypes by *Aleuria aurentia* lectin (figure 4.12 B). These structures might represent proximal tubules that exhibit a glycocalyx and a high amount of glycoproteins at their luminal site, whereas the intermediate as well as the distal tubules do not exhibit a glycocalyx. An aquaporin2-specific antibody was used as a marker for renal collecting ducts and a co-staining with the *Aleuria aurentia* lectin was shown. Severely vacuolated cells were found in the collecting ducts of the inner medulla of the *Fuca1*$^{(-/-)}$ kidney. It was already shown by light microscopic analysis that the intercalated cells of the renal collecting ducts are highly affected from storage and also giant storage vacuoles were found in some of these cells (figure 4.7 E). Similar structures were seen using the *Aleuria aurentia* lectin (figure 4.12 B, marked by stars). Remarkably, vacuolated cells were exclusively seen in the *Fuca1*$^{(-/-)}$ kidney but not in the wildtype tissue.

Aleuria aurentia lectin staining of the brain resulted in no obvious differences between *Fuca1*$^{(-/-)}$ and wildtype littermates. The lectin recognized predominately areas of grey matter, whereas the white matter remained unstained (appendix A.5).

4.1.8 Urine analysis and haematology

The histological findings of the kidney of *Fuca1*$^{(-/-)}$ mice are described in section 4.1.6. As high amounts of storage vacuoles were found in the glomerular podocytes as well as in different tubular segments, the functionality of the kidney was tested with regard to a potential proteinuria describing an excess of serum proteins in the urine. In healthy individuals, high molecular weight proteins (≥ 60 kDa) are retained by the renal glomeruli during blood filtration. If the blood-urine barrier, which is composed of podocytes, is not functional, these proteins are excreted with the urine. In contrast, low molecular weight proteins (≤ 60 kDa) are initially excreted with the urine and later reabsorbed by the renal tubuli. Thus, a damage of the tubuli would lead to an increase of low molecular weight proteins in the urine.

Spot urine of wildtype and *Fuca1*$^{(-/-)}$ mice was monitored in a reducing SDS-PAGE followed by silver staining (figure 4.13). Remarkably, neither high nor low molecular weight proteins were excessively excreted with the urine of *Fuca1*$^{(-/-)}$ mice indicating that the blood-urine

barrier as well as renal tubular segments were still functional, although they were severely affected by vacuolation.

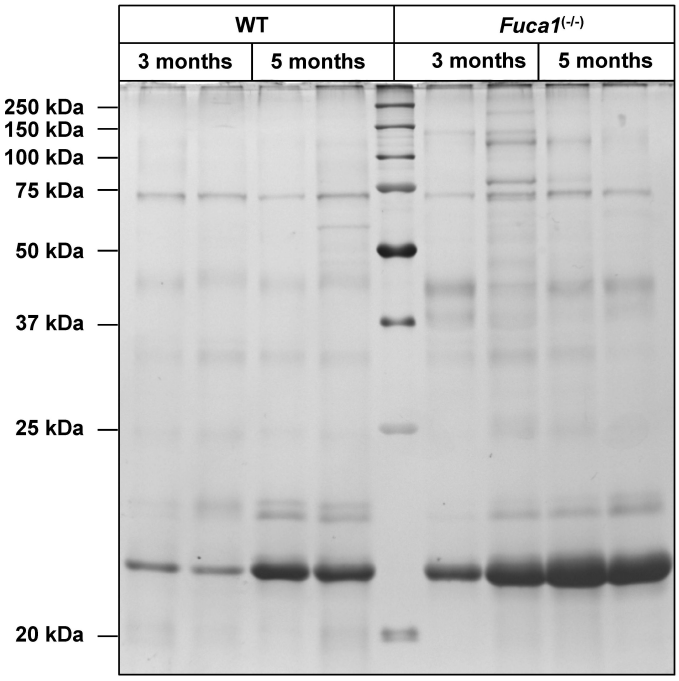

Figure 4.13: Analysis of urine samples
Spot urine from 3- and 5-month-old wildtype as well as *Fuca1*$^{(-/-)}$ mice was collected. The protein concentration was determined and 100 μg were loaded on a reducing SDS-PAGE. After gel electrophoresis the proteins were silver-stained.

Due to the histological findings in liver and kidney of the *Fuca1*$^{(-/-)}$ mice (section 4.1.6), serum parameters of 5-month-old animals were analyzed. Due to technical problems, most of the

Table 4.1: Serum parameters from wildtype and *Fuca1*$^{(-/-)}$ mice (WT: n = 7; *Fuca1*$^{(-/-)}$: n = 3), AST: aspartate aminotransferase, GGT: gamma-glutamyl transpeptidase

Parameter	Unit	Wildtype	*Fuca1*$^{(-/-)}$
Sodium	mmol / l	142.75 ± 2.49	139.67 ± 0.47
Calcium	mmol / l	2.12 ± 0.08	2.02 ± 0.03
Phosphate	mg / dl	6.04 ± 1.04	6.07 ± 0.38
Chloride	mmol / l	110.00 ± 2.12	104.67 ± 0.47
Urea	mg / dl	50.88 ± 5.58	52.33 ± 1.25
Creatinine	mg / dl	0.37 ± 0.03	0.35 ± 0.01
Albumin	mg / dl	1277.38 ± 104.89	1197.33 ± 29.94
AST	U / l	123.13 ± 35.00	167.67 ± 91.69
GGT	U / l	≤ 4	≤ 4

blood samples were slightly hemolytic, which prevented the analysis of the lactate dehydrogenase and the potassium values. Remarkably, no differences in the liver parameters were found between wildtype and *Fuca1*$^{(-/-)}$ mice (table 4.1). Also the kidney parameters including urea, creatinine and albumin values were inconspicuous. In contrast, the electrolytes (sodium, calcium and chloride) were significantly decreased in the *Fuca1*$^{(-/-)}$ mice, indicating functional disabilities in the renal collecting ducts caused by the accumulation of storage material. The collecting ducts are participating in electrolyte homeostasis, as they are responsible for urea reabsorption. An osmotic gradient is formed that triggers the reabsorption of electrolytes into the Henle's loop. Due to the immense accumulation of storage material observed in the collecting ducts, the formation of the osmotic gradient might be insufficient. As a consequence, the reabsorption of the electrolytes might be inhibited, which would lead to a decreased concentration of electrolytes in the blood.

In addition, blood cell parameters were analyzed from wildtype and *Fuca1*$^{(-/-)}$ mice at 5 months of age (table 4.2). The number of erythocytes was found to be slightly reduced in *Fuca1*$^{(-/-)}$ mice, indicating a milder form of a renal anemia. All other parameters were unaffected by the *Fuca1* gene knock-out.

Table 4.2: Blood parameters from wildtype and *Fuca1*$^{(-/-)}$ mice (WT: n = 8; *Fuca1*$^{(-/-)}$: n = 4)

Parameter	Unit	Wildtype	*Fuca1*$^{(-/-)}$
Erythocytes	M / μl	8.10 ± 0.16	7.34 ± 0.15
Hemoglobin	g / dl	12.25 ± 0.47	11.20 ± 0.45
Hematocrit	%	34.83 ± 1.05	31.92 ± 1.28
MCV	fl	48.93 ± 1.27	48.38 ± 1.60
MCH	pg	17.20 ± 0.51	16.94 ± 0.58
MCHC	g / dl	39.92 ± 0.63	38.92 ± 0.50
RDW	%	13.49 ± 0.31	12.79 ± 0.48
Thrombocytes	K / μl	629.24 ± 270.80	682.30 ± 56.46
Thrombocrit	%	0.23 ± 0.06	0.24 ± 0.02

4.1.9 Neuropathology

4.1.9.1 Storage pathology of the CNS

Pathological alteration of the brain is the leading symptom of human fucosidosis and similar findings were expected in the *Fuca1*$^{(-/-)}$ mice. The CNS was extensively studied by light and electron microscopy in cooperation with Prof. Lüllmann-Rauch (University of Kiel, Germany) and storage vacuoles were found in all analyzed regions of the *Fuca1*$^{(-/-)}$ brain. Neuronal perikarya of the hippocampus (figure 4.14 B) and cerebral cortex (figure 4.14 D) were severely affected and filled with cytoplasmic translucent vacuoles. Moreover, high amounts of axon spheroids were identified in the hippocampus (figure 4.14 B (marked by arrows) and C) and to a lesser extend also in the cerebellum (data not shown). Ultrastructural analysis detected disorientated neurotubules, neurofilaments and heterogeneous material in the axoplasm of the spheroids. In the cerebellum, large storage vacuoles containing floccular material of moderate electron-density were found in Purkinje cells of *Fuca1*$^{(-/-)}$ mice, whereas Bergmann-glia cells were filled with numerous small empty vacuoles (figure 4.14 E). The granular cells were also affected from storage, even through to a much lesser extend (data not shown).

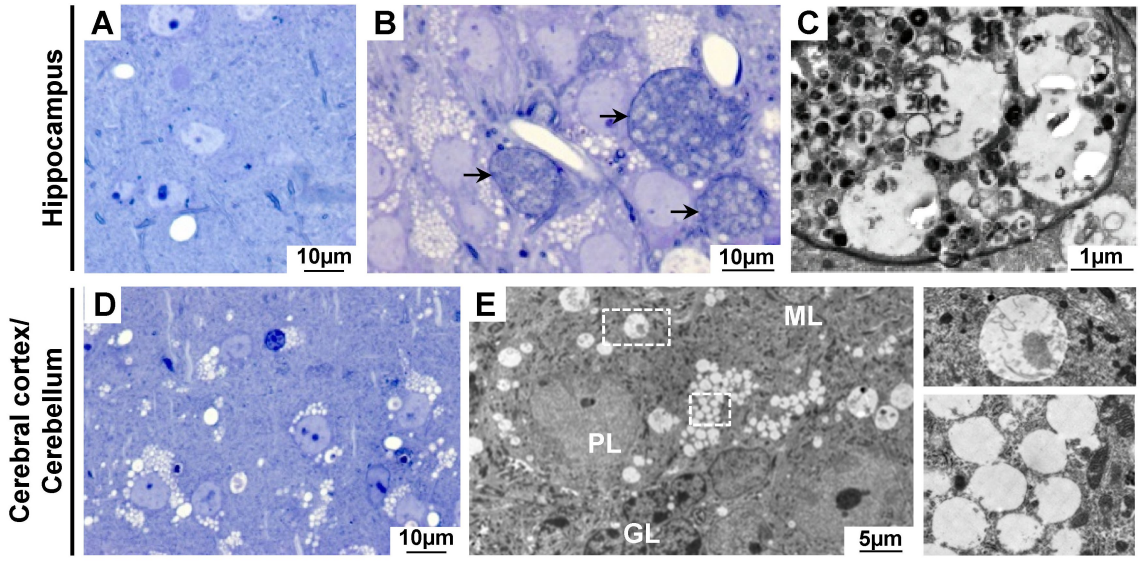

Figure 4.14: Storage pathology of the CNS
The brains of wildtype and *Fuca1*$^{(-/-)}$ mice were analyzed by light (**A**, **B** and **D**) or transmission electron microscopy (TEM; **C** and **E**) in cooperation with Prof. Lüllmann-Rauch (University of Kiel, Germany). (**A** – **C**) Hippocampus (CA3 region) from 9-month-old mice. (**A**) wildtype. (**B**) Neuronal perikarya from *Fuca1*$^{(-/-)}$ mice contained storage vacuoles. Abnormal axon spheroids are marked by arrows. (**C**) Higher magnification of an axon spheroid. (**D**) Cerebral cortex of the same mouse as in (B). Storage vacuoles were found in the neuronal perikarya. (**E**) Cerebellum of a 3.5-month-old *Fuca1*$^{(-/-)}$ mice. Purkinje cells contained large vacuoles filled with some floccular material, whereas Bergmann glia cells contained numerous small empty vacuoles. ML: molecular layer; PL: Purkinje cell layer; GL: granular layer.

An increase in Lamp1 protein (lysosome-associated membrane protein 1) is commonly used as marker for LSDs (Meikle et al. 1997) and was already shown by immunoblotting in the cerebrum of the *Fuca1*$^{(-/-)}$ mice (section 4.1.4). Using immunostainings, a massive increase in Lamp1 protein was confirmed in the *Fuca1*$^{(-/-)}$ brain (figure 4.15 A) indicating an enlarged endosomal-lysosomal compartment in the hippocampus, cerebral cortex and cerebel-

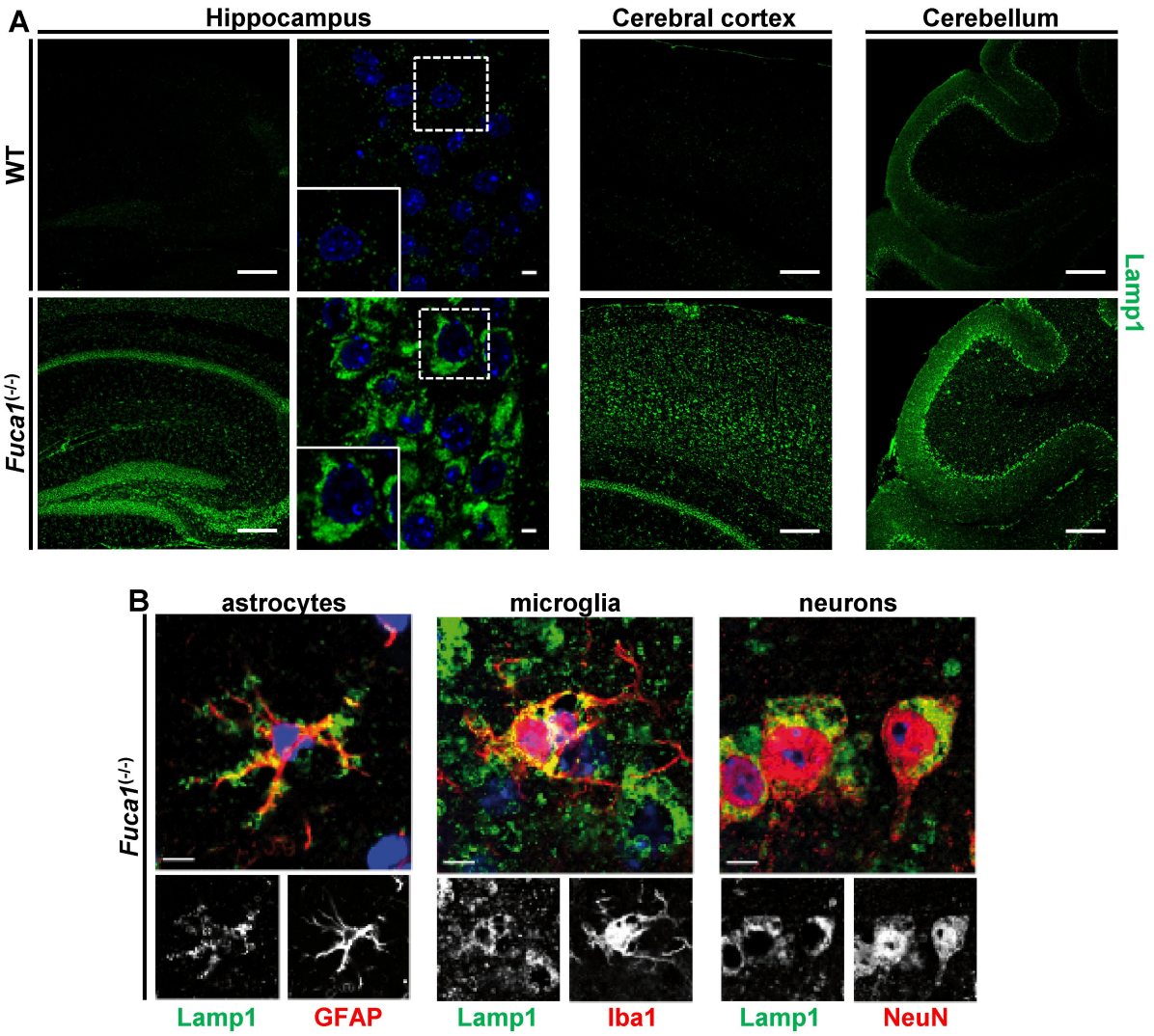

Figure 4.15: The endosomal-lysosomal compartment of the brain is enlarged in *Fuca1*$^{(-/-)}$ mice
(**A**) Semi-thin sections of the brain of 3.5-month-old wildtype and *Fuca1*$^{(-/-)}$ mice were stained with a Lamp1-specific antibody. The hippocampus, cerebral cortex and cerebellum is shown. Bars correspondent to 200 μm or 5 μm (magnification of the hippocampus). (**B**) Co-staining of Lamp1-positive cells with different cell type-specific markers (GFAP for astrocytes, Iba1 for microglia and NeuN for neurons). Cell nuclei were stained with DAPI (blue). Bars correspondent to 5 μm. Co-stainings using Iba1 and NeuN were performed by Dr. Damme (University of Kiel, Germany).

lum. Co-stainings of Lamp1-positive cells with different cell type-specific markers for astrocytes (GFAP), microglia (Iba1) and neurons (NeuN) revealed that all tested cell types of the CNS were affected from storage (figure 4.15 B).

4.1.9.2 Secondary storage material accumulate in the *Fuca1*$^{(-/-)}$ brain

Secondary storage pathology of lipids is a common feature of many LSDs and contribute to the complex pathological cascade underlying these diseases as unesterified cholesterol, gangliosides and autofluorescent material were detected in several mucopolysaccharidoses and in α-mannosidosis (Walkley 2004, Walkley et al. 2010, Damme et al. 2011, Kowalewski et al. 2015). So far, secondary storage pathology was not investigated in detail in human fucosidosis patients and the fucosidosis dog model.

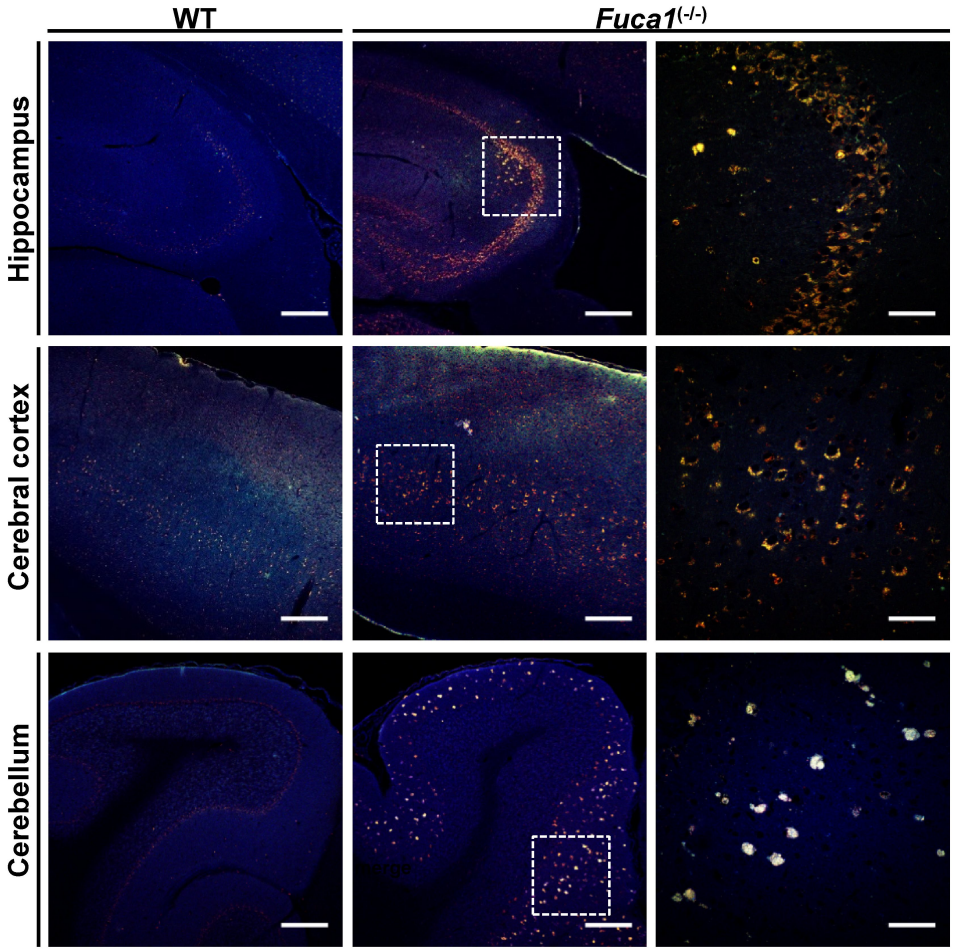

Figure 4.16: Autofluorescent material accumulate in the *Fuca1*$^{(-/-)}$ brain
Unstained, semi-thin brain sections of 11-month-old animals were analyzed at different wavelengths (410 nm, 488 nm, 594 nm). Bars correspondent to 200 μm (left and middle) and 50 μm (right).

The accumulation of autofluorescent material in *Fuca1*$^{(-/-)}$ mice was investigated by analyzing unstained semi-thin section of the brain at different wavelengths, revealing autofluorescent compounds in cellular structures exclusively in the brain of *Fuca1*$^{(-/-)}$ mice (figure 4.16). Here, the hippocampus, cerebral cortex and the cerebellum, particularly the molecular layer was affected. The accumulation of autofluorescent material was observed only in late stages of the disease in 11-month-old *Fuca1*$^{(-/-)}$ mice, while it was absent in younger animals (data not shown). Although autofluorescent material often accumulates in aging brains, a pathological storage was shown, as the autofluorescent material was absent in brain sections of wildtype mice at the same age.

In order to further analyze the autofluorescent material, semi-thin sections were stained with Sudan Black B, which is a fat-soluble diazo dye and stains lipid-rich structures. It is often used for detection of lipofuscin, which is known to be composed of oxidized lipids, proteins and metal ions. The Sudan Black B staining resulted in a general staining of the cerebellar white matter, but also a moderate staining of macrophage-like structures was detected in the molecular layer of the cerebellum of *Fuca1*$^{(-/-)}$ mice but not of wildtype animals at 11 months of age (figure 4.17). The staining pattern was comparable with the distribution of autofluorescent material, indicating that these storage compounds might be composed lipofuscin. Of

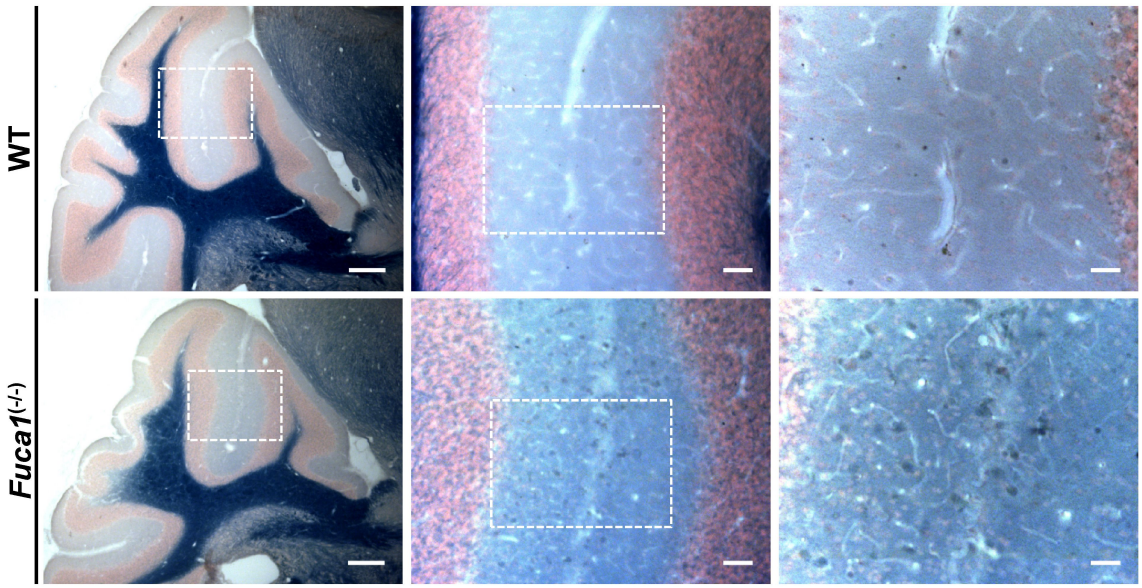

Figure 4.17: Accumulation of Sudan Black B-positive material in the *Fuca1*$^{(-/-)}$ brain
Semi-thin brain sections of 11-month-old animals were stained with Sudan Black B and Nuclear Fast Red (counterstaining). Bars correspondent to 250 μm (lowest magnification), 50 μm (medium magnification) or 25 μm (highest magnification).

note, the accumulation of lipofuscin was only seen in late stages of the disease and was absent in younger *Fuca1*$^{(-/-)}$ mice (e. g. 3 and 5 months of age; data not shown).

The *Fuca1*$^{(-/-)}$ mice were further analyzed with regard to accumulation of gangliosides as secondary storage material. Semi-thin brain section were stained with an GM2-specific antibody and GM2-gangliosides were detected in small, vesicle-like structures in the hippocampus, cerebral cortex and molecular layer of the cerebellum of 3-month-old *Fuca1*$^{(-/-)}$ mice (figure 4.18). Interestingly, this GM2-staining pattern was nearly completely absent in 11-month-old animals (data not shown), indicating a progressive loss of that particular storage material.

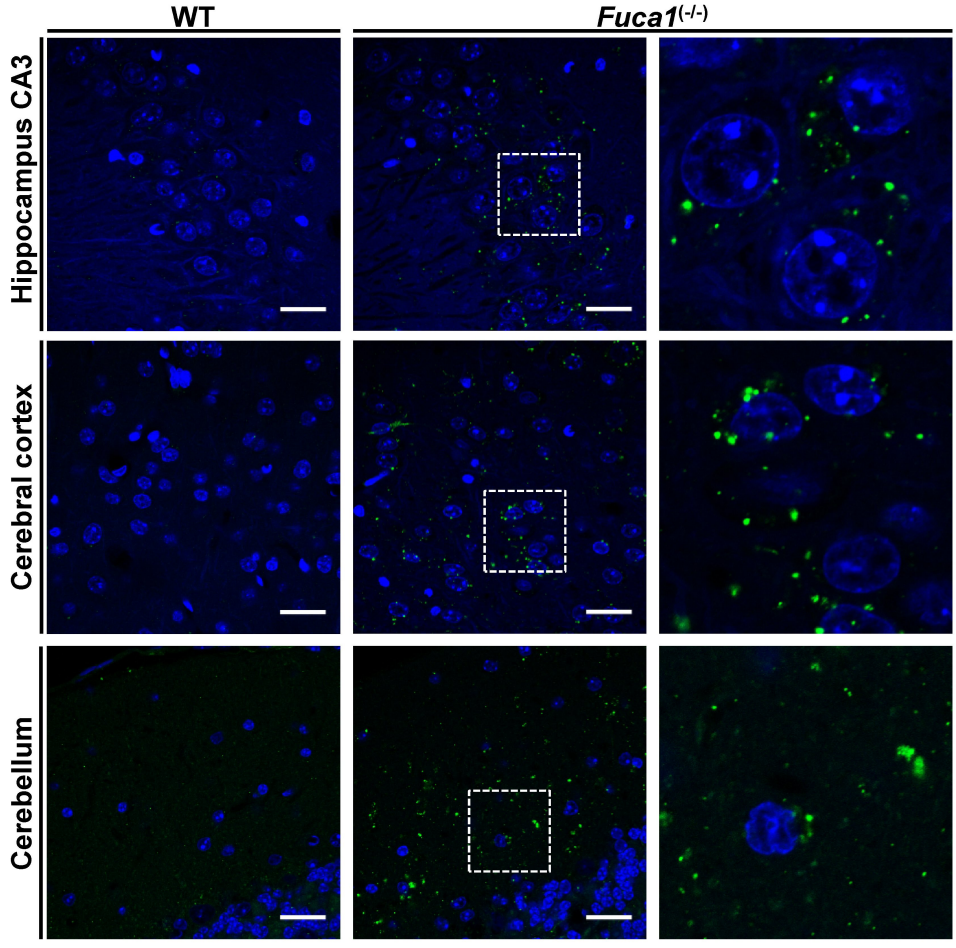

Figure 4.18: GM2-ganglioside accumulate in the brain of *Fuca1*$^{(-/-)}$ mice
Immunofluorescence staining on semi-thin brain sections from 3-month-old animals using a GM2-ganglioside-specific antibody. In the cerebellum, the molecular layer is shown. Cell nuclei were stained with DAPI (blue). Bars correspondent to 25 μm.

Filipin is a fluorescent dye that is excitated in the UV-spectrum and binds specifically to unesterified cholesterol. Brain sections of wildtype and *Fuca1*$^{(-/-)}$ mice at 3 and 11 months of age were analzyed by filipin staining and large deposits of unesterified cholesterol were exclusively detected in the cerebellum of *Fuca1*$^{(-/-)}$ animals, where the staining pattern was restricted to the molecular layer (figure 4.19). Of note, the filipin staining in 11-month-old animals did only partially co-localize with the autofluorescent material.

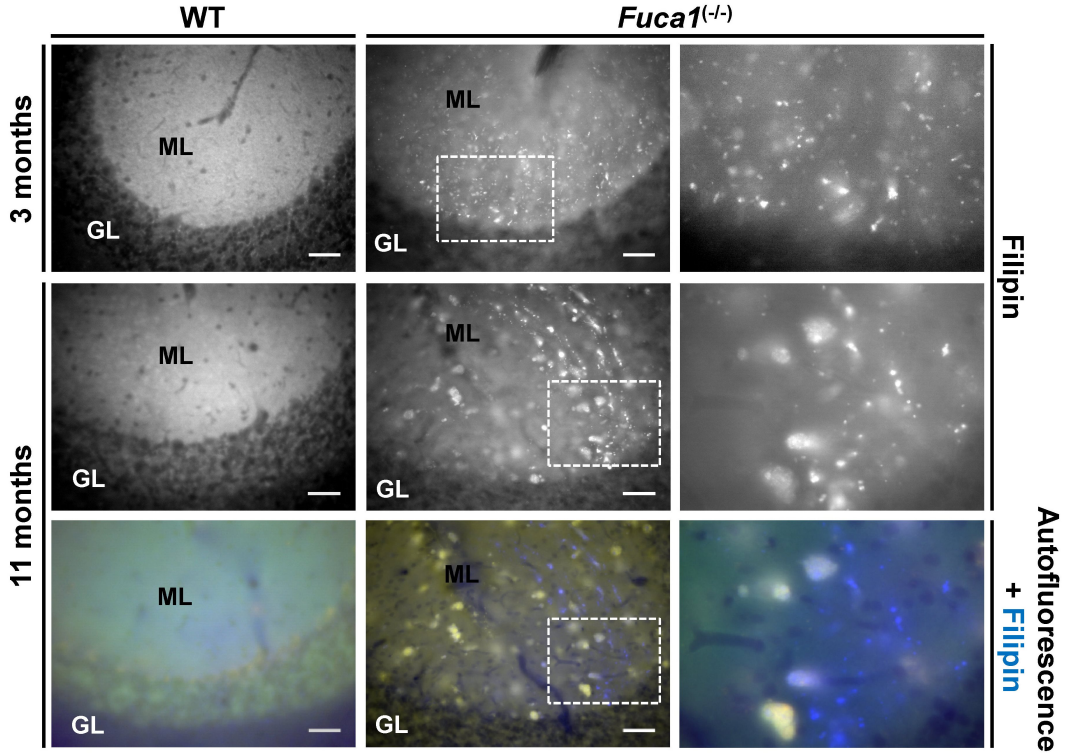

Figure 4.19: Unesterified cholesterol accumulate in the cerebellum of *Fuca1*$^{(-/-)}$ mice
Accumulation of unesterified cholesterol was found by filipin staining of semi-thin brain sections in the cerebellum particularly in the molecular layer of 3- and 11-month-old *Fuca1*$^{(-/-)}$ (upper and middle panel). Lower panel: Filipin staining (blue) partially co-localize with autofluorescent material (green and red) in 11-month-old *Fuca1*$^{(-/-)}$ animals. Bars correspondent to 50 μm.

Accumulation of lipid-rich secondary storage material was monitored also by TLC in 3-, 5- and 10.5-month-old animals. However, no obvious differences between the genotypes were observed (appendix A.6), indicating that TLC was not sensitive enough to detect e. g. the accumulation of cholesterol, GM2-gangliosides or other lipids in *Fuca1*$^{(-/-)}$ mice.

4.1.9.3 *Fuca1* gene knock-out leads to neuronal loss

Many lysosomal storage diseases that exhibit a neuropathological phenotype are characterized by a progressive loss of neuronal cells (Platt et al. 2012). Although neuropathological alterations are the main symptom in human fucosidosis, only little information is available

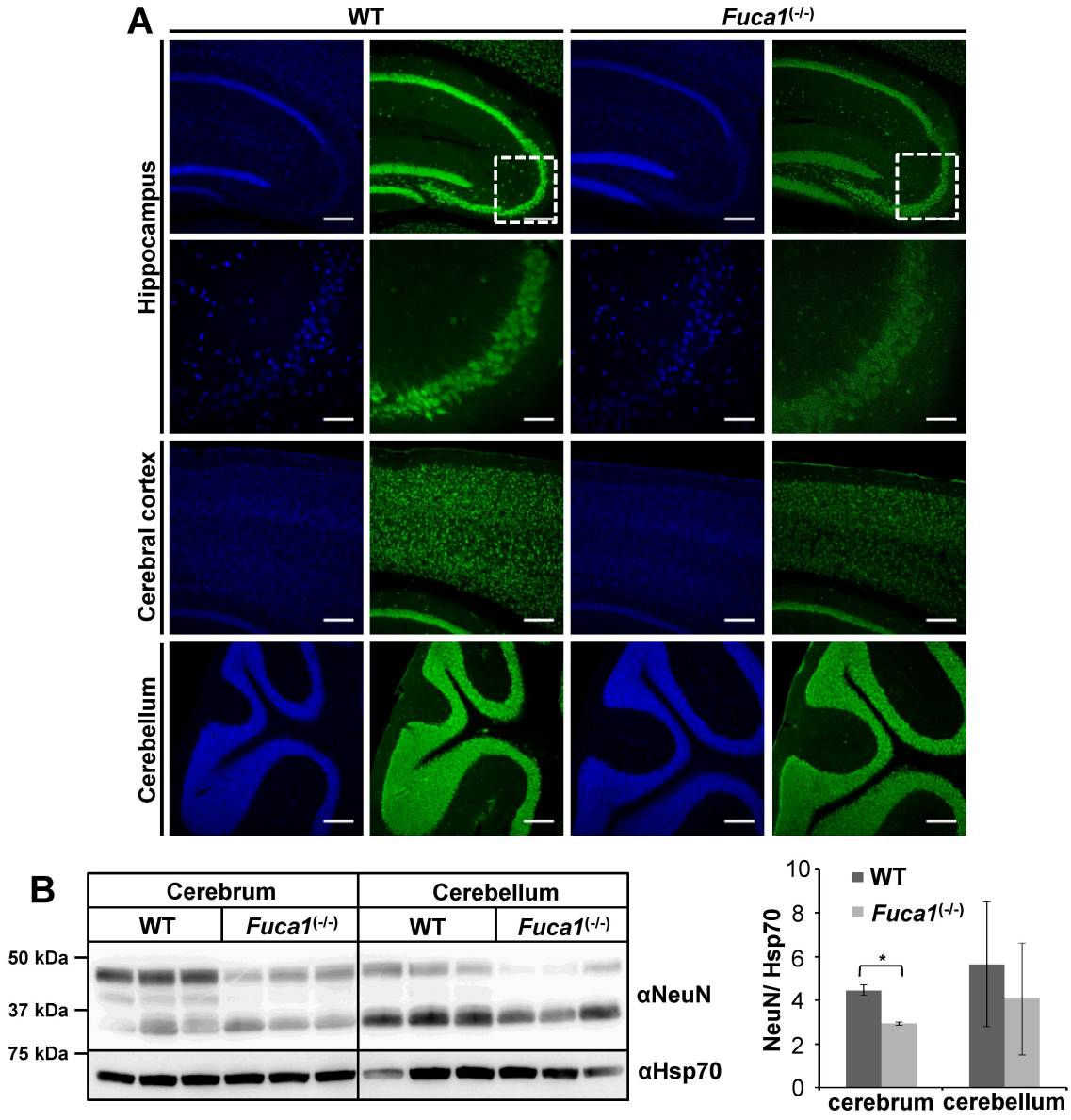

Figure 4.20: Neuronal loss in the *Fuca1*$^{(-/-)}$ cerebrum
(**A**) Immunofluorescence stainings on semi-thin sections of 5-month-old wildtype and *Fuca1*$^{(-/-)}$ mice for the neuron-specific cell marker NeuN. Cell nuclei were stained with DAPI (blue). Bars correspondent to 200 μm and 50 μm (magnification of hippocampus). (**B**) Cerebral and cerebellar tissue homogenates of 5-month-old animals were analyzed by immunoblotting using a NeuN-specific antibody. Hsp70 was used for normalization. *$p < 0.05$

regarding neuronal cell death. As numerous storage vacuoles have been found in neuronal perikarya of the hippocampus and cerebral cortex (figure 4.14 B and D), these cells were evaluated in more detail by immunofluorescence stainings of the neuron-specific cell marker NeuN. A slightly decreased staining intensity of NeuN-positive cells in the hippocampus and cerebral cortex of *Fuca1*$^{(-/-)}$ mice was detected, while the cerebellum was unaffected (figure 4.20 A). This result was confirmed by immunoblotting showing a significant decrease in NeuN-protein in the cerebrum but not in the cerebellum of *Fuca1*$^{(-/-)}$ mice (figure 4.20 B).

Durand et al. (1969) described a loss of Purkinje cells in a brain biopsy of a severely affected fucosidosis patients. In the *Fuca1*$^{(-/-)}$ mice, these cells were also affected and contained several storage vacuoles (figure 4.14 E). Further analyses were performed by immunofluorescence stainings of the Purkinje cell-specific marker calbindin in cerebellar sections of mice of different ages (figure 4.21). At 3.5 months of age the layer of Purkinje cell perikarya as well as their dendritic trees in the molecular layer of the cerebellum were comparable between the genotypes. In contrast, at 7.5 months of age the Purkinje cells were already severely diminished in *Fuca1*$^{(-/-)}$ mice, and at 11 months of age they were nearly completely lost as reflected by the

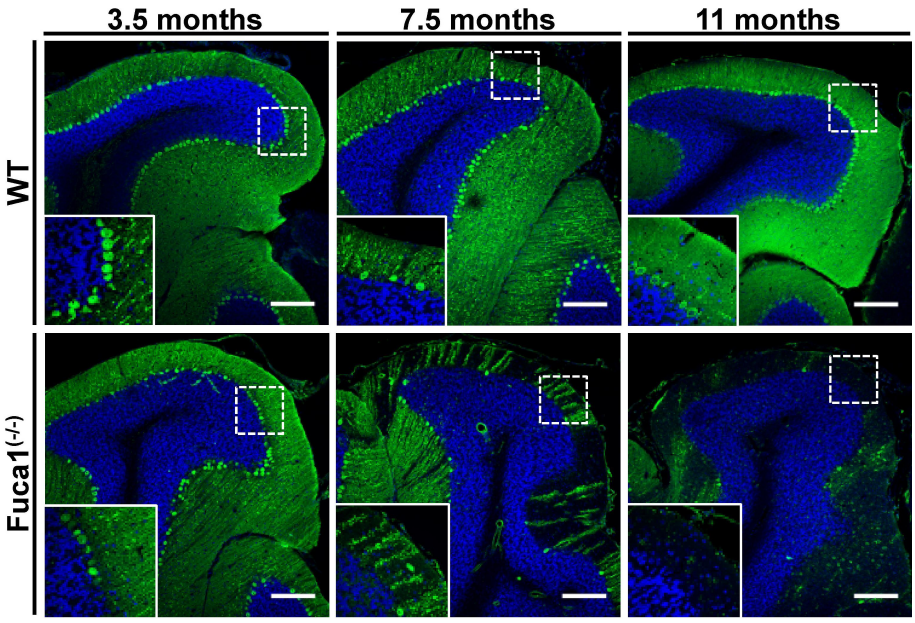

Figure 4.21: Loss of Purkinje cells in *Fuca1*$^{(-/-)}$ mice
Immunofluorescence stainings on semi-thin sections of wildtype and *Fuca1*$^{(-/-)}$ mice at 3.5, 7.5 and 11 months of age for the Purkinje cell-specific marker calbindin. Cell nuclei were stained with DAPI (blue). Bars correspondent to 200 μm.

absence of Purkinje cell perikarya as well as dentritic trees. The residual immunofluorescence staining in the cerebellar sections of 11-month-old *Fuca1*$^{(-/-)}$ mice was most likely due to autofluorescent material (compare with figure 4.16).

4.1.9.4 *Fuca1*$^{(-/-)}$ mice exhibit neuroinflammation

Loss of neurons is often accompanied by neuroinflammation and is commonly observed in LSDs (Vitner et al. 2010). The inflammatory processes are due to an activation of astrocytes and microglia in response to neuronal cell death. However, only limited data are available from human fucosidsosis patients. In order to analyze whether the fucosidosis mouse model exhibits neuroinflammation, the expression of the astrocyte-specific marker GFAP (glial fibrillary acidic protein) was determined by Real-Time PCR analysis on whole brain cDNA and was found to be 6.5-fold increased in *Fuca1*$^{(-/-)}$ brains (figure 4.22 A). Western blot analysis detected an increase in GFAP protein by 8.5-fold in the *Fuca1*$^{(-/-)}$ cerebrum and by nearly six fold in the cerebellum (figure 4.22 B and C). High numbers of GFAP-positive cells were confirmed by immunofluorescence analysis especially in the cerebral cortex and in the CA3-region of the hippocampus. An increase in GFAP-positive cells was also shown in the cerebellum. This effect, however, was closely restricted to the Purkinje cell layer (figure 4.22 D). CD68 and Iba1 (ionized calcium-binding adapter molecule 1) were used as specific markers for macrophages and microglia and a nearly 17-fold and three-fold increased mRNA expression was detected by Real-Time PCR on whole brain cDNA, respectively (figure 4.22 A). At the protein level, immunofluorescence analysis clearly confirmed a massive increase in CD68-positive cells in all regions of the brain (figure 4.22 E). Furthermore, the expression of the inflammatory marker Ccl-3 (macrophage inflammatory protein 1a) was analyzed by Real-Time PCR on whole brain cDNA and was shown to be massively increased in the *Fuca1*$^{(-/-)}$ brain. Here, an exact quantification was not possible, as the abundance of Ccl-3 transcript in the wildtype tissue was at background level and could not be properly determined (data not shown). In summary, these results clearly show that the *Fuca1*$^{(-/-)}$ mice exhibit astro- and microgliosis.

4.1.9.5 Myelination is unaffected by the *Fuca1* gene knock-out

Myelination defects are commonly described in human fucosidosis as well as in the fucosidosis dog model. In order to evaluate the myelination state in the *Fuca1*$^{(-/-)}$ mice, the

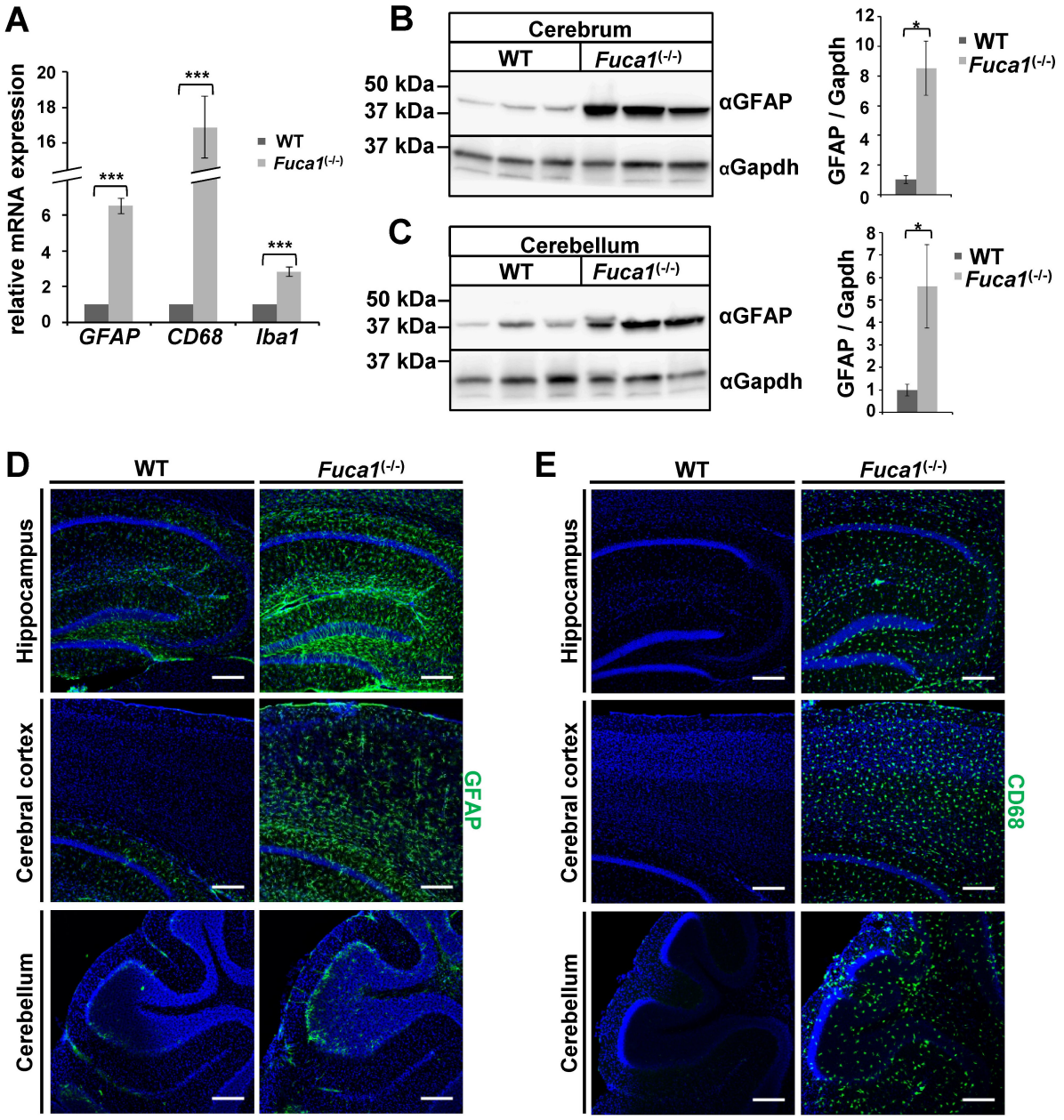

Figure 4.22: Micro- and astrogliosis in *Fuca1*$^{(-/-)}$ mice
(**A**) The expression of markers for astrogliosis (GFAP) and microgliosis (CD68 and Iba1) were analyzed by Real-Time PCR analysis on whole brain cDNA from 5-month-old wildtype and *Fuca1*$^{(-/-)}$ mice. Cerebral (**B**) and cerebellar tissue homogenates (**C**) of 5-month-old animals were analyzed by immunoblotting using a GFAP-specific antibody. Gapdh was used for normalization. ***$p < 0.0005$, *$p < 0.05$. Immunofluorescence stainings on semi-thin sections of 3.5-month-old wildtype and *Fuca1*$^{(-/-)}$ mice using a GFAP- (**D**) and CD68-specific antibody (**E**). The hippocampus, cerebral cortex and cerebellum is shown. Cell nuclei were stained with DAPI (blue). Bars correspondent to 200 μm.

expression of the myelin markers MBP (myelin basic protein) and Plp1 (proteolipid protein 1) were analyzed by Real-Time PCR on whole brain cDNA (figure 4.23 A). The mRNA level of Plp1 was unaffected by the *Fuca1* gene knock-out, whereas a slight but significant increase in MBP transcript (1.3 fold) was detected. However, no alterations in MBP expression could be detected at the protein level neither by immunoblotting of cerebral and cerebellar tissue homogenates (figure 4.23 B and C) nor by immunofluorescence stainings on brain sections (figure 4.23 D), suggesting an increase in MBP protein turnover that does not affect the steady-state protein level.

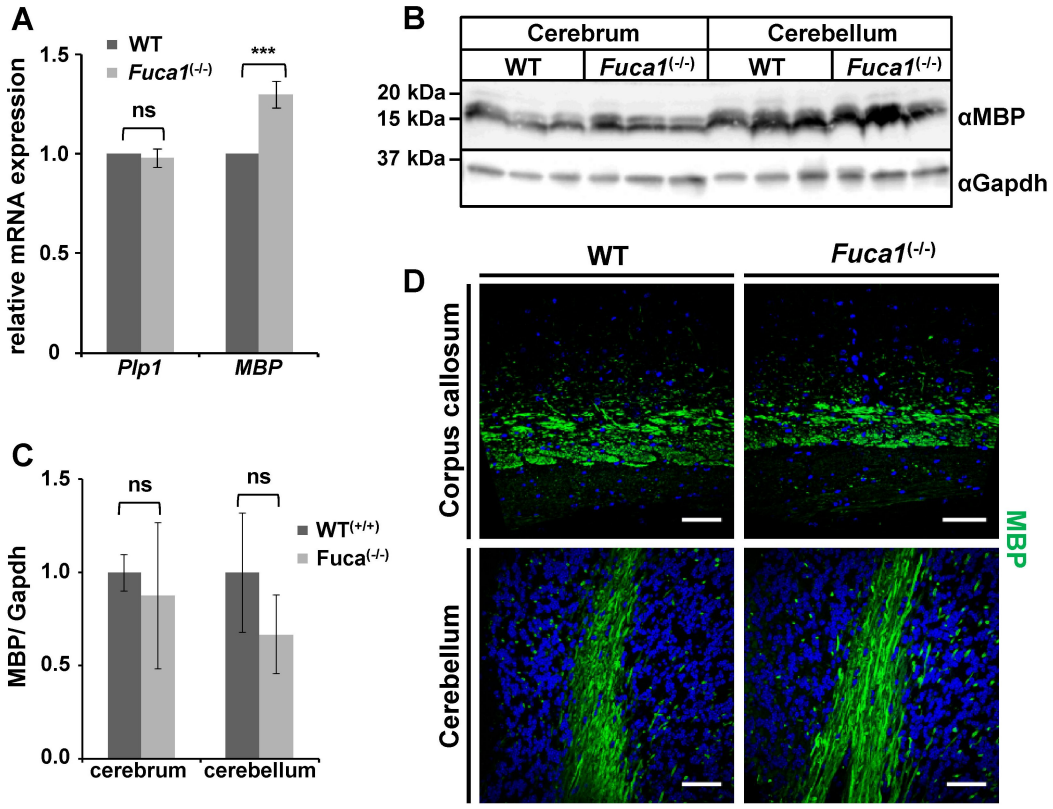

Figure 4.23: Myelination is not affected in *Fuca1*$^{(-/-)}$ mice
(**A**) The expression of the myelination markers *Plp1* and *MBP* were analyzed by Real-time PCR on whole brain cDNA of 5-month-old wildtype and *Fuca1*$^{(-/-)}$ mice. (**B** and **C**) Immunoblotting of cerebral and cerebellar tissue homogenates from 5-month-old mice using a MBP-specific antibody. Gapdh was used for normalization. ***$p < 0.0005$; ns = not significant. (**D**) Immunofluorescence staining on semi-thin sections of 3.5-month-old animals using an MBP-specific antibody. The corpus callosum and cerebellar white matter is shown. Cell nuclei were stained with DAPI (blue). Bars correspondent to 50 μm.

4.1.10 Behavior

As neuropathological alterations are often connected with behavioral deficits, *Fuca1*$^{(-/-)}$ mice were analyzed at 3 and 7 months of age regarding motor and coordinatory performance, overall activity and exploration as well as learning and memory performance. All experiments described here, were performed by Dr. Stroobants and Prof. D'Hooge (University of Leuven, Belgium).

A grip strength test was used to analyze the motor performance, where the mice had to grap a T-shaped bar, that was connected to a digital dynamometer. *Fuca1*$^{(-/-)}$ mice showed a reduced forelimb grip strength at 3 months of age (figure 4.24 A) as well as an enhanced rate of paw misplacements (40 % of *Fuca1*$^{(-/-)}$ mice (6/15); 7 % of wildtype mice (1/15)) . As the differences between the *Fuca1*$^{(-/-)}$ mice and their wildtype littermates were not that significant, the animals were re-tested at 7 months of age. However, no obvious progression was detected regarding the reduced forelimb strength (figure 4.24 A; paw misplacements: 50 % of *Fuca1*$^{(-/-)}$ mice (4/8); 0 % of wildtype mice (0/10)). In addition, motor and coordinatory performance was evaluated using a *rotarod* test. The animals were placed on a horizontally located, rotating rod. Rotation was accelerating from 4 to 40 rpm during 5 min and the drop latency of the animals was measured over four test trials. No differences were detected between wildtype and *Fuca1*$^{(-/-)}$ mice at 3 months of age (figure 4.24 D). The drop latencies increased in subsequent trials indicating a similar motor learning in both genotypes. However, at 7 months of age the *Fuca1*$^{(-/-)}$ mice showed a significant decreased drop latency in comparison to their wildtype littermates (figure 4.24 E). A progressive impairment of motor skills was evident, as all tested *Fuca1*$^{(-/-)}$ mice performed worse at 7 months of age (figure 4.24 F).

Hypoactivity was already observed in *Fuca1*$^{(-/-)}$ mice starting at approximately 6 months of age (section 4.1.5) and could be confirmed by analyzing the cage activity. Transparent cages were used, placed between 3 infrared beams and the total number of beam crossings was recorded over 23 h. The activity of 3-month-old wildtype animals showed an initial exploratory peak and a characteristic pattern of circadian activity. In contrast, these movement peaks were less pronounced or completely absent in the *Fuca1*$^{(-/-)}$ mice, indicating a hypoactive behavior (figure 4.24 B), although no obvious progression was detected in 7-month-old animals (figure 4.24 C).

The cognitive abilities were analyzed at 7 months of age using a contextual and cued fear conditioning test recording the freezing behavior of the mice (figure 4.24 G). The animals were

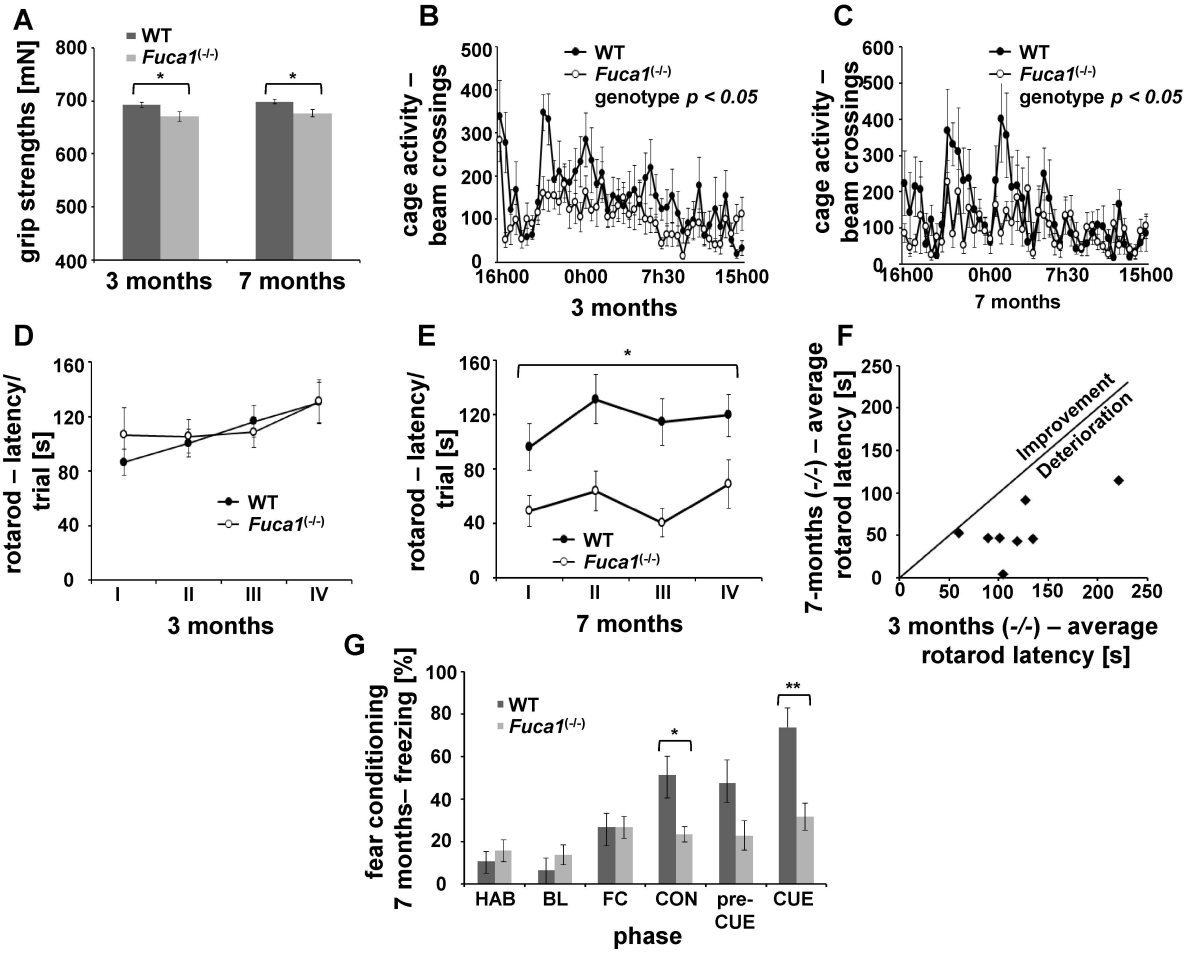

Figure 4.24: Fucosidase knock-out mice show behavioral deficits
(**A**) Grip strength test: *Fuca1*$^{(-/-)}$ mice showed a reduced forelimb strength at 3 and 7 months of age. An age-dependent progression was not detected. (**B**) and (**C**) Home cage activity was recorded over 23 h. Both, 3- and 7-month-old *Fuca1*$^{(-/-)}$ mice showed hypoactive behavior. (**D**) Using a *rotarod* test, no differences between the genotypes were detected at 3 months of age. (**E**) 7-month-old *Fuca1*$^{(-/-)}$ mice showed a decreased drop latency across four subsequent trials. (**F**) A progressive impairment of motor function was detected in all investigated *Fuca1*$^{(-/-)}$ animals. The scatter plot shows the rotarod drop latency of *Fuca1*$^{(-/-)}$ mice at 3 and 7 months of age. (**G**) Contextual and cued fear memory: No difference in baseline freezing levels or fear acquisition was observed between the genotypes. However, contextual and cued fear memory is impaired as shown by the decreased freezing percentage during fear memory evaluations in *Fuca1*$^{(-/-)}$ mice. HAB = habituation, BL = baseline, FC = fear conditioning, CON = context fear, preCUE = pre cued fear, CUE = cued fear; n = 15 for 3 months-old mice, n = 10 (WT) and n = 8 (Fuca1(-/-)) for 7 months-old mice. *p < 0.05 ; **p < 0.01

placed in the test environment for 5 min (*habituation* time). On the next day, the mice were placed in the same environment and received 2 min of exploration time (*baseline*-score). No differences between wildtype and *Fuca1*$^{(-/-)}$ mice were observed regarding freezing behavior

during the preparatory phases of the experiment (habituation and baseline). After baseline scoring, an auditory stimulus (buzzer = conditional stimulus (CS)) was sounded for 30 sec and an electric foot shock (0.3 mA) was applied for 2 sec (= averse, unconditional stimulus (US)). After 1 min of exploration, the CS-US was presented for a second time followed by a final exploration time of 1 min (*fear conditioning* phase). Fear acquisition was successful, as the freezing percentage of both genotypes increased during fear conditioning. On the third day, the *contextual fear* memory was recorded by placing the animals in the same environment for 5 min. *Fuca1*$^{(-/-)}$ mice showed a decreased freezing behavior indicating an impaired contextual fear memory. After 90 min the animals were presented to environmental alterations and received 3 min of exploration (*pre-cue* phase). Here, no differences were observed between the genotypes and freezing behavior was similar to the contextual phase, reflecting similar fear acquisition in the context of the newly created environment. Then the auditory stimulus (buzzer) was presented for 3 min resulting in substantial increase of freezing in wildtype mice (cue phase). This reaction was very weak pronounced in the *Fuca1*$^{(-/-)}$ mice, indicating an impaired cued fear memory. All these results demonstrate that the *Fuca1*$^{(-/-)}$ mice suffered from motor and coordinatory dysfunction and showed reduced activity as well as cognitive impairment.

4.2 Production and purification of human α-L-fucosidase

4.2.1 Establishment of an α-L-fucosidase expression system in CHO-K1 cells

Recombinant lysosomal enzymes used for ERTs are commonly produced in CHO-K1 cells and their derivatives like DG44 (e. g. for ERTs of Morbus Gaucher (Van Patten et al. 2007) and Fabry disease (Ioannou et al. 2001)). The synthesis of the enzymes results in a high protein overload of ER and Golgi apparatus of the cells. Hence, the majority of the produced enzymes escapes the lysosomal transport pathways and is secreted into the cell culture medium. The conditioned medium is harvested and used for further purification of the enzymes. For human α-L-fucosidase production, CHO-K1 cells were transfected with an expression plasmid for the untagged and the *C*-terminal His_6-tagged enzyme, respectively. After selection of stably transfected cells, the synthesis of the enzyme was tested by culturing the cells in FCS-free medium for 24 h. α-L-fucosidase activity was measured in the cell culture supernatant and a cell clone displaying the highest fucosidase secretion capacity (untagged: # C1; His_6-tagged: # C2) was further subjected to a limited dilution procedure in order to establish single cell clones. After cell propagation, the cell clone displaying the highest fucosidase secretion capacity (untagged: # C1/A5; His_6-tagged: # C2/C1) was expanded and characterized in detail.

No α-L-fucosidase activity was detected in the cell culture supernatant of untransfected cells, while the stably transfected CHO-K1 cell lines displayed a high α-L-fucosidase synthesis (figure 4.25 A). Generally, a slightly higher enzyme production was detected in the CHO-K1 cell line expressing the His_6-tagged α-L-fucosidase (10.6 mU/ml) than in the CHO-K1 cell line expressing the untagged enzyme (8.8 mU/ml).

For the initial experiments like the establishment of a purification strategy, only minor amounts of α-L-fucosidase were needed. For this purpose, an adherent cell culture system was established and the optimal production conditions were tested. Using 0.5 % FCS, an optimal cell survival was achieved. The cell culture supernatant was harvested every second day, as extended harvest intervals caused a massive decrease in cell survival. The fucosidase secretion capacity was monitored during the production cycle and was severely reduced after the fourth harvest. In summary, the optimal α-L-fucosidase production in the adherent cell culture system was achieved using culture medium containing 0.5 % FCS with a collecting interval of two days for four times.

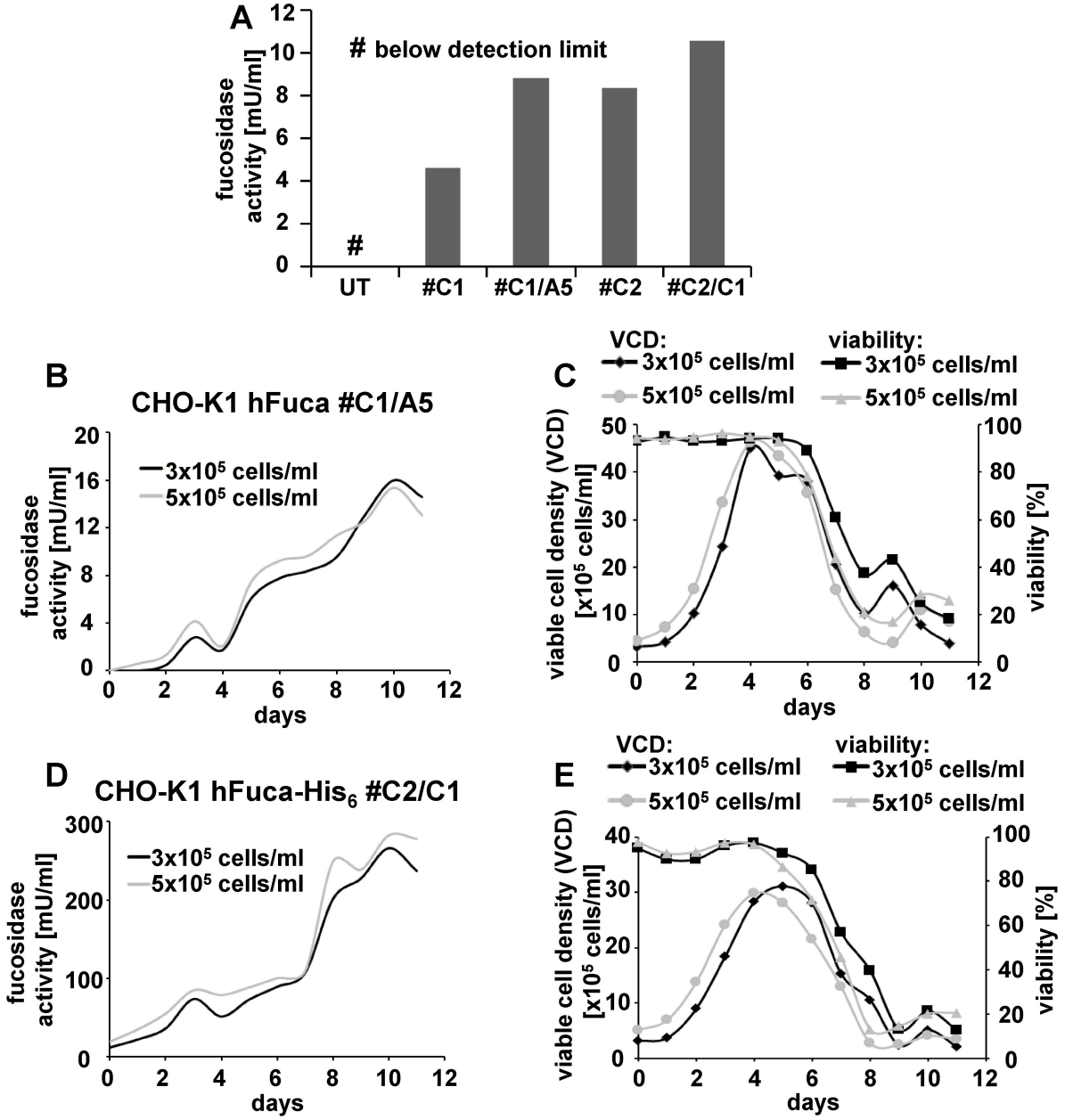

Figure 4.25: Establishment of CHO-K1 cells overexpressing human α-L-fucosidase
(**A**) CHO-K1 cells were stably transfected with an expression plasmid for the untagged and the His_6-tagged human α-L-fucosidase, respectively. Cell clones were picked (untagged: #C1; His_6-tagged: #C2). Single cell clones were established by limited dilution (untagged: #C1/A5; His_6-tagged: #C2/C1). Their fucosidase secretion capacity was monitored in comparison to untransfected cells (UT). Cells were grown for 48 h in FCS-free medium and the α-L-fucosidase activity of the cell culture supernatant was measured. (**B** - **D**) CHO-K1 cells expressing untagged (#C1/A5) or His_6-tagged (#C2/C1) human α-L-fucosidase were inoculated with 3×10^5 and 5×10^5 viable cells/ml (30 ml culture volume). The cells were grown in suspension and the viable cell density (VCD), the viability as well as the α-L-fucosidase activity in the cell culture medium was measured daily.

For ERT purposes, a large-scale production of the human α-L-fucosidase is necessary, which is achieved by adapting the CHO-K1 cell lines to suspension conditions using serum- and protein-free medium (Corning® PF medium). A growth curve was monitored over several days. The cells were seeded at concentrations of 3 x 10^5 and 5 x 10^5 viable cells/ml in 30 ml culture volume, respectively, and the viable cell density (VCD), the total viability as well as the α-L-fucosidase activity in the cell culture medium was monitored daily. CHO-K1 cells expressing the untagged enzyme reached higher cell densities, whereas the cells expressing the His_6-tagged enzyme produced considerably more α-L-fucosidase (figure 4.25 B - E). The highest cell densities were measured at day four to six. The viability decreased during the further cultivation period. The highest α-L-fucosidase activities were measured at day ten with 16 mU/ml for the untagged enzyme (vs. 8.8 mU/ml in adherent system) and 282 mU/ml for the His_6-tagged enzyme (vs. 10.6 mU/ml in adherent system).

4.2.2 Purification of His_6-tagged human α-L-fucosidase

The His_6-tagged human α-L-fucosidase was purified from ammonium sulfate precipitated cell culture medium of CHO-K1 cells (# C2/C1) using a Ni^{2+}-affinity chromatography as a first purification step followed by a strong cation exchange chromatography (SCX) as the second purification step. Finally, the enzyme was re-buffered into PBS.

The binding affinity of the His_6-tagged α-L-fucosidase towards the Ni^{2+}-affinity matrix was very high and allowed the presence of 50 mM imidazole in the binding buffer. In prior tests, no α-L-fucosidase activity was detected in flow through and washing fractions, while the enzyme started to elute at 230 mM imidazole during a linear elution gradient with increasing imidazole concentration. Taking this into consideration, a purification protocol was established in which the column was washed with 50 mM imidazole and elution of the His_6-tagged α-L-fucosidase was achieved by flushing the column with 500 mM imidazole resulting in a single and distinct elution peak (figure 4.26 A), where 95 % - 100 % of the initially loaded α-L-fucosidase activity was recovered within 4 ml (fractions F2 - F5). As determined by immunoblotting and on a coomassie-stained SDS-gel (figure 4.26 B), these fractions were highly enriched in α-L-fucosidase (55 kDa) but still contained some high-molecular weight as well as low-molecular weight contaminants. Fractions F2 - F5 were pooled and further applied to a SCX column.

The Ni^{2+}-affinity chromatography used a Tris/HCl-buffered system at pH 7.4, while the SCX was performed at pH 5.0, so that the pooled eluate had to be re-buffered towards the acidic pH.

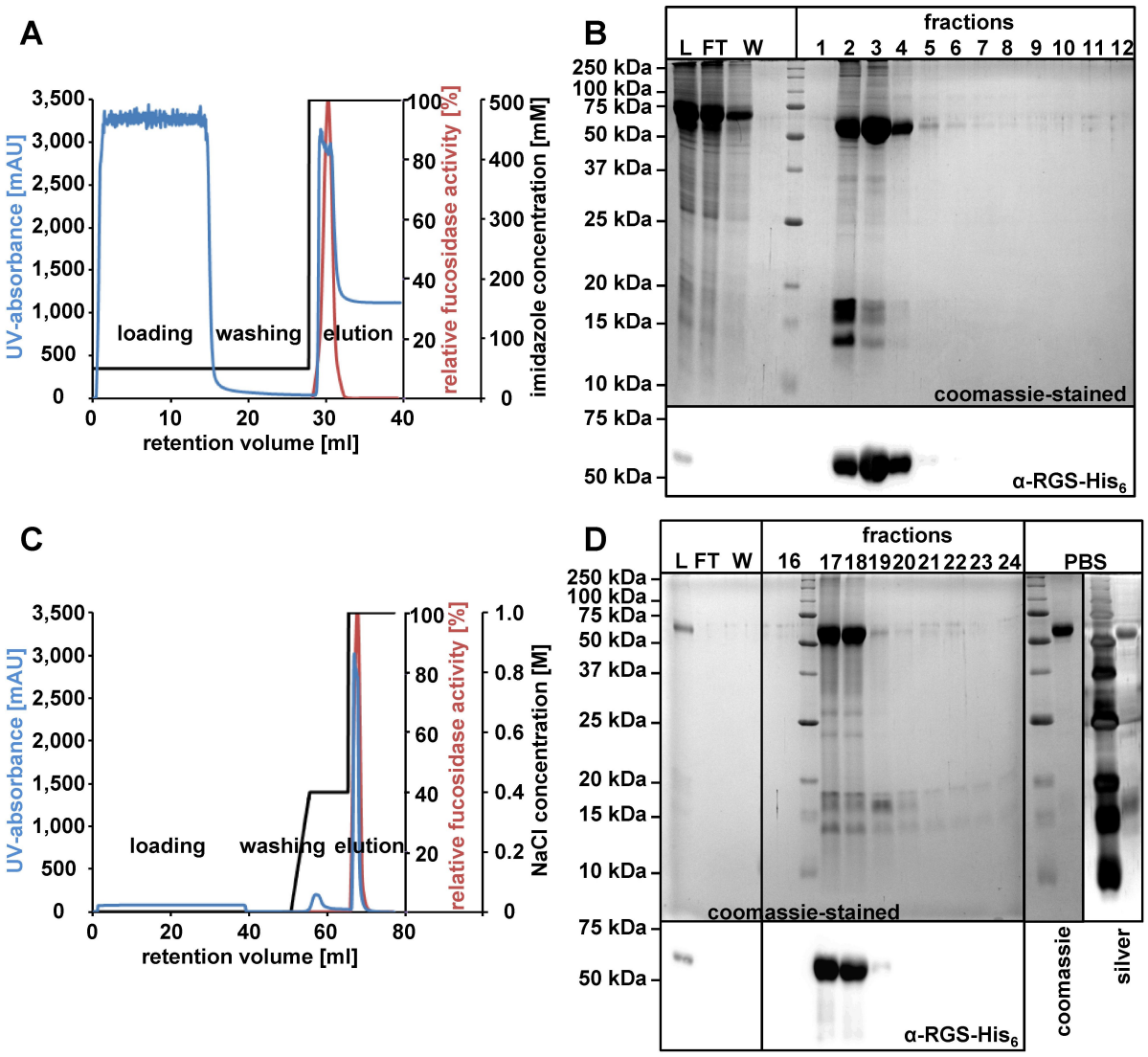

Figure 4.26: Purification of His_6-tagged human α-L-fucosidase
(**A**) Ni^{2+}-affinity chromatography: His_6-tagged human α-L-fucosidase was purified from coditioned cell culture medium of CHO-K1 cells (# C2/C1). The reconstituted ammonium sulfate precipitate was loaded on a HisTrap HP 1 ml column. After washing, the His_6-tagged α-L-fucosidase was eluted using 500 mM imidazole (black line). The UV-absorbance (280 nm, blue line) and the α-L-fucosidase activity (red line) is shown. The majority of the enzyme eluted at 29 - 32 ml (fractions F2 - F5). (**B**) Fractions obtained by Ni^{2+}-affinity chromatography were analyzed on a coomassie-stained SDS-gel and by immunoblotting using a RGS-His_6-specific antibody. α-L-Fucosidase was detected with an apparent molecular weight of 55 kDa. (**C**) Strong cation exchange chromatography (SCX): Ni^{2+}-NTA purified material (F2 - F5) was diluted in SCX binding buffer and loaded on a HiTrap SP HP 1 ml column. Two washing steps (without NaCl and using 400 mM NaCl) were applied and the enzyme was eluted using 1 M NaCl (black line). The UV-absorbance (280 nm, blue line) and the α-L-fucosidase activity (red line) is shown. The majority of the enzyme eluted at 67 - 69 ml (fractions F17 - F19). (**D**) Fractions obtained by SCX were analyzed on a coomassie-stained SDS-gel and by immunoblotting using a RGS-His_6-specific antibody. α-L-Fucosidase was detected at 55 kDa. Moreover, F17 - F19 were pooled, re-buffered into PBS, concentrated and analyzed on a SDS-gel by coomassie- and silver-staining. L: load; FT: flow through; W: washing fractions; PBS: PBS-buffered sample.

Moreover, 500 mM of NaCl were used in the Ni^{2+}-affinity chromatography and had to be removed to enable an efficient binding to the SCX column. In order to re-adjust the buffer, different methods like dialysis and fast diafiltration were tested resulting in a massive loss of α-L-fucosidase activity. Finally, the buffer exchange was performed by simply diluting the pooled fractions F2 - F5 in SCX binding buffer (1 : 10). Approximately 10 % of the α-L-fucosidase activity were lost in this step.

The re-buffered sample was loaded on a HiTrap SP HP 1 ml column and purified by a SCX. While no α-L-fucosidase activity was detected in the flow through and washing fraction, the His_6-tagged enzyme eluted at 850 mM NaCl during a linear elution gradient of increasing salt concentration (data not shown). The high binding affinity towards the column matrix enabled the implementation of an additional washing step using 400 mM NaCl resulting in the elution of contaminants as indicated by the increase in UV-absorbance (figure 4.26 C), while no significant loss of the α-L-fucosidase (< 1 %) was observed. Finally, the His_6-tagged α-L-fucosidase was eluted within a single, distinct peak of 3 ml (fractions F17 - F19) using 1 M NaCl with a recovery of 95 % - 100 % of the α-L-fucosidase activity (based on the SCX load). The elution fractions were further analyzed by immunoblotting and on a coomassie-stained SDS-gel (figure 4.26 D) showing that the α-L-fucosidase was highly enriched and exhibited an apparent molecular weight of 55 kDa. Only some minor impurities of low-molecular weight were detected.

In order to re-adjust buffer conditions suitable for ERT, the His_6-tagged human α-L-fucosidase was re-buffered into PBS. Although a fast diafiltration of the enzyme from neutral towards acidic pH resulted in a massive loss of α-L-fucosidase activity (as described above), only minor amounts (approximately 1 %) were lost during diafiltration from acidic to neutral buffer conditions. The sample was concentrated to a final volume of approximately 0.5 ml.

Table 4.3 summarizes the results of a typical purification procedure of the His_6-tagged human α-L-fucosidase. Here, 900 ml of conditioned cell culture supernatant were used. Based on the load of the Ni^{2+}-affinity chromatography, 80.2 % (70 U) of the fucosidase activity were recovered in the final PBS-buffered sample. The protein concentration of 7.9 mg/ml as well as a specific activity of 15.4 U/mg were determined, reflecting a 31-fold purification. The His_6-tagged α-L-fucosidase was purified to apparent homogeneity, as shown on a coomassie-stained SDS-gel (figure 4.26 D). Only a few low-molecular weight contaminants were detected using a very sensitive silver-staining.

Table 4.3: Purification of the His_6-tagged human α-L-fucosidase using 900 ml conditioned cell culture supernatant

	loaded sample			
	volume [ml]	**α-L-fucoisdase activity [U]**	**specific activity [mU/mg]**	**protein concentration [mg/ml]**
Ni^{2+}-affinity chromatography	20	87.3	0.5	9.3
strong cation exchange chromatography (SCX)	40	71.5	13.1	0.1
buffer exchange via centricon	3	70.8	13.8	1.7
	PBS-buffered sample			
	Volume [ml]	**α-L-fucoisdase activity [U]**	**specific activity [mU/mg]**	**protein concentration [mg/ml]**
PBS-buffered sample	0.6	70.0	15.4	7.9

4.2.3 Purification of untagged human α-L-fucosidase

The application of the His_6-tagged human α-L-fucosidase in an ERT of human fucosidosis patients is not feasible, as the His_6-tag exhibits a high immunogenicity, so that a large-scale production of the untagged human α-L-fucosidase is mandatory. However, the establishment of a purification protocol for the untagged enzyme is challenging, as the specific Ni^{2+}-affinity chromatography used for purification of the His_6-tagged human α-L-fucosidase has to be replaced by other separation techniques. Moreover, a Fuca1-specific antibody was not available at that time. In order to analyze the purification strategies by immunoblotting, the His_6-tagged α-L-fucosidase was used in parallel in some experiments. Different strategies like a fucose- and a concanavalin A-affinity chromatography as well as different ion exchange chromatography protocols were tested and are described below. The enzyme was produced from adherently grown CHO-K1 cells (cell line # C1/A5). The conditioned cell culture medium was harvested, precipitated by ammonium sulfate and the resuspended proteins were dialyzed and applied to various chromatography techniques.

4.2.3.1 Fucose-affinity chromatography

The purification of the α-L-fucosidase from several human tissues has been reported and was achieved by a specific fucose-affinity chromatography (Alhadeff et al. 1975b, Turner 1979, Chien and Dawson 1980). A similar approach was tested in this study by immobilizing *N*-(ε-aminocaproyl)-β-L-fucopyranosylamine on CNBr-activated sepharose beads and on a purification column containing NHS-activated sepharose (HiTrap NHS-activated HP 1 ml), respectively. Due to technical reasons, the matrices were finally combined. 3.7 U α-L-fucosidase were loaded on this affinity matrix and 4 % of the enzyme eluted in flow through and washing fractions. However, loading of higher amounts of α-L-fucosidase resulted in a massively increased elution in the flow through, indicating that the binding capacity of the affinity matrix was rather low.

The α-L-fucosidase was eluted by addition of 100 mM L-fucose. However, analysis of the elution fractions by activity measurements was not possible as the L-fucose completely inhibited the α-L-fucosidase activity (figure 4.27 A). The elution fractions were further analyzed on a silver-stained SDS-gel (figure 4.27 B). The enzyme eluted as a broad smear and con-

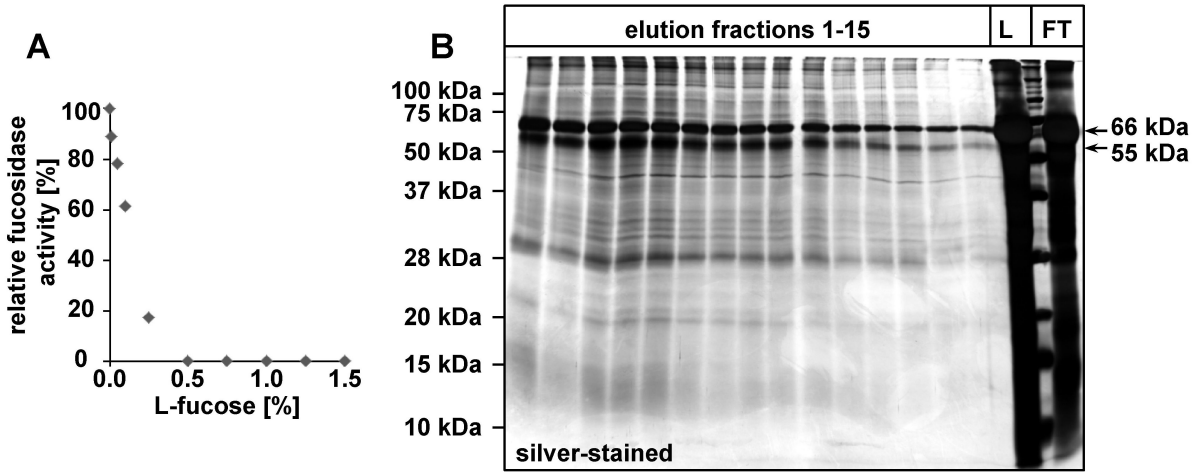

Figure 4.27: Fucose-affinity chromatography
(**A**) CHO-K1 cells overexpressing untagged human α-L-fucosidase were cultured for 72 h in FCS-free medium. The conditioned medium was quenched with different amounts of L-fucose and the α-L-fucosidase activity was measured. (**B**) A silver-stained SDS-gel of an examplified fucose-affinity chromatography is shown. Results were obtained in cooperation with Michael Weber (Master Thesis). Untagged α-L-fucosidase was loaded on a fucosyl-affinity column. The enzyme was eluted using 15 ml of 100 mM L-fucososе including 500 mM NaCl. The expected molecular weight of the α-L-fucosidase (55 kDa) and a 66 kDa protein (probably BSA) is indicated. L: load; FT: flow through.

tained high amounts of impurities, although column binding and washing was performed in the presence of 500 mM NaCl to reduce unspecific interactions. Remarkably, high amounts of a protein with an apparent molecular weight of 66 kDa were detected, which could be BSA.

In summary, the fucose-affinity chromatography should be further optimized to enable a higher binding capacity of the affinity column and to reach a higher purity of the α-L-fucosidase.

4.2.3.2 Concanavalin A-affinity chromatography

Concanavalin A (ConA)-affinity chromatography is widely used for the purification of glycoproteins. The lectin binds specifically to *N*-glycans, particularly internal and terminal non-reducing α-D-glucosyl and α-D-mannosyl residues. For the purification of untagged α-L-fucosidase, ConA-coupled sepharose beads were tested.

In order to enable an analysis of the purification strategy by immunoblotting, the His_6-tagged human α-L-fucosidase was used in the experiments described below. The enzyme was loaded on ConA sepharose beads and elution was performed by adding up to 1 M α-D-methylmannoside, but almost no elution (< 10 %) of the α-L-fucosidase was achieved.

At neutral pH, ConA forms a protein-ion complex with Mn^{2+} and Ca^{2+}, which are essential cofactors for substrate binding. The protein-ion complex is stable at neutral pH even in the absence of Mn^{2+} and Ca^{2+} in the chromatography buffer. However, at acidic pH values below 5.0 the ions are released from the protein. Hence, the ConA sepharose beads were loaded with α-L-fucosidase in the presence of Mn^{2+} and Ca^{2+} at neutral pH. Afterwards, an acidic elution buffer at pH 4.5 including 500 mM NaCl and 1 M α-methylmannoside was applied, but did not improve elution as demonstrated by a α-L-fucosidase activity assay (figure 4.28 A). As little as 2.4 % of the initially loaded fucosidase activity were eluted in the flow through and washing steps, but only 6.9 % were recovered during elution, which means that 90.7 % still remained on the column. An aliquot of the ConA sepharose beads was boiled and analyzed by immunoblotting showing high amounts of α-L-fucosidase sticking to the beads (figure 4.28 B). Consequently, the ConA-affinity chromatography was not further considered as purification strategy as an efficient elution of the α-L-fucosidase was only achieved under denaturating conditions.

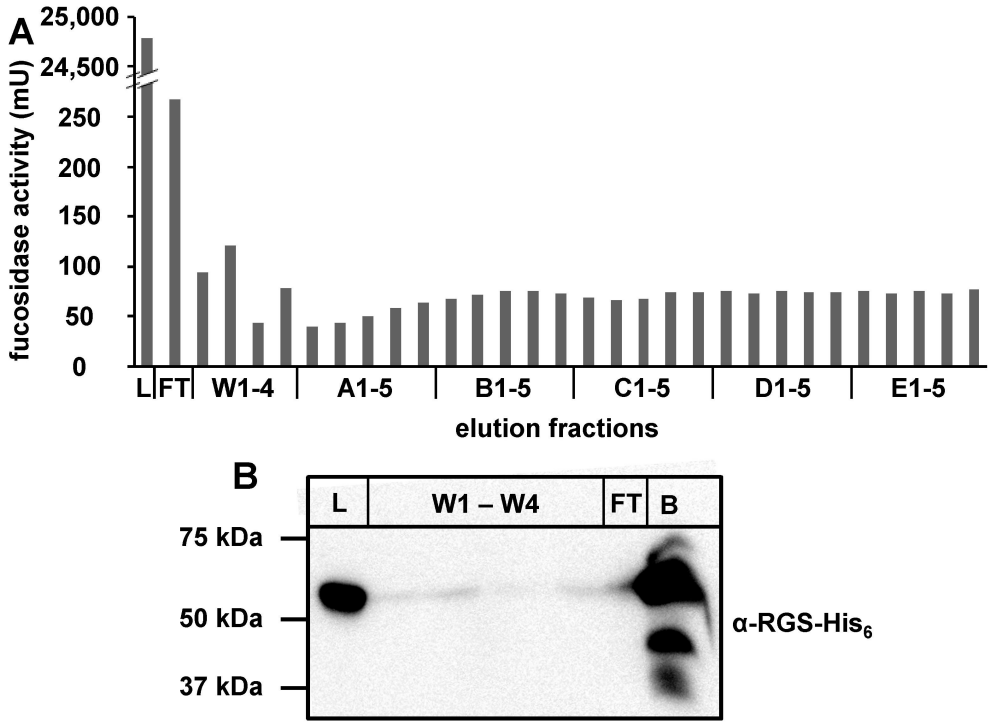

Figure 4.28: Concanavalin A-affinity chromatography
Experiments were performed in cooperation with Michael Weber (Master Thesis). (**A**) His_6-tagged human α-L-fucosidase was loaded on ConA sepharose beads under neutral conditions (pH 7.4) in the presence of Mn^+ and Ca^{2+} as well as 500 mM NaCl. After washing the enzyme was eluted using 5 ml of acidic buffer (pH 4.5) including 500 mM Nacl and 1 M α-methylmannoside. The elution buffer was incubated on the column for 5 min and collected as 1 ml fraction. Elution was repeated for 5 times (A - E) and the α-L-fucosidase activity was determined in each fraction. L: load; FT: flow through; W: washing fractions. (**B**) A part of the ConA sepharose beads was boiled and analyzed by immunoblotting using a RGS-His_6-specific antibody together with the load, flow through and washing fractions. The following volume percentages were loaded: L: load 0.2 %, FT: flow through 0.5 %, W: washing fractions 1 %, B: boiled ConA beads 0.6 %.

4.2.3.3 Ion-exchange chromatography

Ion-exchange chromatography is an easy accessible and low-cost method for a reproducible purification of recombinant proteins. The purification of the His_6-tagged human α-L-fucosidase included a strong cation-exchange chromatography (SCX) as second purification step (section 4.2.2), in which the enzyme showed a strong affinity towards the column matrix. The untagged human α-L-fucosidase was expected to show similar binding properties during SCX, as the RGS-His_6-tag was the only difference between both enzymes. Different ion exchange matrices as well as different purification settings (pH values) were tested for the untagged α-L-fucosidase. An efficient binding and elution was observed at pH 4.0 - 5.0 for the cation

Table 4.4: Purification of the untagged human α-L-fucosidase by ion exchange chromatography

Column	pH	% fucosidase activity in the flow through and washing steps	% fucosidase activity in the elution fractions	elution concentration (mM NaCl)
HiTrap HP SP 1 ml	4.0	0	100	590
HiTrap HP SP 1 ml	4.5	0	100	450
HiTrap HP SP 1 ml	5.0	0	100	450
HiTrap HP SP 1 ml	7.4	15.7	84.3	300
HiTrap DEAE FF 1 ml	4.6	99.0	1.0	0
HiTrap DEAE FF 1 ml	8.0	2.5	97.5	240

exchange matrix and at pH 8.0 for the anion exchange matrix. However, all attempts resulted in a significant lower salt concentration for elution of the untagged α-L-fucosidase than for the His_6-tagged enzyme (table 4.4). As a consequence, it was not possible to separate the contaminants efficiently. In figure 4.29 a coomassie-stained SDS-gel from an anion-exchange chromatography using an HiTrap DEAE FF column at pH 8.0 is shown exemplarily.

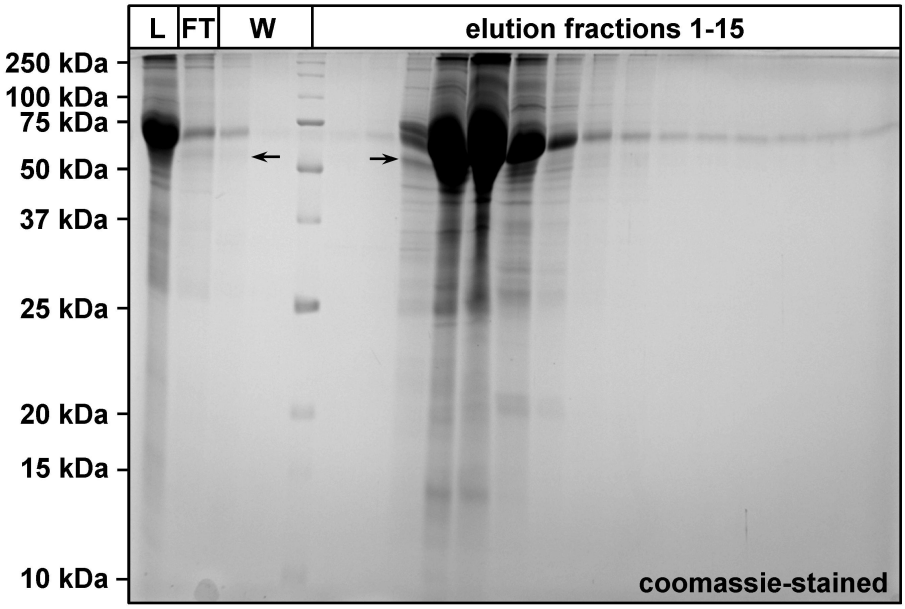

Figure 4.29: Ion-exchange chromatography of the untagged human α-L-fucosidase
(**A**) Untagged human α-L-fucosidase was loaded on a HiTrap DEAE FF 1 ml at pH 8.0. After washing the enzyme was eluted using a linear gradient from 0 - 1 M NaCl over 15 ml. The fractions were analyzed on a coomassie-stained SDS-gel. The expected molecular weight of the α-L-fucosidase (55 kDa) is marked by arrows. L: load, FT: flow through, W: washing fractions.

The analysis of different ion exchange chromatographies uncovered the presence of a prominent contaminant (figure 4.29) with an apparent molecular weight of 66 kDa (most likely BSA), that could not be removed so far. In a further experiment the adherent CHO-K1 cells were cultured in FCS-free medium and the conditioned medium was either applied to an ammonium sulfate precipitation or was directly dialyzed over night and loaded on a HiTrap SP HP 1 ml column, respectively. In both cases the α-L-fucosidase eluted in fraction 7 (figure 4.30 A and C). However, different UV-absorbances were recorded suggesting an

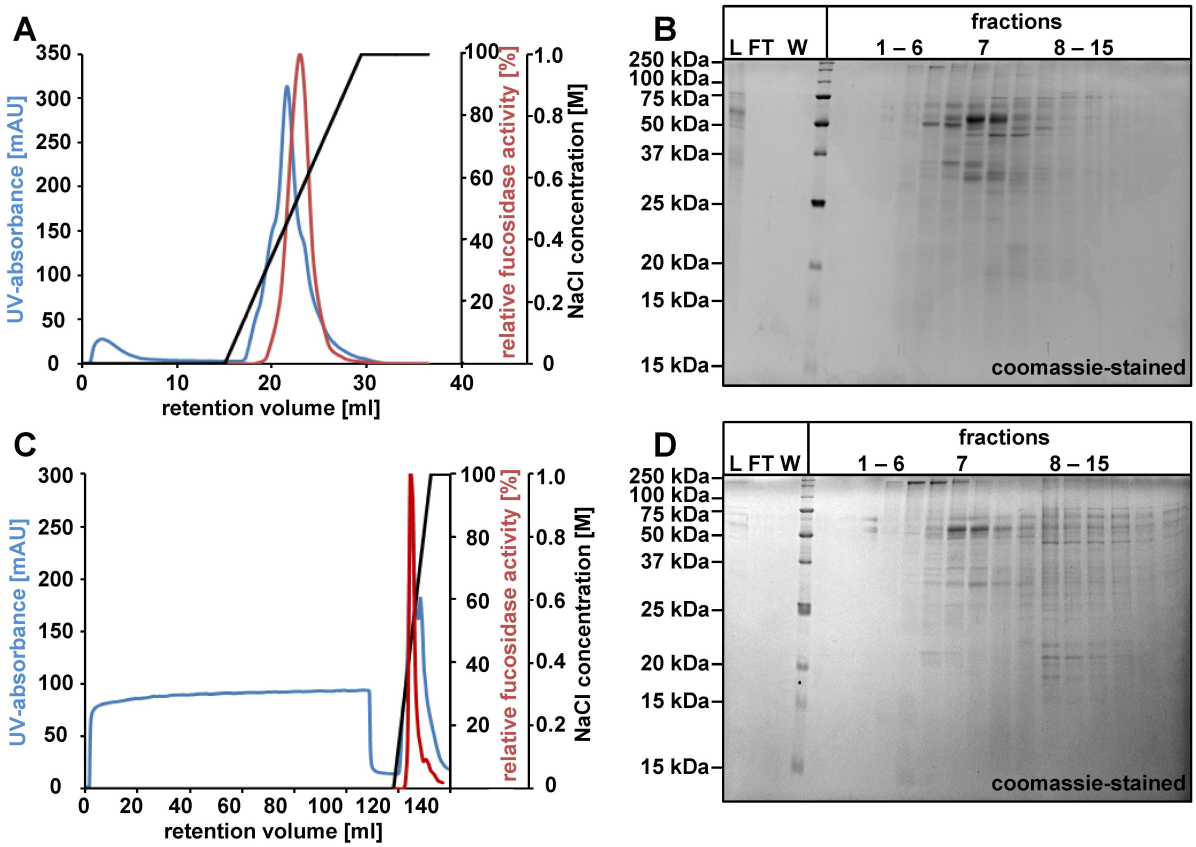

Figure 4.30: Ion-exchange chromatography using precipitated as well as non-precipitated untagged human α-L-fucosidase

Untagged human α-L-fucosidase was produced using adherent CHO-K1 cells (#C2/C1). The cells were cultured in FCS-free medium for three days. (**A**) The conditioned medium was precipitated using ammonium sulfate, reconstituted in binding buffer (pH 5.0), dialyzed and loaded on a HiTrap SP HP 1 ml column. The α-L-fucosidase was eluted using a linear gradient of increasing salt concentrations (0 - 1 M NaCl, black line) over 15 ml. The UV-absorbance is shown as blue line and the α-L-fucosidase activity as red line. (**B**) The purification strategy was analyzed on a coomassie-stained SDS-gel. The expected molecular weight of the α-L-fucosidase is 55 kDa. (**C**) The conditioned medium was directly dialyzed against binding buffer (pH 5.0) and the purification was performed as described in (A) and (**D**) was further analyzed on a coomassie-stained SDS-gel. The expected molecular weight of the α-L-fucosidase is 55 kDa. L: load, FT: flow through, W: washing fractions.

altered elution of the contaminants, which was further analyzed on a coomassie-stained SDS-gel. Similar to the results described above, most of the contaminants from the precipitated starting material eluted together with the α-L-fucosidase (figure 4.30 B), while some of the impurities from the non-precipitated starting material eluted at higher salt concentrations than the enzyme (figure 4.30 D). Further experiments are necessary to analyze this phenomenon and the experiment should be repeated using conditioned medium from CHO-K1 cells cultured under FCS-free suspension conditions.

4.2.3.4 Ni^{2+}-affinity chromatography

Berteau et al. (2002) described the purification of an untagged α-L-fucosidase from *P. maximus* (starfish) by Ni^{2+}-affinity chromatography amongst other purification techniques. It was postulated that the binding of the untagged enzyme was achieved by histidine residues located at the protein surface. The NetSurfP prediction program, which checks out the protein surface accessibility, predicted that seven out of twelve histidine residues might be located at the protein surface of the human α-L-fucosidase.

The untagged human α-L-fucosidase was applied to a Ni^{2+}-affinity chromatography on a HisTrap HP 1 ml column at pH 7.4 in the presence of 500 mM NaCl. 55 % of the α-L-fucosidase activity was detected in the flow through or washing steps. 45 % of the α-L-fucosidase eluted specifically by addition of imidazole with the highest enzyme activity at approximately 50 mM imidazole. The majority of contaminants was detected in the same fractions as the α-L-fucosidase (figure 4.31). Therefore, the Ni^{2+}-affinity chromatography was not further considered as purification strategy for the untagged human α-L-fucosidase.

4.2.4 Characterization of the recombinant α-L-fucosidase with regard to its application in ERT

An aim of this work was the application of the purified human α-L-fucosidase in an ERT of *Fuca1*$^{(-/-)}$ mice. Therefore, the recombinant enzyme was characterized regarding its pH optimum and oligomerization. As the latter might also influence enzyme stability, this aspect was also analyzed. Moreover, the glycosylation pattern and especially the mannose-6-phosphorylation of the recombinant α-L-fucosidase was determined as these properties might influence the uptake of the enzyme during ERT.

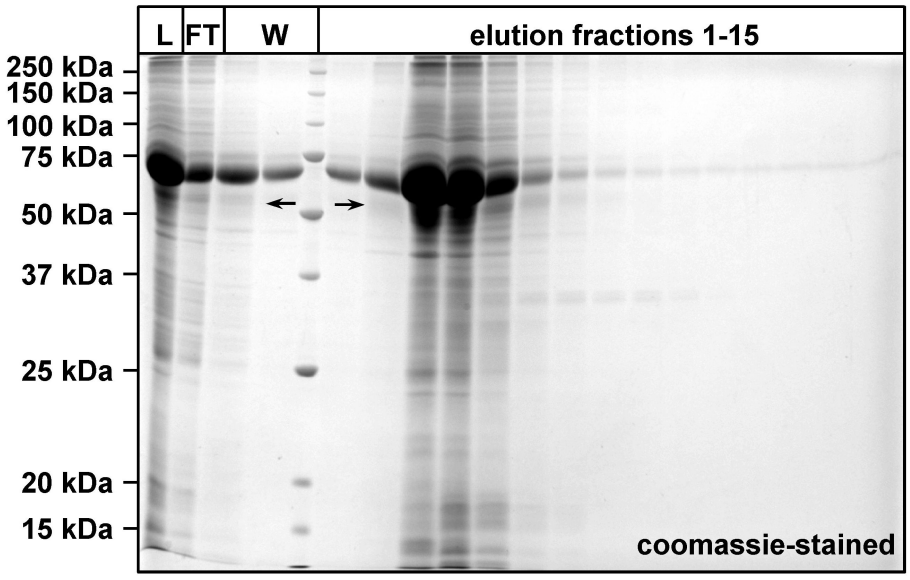

Figure 4.31: Ni^{2+}-affinity chromatography of untagged human α-L-fucosidase
The untagged human α-L-fucosidase was loaded on a HisTrap HP 1 ml column. The column was washed and elution was performed using a linear gradient from 0 - 500 mM imidazole over 15 ml. The highest fucosidase activity was measured in elution fraction 3. All fractions were analyzed on a coomassie-stained SDS-gel. The expected molecular weight of the α-L-fucosidase (55 kDa) is marked by arrows.

4.2.4.1 pH optimum of α-L-fucosidase

The standard α-L-fucosidase activity assay is carried out using an acidic citrate buffered system. For analysis of the pH optimum of the enzyme, a buffer system described by McIlvaine (1921) (citrate-phosphate buffer) was used instead, that enabled investigations over a broader pH spectrum (pH 4.0 - 8.0), than citrate alone. As control, the pH optimum of the genuine α-L-fucosidase was determined using lysosome-enriched fractions from liver of wildtype mice with the highest α-L-fucosidase activity at pH 5.5 (figure 4.32 A). At pH 7.0, still 50 % of the maximal enzyme activity was measured. Next, the untagged human α-L-fucosidase derived from CHO-K1 cells was analyzed and the pH optimum of the recombinant enzyme slightly differed from that of the genuine enzyme and was recorded at pH 5.0 (figure 4.32 B). In order to exclude a possible influence of McIlvaine's buffer on the pH-dependency of the α-L-fucosidase, the experiment was repeated using the citrate buffer in a suitable pH spectrum (pH 4.5 - 6.5). Here, the recombinant α-L-fucosidase exhibited a pH-dependency comparable to that of lysosome-enriched fractions from mouse liver with an pH optimum at 5.5 (figure 4.32 C), indicating that the recombinant enzyme is highly active at lysosomal pH.

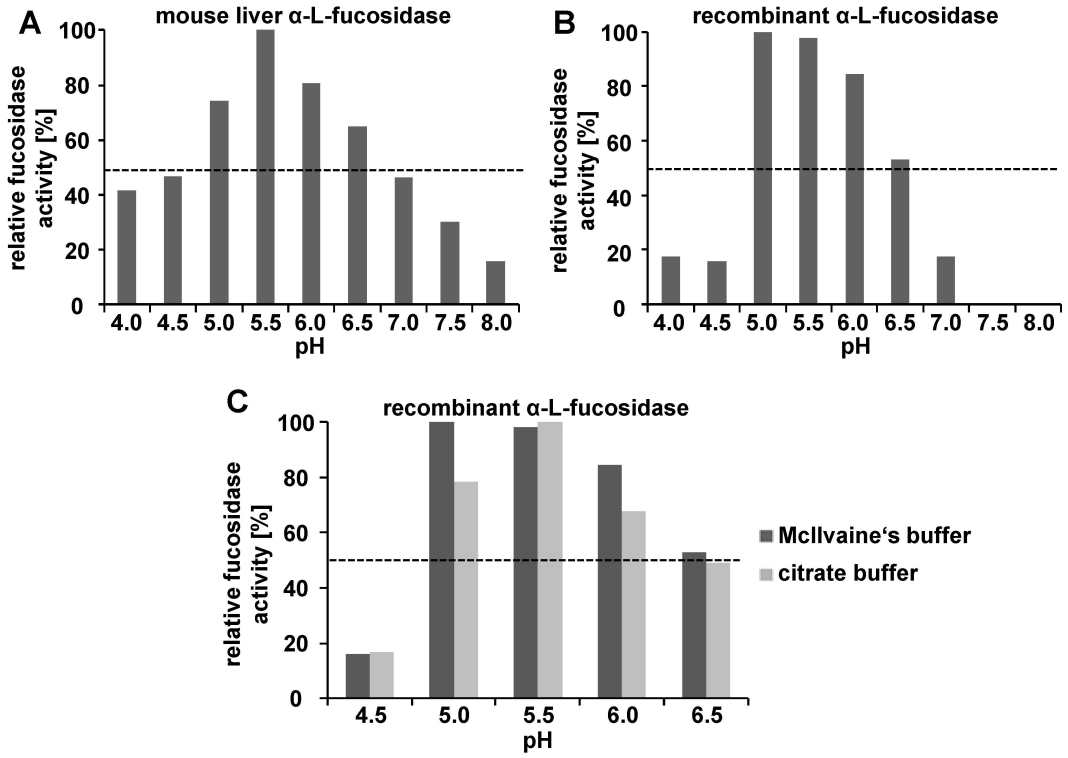

Figure 4.32: pH optimum of the α-L-fucosidase
(**A**) The α-L-fucosidase activity of lysosome-enriched fractions from liver of wildtype mice was analyzed over a broad pH spectrum (pH 4.0 - 8.0) using McIlvaine's buffer system (McIlvaine 1921). (**B**) The activity of CHO-K1 cell-derived untagged human α-L-fucosidase was determined using McIlvaine's buffer system adjusted to the stated pH values. (**C**) Same experiment as in (B). In addition the α-L-fucosidase activity was determined at pH 4.5 - 6.5 using citrate buffer instead of McIlvaine's buffer.

4.2.4.2 Oligomerization

A homooligomerization of the α-L-fucosidase has been reported including dimeric, tetrameric as well as hexameric forms (Alhadeff et al. 1975b, Turner 1979 and Chien and Dawson 1980). The fact that the His_6-tagged human α-L-fucosidase exhibited an unexpected strong binding towards the HisTrap HP column as well as the HiTrap SP HP column suggested an oligomerization of the enzyme that accordingly increased the avidity of this interaction. Hence, the molecular weight of the purified human α-L-fucosidase was determined by size exclusion chromatography on a Superdex 200 10/30 column using recombinant untagged as well as His_6-tagged enzyme at pH 4.6 and 7.4, respectively. Several standard proteins were also separated at neutral and acidic pH and were used for molecular weight calculation (figure 4.33 A and B). As expected, the His_6-tagged human α-L-fucosidase was detected as an oligomer

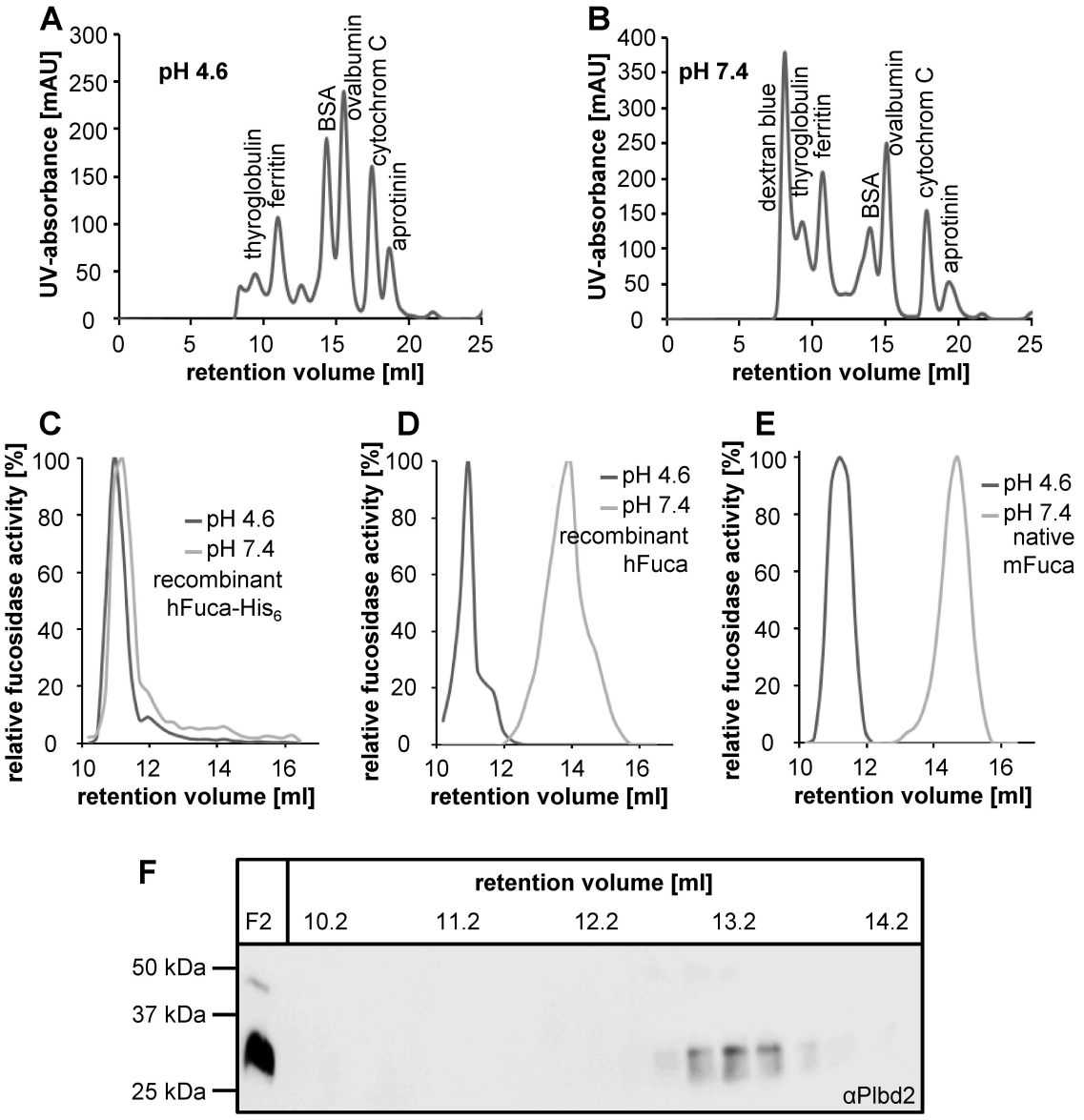

Figure 4.33: Oligomerization of the α-L-fucosidase
Experiments were performed in cooperation with Michael Weber and Marcel Strüve (practical internship). (**A** and **B**) Standard proteins were separated by size exclusion chromatography (SEC) using a Superdex 200 10/30 column and were used for molecular weight calculation. PBS pH 7.4 or McIlvaine's buffer pH 4.6 supplemented with 140 mM NaCl was used as running buffer. dextran blue = 2000 kDa; thyroglobulin = 670 kDa; ferritin = 440 kDa; BSA = 66 kDa; ovalbumin = 45 kDa; cytochrom C = 12.5 kDa; aprotinin = 6.5 kDa; His_6-tagged human α-L-fucosidase (**C**) as well as untagged human α-L-fucosidase (**D**) was dialyzed against PBS pH 7.4 or McIlvaine's buffer pH 4.6 supplemented with 140 mM NaCl and analyzed by SEC. Fractions of 250 µl were collected. The enzyme was detected in the elution fractions by α-L-fucosidase activity measurements. (**E** and **F**) Lysosome-enriched fraction were isolated from liver of wildtype mice. The lysosomes were pelleted by centrifugation and were resuspended in either PBS pH 7.4 or McIlvaine's buffer pH 4.6 supplemented with 140 mM NaCl. The SCX was performed as described above. (**E**) The α-L-fucosidase was detected by activity measurements. (**F**) Plbd2 was detected by immunoblotting. The 25 kDa, 28 kDa and 40 kDa subunit is visible. Isolated lysosomes (F2) were used as internal control.

with calculated molecular weights of 276 kDa and 356 kDa at pH 7.4 and 4.6, respectively (figure 4.33 C). For the untagged human α-L-fucosidase, a pH-dependent oligomerization was observed with calculated molecular weights of 79 kDa at pH 7.4 and of 355 kDa at pH 4.6 (figure 4.33 D). Moreover, liver-derived murine α-L-fucosidase was analyzed by SEC and the pH-dependent oligomerization seen before for the recombinant human protein was confirmed (figure 4.33 E). At pH 7.4 the monomeric form of the fucosidase was detected (56 kDa), whereas at pH 4.6 a molecular weight of 312 kDa was determined suggesting a hexamerization at lysosomal pH. As internal control, the lysosomal protein Plbd2 was confirmed as a dimer (112 kDa) at pH 4.6 (figure 4.33 F).

4.2.4.3 Stability after short-term storage

In order to analyze the stability of the purified His_6-tagged human α-L-fucosidase, the enzyme activity was measured during short-term storage either at room temperature or at 4 °C. After ten days, only a slight decrease of 22 % (storage at room temperature) and 15 % (storage at 4 °C) of α-L-fucosidase activity was observed (figure 4.34 A). Using a coomassie-stained SDS-gel, a protein degradation was visible after four days of storage at room temperature, whereas no degradation of the enzyme was detected even after ten days of storage at 4 °C (figure 4.34 B), indicating a high stability of the His_6-tagged human α-L-fucosidase.

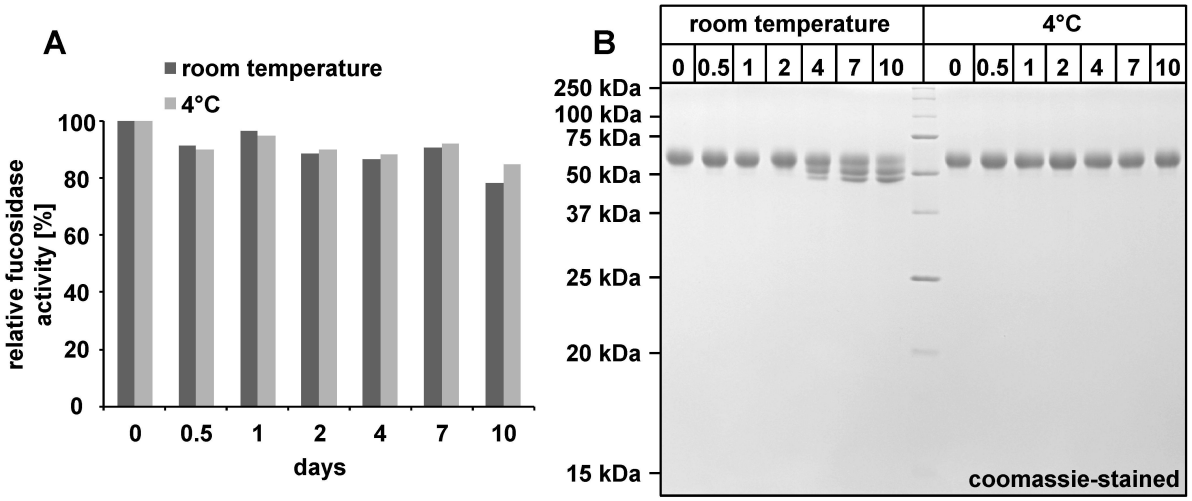

Figure 4.34: Stability of the His_6-tagged human α-L-fucosidase after short-time storage
Purified His_6-tagged human α-L-fucosidase was stored at room temperature and 4 °C for up to ten days, respectively. Samples were analyzed at defined time points (0.5, 1, 2, 4, 7 and 10 days). (**A**) The α-L-fucosidase activity was measured and (**B**) the enzyme was analyzed for protein degradation by SDS-PAGE followed by coomassie-staining.

4.2.4.4 Glycosylation

Many lysosomal proteins are known to be highly glycosylated. The α-L-fucosidase was previously reported to exhibit high-mannose as well as complex type *N*-glycans (Johnson et al. 1992). In order to analyze the glycosylation of the recombinant human α-L-fucosidase, the purified His_6-tagged enzyme was digested with PNGase F and EndoH. PNGase F cleaves high-mannose as well as complex type *N*-glycans between the GlcNAc and the asparagine residue, whereas EndoH only cleaves high-mannose type *N*-glycans between the two core-GlcNAc residues. Using immunoblotting, the untreated His_6-tagged α-L-fucosidase was detected at 55 kDa (figure 4.35), while the PNGase F digest resulted in a substantial decrease in molecular weight to 45 kDa. In contrast, a molecular weight of 50 kDa was detected after EndoH digest, indicating that the His_6-tagged human α-L-fucosidase exhibited both types of *N*-glycans.

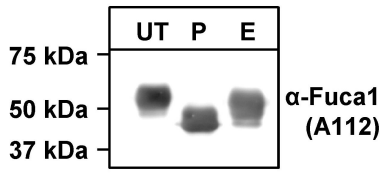

Figure 4.35: Glycosylation pattern of the His_6-tagged human α-L-fucosidase
Purified His_6-tagged human α-L-fucosidase was digested with PNGase F (P) and EndoH (H) respectively. The samples were analyzed by immunoblotting using a Fuca1-specific antibody (A112). UT - untreated.

4.2.4.5 Mannose-6-phosphorylation

The lysosomal targeting of the α-L-fucosidase was shown to be strictly dependent on the mannose-6-phosphate (M6P) receptor pathway (Kollmann et al. 2012, Markmann et al. 2015). Thus, a high M6P phosphorylation of the recombinant enzyme is desired to achieve an efficient ERT. However, a complete M6P modification of recombinant proteins is often not achieved in overexpression systems due to high protein overload of the M6P-generating system (Roces et al. 2004).

The degree of M6P phosphorylation of the His_6-tagged human α-L-fucosidase was quantified using an affinity column with immobilized M6P receptors (Braulke et al. 1990; kind gift of Siva Kumar, Hyderabad, India). The purified enzyme was loaded and unbound material was washed off using 5 mM Glc-6-phosphate, the epimer of M6P. 37.1 % of the enzyme eluted already in the flow-through and washing fractions, whereas only 4 % of the His_6-tagged α-L-fucosidase eluted specifically by addition of 5 mM M6P (figure 4.36 A and B), indicating an

incomplete elution of the loaded enzyme. The experiment was repeated and additional washing steps including a stringent acidic elution buffer and 20 % ethanol were performed (figure 4.36 C). Again, the α-L-fucosidase activity could not be completely recovered, but a substantial amount of the enzyme eluted after addition of 20 % ethanol indicating an unspecific interaction of the His_6-tagged α-L-fucosidase with the column matrix. In order to exclude that the column matrix was irreversibly damaged, recombinant Scpep1 with a high M6P phosphorylation degree was used as positive control (figure 4.36 D). Scpep1 could be specifically eluted upon addition of 5 mM M6P. These results indicate that a considerable amount of the His_6-tagged α-L-fucosidase was M6P phosphorylated, but the degree of the M6P modification could not be precisely quantified.

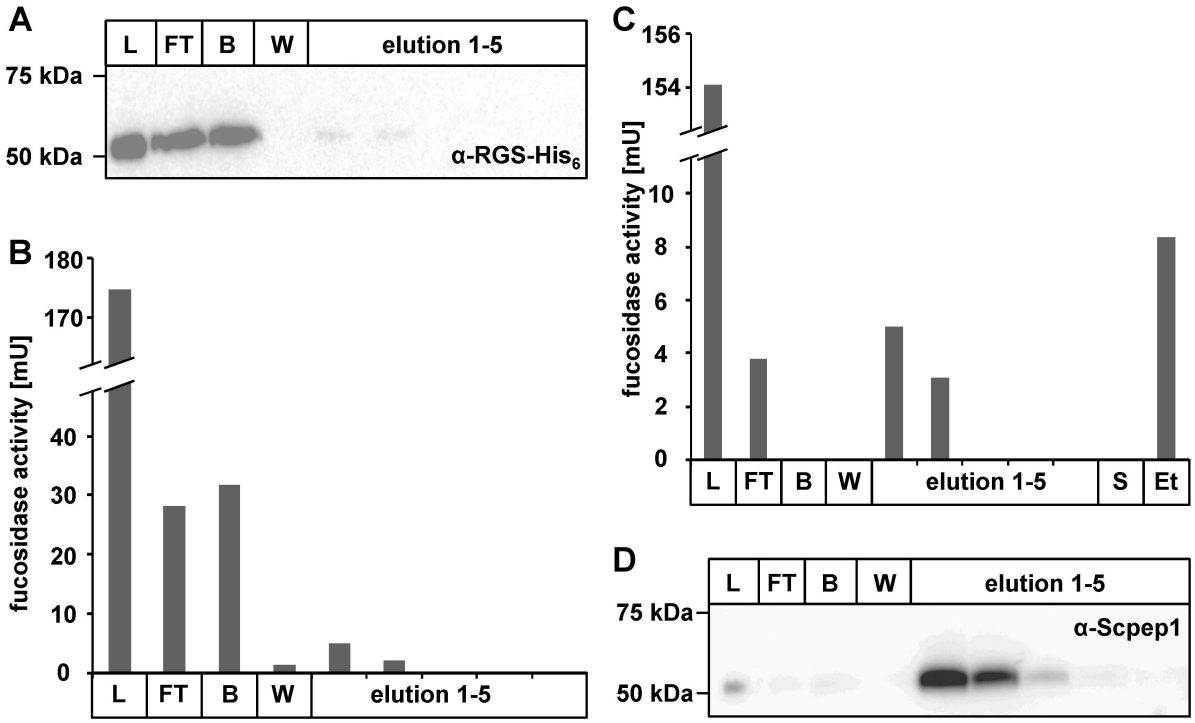

Figure 4.36: Quantification of the M6P phosphorylation of the His_6-tagged α-L-fucosidase
(**A**) Purified His_6-tagged α-L-fucosidase was loaded on a MPR-affinity matrix. The flow through (FT) was collected, the matrix was washed with binding buffer (B) followed by binding buffer containing 5 mM Glc-6-phosphate (W). Elution was performed by addition of 5 mM M6P. 5 % (v/v) of each fraction was precipitated with TCA and analyzed by immunoblotting (RGS-His_6-specific antibody). (**B**) The α-L-fucosidase activity was determined in each fraction. (**C**) The experiments described in (A) was repeated and expanded by additional washing steps with a stringent acidic elution buffer (S) and 20 % ethanol (Et). The α-L-fucosidase activity was determined in each fraction. (**D**) Recombinant Scpep1 exhibiting a high M6P phosphorylation degree was used as positive control. The experiment was performed as described in (A). 5 % (v/v) of each fraction was precipitated with TCA and analyzed by immunoblotting.

4.3 Enzyme replacement therapy

4.3.1 *In vitro* digest of fucosidosis storage material

It is mandatory for an ERT of fucosidosis that the recombinant α-L-fucosidase is able to digest the accumulated storage material. In order to perform an *in vitro* digest, storage material derived from *Fuca*$^{(-/-)}$ kidney and cerebrum was isolated, incubated with the purified His_6-tagged enzyme and analyzed by thin-layer chromatography. As shown in figure 4.37, the *in vitro* digest resulted in the disappearance or at least a shift of TLC bands towards higher retention factors indicating that the storage material exhibited less hydrophilic properties as expected by an elimination of a sugar residue like α-L-fucose. Of note, L-fucose was

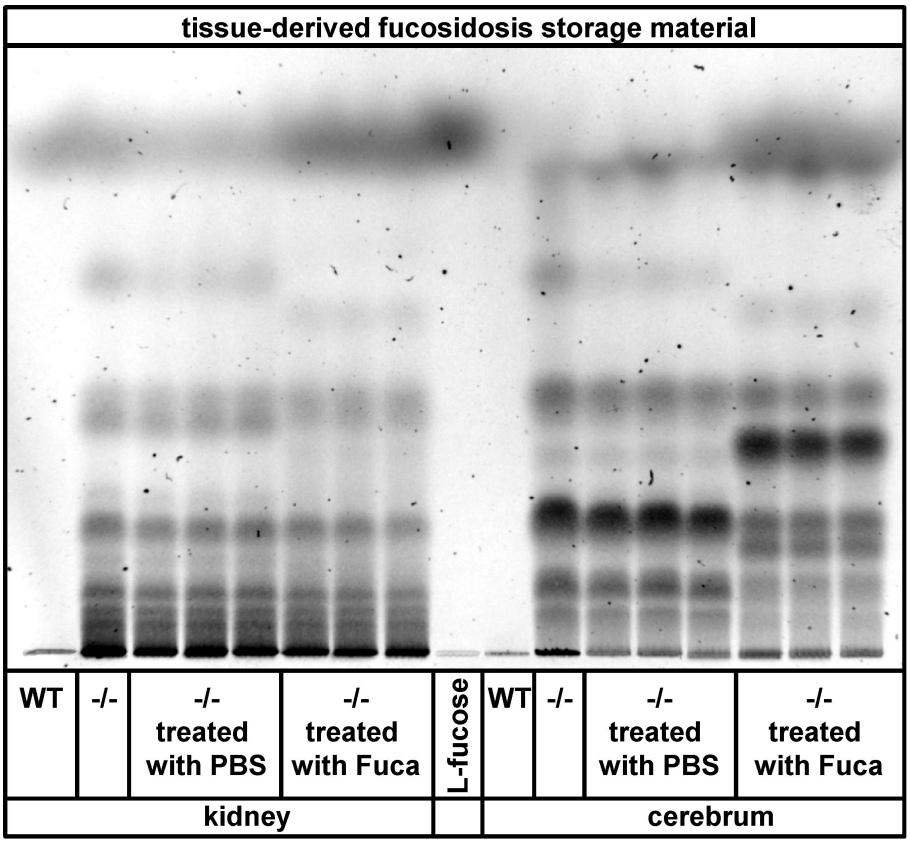

Figure 4.37: *In vitro* digest of fucosidosis storage material
Neutral oligosaccharides were isolated from wildtype and *Fuca1*$^{(-/-)}$ kidney and cerebrum and were incubated with purified His_6-tagged human α-L-fucosidase or with PBS, respectively. The experiment was done in technical triplicates and the samples were analyzed by TLC. L-Fucose was loaded as internal standard.

loaded as internal standard on the TLC and α-L-fucosidase-treated samples showed an increased intensity of the TLC band corresponding to L-fucose in comparison to the PBS-treated samples. These results indicate that the His_6-tagged human α-L-fucosidase is able to digest storage material from *Fuca1*$^{(-/-)}$ mice *in vitro*.

4.3.2 Endocytosis of recombinant α-L-fucosidase

An efficient uptake of recombinant enzymes into affected cells and tissues is a prerequisite for a successful ERT. The endocytosis of the His_6-tagged human α-L-fucosidase was analyzed using immortalized wildtype and *Fuca1*$^{(-/-)}$ mouse embryonic fibroblasts (MEFs). The purified enzyme was applied to the cell culture medium and the α-L-fucosiase activity was subsequently measured in the cell lysates. Here, the enzyme activity was increased five to ten times in the α-L-fucosidase-treated wildtype MEFs compared to PBS-treated cells (figure 4.38 A). As expected, no α-L-fucosidase activity could be detected in PBS-treated *Fuca1*$^{(-/-)}$ MEFs, while the amount of endocytosed α-L-fucosidase was comparable to wildtype MEFs. These results clearly indicate that the recombinant enzyme is endocytosed by wildtpye and *Fuca1*$^{(-/-)}$ MEFs.

The endocytosis of the α-L-fucosidase was shown to be dose-dependent (figure 4.38 B), when different amounts of enzyme were applied to wildtype and *Fuca1*$^{(-/-)}$ MEFs. The enzyme activity of the cell lysates increased linearly with increasing α-L-fucosidase concentrations in the medium. Moreover, a linear correlation was determined for the α-L-fucosidase activity and the incubation time of the recombinant enzyme (figure 4.38 C). However, the *Fuca1*$^{(-/-)}$ MEFs exhibited always a lower endocytosis rate than the wildtype MEFs as depicted by the flatter slope of the linear regression lines (figure 4.38 B and C). It remains to be analyzed whether this result is dependent on the *Fuca1* gene knock-out or whether it is a feature of the particular clonal cell lines, which were used to evaluate the dose and time dependency. Other *Fuca1*$^{(-/-)}$ MEF cell lines might exhibit a higher endocytosis rates comparable to that of the wildtype cell line.

Markmann et al. (2015) reported that the lysosomal targeting of the α-L-fucosidase is highly dependent on the M6P residue. Their study was based on ML II MEFs, which are deficient in GlcNAc-1-phosphotransferase thereby lacking the M6P modification of lysosomal proteins. Endogenous lysosomal proteins depending on the MPR-pathway are not transported towards the lysosome and are secreted. Of note, some hydrolases, but not the α-L-fucosidase reach

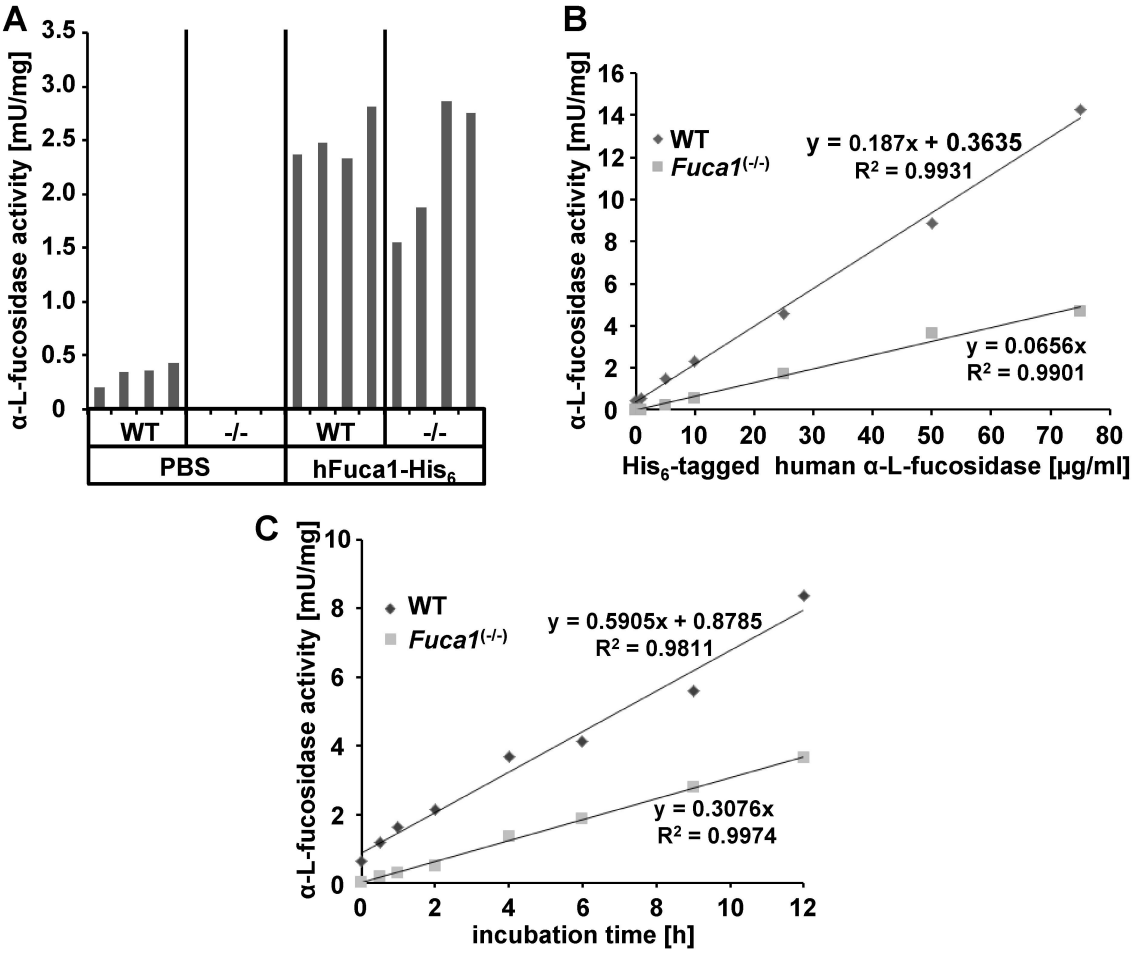

Figure 4.38: His$_6$-tagged human α-L-fucosidase is endocytosed by MEFs
(**A**) 20 μg/ml purified His$_6$-tagged human α-L-fucosidase or equal amounts of PBS were applied to the cell culture medium of wildtype and *Fuca1*$^{(-/-)}$ MEFs (n = 4) for 5 h. The cells were harvested by trypsination and the α-L-fucosidase activity was measured in the cell lysates. (**B**) Same experiment as in (A) but using different concentrations of His$_6$-tagged human α-L-fucosidase (n = 1 for wildtype and *Fuca1*$^{(-/-)}$ MEFs). (**C**) Same experiment as in (A) but cells were harvested after different incubation times (n = 1 for wildtype and *Fuca1*$^{(-/-)}$ MEFs).

the lysosomal compartment through M6P-independent pathways, e. g. β-glucocerebrosidase via Limp 2 (Reczek et al. 2007) or cathepsin D and cathepsin B via Lrp1 (Markmann et al. 2015). Moreover, ML II MEFs are also able to endocytose recombinant proteins that exhibit a M6P-modification. Here, ML II MEFs were used that harbored the same genetic modification as described by Markmann et al. (2015). After incubation with recombinant His$_6$-tagged α-L-fucosidase, a more than 100-fold increased intracellular α-L-fucosidase activity was detected. Of note, the endocytosis could be inhibited by 96 % by the addition of 5 mM M6P. These results confirm, that the endocytosis of the α-L-fucosidase in ML II MEFs is highly dependent

on the MPR-pathway. However, this effect was less pronounced in wildtype and *Fuca1*$^{(-/-)}$ MEFs (figure 4.39 A). The addition of 5 mM M6P resulted in a decreased endocytosis by only 37 - 85 % dependent on the individual cell line (n = 2 for wildtype and *Fuca1*$^{(-/-)}$ MEFs), indicating that the degree of the M6P-dependency might by cell line-specific and other endocytosis pathways might be involved. The inhibitory effect of M6P was further analyzed by adding different amounts of M6P during the incubation with His$_6$-tagged human α-L-fucosidase. The α-L-fucosidase activity in the cell lysates was decreased by approximately 50 % when using 0.1 mM M6P, while the maximal inhibition was reached by using 1 mM M6P (figure 4.39 B).

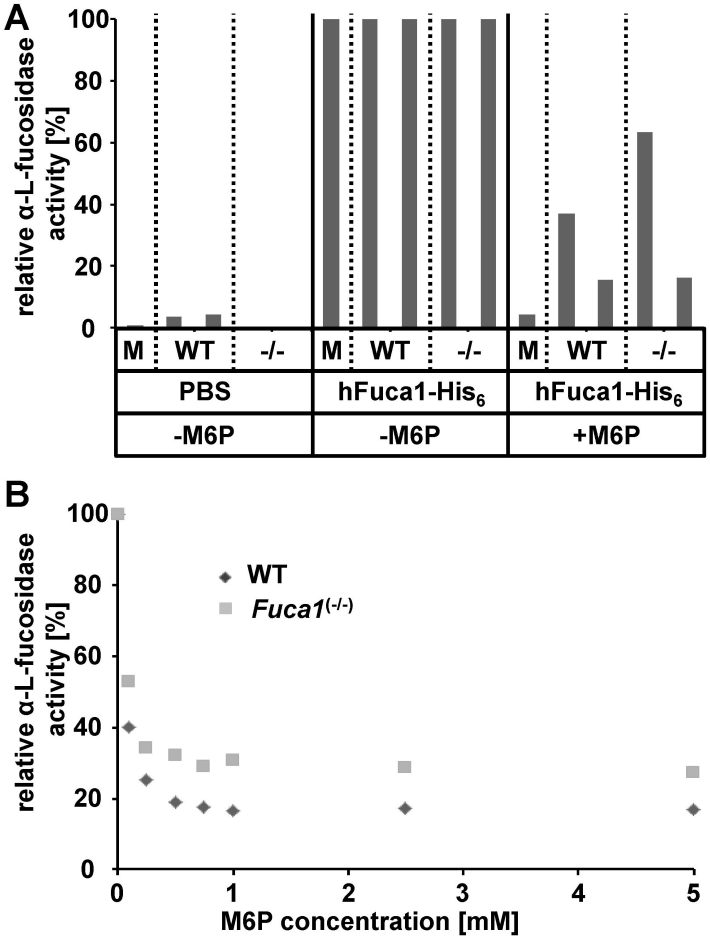

Figure 4.39: Endocytosis of His$_6$-tagged human α-L-fucosidase is dependent on the MPR pathway

(**A**) ML II MEFs (M; n = 1), wildtype as well as *Fuca1*$^{(-/-)}$ MEFs (n = 2) were treated with His$_6$-tagged human α-L-fucosidase. The endocytosis was performed in the presence or absence of 5 mM M6P. The cells were harvested by trypsination and the α-L-fucosidase activity was determined in the cell lysates. (**B**) Wildtpye and *Fuca1*$^{(-/-)}$ MEFs (n = 1) were treated with His$_6$-tagged human α-L-fucosidase in the presence of different amounts of M6P. The cells were harvested by trypsination and the α-L-fucosidase activity was determined in the cell lysates.

4.3.3 ERT of the constitutive fucosidosis mouse model

So far, it was shown that the His$_6$-tagged human α-L-fucosidase is able to digest storage material from *Fuca1*$^{(-/-)}$ mice *in vitro* and that the enzyme is endocytosed by mouse fibroblasts.

In order to analyze the effect of an ERT *in vivo*, 250 mU/g body weight of purified His_6-tagged human α-L-fucosidase were intravenously injected into the tail vein of a *Fuca1*$^{(-/-)}$ mouse. A short-term ERT was performed by applying two injections within one week (figure 4.40 A). As a control, a wildtype as well as a *Fuca1*$^{(-/-)}$ mouse were treated with PBS. After sacrificing, the mouse tissues were analyzed by enzyme activity assays and TLC for storage material. As expected, α-L-fucosidase activity was detected in tissue homogenates of the PBS-treated wildtype, but not of the PBS-treated *Fuca1*$^{(-/-)}$ mouse. The injection of the recombinant enzyme resulted in a massive increase in α-L-fucosidase activity that was more than 400-fold and 37-fold elevated in homogenates of the *Fuca1*$^{(-/-)}$ liver and spleen, respectively, compared to the PBS-treated wildtype tissue homogenates (table 4.5). In the α-L-fucosidase-treated *Fuca1*$^{(-/-)}$ kidney, one-third of the enzyme activity of the PBS-treated wildtype tissue was detected. The bioavailability of the α-L-fucosidase in the brain was rather low as only 1/10 of the enzyme activity of the PBS-treated wildtype brain was detected in α-L-fucosidase-treated *Fuca1*$^{(-/-)}$ brain. Of note, the mice were not perfused with PBS prior to sacrifice and a part of the α-L-fucosidase activity in the brain might be derived from recombinant enzyme that was still present in the circulation of the mouse.

In order to analyze the benefit of the short-term ERT, neutral oligosaccharides were isolated from kidney, spleen and brain and separated by TLC. The liver was not analyzed, as the high amount of glycogen prevented the proper analysis by TLC. As shown in figure 4.40 B, the storage material was completely absent in the spleen of the α-L-fucosidase-treated *Fuca1*$^{(-/-)}$ mouse. In the kidney some TLC bands disappeared or at least shifted towards higher retention factors, indicating an incomplete degradation of the storage material. However, no effects were visible in the composition and presence of storage material of the brain.

Table 4.5: α-L-fucosidase activity after short-term ERT

genotype	**WT**	***Fuca1*$^{(-/-)}$**		***Fuca1*$^{(-/-)}$**
injection of	**PBS**	**PBS**		**hFuca1-His_6**
	α-L-fucosidase activity [mU/mg]			
liver	0.13	0.0*	(*below detection limit)	56.59
kidney	2.64	0.0*		0.96
spleen	0.65	0.0*		24.01
brain	0.24	0.0*		0.02

As described in section 4.1.4, the *Fuca1* gene knock-out resulted in an altered expression of lysosomal glycosidases like β-hexosaminidase and α-mannosidase. In order to analyze the benefit of the short-term ERT on this secondary *Fuca1*$^{(-/-)}$ pathology, the β-hexosaminidase activity was determined in tissue homogenates of the ERT-treated mice. As expected, an elevated enzyme activity was found in PBS-treated *Fuca1*$^{(-/-)}$ tissues in comparison to the PBS-treated wildtype organs (figure 4.40 C), although the β-hexosaminidase activities slightly differed from those shown in section 4.1.4. This might be due to the fact, that the animals were of different ages (5 months of age in the former experiment and 3 months of age in the ERT study). In kidney and brain, almost no differences were found between the β-hexosaminidase activities of the α-L-fucosidase-treated and the PBS-treated *Fuca1*$^{(-/-)}$ mouse (figure 4.40 C). In contrast, a reduction in β-hexosaminidase activity was found in the liver and spleen of the α-L-fucosidase-treated *Fuca1*$^{(-/-)}$ mouse in comparison to the PBS-treated *Fuca1*$^{(-/-)}$ mouse. However, the enzyme activities were still elevated in comparison to the PBS-treated wildtype

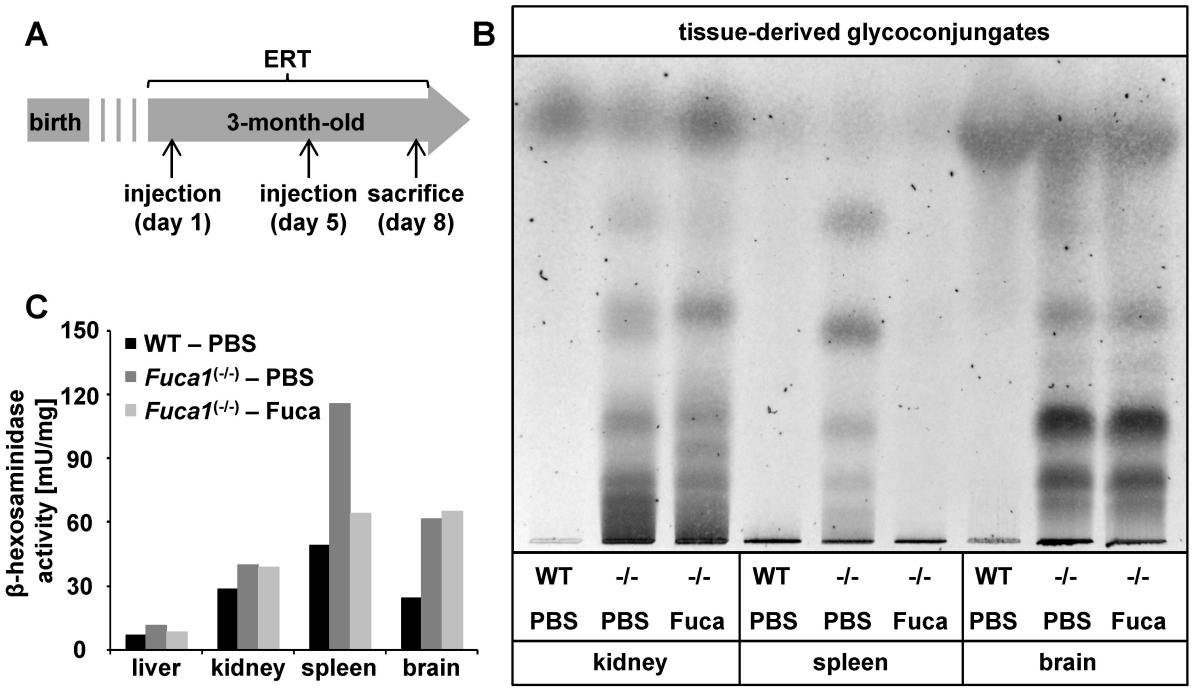

Figure 4.40: Short-term ERT of the fucosidosis mouse model
3-month-old mice were used for short-term ERT including two injections with 250 mU His_6-tagged α-L-fucosidase per 1 g body weight. As control, similar volumes of PBS were injected into a wildtype and a *Fuca1*$^{(-/-)}$ mouse. (**A**) Injections were performed at day one and five and organs were dissected at day eight. (**B**) Neutral oligosaccharides were extracted from kidney, spleen and brain and analyzed by TLC. (**C**) β-hexosaminidase activity was measured in tissue homogenates of ERT-treated mice.

mouse. It was not possible to analyze the significance of this effect, as only one mouse was used for each condition.

In summary, after short-term ERT with 250 mU/g body weight of His_6-tagged α-L-fucosidase, a high α-L-fucosidase activity was detected in liver and spleen, resulting in a complete digestion of storage material in the spleen. Moreover, the β-hexosaminidase activity was analyzed as secondary pathology and intermediate values between the activities of the PBS-treated wild-type and PBS-treated *Fuca1*$^{(-/-)}$ mouse were found. In contrast, minor α-L-fucosidase activities were detected in kidney and brain of the α-L-fucoisdase-treated *Fuca1*$^{(-/-)}$ mouse and only moderate or no effects were found regarding the digestion of the storage material and the β-hexosaminidase activities. These preliminary results suggest that the bioavailability of the His_6-tagged α-L-fucosidase is low in the kidney and especially in the brain. As expected, the major amount of the injected enzyme was taken up by liver and spleen.

4.4 Generation of an α-L-fucosidase-specific antibody

So far, a monoclonal antibody recognizing the RGS-His_6-tag was used to analyze the His_6-tagged human α-L-fucosidase. In order to enable the detection of the untagged human α-L-fucosidase as well as of the endogenous murine enzyme, a monoclonal α-L-fucosidase-specific antibody was generated. As a higher immunogenicity of the enzyme was expected in *Fuca1*$^{(-/-)}$ than in wildtype mice, *Fuca1*$^{(-/-)}$ mice were immunized in cooperation with Prof. Koch-Nolte (University Medical Center Hamburg-Eppendorf, Germany) by ballistic injection of coated gold particles carrying an expression plasmid encoding the murine α-L-fucosidase. The resulting antisera were tested by Western blot analysis of lysosome-enriched fractions from liver of wildtype and *Fuca1*$^{(-/-)}$ mice and against recombinant α-L-fucosidase, but no specific reactivity could be detected (data not shown). Nevertheless, the animals received a final immunization boost using purified His_6-tagged human α-L-fucosidase, resulting in a high specificity of the antisera against the recombinant enzyme in a dose-dependent manner (data not shown).

The mice were further used to generate hybridoma cell lines secreting monoclonal antibodies specific for α-L-fucosidase by the fusion of spleen-derived B-lymphocytes with a myeloma cell line (performed by Prof. Koch-Nolte, University Medical Center Hamburg-Eppendorf, Germany). The conditioned media of the cell lines were harvested and used to analyze the specificity of the secreted antibodies. Three hybridoma cell lines produced monoclonal antibodies that recognized the human α-L-fucosidase (A112, A177 and A180), as shown by immunoblotting of His_6-tagged human α-L-fucosidase (data not shown). Immunoblotting of tissue homogenates (data not shown) as well as lysosome-enriched fractions from wildtype and *Fuca1*$^{(-/-)}$ liver did not results in specific signals for α-L-fucosidase. In wildtype lysosomes, a band slightly above 50 kDa was detected, which could correspondent to the expected molecular weight of the α-L-fucosidase. However, a similar band was also seen in the *Fuca1*$^{(-/-)}$ sample, indicating an unspecific signal (figure 4.41 A, data were shown for A112 only). Moreover, wildtype MEFs were transfected with an expression plasmid for the human α-L-fucosidase and were analyzed by immunofluorescence staining. While PFA-fixation of the MEFs and permeabilisation using saponin showed no staining at all, a specific staining was observed after methanol fixation, in which hybridoma supernatants detected the overexpressed human enzyme (figure 4.41 B, data were shown for A112 and A180). Under these expressing conditions an intensive staining of the ER, but also a slight staining of the lysoso-

mal compartment was visible. Moreover, one hybridoma supernatant (A112) also recognized the overexpressed murine enzyme, whereas the endogenous enzyme in untransfected cells was not detected.

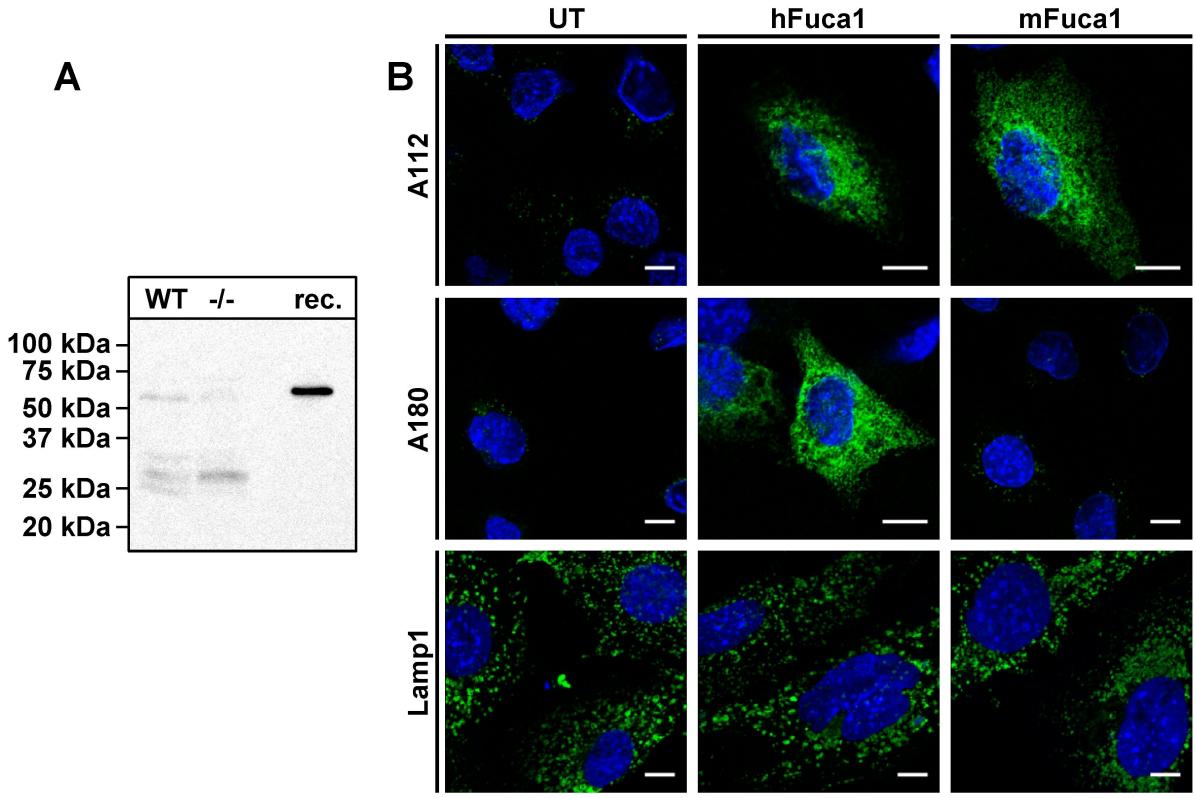

Figure 4.41: Analysis of the specificity of the Fuca1-specific monoclonal antibodies
(**A**) Experiment was performed in cooperation with Michael Weber (Master Thesis). 25 µg of lysosome-enriched fractions from wildtpye and *Fuca1*$^{(-/-)}$ mice as well as 100 ng of purified His_6-tagged human α-L-fucosidase (rec.) were used to analyze the specificity of the hybridoma cell culture supernatants against the α-L-fucosidase by immunoblotting. The results for the hybridoma cell line A112 are shown exemplarily. (**B**) Wildtpye MEFs were seeded on cover slips, were transfected with an expression plasmid for the human and the murine α-L-fucosidase, respectively, and were further applied to a methonal fixation. An immunofluorescence staining was performed using cell culture supernatants of the hybridoma cell lines A112 and A180. Untransfected cells were used as control. In parallel, MEFs were stained with an Lamp1-specific antibody and used as control for a lysosomal staining pattern. Cell nuclei were stained with DAPI (blue). Bars correspondent to 10 µm.

The hybridoma cell lines A112 and A180 were further re-selected to establish single cell clones with a high antibody secretion capacity. The cell clones were screened for specificity against the His_6-tagged human α-L-fucosidase by ELISA tests (re-selection and screening

was performed in cooperation with Prof. Koch-Nolte, University Medical Center Hamburg-Eppendorf, Germany). Those cell clones displaying the highest antibody production were further expanded, the cell culture supernatants were harvested and further analyzed by immunoblotting. Both hybridoma supernatants (A112 and A180) detected the His_6-tagged human α-L-fucosidase in a dose-dependent manner (figure 4.42). An optimal dilution to detect at least 50 ng of the recombinant enzyme was determined with 1 : 1000.

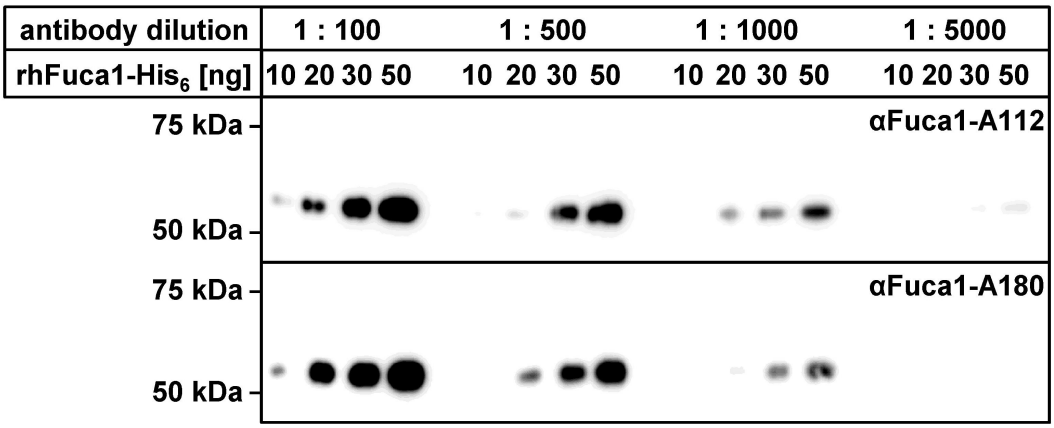

Figure 4.42: Fuca1-specific monoclonal antibodies detect the recombinant enzyme in a dose-dependent manner

The specificity of the hybridoma supernatants A112 and A180 against the human α-L-fucosidase was analyzed by immunoblotting using different amounts (10, 20, 30 and 50 ng) of the His_6-tagged enzyme. Different dilutions of hybridoma supernatants were tested (1 : 100 – 1 : 5000).

The specificity of the hybridoma supernatants was further analyzed by immunoblotting of cell lysates from transfected Neu2A cells. The supernatant of the hybridoma cell line A112 showed a higher reactivity against the murine enzyme than against the human α-L-fucosidase (figure 4.43 A). However, the endogenous murine enzyme in untransfected cells was not detected. The supernatant of the hybridoma cell line A180 recognized only the human enzyme (figure 4.43 B). Of note, both monoclonal antibodies detected the purified recombinant His_6-tagged α-L-fucosidase at approximately 55 kDa (figure 4.42), whereas two bands were visible in transfected cells (52 kDa and 48 kDa; figure 4.43).

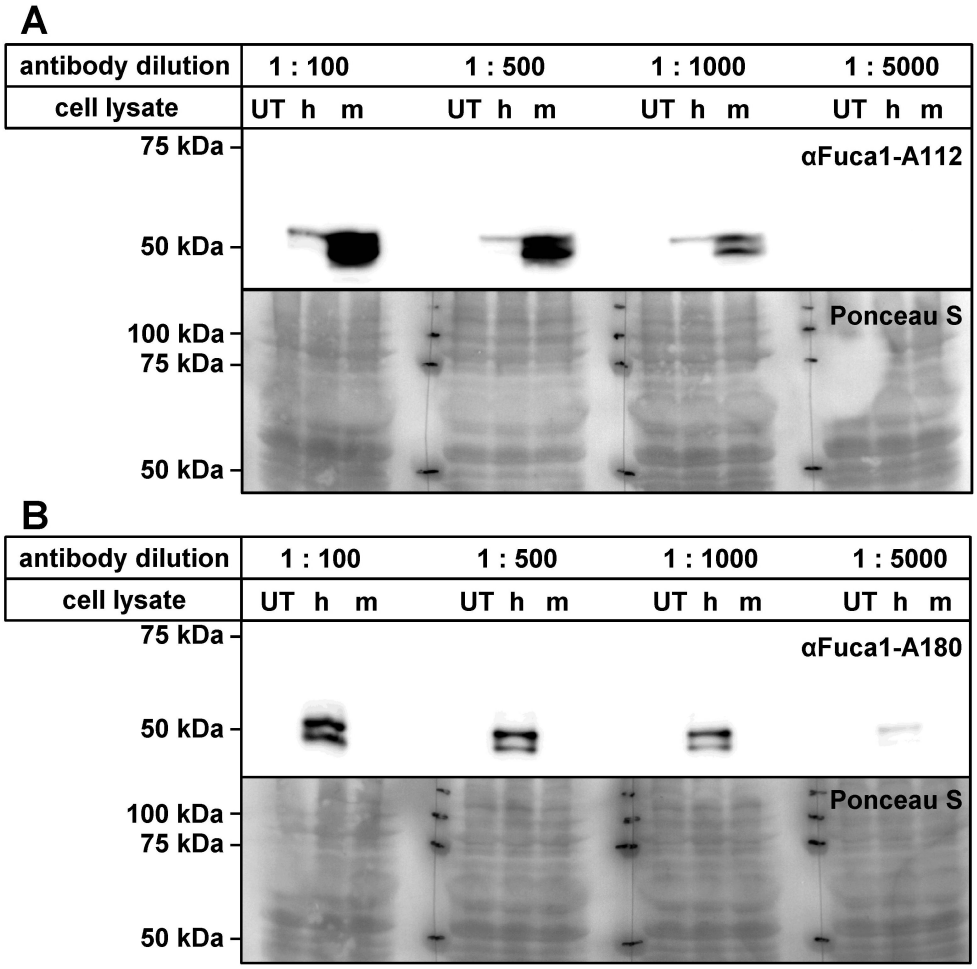

Figure 4.43: Fuca1-specific monoclonal antibodies do not detect endogenous murine α-L-fucosidase by immunoblotting

Neu2A cells were transfected with an expression plasmid for the human (h) and the murine (m) α-L-fucosidase, respectively. Untransfected cells (UT) were used as control. The specificity of the hybridoma supernatants A112 and A180 against the α-L-fucosidase was analyzed by immunoblotting of the cell lysates. Different dilutions were tested (1 : 100 – 1 : 5000). A ponceau S staining was performed as loading control.

5 Discussion

The lysosomal storage disease is mainly characterized by progressive mental retardation and neurological deterioration leading to premature death (Durand et al. 1966, Willems et al. 1991). The disease is caused by the deficiency of the lysosomal enzyme α-L-fucosidase (van Hoof and Hers 1968b) that is responsible for cleaving off fucose residues during the degradation of fucosylated *N*-glycans and glycolipids. α-L-Fucosidase deficiency leads to the accumulation of fucosylated glycocompounds (Michalski and Klein 1999). Here, the generation and characterization of the first fucosidosis mouse model is described, which resembles a mild phenotype of the human disease. As an initial step towards a disease therapy, the production and purification of a His_6-tagged human α-L-fucosidase derived from CHO-K1 cells was shown. The purified enzyme was finally used in a first ERT approach of the fucosidosis mouse model, resulting in a complete digestion of the accumulated storage material in the spleen. These preliminary results provide promising data with regard to a successful ERT of the fucosidosis disease.

5.1 The fucosidosis mouse model

Although fucosidosis is known since 1966 (Durand et al. 1966), only limited data are available from human patients. Besides the human fucosidosis, a naturally occurring dog model in English Springer spaniel was used for disease characterization (Kelly et al. 1983, Kondagari et al. 2011a, Fletcher et al. 2014), as well as basic studies on an intracisternal ERT (Kondagari et al. 2011b, Kondagari et al. 2015). Nevertheless, the generation of a fucosidosis mouse model was addressed, as the mice exhibit several advantages over the dog model e. g. easier breeding and housing, a controlled genetic background, a shorter life span and a high number of available animals. With regard to establish an ERT for the fucosidosis disease, particularly the much lower body weight reduces the expenses of a pre-clinical study in the mouse model.

5.1.1 Generation and validation of the *Fuca1* gene knock-out

Fuca1$^{(-/-)}$ mice were generated by a gene targeting strategy which is a commonly used technique to introduce genomic modifications in mice (Capecchi 2005), where the open reading frame of the target gene is disrupted by insertion of the bacterial *nptI* gene. The *Fuca1*$^{(-/-)}$ allele was successfully validated on genomic level by PCR and the precise site of homologous recombination was analyzed by sequencing. On transcript level, the expression of the *Fuca1* gene was reduced to 1 % in *Fuca1*$^{(-/-)}$ liver and kidney, whereas still 10 % - 20 % of the *Fuca1* transcript were detected in spleen and brain. As expected, the gene targeting did not abolish the transcription of the *Fuca1* gene. Rather, the insertion of the *nptI* gene into exon 1 of the *Fuca1* gene resulted in the transcription of mRNA harboring a premature termination codon (PTC). Such mRNAs are recognized by the so-called nonsense-mediated mRNA decay (NMD), a conserved quality control mechanism that degrades mRNAs containing PTC elements (Chang et al. 2007, Schweingruber et al. 2013). Thus, the *Fuca1*$^{(-/-)}$ allele is recognized by the transcription machinery but the resulting mRNA is degraded immediately. In this study, the transcript level was analyzed by Real-Time PCR determining the steady-state mRNA amounts in tissues, where a part of the newly synthesized mRNA of the *Fuca1*$^{(-/-)}$ allele could still be detected before it was recognized and degraded by NMD. As described above, tissue-specific differences in the extent of *Fuca1* transcript reduction in the *Fuca1*$^{(-/-)}$ mice were observed and might be caused by differences in the tissue-specific *Fuca1* expression. In tissues with high *Fuca1* expression, a larger amount of *Fuca1* transcript is synthesized and subsequently degraded by NMD compared with tissues with low *Fuca1* expression, resulting in a larger extent of *Fuca1* transcript reduction.

It is supposed that the transcript degradation is initiated during the first round of translation (Chang et al. 2007, Schweingruber et al. 2013) resulting in a shortened polypeptide that is not functional, as only the first 77 out of 452 amino acids of the α-L-fucosidase were translated. Here, the complete *Fuca1* gene knock-out was confirmed by activity measurements for α-L-fucosidase in tissue homogenates as well as lysosome-enriched fractions demonstrating the absence of enzyme activity.

5.1.2 The *Fuca1* gene knock-out causes a differential regulation of other lysosomal proteins

N-glycans are degraded stepwise by different exoglycosidases. For complex *N*-glycans, the lysosomal α-L-fucosidase catalyzes the initial step in the degradation process (figure 1.3).

Its deficiency leads to the termination of the degradation process and the accumulation of the residual *N*-glycan. These pathological circumstances result in lysosomal storage (Winchester 2005), and as a cellular response, an altered regulation of several lysosomal proteins, besides the deficient protein, was often observed in LSDs, e. g. changes in the expression of genes for several lysosomal hydrolases were recorded in a mouse model for MPS VII (Woloszynek et al. 2004). Moreover, increased specific activities of lysosomal enzymes were measured in tissues from human LSD patients (van Hoof and Hers 1968b, Sandhoff et al. 1971). With respect to fucosidosis, an enhanced activity of several glycosidases was detected in the liver of three human patients (van Hoof and Hers 1968a). In the *Fuca1*$^{(-/-)}$ mice, the regulation of lysosomal enzymes participating in the degradation of *N*-glycans as well as of the lysosomal membrane protein Lamp1 was investigated and an enhanced transcription of all analyzed genes was found in the *Fuca*$^{(-/-)}$ brain. The increased gene expression might represent a cellular response to lysosomal storage and lysosomal stress resulting in an activation and nuclear translocation of the transcription factor EB (TFEB) and / or E3 (TFE3) and an upregulation of genes harboring one or several CLEAR (coordinated lysosomal expression and regulation) elements. In fact, a CLEAR consensus sequence was reported in the promoter regions of all genes analyzed in this study, except the *Fuca1* itself which lacks the CLEAR motif (Sardiello et al. 2009). However, the expression of genes for several lysosomal proteins was tissue-dependent. As mentioned above, a general upregulation was detected in the *Fuca*$^{(-/-)}$ brain, while the expression of nearly all analyzed genes was unaffected in the *Fuca*$^{(-/-)}$ kidney. Hence, the putative regulation of these genes by TFEB / TFE3 is obviously tissue-dependent and could be due to a tissue-specific expression of the transcription factors, which has to be further analyzed. Moreover, other regulatory factors besides TFEB / TFE3 might be involved, as the expression of nearly all analyzed genes in the kidney was unaffected by the *Fuca1* gene knock-out, whereas the expression of β-hexosaminidase and α-mannosidase was decreased, indicating a differential regulation of single genes. Interestingly, the enzyme activities of these two glycosidases were increased in the *Fuca*$^{(-/-)}$ kidney, indicating an enhanced stability of the proteins. The half-life of the enzymes might be increased due to the general inhibition of lysosomal proteolysis, which could result from the high storage burden of the endosomal-lysosomal compartment (Platt et al. 2012).

An increased amount of Lamp1 protein has been described as a diagnostic marker in a large subset of LSDs, e. g. in mouse models for α-mannosidosis (Stinchi et al. 1999) and mucolipidosis II (Kollmann et al. 2012). Moreover, the amount of Lamp1 protein is increased in

blood plasma of patients suffering from, e. g., α-mannosidosis, galactosialidosis and several mucopolysaccharidoses (Meikle et al. 1997). The accumulation of storage material in LSDs results in a massively increased number and size of lysosomes rising from 1 % of total cell volume up to 50 % (Meikle et al. 1997). Such an increased amount of lysosomal membranes needs additional lysosomal membrane proteins like Lamp1. Indeed, elevated levels of Lamp1 protein were also found in several tissues of the *Fuca*$^{(-/-)}$ mice, indicating the formation of a LSD-like phenotype in the mouse model.

5.1.3 The phenotype of *Fuca1*$^{(-/-)}$ mice resembles a mild form of the human disease

Although there exists a continuous clinical spectrum in human fucosidosis, the disease is classically divided into a severe type 1 and a milder type 2. Patients suffering from type 1 fucosidosis are characterized by an early onset and rapid progression of clinical symptoms, particularly of neurodegenerative symptoms, leading to death within the first decade of life. In contrast, disease progression in type 2 fucosidosis is slower and patients may survive until the second or third decade of life (Willems et al. 1991). Initially it had been suggested, that type 2 fucosidosis is characterized by development of angiokeratoma corporis diffusum. However, several type 2 fucosidosis cases lacking angiokeratoma as well as several type 1 fucosidosis cases with prominent angiokeratoma were described. Hence the occurrence of angiokeratoma was designated to a third (juvenile) type of fucosidosis (Willems et al. 1991, Kanitakis et al. 2005). In this work, the phenotype of the *Fuca1*$^{(-/-)}$ mice was characterized. The animals suffered from progressive clinical symptoms leading to premature death in the first half of their lives. However, an onset of clinical symptoms was not observed before six months of age and no skin abnormalities were seen so far. Hence, the phenotype of the *Fuca1*$^{(-/-)}$ mice closely resembled that of the milder type 2 fucosidosis in human. Interestingly, no genotype - phenotype correlation was found for human fucosidosis (Willems et al. 1991) and as well as other glycoproteinoses (except sialidosis; Malm et al. 2013). Comparably, the manifestation of a mild LSD phenotype was also observed in a mouse model for α-mannosidosis, despite its total lack of α-mannosidase activity (Stinchi et al. 1999), and was also seen in mice with arylsulfatase B and arylsulfatase A deficiency, respectively (Evers et al. 1996, Hess et al. 1996).

Willems et al. (1991) reported a continuous spectrum of clinical phenotypes in fucosidosis patients rather than a strict classification into type 1 and 2 fucosidosis. However the severity

of the disease is not connected to residual α-L-fucosidase activity or the genetic heterogeneity of the fucosidosis patients. Other disease modifying factors were suggested to influence the clinical phenotype. A plausible potential candidate is the second α-L-fucosidase (*Fuca2*) that is also referred to as plasma α-L-fucosidase, although it was recently identified as putative lysosomal protein by analysis of the lysosomal proteome (Sleat et al. 2008) and by localization studies using mCherry-fusion constructs (Huang et al. 2014). However, a specific activity assay for α-L-fucosidase 2 as well as data regarding its substrate specificities are not available so far. However, Sobkowicz et al. (2014) reported activity of the α-L-fucosidase 2 against the pseudosubstrate 4-MUF under overexpressing conditions in CHO cells, but this fucosidase activity might also be derived from endogenous α-L-fucosidase 1. Here, the *Fuca1*$^{(-/-)}$ mice might serve as an ideal model to study α-L-fucosidase 2 activity, as these measurements are not influence by activity derived from α-L-fucosidase 1. So far, no α-L-fucosidase activity could be detected in *Fuca1*$^{(-/-)}$ tissues and lysosome-enriched fractions whatever pH value was tested. Hence, the α-L-fucosidase 2 might not be translated or possesses no activity under the specific conditions of the *in vitro* assay. In further experiments, the α-L-fucosidase activity in the plasma of the *Fuca1*$^{(-/-)}$ mice should be also measured, but so far, there exists no evidence for α-L-fucosidase 2 as a disease modifying factor for fucosidosis.

5.1.3.1 Storage pathology of visceral organs

The *Fuca1*$^{(-/-)}$ mice showed accumulation of storage material with variable degree and heterogeneous nature in several visceral organs like liver, kidney, spleen, urinary bladder, gall bladder and pancreas. Most of these findings were comparable to those seen in human fucosidosis patients. The hepatic sinusoidal cells as well as the Kupffer cells contained translucent foam-like storage vesicles in human patients as well as in *Fuca1*$^{(-/-)}$ mice. In contrast, mainly heterogeneous storage material of moderate electron density was found in human hepatocytes. Interestingly, Freitag et al. (1971) reported that this storage material tended to aggregate in hepatocytes near the bile canaliculus in a severely affected human patient and a similar localization of electron-dense storage vacuoles was also observed in the *Fuca1*$^{(-/-)}$ mice. The accumulation of storage material in the different human hepatic cell types may contribute to the hepatomegaly that is observed in approximately 40 % of the fucosidosis cases (Willems et al. 1991). Here, the *Fuca1*$^{(-/-)}$ mice resemble the phenotype of the majority of fucosidosis patients, where no hepatomegaly was observed.

The spleen of human fucosidosis patients was not investigated so far by ultrastructural analysis. In English Springer spaniel, a vacuolation of splenic macrophages has been reported (Kelly et al. 1983), whereas in *Fuca1*$^{(-/-)}$ mice several cell types of the spleen like macrophages, sinusoidal endothelial cells as well as reticular cells were found to contain storage vacuoles. By electron microscopic analysis it was shown that the lymphocytes of *Fuca1*$^{(-/-)}$ mice are affected. This was also seen in peripheral blood smears of human fucosidosis patients (Durand et al. 1969). A splenomegaly was not observed in *Fuca1*$^{(-/-)}$ mice, comparable to the majority of human fucosidosis patients, as a splenomegaly was observed in only 25 % of all fucosidosis cases (Willems et al. 1991). Moreover, pathological alterations of the pancreas had been described in human patients (Willems et al. 1991) as well as affected English Springer spaniel (Kelly et al. 1983) and were also seen in the *Fuca1*$^{(-/-)}$ mice.

In the kidney, foam-like vacuoles were observed in glomerular podocytes and in the collecting ducts, especially in intercalated cells of *Fuca1*$^{(-/-)}$ mice. Comparably, vacuolation of renal tubular cells is also known from a naturally occurring fucosidosis case in a domestic short hair cat (Arrol et al. 2011) and was also reported in English Springer spaniel (Kelly et al. 1983). With regard to human fucosidosis, Durand et al. (1969) identified a degeneration of the kidney as well as storage vacuoles in glomerular epithelial cells in two severely affected children, but a renal pathology is no common clinical symptom of human fucosidosis so far. Besides the histological findings, the renal functionality was addressed in the *Fuca1*$^{(-/-)}$ mice. Glomerular podocytes represent the blood-urine-barrier of the kidney. Although they were affected from storage pathology, a proteinuria was not observed indicating that the blood-urine-barrier is still functional. The clinical chemistry revealed slightly decreased electrolyte concentrations in the blood serum of *Fuca1*$^{(-/-)}$ mice. In the collecting ducts, urea is reabsorbed as a prerequisite for the formation of an osmotic gradient in the interstitium of the kidney, which triggers the uptake of electrolytes from urine into the blood and disabilities in the formation of the osmotic gradient due to the severe accumulation of storage material in the collecting ducts might result in slightly decreased electrolyte concentrations as observed in the blood serum of *Fuca1*$^{(-/-)}$ mice. Especially the intercalated cells of the collecting ducts were affected from storage, which participate in the maintenance of the acid-base homeostasis by secretion of protons. The pH value of the urine was not analyzed so far in *Fuca1*$^{(-/-)}$ mice but should be addressed in further studies. Analysis of clinical chemistry was not reported so far for human fucosidosis patients, but should be routinely included in examinations of patients, especially as blood and urine are easy accessible.

5.1.3.2 Neuropathology and behavior

Human fucosidosis patients are mainly characterized by neurological symptoms like mental retardation, neurological decline resulting in severe motor disabilities, hypertonia and to a lesser extent hypotonia as well as seizures (Willems et al. 1991). The underlying pathological processes remain largely unknown and only a few reports regarding the histological alterations of the disease are available. A recent MR study (magnetic resonance tomography) reported increased cerebellar volumes in early childhood of fucosidosis patients (Kau et al. 2011). Additionally, cerebral and cerebellar atrophy was reported in later stages of the disease (Inui et al. 2000) and might result from neuronal cell death that was reported in a few fucosidosis cases (Durand et al. 1969, Galluzzi et al. 2001). The macroscopic inspection of the *Fuca1*$^{(-/-)}$ mice revealed several comparable pathological alterations like the swollen cerebellum and the reduced size of the cerebrum. So far, the observed encephalic volume alterations are based on only few animals and continued analyses are necessary to confirm these observations.

The microscopic alterations of the brain are well studied in English Springer spaniel, where foam-like storage vacuoles and axon spheroids were seen throughout the whole brain together with a progressive neuronal cell death, myelination defects and inflammatory reactions like the activation of astrocytes and microglia (Kondagari et al. 2011a, Fletcher et al. 2011, Fletcher et al. 2014). In the *Fuca1*$^{(-/-)}$ mice, mainly translucent storage vacuoles were found in all regions of the brain, particularly in the neuronal perikarya of the hippocampus, cerebral cortex and cerebellum. Moreover, axon spheroids are common to many LSDs and were observed in mouse models for e. g. α-mannosidosis (Stinchi et al. 1999), mucolipidosis II (Kollmann et al. 2012), MPS IIIE (Kowalewski et al. 2015) and Niemann-Pick disease type C (NPC; Zervas et al. 2001). The formation of such axonal swellings is often accompanied with neuronal cell death (Walkley et al. 2010). In the canine fucosidosis model, an increasing number of axon spheroids was found in the hippocampus and the cerebellum (Kondagari et al. 2011a) and was similarly observed in the *Fuca1*$^{(-/-)}$ mice. In human patients, neuronal ballooning was also observed by MR analysis (Galluzzi et al. 2001, Oner et al. 2007).

The most prominent neuronal pathology of the *Fuca1*$^{(-/-)}$ mice was observed in Purkinje cells. A massive loss of this cell type was shown during disease progression and at 11 months of age almost no Purkinje cells were found in the *Fuca1*$^{(-/-)}$ cerebellum. A degeneration of Purkinje cells is commonly observed in LSDs affecting the CNS, e. g. in Niemann-Pick disease type C, where this neuronal cell type seems particularly vulnerable to lysosomal storage (Elrick et al.

2010). The exact mechanisms underlying the early Purkinje cell death remain to be analyzed, especially as some cells located in the cerebellar lobi X of a mouse model for Niemann-Pick disease type C are highly resistant to cell death (Chung et al. 2016). Loss of Purkinje cells was also found in English Springer spaniel suffering from fucosidosis (Kondagari et al. 2011a) and in brain biopsies of two severely affected human patients (Durand et al. 1969). These cells are the only efferent neurons of the cerebellar cortex and are essential for the modulation of motor function. Hence, the reduced number of efferent neurons may contribute to motor deterioration and coordinatory deficits observed in fucosidosis. In the dog model, prominent motor deficits, delayed learning and, in late disease, severe mental decline and disorientation were reported (Fletcher et al. 2014). Detailed behavioral analysis of the *Fuca1*$^{(-/-)}$ mice were performed at 3 and 7 months of age indicating motor dysfunction and coordinatory deficits, reduced activity as well as cognitive impairment. In some behavioral tests (e. g. rotarod test), differences between the *Fuca1*$^{(-/-)}$ and control mice were not observed in young animals, but became more significant at older ages, indicating a disease progression coinciding with the Purkinje cell degeneration. In the cerebrum, storage vacuoles were seen in neuronal perikarya and neuronal cell death was observed in the hippocampus and cerebral cortex. These pathological alterations might contribute to the deficits of contextual and cued fear memory. The neuropathology and behavioral deficits of *Fuca1*$^{(-/-)}$ mice closely resemble that of human patients and reflect the main clinical hallmark of fucosidosis.

Neuronal cell loss is often accompanied by inflammatory reactions and inflammation of the brain as well as an excessive appearance of reactive astrocytes are common features of an affected CNS in many LSDs (Vitner et al. 2010). This was also analyzed in detail in the canine fucosidosis model. Kondagari et al. (2011a) reported an increasing number of microglia during disease progression as well as an increased astrocytosis in the cerebral cortex and the cerebellum. A recent study based on MRS analysis (magnetic resonance spectroscopy) also revealed astrocytosis in the brain of a human patient (Oner et al. 2007). Similar results were shown for the *Fuca1*$^{(-/-)}$ mice. A prominent microgliosis and astrogliosis was seen in all regions of the brain. Especially in the cerebellum, reactive astrocytes were closely restricted to the Purkinje cell layer at already 3.5 months of age, which is a disease stage, where the Purkinje cells are still intact. Although neuroinflammation is typically a protective response of the innate immune system, chronic inflammation and astrocyte activation may contribute to neurodegeneration and loss of Purkinje cells observed in later stages of the disease and may result from the chronic production of cytokines and chemokines creating a neurotoxic environment

(Platt et al. 2012, Bosch and Kielian 2015). The contribution of astrocytes to neurodegeneration was analyzed in more detail in a mouse model for multiple sulfatase deficiency, which is caused by mutations in the *Sumf1* gene. The mice harbored an astrocyte-specific *Sumf1* depletion and the severe lysosomal storage in astrocytes resulted in the degeneration of cortical neurons *in vivo* indicating a cell-autonomous mechanism for neurodegeneration (Di Malta et al. 2012), which was also suggested in a mouse model of Niemann-Pick disease type C (Elrick et al. 2010).

Over the last decades, information based on MR findings of fucosidosis patients have been published, revealing neuropathological changes in the white matter as a common feature of the disease. However, there is an open question, whether these pathological findings were caused by hypomyelination or demyelination (Galluzzi et al. 2001, Oner et al. 2007, Alexander et al. 2014, Jain et al. 2014). Hypomyelination describes an incomplete myelin formation, whereas an initial complete myelination is achieved in an demyelinating disease, which subsequently decreases during disease progression. A hypomyelination was identified in the canine model (Fletcher et al. 2011). This defect is caused by an early apoptosis of oligodendrocytes for a yet unknown reason (Fletcher et al. 2014). In contrast, no myelination defects were observed in the *Fuca1*$^{(-/-)}$ mice. Real-Time PCR results revealed no differences in the major myelin structural protein Plp1 mRNA expression between wildtype and *Fuca1*$^{(-/-)}$ mice, whereas a significantly decreased expression was detected in the canine model (Fletcher et al. 2011). In contrast, MBP mRNA expression was increased in the *Fuca1*$^{(-/-)}$ mice, whereas no differences in MBP protein expression could be verified, which could indicate an increased MBP protein turnover. Hence, oligodendrocytes of the fucosidosis mouse model seem to be affected, but to a lesser extent than in the dog model or in human patients and they may compensate their deficits by an enhanced turnover of some myelin components like MBP. Interestingly, species-specific differences in myelination defects were also reported for metachromatic leukodystrophy (MLD), a LSD caused by the deficiency of arylsulfatase A. A MLD mouse model as well as human MLD patients showed prominent pathological alterations in the CNS, especially in oligodendrocytes, but the mouse model lacks the massive myelin degeneration that is characteristic for the human disease (Hess et al. 1996, Gieselmann et al. 1998).

5.1.4 Storage material

5.1.4.1 Core-fucosylated *N*-glycans are the primary storage material in mouse fucosidosis

The accumulation of fucose-containing oligosaccharides, glycoasparagines and glycosphingolipids are a basic feature of human fucosidosis and more than ten different oligosaccharide and glycoasparagine species were identified, which were also partially excreted with the urine (Michalski and Klein 1999). As in human patients (Tsay and Dawson 1976, Yamashita et al. 1979, Michalski and Klein 1999), the corefucosylated glycoasparagine Asn-GlcNAc-Fuc is the major storage material that is excreted with the urine of *Fuca1*$^{(-/-)}$ mice, while it was not detected in wildtype animals. This fucosylated glycocompound may serve as a biomarker for the disease and may improve diagnosis, especially as urine samples of patients are easily accessible.

Moreover, Asn-GlcNAc-Fuc was also identified as storage material in different tissues of the *Fuca1*$^{(-/-)}$ mice along with other glycoasparagines like the asparaginyl-linked pentasaccharide Asn-GlcNAc-(Fuc)-GlcNAc-Man-Man. Both storage compounds are also known from human patients (Tsay et al. 1976, Tsay and Dawson 1976, Michalski and Klein 1999) and Asn-GlcNAc-Fuc was also found in tissues of affected English Springer spaniel (Abraham et al. 1984). However, the nature of some storage conjungates derived from urine as well as from tissues of the *Fuca1*$^{(-/-)}$ mice are still unknown, indicating a complex mixture of undigested fucosylated glycocompounds, which has to be further analyzed. Of note, only single spots of TLC separated storage material were analyzed so far by mass spectrometry. These analyses have to be expanded, as considerable more (>10) oligosaccharide and glycoasparagine species are known to accumulate in human fucosidosis. So far, the TLC-separated storage material of the *Fuca1*$^{(-/-)}$ mice was first derivatized with the fluorescent label 2-AB, was then applied to a hydrophobic interaction chromatography (HILIC) and analyzed by mass spectrometry. However, a derivatization of the storage material is only possible in the presence of a free reducing end on the oligosaccharides and, hence, asparaginyl-linked oligosaccharides are not labeled. However, only asparaginyl-linked storage material (non-derivatized), but no free oligosaccharides were identified so far in *Fuca1*$^{(-/-)}$ tissues (as discussed below) and the non-derivatized storage material resulted in very low signal intensities in the mass spectrometry. As an alternative, the storage material could be permethylated prior to mass spectrometry, as a permethylation converts the hydroxyl groups of the sugar residue to methyl ethers, which

increases the efficiency of the ionization at these positions resulting in an increased signal intensity (Desantos-Garcia et al. 2011, Harvey 2011) and may enable the detection of more storage material species. This technique was also used for analysis of storage material in the urine of patients suffering from aspartylglucosaminuria, a LSD where also asparaginyl-linked *N*-gylcans accumulate (Aula et al. 1980).

In *Fuca1*$^{(-/-)}$ mice, all identified storage compounds represented structures of core-fucosylated *N*-glycans that were still linked to the asparagine residue. The presence of the α1,6-(core)-fucosylation is known to sterically inhibit the lysosomal aspartylglucosaminidase so that the asparagine residue can not be removed (Noronkoski and Mononen 1997). However, in human fucosidosis patients, several oligosaccharides with terminal fucose residues but without the core-fucosylation were identified that lacked the asparagine residue (Tsay et al. 1976, Tsay and Dawson 1976, Nishigaki et al. 1978, Michalski and Klein 1999). Due to the lack of a core-fucose residue the asparagine residue became accessible to the aspartylglucosaminidase. However, storage material with terminal fucose residues was not identified so far in the *Fuca1*$^{(-/-)}$ mice and may reflect species-specific differences in the degree of terminal fucosylation of *N*-glycans.

In human patients, glycosphingolipid-derived fucose-containing H- and Lewis^{X}-antigens were also found as storage material. In particular, the H-antigen was identified as the major storage product of the liver (Dawson and Spranger 1971, Tsay et al. 1976, Michalski and Klein 1999). However, such storage compounds were not described so far in the canine model and were not found in the *Fuca1*$^{(-/-)}$ mice. The Lewis blood group antigens can be divided into four subtypes: Le^{a}, Le^{b}, Le^{x} and Le^{y} (figure 1.4) and it is reported that mice do not possess Le^{x} and Le^{y} antigens (Thorpe and Feizi 1984). However, there exists no information, whether mice exhibit a fucosyltransferase activity that enables the synthesis of Le^{a} and Le^{b} antigens. Moreover, the expression of Lewis antigens in humans is restricted to tissues originating from endoderm (e. g. digestive and respiratory mucosa, epithelium of the biliary ducts and the urinary tract; Oriol et al. 1986), whereas little is known about tissue-specific expression of Lewis antigens in mice. Besides these Lewis antigens, there exist also species-specific differences in synthesis and availability of the blood group antigens H, A and B between mouse and men. Comparable with the human ABO system, also mice do express the H-, A- and B-antigens. However, the murine ABO locus encodes a glycosyltransferase with both A and B transferase activity and all mouse strains tested by Yamamoto et al. (2001) were of blood group AB. Moreover the tissue-specific localization of the blood group antigens is different. During evolution,

men and some primates were the only species that adapted blood group antigen expression on their erythrocytes. The red blood cells of other mammals are completely devoid of ABH antigens (Oriol et al. 1986). Hence, it is likely that no differences in the glycosphingolipid content were found between wildtype and *Fuca1*$^{(-/-)}$ mice by TLC. Nevertheless, at least the H antigens should be expressed in murine tissues originating from endoderm and in further studies these tissues should be analyzed in more detail by immunofluorescence staining using the lectin from *Ulex europaeus*, which recognizes the H-antigen.

The *Aleuria aurentia* lectin was used to stain α1,6-core-fucosylated storage material in histological sections of different organs from *Fuca1*$^{(-/-)}$ mice. However, this particular lectin stained only the membrane of storage vacuoles whereas their content remained unstained, which might reflect the water-soluble properties of the storage material. Most of the accumulated glycocompounds might be washed out during tissue fixation and staining, as the majority of storage vacuoles appeared also empty in light-microscopy analysis and electron-translucent in TEM. However, the use of the *Aleuria aurentia* lectin resulted in a stronger staining intensity in the *Fuca1*$^{(-/-)}$ tissues which might be due to the increased amount of lysosomal membrane proteins harboring complex *N*-glycans like Lamp1. Prior to the lectin staining, the tissues were fixed with formaldehyde, which might result in a cross-linkage of free amino groups (mainly lysine residues) to other free amino acid residues at the surface of proteins (e. g. arginine, asparagine, glutamine, histidine, tryptophan, tyrosine; Metz et al. 2004). The cross-linkage can occur in an intra- and intermolecular manner by formation of methylene bridges. As the storage material of the *Fuca1*$^{(-/-)}$ mice is still connected to the asparagine residue, it contains a free primary amino group. However, formaldehyde does not cross-link two primary amino groups (Metz et al. 2004). Thus, the storage material can not be linked together but only to other lysosomal proteins (e. g. lysosomal membrane proteins at the limiting membrane of the storage vacuoles). Although the majority of the storage material is washed out during tissue preparation, a proportion may be fixed in close proximity to the lysosomal membrane, which might result in a brighter lectin staining intensity in the *Fuca1*$^{(-/-)}$ mice.

In contrast to formaldehyde, glutaraldehyde contains two reactive aldehyde groups resulting in a different cross-linking mechanism. Only primary amino groups are addressed and connected intra- and intermolecularly (Migneault et al. 2004). Thus, glutaraldehyde might be able to cross-link and immobilize storage material that is washed out when using formaldehyde. It should be noted, that glutaraldehyde can not be used prior to immunofluorescence stainings, as it leads to a masking of the majority of antigens. However, it is widely used for tissue

fixation and preparation for electron microscopiy analysis. Indeed, TEM analysis revealed storage vacuoles in the *Fuca1*$^{(-/-)}$ mice tissues (e. g. in the renal collecting ducts or in Purkinje cells) that were partially filled with floccular material of moderate electron density. These results might represent water-soluble storage material that was cross-linked by glutaraldehyde thereby forming large aggregates unable to cross the permeabilized lysosomal membrane.

In summary, the biochemical phenotype of the *Fuca1*$^{(-/-)}$ mice resembled that of human fucosidosis patients and affected English Springer spaniel. Neutral glycoasparagines were found as the major storage material in the mice and were also partially excreted with the urine. However, the analysis of the accumulating glycoasparagine and oligosaccharide species should be extended and especially the investigations of fucosylated glycolipids as storage material should be addressed in more detail.

5.1.4.2 Secondary storage material

The monogenetic defect of a certain lysosomal hydrolase leads to the accumulation of the corresponding primary storage material. However, a LSD is often characterized by accumulation of secondary storage products unrelated to the enzyme defect. So far, this aspect was not investigated in human fucosidosis patients and English Springer spaniel. In several mucopolysaccharidoses and in α-mannosidosis, the storage of lipofuscin-like autofluorescent material was observed (Walkley 2004, Walkley and Vanier 2009, Damme et al. 2011, Kowalewski et al. 2015) and also the *Fuca1*$^{(-/-)}$ mice exhibited accumulation of autofluorescent material in the molecuar layer of the cerebellum, hippocampus and cerebral cortex, which most likely represented lipofuscin and appeared only during late disease progression. In particular, neuronal perikarya of the hippocampus and cerebral cortex were heavily affected from *Fuca1* gene knock-out and contained a high amount of translucent storage vacuoles. Hence, the additional accumulating lipufuscin-like material might result from a more general impairment of the endosomal-lysosomal system in the affected cell populations resulting in a decreased proteolytic activity (Platt et al. 2012). However, the distribution of the autofluorescent material in the molecular layer of the cerebellum differed from that of hippocampus and cerebral cortex and probably occurred in macrophage/microglia-like cells rather than in neurons.

As described in many other LSDs (Walkley 2004, Walkley and Vanier 2009), unesterified cholesterol and GM2-gangliosides were also identified as secondary storage materials in the CNS of *Fuca1*$^{(-/-)}$ mice in small vesicle-like structures. Interestingly, these storage compounds

were identified by filipin staining and immunofluorescence analysis but could not be detected by TLC. Similar results were reported for α-mannosidosis, where the accumulation of gangliosides was not detectable by TLC but only by immunofluorescence stainings (Walkley 2004). Moreover, it is known that accumulation of unesterified cholesterol in certain cell-types of the CNS is not connected to a general increase in total cholesterol, indicating that only the intracellular distribution and trafficking, but not the total amount of these secondary storage compounds, is altered due to the general impairment of the endosomal-lysosomal compartment in LSDs and the reduced or decelerated vesicle transport and fusion (Walkley and Vanier 2009). Although it was often postulated that cholesterol and gangliosides are sequestered together from lipids rafts of the plasma membrane, they accumulate in separate vesicles and only in a few cases a partial co-localization was observed (McGlynn et al. 2004). This indicates, that the processing of cholesterol and gangliosides might involve different, yet unknown, biochemical routes, although these secondary storage materials often occur within the same cell. So far, no co-localization studies of unesterified cholesterol and GM2-ganglioside accumulation was performed in *Fuca1*$^{(-/-)}$ mice, but should be addressed in the future. Moreover, secondary storage materials might also have an impact on the function of affected cells, as increased amounts of GM2-gangiosides were reported to result in a depletion of intracellular Ca^{2+} stores causing ER stress and apoptosis (Walkley and Vanier 2009). In this context, accumulation of GM2-gangliosides was only observed in young *Fuca1*$^{(-/-)}$ mice but was absent during late stages of the disease, indicating that the affected cell types died and were lost during disease progression. The exact nature of the affected cell type remains to be analyzed by co-stainings of GM2-ganglioside and different neural cell type-specific markers.

5.2 Production and purification of human α-L-fucosidase

5.2.1 CHO-K1 cells are a suitable production system for recombinant human α-L-fucosidase

With regard to a planned ERT of fucosidosis patients, the production of the human form of α-L-fucosidase was envisaged in this work. The human enzyme has to be synthesized in a biological active form including proper protein folding and post-translational modifications, whereby the latter are of particular importance as a proper glycosylation and sufficient mannose-6-phosphorylation is essential for the efficient cellular uptake of the recom-

binant enzyme in the patients (Kollmann et al. 2012, Markmann et al. 2015). Moreover, post-translational modifications influence the pharmacodynamic properties of a recombinant protein e. g. its solubility, stability, activity and biodistribution (Jayapal et al. 2007). As prokaryotic systems like *Escherichia coli* are not able to produce glycosylated proteins, the use of a mammalian production system was favored, so that CHO-K1 cells were chosen as host system for the production of recombinant human α-L-fucosidase. Over the last decades, this cell line has been proven as a safe and robust system for production of therapeutic proteins for human diseases. Amongst others, also the production of ERT-applied lysosomal enzymes like e. g. α-glucosidase, α-L-iduronidase, *N*-acetylgalactosamine-4-sulfatase, α-galactosidase, β-glucocerebrosidase (Jayapal et al. 2007) is carried out in CHO cells.

In this work, CHO-K1 cells were transfected with an expression plasmid for the untagged as well as a *C*-terminal His_6-tagged human α-L-fucosidase. Stable transfected cells were selected and single cell clones were established by limited dilution. As only small amounts of the recombinant enzyme were needed for initial studies like the establishment of a purification strategy, an adherent cell culture system was generated. For the His_6-tagged enzyme, a two-step purification procedure yielded 5 mg of α-L-fucosidase out of 1 L conditioned cell culture supernatant, which was sufficient for initial ERT studies in the mouse model. However, for extended experiments and especially for a therapy of human patients a large-scale production is mandatory and thus, cells were adapted to suspension conditions, which would allow further volumetric scale-up processes and the use of large bio-reactors in a commercial environment. Moreover, a FCS-free and protein-free medium was used for cultivation, which minimizes the amount of contaminants and should ease enzyme purification especially with regard to the untagged α-L-fucosidase. However, purification of untagged and His_6-tagged human α-L-fucosidase from conditioned medium of the suspension culture system was not tested so far.

In the suspension culture system, densities of 3×10^6 - 4×10^6 cells / ml were reached and for both enzymes, the untagged and the His_6-tagged human α-L-fucosidase, an increased synthesis rate was monitored compared to the adherent culture system, particularly for the His_6-tagged enzyme. In general, CHO-K1 cells producing the untagged enzyme reached higher cell densities, whereas His_6-tagged α-L-fucosidase producing cells yielded more recombinant enzyme. This might be due to the fact, that during transfection the target DNA integrates randomly into the host genome. The insertion of the cDNA for the untagged enzyme might have occurred in a transcriptional more inactive genomic region, whereas the cDNA for the

His_6-tagged α-L-fucosidase might have integrated at a DNA locus of high transcriptional activity. Moreover, the His_6-tagged α-L-fucosidase producing CHO cells might have integrated a higher copy number of the transfected plasmid resulting in enhanced synthesis rates. In the future, the re-transfection of the cell lines should be considered. Moreover, the use of the CHO-DG44 cell line, which is deficient in dihydrofolate reductase, might be of benefit, as this allows the amplification of the gene of interest by selection with methotrexate resulting in highly elevated transcription rates (Jayapal et al. 2007, will be further discussed in section 5.4).

5.2.2 Purification of the His_6-tagged human α-L-fucosidase

The His_6-tagged human α-L-fucosidase was produced in adherently grown CHO-K1 cells and purified to apparent homogeneity in a two-step purification procedure using a Ni^{2+}-affinity chromatography (IMAC) followed by a strong cation exchange chromatography (SCX). A 31-fold purification was achieved resulting in a specific activity of 15.4 U/mg. For comparison, the specific activities of genuine enzyme purified from human liver and brain were determined with 24.2 U/mg and 7.5 U/mg, respectively (Alhadeff et al. 1975a, Alhadeff and Janowsky 1977).

The His_6-tagged human α-L-fucosidase displayed a comparatively strong binding towards both column matrices and eluted at 230 mM imidazole from the IMAC and with 850 mM NaCl from the SCX. In further experiments, a pH-independent oligomerization of the His_6-tagged α-L-fucosidase was detected (will be discussed in section 5.2.4), which might cause an increased avidity resulting in a strong binding of the enzyme towards the column matrices. Nearly no α-L-fucosidase activity was detected in the flow through and washing fractions of both chromatographies and elution of the enzyme was performed by flushing the columns with high concentrations of imidazole and NaCl, respectively, resulting in a highly concentrated eluate containing α-L-fucosidase. In both chromatographies, 95 % - 100 % of the loaded activity was recovered in the elution fractions, respectively. However, the enzyme had to be re-buffered between both chromatographies from neutral pH of the IMAC towards the acidic pH of the SCX, which needed some optimization to prevent loss of enzyme. Finally, the loss of α-L-fucosidase in this step was minimized to 10 % by diluting the fractions received during IMAC in binding buffer of the SCX. After the SCX, the enzyme was again re-buffered towards PBS at neutral pH. Interestingly the first re-buffering from neutral towards acidic pH

resulted in a substantial loss of α-L-fucosidase when using a centricon, whereas nearly the entire amount of enzyme was recovered during buffer exchange via centricon from acidic to neutral pH. In summary, up to 80 % of the initially loaded α-L-fucosidase activity could be recovered in the final concentrated PBS-buffered sample. 70 U were obtained from 900 ml cell culture supernatant. In comparison, 250 mU/g body weight of His_6-tagged human α-L-fucosidase were used in a preliminary high-dose ERT of the mouse model. Assuming an average body weight of 25 g of the mice, up to ten injections could be performed using one enzyme preparation. As stated above, an even higher enzyme production was monitored in the suspension culture system, which should result in increased yields of His_6-tagged human α-L-fucosidase.

5.2.3 Purification of the untagged human α-L-fucosidase

Although a purification protocol for the His_6-tagged human α-L-fucosidase was successfully established, the purification of the untagged enzyme is absolutely essential with respect to a further ERT of human fucosidosis patients, due to the high immunogenicity of the His_6-tag. Several chromatography techniques have been tested for purification of the untagged enzyme and are discussed below, but a sufficient purification protocol could not be established so far and should be the issue of further research.

5.2.3.1 Fucose-affinity chromatography

The purification of genuine human α-L-fucosidase had been commonly carried out using a specific agarose-ε-aminocaproyl-fucosamine affinity matrix (Alhadeff et al. 1974a, Alhadeff et al. 1975a, Alhadeff and Janowsky 1977, Chien and Dawson 1980), where fucose was coupled to a six-carbon-atom spacer. The affinity matrix, which was used in these studies, is no longer available. In a similar approach, Bielicki et al. (2000) purified recombinant canine α-L-fucosidase using an affinity matrix where fucose was coupled to a 24-carbon-atom spacer, but this matrix is also no longer available. In this study, *N*-(ε-aminocaproyl)-β-L-fucopyranosylamine (6-carbon-atom spacer) was immobilized on CNBr-activated sepharose beads and, alternatively, on a NHS-activated column. However, the coupling efficiency of both matrices was rather low, as only small amounts of α-L-fucosidase (< 5 U) could be efficiently bound, whereas increasing amounts resulted in a high α-L-fucosidase activity in flow through and washing fractions. In further studies, additional coupling conditions should be tested in order to increase coupling efficiency. Moreover, other commercial available fucose-affinity

matrices could be tested (e. g. from Vector Laboratories # AC-1002) and the use of another spacer should be considered. Bielicki et al. (2000) reported, that the length of the spacer influences the binding efficiency, as the use of a 24-atom spacer resulted in binding of 98 % of the canine α-L-fucosidase, whereas only 9 % were bound to an affinity matrix, where fucose was coupled to a one-carbon-atom spacer.

Despite the general difficulties regarding the coupling efficiency, an efficient elution by addition of L-fucose could not be established so far. The α-L-fucosidase eluted as a broad smear and contained multiple impurities, particularly a protein with an apparent molecular weight of 66 kDa, which is most likely BSA. An enrichment of the enzyme was not achieved, although 500 mM NaCl were already included in the washing buffer. Similar results were also observed using other chromatography techniques and might suggest, that the enzyme forms aggregates with other proteins (will be further discussed in section 5.2.3.3).

5.2.3.2 Concanavalin A-chromatography

In order to establish a purification protocol for the untagged human α-L-fucosidase the use of a lectin-chromatography (concanavalin A, ConA) was tested. As a matter of fact, no sufficient elution was achieved and approximately 90 % of the enzyme remained on the column whatever elution conditions were tested. A comparable study was presented by Gramer et al. (1994), in which a Tris-buffered system containing 0.5 M α-D-methylmannoside resulted in the elution of only 41 % of the loaded α-L-fucosidase (produced in CHO cells). Moreover, Alhadeff and Watkins (1979) used an acidic buffer system at pH 4.0 that resulted in the loss of Mn^{2+} and Ca^{2+} as essential co-factors for substrate binding of the lectin. The application of an acidic buffer system was considered to cause a complete elution of the bound enzyme, but only 50 % of human liver α-L-fucosidase were released from ConA material. The binding of the α-L-fucosidase to the ConA material seemed to be extremely strong, since the enzyme could be released only under denaturating conditions.

5.2.3.3 Further purification techniques

Besides the affinity chromatographies using immobilized fucose residues as well as ConA material, different ion-exchange chromatographies (IEX) as well as a Ni^{2+}-affinity chromatography (IMAC) were tested to purify the untagged α-L-fucosidase. Although an efficient binding of the enzyme could be achieved for the IEX using a HiTrap HP SP column at acidic pH values

and a DEAE matrix at pH 8.0, the enzyme always eluted together with the majority of impurities independent on the chromatography technique or the chosen pH value. Similar results were obtained for the IMAC and were also seen during fucose-affinity chromatography (discussed in section 5.2.3.1). This might be due to a complex formation of the α-L-fucosidase with several other proteins. Further results suggested that these aggregates might be formed during the ammonium sulfate precipitation of freshly harvested cell culture supernatants, as a high amount of contaminants showed an altered elution profile during ion-exchange chromatography when the cell culture supernatant was directly loaded onto the SP column. A formation of aggregates is not reported in the literature, although ammonium sulfate precipitation was often used during purification of α-L-fucosidase from human tissues (Robinson and Thorpe 1973, Turner 1979, Chien and Dawson 1980). In further experiments, particularly the use of conditioned medium from suspension cells cultivated in FCS-free and protein-free medium seems to be promising, as this medium should minimize the amount of contaminants.

5.2.4 Characterization of the recombinant α-L-fucosidase with regard to its application in ERT

The recombinant human α-L-fucosidase was characterized regarding its enzymatic properties and suitability for ERT studies. In a first experiment, the pH optimum of the enzyme was determined and the highest α-L-fucosidase activity was observed at pH 5.5, which is comparable to genuine enzyme from mouse liver, indicating that the recombinant α-L-fucosidase is highly active at lysosomal pH. A slightly lower pH optimum at pH 5.0 for human α-L-fucosidase was reported by Robinson and Thorpe (1973), whereas Wiederschain et al. (1973) distinguished between a low molecular weight form of human α-L-fucosidase with a pH optimum of 4.5 - 5.0 and a high molecular weight form with a pH optimum of 5.5. In contrast, Alhadeff et al. (1975a) reported a pH optimum of 4.6. These data indicate, that the human α-L-fucosidase exhibits its pH optimum at lysosomal pH and slight differences between the individual data might be due to the different enzyme preparation or different sources of the enzyme resulting in an altered glycosylation pattern that was already shown to slightly influence enzyme activity and pH optimum (Alhadeff 1978).

In particular, a proper glycosylation of the recombinant human α-L-fucosidase is important regarding its further use in an ERT, as the glycosylation pattern might influence the pharmacodynamic properties and biodistribution of the enzyme. The human α-L-fucosidase contains

four putative glycosylation sites, but the usage of one is unlikely, as it contains a proline residue in the recognition sequence (Johnson and Alhadeff 1991). The *N*-glycans were shown to exhibit high-mannose as well as complex type *N*-glycans (Johnson et al. 1992). Similar results were obtained during this study by PNGase F and EndoH treatment of recombinant His_6-tagged α-L-fucosidase indicating the presence of a mixed glycosylation pattern. The proper glycosylation of the recombinant enzyme is of special importance, as it is a prerequisite for addition of M6P residues, which are essential for the lysosomal targeting of the α-L-fucosidase (Kollmann et al. 2012, Markmann et al. 2015). The exact site of M6P phsophorylation was determined at position ^{377}NTT of the α-L-fucosidase purified from human brain (Sleat et al. 2005). The transfer of the phosphate residue is carried out by the UDP-*N*-acetylglucosamine 1-phosphotransferase (GNPT) that consists of two α and two β-subunits encoded by the *GNPTAB* gene as well as two γ-subunits encoded by the *GNPTG* gene. The α/β-subunits are responsible for phosphotransferase activity and recognition of the lysosomal hydrolases, whereas the γ-subunits are supposed to enhance the phosphorylation of a subset of hydrolases, especially lysosomal glycosidases like α-mannosidase. In contrast the α-L-fucosidase is efficiently recognized by α/β-subunits and its lysosomal targeting is not impaired by *GNPTG*-deficiency (Flanagan-Steet et al. 2016). The degree of mannose-6-phosphorylation of the recombinant His_6-tagged enzyme was analyzed in this study using a specific M6P receptor affinity matrix. Although a partial elution of the recombinant enzyme by addition of M6P was shown, the exact degree of mannose-6-phosphorylation could not be estimated, as an unspecific binding towards the column matrix occurred and only an incomplete elution was achieved. Nevertheless, the His_6-tagged human α-L-fucosidase was shown to be partially mannose-6-phosphorylated and hence the enzyme offers great potential regarding ERT studies. Besides the M6P-mediated endocytosis, other glycoprotein receptors could also participate in the uptake of the recombinant α-L-fucosidase. The mannose-receptor is expressed in macrophages and dentritic cells as well as in hepatic, spleenic, lymphatic and dermal microvascular endothelium and specifically mediates the uptake of glycoproteins with terminal mannose, fucose and *N*-acetylglucosamine residues (Martinez-Pomares 2012), whereas the asialoglycoprotein receptor is expressed in hepatocytes and binds terminal galactose and *N*-acetylgalactosamine residues (Ashwell and Harford 1982). In this context, an efficient uptake of the recombinant His_6-tagged α-L-fucosidase was observed in MEFs and during ERT of the mouse model, indicating that the endocytosis is not restricted to the M6P receptors and other receptors might contribute to the cellular uptake.

As discussed earlier (section 5.2.2), the His_6-tagged human α-L-fucosidase displayed an unexpected strong affinity towards the IMAC and SCX matrix suggesting an oligomerization of the enzyme that increased the avidity of this interaction. Indeed, a pH-independent oligomerization of the His_6-tagged enzyme was shown by size exclusion chromatography (SEC), which might be tag-induced. The molecular weight of untagged human α-L-fucosidase was determined by SEC at 60 kDa at pH 7.5 (Turner 1979), whereas the enyzme was detected at 79 kDa (pH 7.4) in this study. The reason for this difference is still unclear, but might at least partially represent differences in the degree and type of glycosylation, especially in the sialic acid content. The human liver α-L-fucosidase is a sialoglycoprotein and seven isoforms have been isolated, which differ in the sialic acid content and display distinct behavior during SEC (Alhadeff 1978). In order to exclude unexpected buffer effects during SEC, the lysosomal protein Plbd2 was used as oligomerization control and its dimerization (Lakomek et al. 2009) was also observed in this study, indicating proper conditions for lysosomal proteins during the SEC. The molecular weight of genuine murine α-L-fucosidase was determined with 56 kDa at pH 7.4 and is comparable to results from Laury-Kleintop et al. (1987), who reported two fucosidase isoforms with an apparent molecular weight of 57 kDa and 63 kDa by SDS-PAGE. The molecular weight differences are probably caused by distinct glycosylation patterns. However, no SEC studies of the murine α-L-fucosidase are available so far. For the human α-L-fucosidase the formation of homooligomers has been reported and dimeric, tetrameric as well as hexameric forms were described (Chien and Dawson 1980; Alhadeff et al. 1975a and Turner 1979). In this study, the molecular weight of the human enzyme oligomer was determined with 312 kDa at pH 4.6 and corresponded well with results by Turner (1979), who also reported a pH-dependent oligomerization of the human fucosidase with a hexameric form of 305 kDa at pH 5.0 and a fucosidase monomer of 60 kDa at pH 7.5. In summary, the recombinant His_6-tagged as well as the untagged human α-L-fucosidase exhibited an oligomeric form at lysosomal pH that might increase the stability of the enzyme. Indeed, a high stability of the purified His_6-tagged α-L-fucosidase was detected during short-term storage in PBS at 4 °C, where no protein degradation could be detected after ten days. A similar finding was reported for arylsulfatase A (ARSA), a lysosomal sulfatase, which also exhibits a pH-dependent oligomerization and forms an octamer at lysosomal pH. Deficiency of ARSA causes the LSD metachromatic leukodystrophy, e. g. due to a P426L mutation of the *ARSA* gene. The P426L-ARSA mutant showed normal activity and lysosomal targeting, but the lysosomal octamerization is impaired. This caused lysosomal instability of the mutant, as a cathepsin L cleavage site became accessible which is normally hidden in the octamer (von Bülow et al. 2002).

5.3 Enzyme replacement therapy of *Fuca1*$^{(-/-)}$ mice

ERT has been proven as a safe and efficient therapy in a subset of LSDs (e. g. Gaucher disease, MPS I, MPS II, MPS VI and Pompe disease; Cox 2013). In this study, a high-dose, short-term ERT of the constitutive fucosidosis mouse model was performed using 250 mU/g body weight of purified His_6-tagged human α-L-fucosidase in two injections within one week. The therapy resulted in a massive uptake of the recombinant enzyme into visceral organs like liver and spleen and to a lower extend also into the kidney, but trace amounts were also detected in the brain. As the ERT-treated *Fuca1*$^{(-/-)}$ mouse was not perfused prior to sacrifice, the α-L-fucosidase activity detected in the brain could result from recombinant enzyme that was still present in the circulation of the mouse, or that was taken up into extra-neural cells of the brain in the endothelia or meninges. A high bioavailability of the α-L-fucosidase in liver and spleen was expected, as recombinant α-mannosidase and *N*-acetylglucosaminidase were also mainly taken up by liver and spleen in short-term ERTs of α-mannosidase knock-out mice (Roces et al. 2004) and a mouse model for MPS IIIB (Yu et al. 2000), respectively, whereas the delivery into the kidney was also low in both studies. The main critical aspect of ERTs in LSDs with CNS involvement is the treatment of the brain, as delivery of intravenously administered enzymes into the CNS is normally prevented by the blood-brain-barrier. However, high-dose ERT of knock-out mouse models for α-mannosidosis and metachromatic leukodystrophy resulted in an uptake of recombinant α-mannosidase and arylsulfatase A, respectively, into the CNS, amelioration of the storage pathology and improvement of motor disabilities (Roces et al. 2004, Blanz et al. 2008, Matzner et al. 2009). Further investigations are necessary to evaluate, whether the α-L-fucosidase is efficiently delivered into the brain e. g. by using a higher dosis of the recombinant enzyme or by repeated injections. Another ERT strategy is the intracisternal injection of the recombinant enzyme directly into the CNS as performed in the canine fucosidosis model (Kondagari et al. 2011a). However, this method bears a high risk for CNS infections due to the invasive procedure (Burrow and Grabowski 2013).

Besides the determination of α-L-fucosidase activity, the effects of the ERT were also monitored by analysis of storage material by TLC. The liver was excluded from this experiment, as the high amount of glycogen prevented its proper analysis by TLC. A complete disappearance of storage material was detected in the spleen, while a partial digestion of storage material was detected in the kidney. This might be due to the higher bioavailability of the recombinant α-L-fucosidase in the spleen in comparison to the kidney and further studies are necessary to

analyze whether a complete clearance of storage material in the kidney could be achieved by a higher dosis of the recombinant enzyme or by repeated injections. Comparably, the disappearance of storage material in ERT-treated α-mannosidosis mice was tissue- and dose-dependent and also relied on the number of injections (Roces et al. 2004, Blanz et al. 2008). As expected, no effect of the ERT was seen by TLC in the *Fuca1*$^{(-/-)}$ brain, indicating that the measured α-L-fucosidase activity was indeed due to residual recombinant enzyme in the circulation of the mice, or that the amount of administered α-L-fucosidase was too low to detect a benefit in the CNS. Again, further investigations are necessary to optimize the bioavailability of the recombinant enzyme. However, these preliminary results are very promising and indicate that an ERT of fucosidosis might improve storage pathology and clinical symptoms.

As discussed earlier (section 5.1.2), alterations in the regulation of lysosomal proteins are a common feature of LSDs and an increase in β-hexosaminidase activity was seen in several organs of the *Fuca1*$^{(-/-)}$ mice. The elevated levels of β-hexosaminidase activity were reduced by approximately the half in liver and spleen after ERT-treatment, indicating that a high bioavailability of the recombinant α-L-fucosidase might not only diminish primary storage material but might also lead to an improvement of secondary pathologies. Similar findings were also reported for a mouse model of MPS IIIB, where the treatment with recombinant *N*-acetylglucosaminidase also resulted in reduction of the elevated β-hexosaminidase activities by approximately the half (Yu et al. 2000).

5.4 Outlook

In this study, the generation of a constitutive fucosidosis mouse model was described. The *Fuca1* gene knock-out was successfully validated and a basic characterization of *Fuca1*$^{(-/-)}$ mice was realized. A number of questions remain still open: A detailed analysis of the fucosidosis storage material should be addressed, particularly as it is currently unknown whether the *Fuca1*$^{(-/-)}$ mice accumulate fucosylated glycosphingolipids comparably to human fucosidosis patients. An analysis by TLC revealed no differences in the glycosphingolipid content between wildtype and *Fuca1*$^{(-/-)}$ mice, but the TLC might be not sensitive enough. Hence, an analysis by immunofluorescence staining of different tissues or by mass spectrometry of isolated lipids should be considered. Here, the liver is of particular interest, as glycosphingolipids bearing the H-antigen have been found as the major storage material in the liver of human fucosidosis patients (Michalski and Klein 1999). Also the analysis of the water-soluble storage material

should be extended, as only a few storage material species were identified so far, whereas more than ten different fucosylated glycocompounds have been reported in human fucosidosis (Michalski and Klein 1999). Of note, Asn-GlcNAc-Fuc was identified in tissues and urine of *Fuca1*$^{(-/-)}$ mice and of human fucosidosis patients (Michalski and Klein 1999), respectively and may serve as a biomarker for the disease. Moreover the analysis of secondary storage material should be extended. Lipofuscin-like autofluorescent material, GM2-gangliosides and unesterified cholesterol were already detected in the brain of *Fuca1*$^{(-/-)}$ mice, whereas the visceral organs have not been analyzed so far.

The *Fuca1*$^{(-/-)}$ mouse model was treated by high-dose, short-term ERT using purified His_6-tagged human α-L-fucosidase. A high bioavailability of the recombinant enzyme was observed in liver and spleen, resulting in a complete disappearance of primary storage material in the spleen as well as an improvement of secondary storage pathology in terms of normalized β-hexosaminidase activity. Certainly, this initial experiment has to be repeated in order to verify the results and it should be further expanded: An important aspect is the analysis of pharmacokinetics of the recombinant enzyme like clearance velocity from the serum of the mice, half life of the enzyme in the mouse tissues, time-dependent depletion of primary storage material as well as duration time between single injections. All these preclinical trials will help to establish a proper and safe ERT for human fucosidosis patients. As already discussed, the accessibility of the CNS is of special interest, as neurological implications are the major clinical symptom of fucosidosis in human. The delivery into the brain could be further optimized by generation of an α-L-fucosidase fusion protein with the RTB-lectin, which is the nontoxic carbohydrate-binding subunit B of ricin AB toxin from *Ricinus communis*. Recently, such fusion constructs with human α-L-iduronidase and human β-galactosidase were shown to amoriliate storage pathology in human MPS I and GM1-gangliosidosis fibroblasts, respectively. The lectin mediated the uptake of the recombinant enzyme by binding to galactose or galactosamine residues on glycoproteins and glycolipids at the cell surface. The delivery is not receptor-mediated, but was provided through adsorptive-mediated endocytosis. Due to this braod spectrum of endocytosis routes, intravenously administered RTB fusion constructs are believed to enter the CNS, although this was not tested so far *in vivo* (Acosta et al. 2015, Condori et al. 2016). Moreover, ERT of the MPS I mouse model using a recombinant fusion construct of α-L-iduronidase and a monoclonal antibody against the murine transferrin receptor was shown to enhance transport across the blood-brain-barrier and to improve the CNS storage pathology (Boado et al. 2011). Similar approaches are also feasible regarding

the fucosidosis mouse model.

The production of the human α-L-fucosidase was performed in CHO-K1 cells. Although the yield of recombinant enzyme was sufficient to perform an initial ERT study, extended experiments might be limited by the availability of untagged α-L-fucosidase. The production yield has to be increased especially when aiming a further ERT of human fucosidosis patients. Towards this end, the use of the CHO-DG44 cell line is promising, which is deficient in dihydrofolate reductase (DHFR) resulting in an auxotrophy for glycine, hypoxanthine and thymidine. The gene of interest (human *Fuca1*) is cloned into an expression vector containing a functional *dhfr* gene. Both genes are included into a bicistronic system, so that their expression is linked. The expression vector is transfected into CHO-DG44 cells and clonal selection is performed in a growth medium lacking glycine, hypoxanthine and thymidine. Subsequently, the DHFR system allows the amplification of the cDNA by selection with methotrexate, a folic acid analogue that blocks DHFR activity. Hence, cell survival is only achieved, when several copies of the DHFR system are present, which is amplified under increasing selection pressure. As the expressions of the DHFR and the gene of interest are connected, a high production CHO-DG44 strain can be generated (Jayapal et al. 2007).

Here, a purification protocol for the His_6-tagged human α-L-fucosidase was established, but sufficient purification of the untagged enzyme proved to be a difficult task. Moreover, the His_6-tagged α-L-fucosidase was used in two injections during ERT of the fucosidosis mouse model. The immunogenicity of the enzyme was not analyzed so far, but a humoral immune response in the *Fuca1*$^{(-/-)}$ mice and the generation of α-L-fucosidase-specific IgG are expected. The *Fuca1*$^{(-/-)}$ mice are completely devoid of α-L-fucosidase resulting in a high immunogenicity of the enzyme, regardless of its source or the presence of any tags, as it was recently described for α-mannosidase knock-out mice receiving repeated injections of recombinant human α-mannosidase (Damme et al. 2015). The authors reported, that the survival of the animals was reduced to 50 % after the sixth injection, whereas the α-mannosidase-specific IgG concentration was already markedly increased after the second injection during high-dose ERT (500 mU/g). Similar results were also obtained for short-term ERT of arylsulfatase A-deficient mice (Matzner et al. 2009). Hence, the α-L-fucosidase knock-out mouse model described in this study is only suitable for analyzing the effects of a short-term ERT, whereas studying a chronic therapy requires the establishment of an immunotolerant mouse model, as recently described for α-mannosidosis. Damme et al. (2015) reported the genomic integration of an inactive form of the human α-mannosidase into the knock-out mouse model which had

been used in previous studies of short-term ERT (Roces et al. 2004, Blanz et al. 2008). The human α-mannosidase was inactivated by active site mutagenesis and the knock-in mice displayed a comparable phenotype to the former knock-out animals, but tolerated repeated and even high doses of recombinant human α-mannosidase (Damme et al. 2015). In the context of the present study, the establishment of a purification strategy for the untagged human α-L-fucosidase is mandatory, as the His_6-tagged enzyme would lead to a high immunogenicity in a fucosidase knock-in mouse model, whereas the untagged enzyme should be tolerated. As the purification using a fucose-affinity matrix is the most commonly described technique (Johnson and Alhadeff 1991), the establishment of an efficient immobilization procedure of fucose residues or the test of commercially available fucose-affinity matrices (e. g. from Vector Laboratories # AC-1002) should be addressed.

Bibliography

Abraham, D., W. F. Blakemore, A. Dell, M. E. Herrtage, J. Jones, J. T. Littlewood, J. Oates, A. C. Palmer, R. Sidebotham, and B. Winchester (1984). "The enzymic defect and storage products in canine fucosidosis". In: *The Biochemical journal* 222.1, pp. 25–33.

Acosta, W., J. Ayala, M. C. Dolan, and C. L. Cramer (2015). "RTB Lectin: a novel receptor-independent delivery system for lysosomal enzyme replacement therapies". In: *Scientific Reports* 5, p. 14144.

Alexander, M., S. Mani, R. Benjamin, K. Muthusamy, M. Thomas, and R. George (2014). "Siblings with fucosidosis". In: *Journal of Pediatric Neurosciences* 9.2, p. 156.

Alhadeff, J. A. (1978). "Gel filtration of sialoglycoproteins". In: *The Biochemical journal* 173.1, pp. 315–319.

Alhadeff, J. A., G. Cimino, and A. Janowsky (1978). "Isoenzymes of human liver alpha-L-fucosidase: chemical relationship, kinetic studies, and immunochemical characterization". In: *Molecular and cellular biochemistry* 19.3, pp. 171–180.

Alhadeff, J. A. and H. Freeze (1977). "Carbohydrate composition of purified human liver alpha-L-fucosidase". In: *Molecular and cellular biochemistry* 18.1, pp. 33–37.

Alhadeff, J. A. and A. J. Janowsky (1977). "Purification and properties of human brain alpha-L-fucosidase". In: *Journal of neurochemistry* 28.2, pp. 423–427.

Alhadeff, J. A., A. L. Miller, and J. S. O'Brien (1974a). "Purification of human placental alpha-L-fucosidase by affinity chromatography". In: *Analytical biochemistry* 60.2, pp. 424–430.

Alhadeff, J. A., A. L. Miller, H. Wenaas, T. Vedvick, and J. S. O'Brien (1975a). "Human liver alpha-L-fucosidase. Purification, characterization, and immunochemical studies". In: *The Journal of biological chemistry* 250.18, pp. 7106–7113.

Alhadeff, J. A., A. L. Miller, D. A. Wenger, and J. S. O'Brien (1974b). "Electrophoretic forms of human liver alpha-L-fucosidase and their relationship to fucosidosis (mucopolysaccharidosis F)". In: *Clinica chimica acta; international journal of clinical chemistry* 57.3, pp. 307–313.

Alhadeff, J. A., L. Tennant, and J. S. O'Brien (1975b). "Isoenzyme patterns of human liver alpha-L-fucosidase during development". In: *Developmental biology* 47.2, pp. 319–324.

Alhadeff, J. A. and P. Watkins (1979). "Differential concanavalin A binding of cystic fibrosis and normal liver alpha-L-fucosidase". In: *Biochemical and biophysical research communications* 86.3, pp. 787–792.

Arrol, L. P., A. M. Kerrins, Y. Yamakawa, and P. M. Smith (2011). "Fucosidosis in a domestic shorthair cat". In: *Journal of feline medicine and surgery* 13.2, pp. 120–124.

Ashwell, G. and J. Harford (1982). "Carbohydrate-specific receptors of the liver". In: *Annual review of biochemistry* 51, pp. 531–554.

Aula, P., K. O. Raivio, and P. Maury (1980). "Variation of urinary excretion of aspartylglucosamine and associated clinical findings in aspartylglucosaminuria". In: *Journal of Inherited Metabolic Disease* 3.1, pp. 159–161.

Austyn, J. M. and S. Gordon (1981). "F4/80, a monoclonal antibody directed specifically against the mouse macrophage". In: *European journal of immunology* 11.10, pp. 805–815.

Bar-Peled, L. and D. M. Sabatini (2014). "Regulation of mTORC1 by amino acids". In: *Trends in cell biology* 24.7, pp. 400–406.

Beck, M. (2009). "Therapy for lysosomal storage disorders". In: *IUBMB Life*, n/a.

Berteau, Olivier, Isabelle McCort, Nicole Goasdoué, Bérangère Tissot, and Régis Daniel (2002). "Characterization of a new alpha-L-fucosidase isolated from the marine mollusk Pecten maximus that catalyzes the hydrolysis of alpha-L-fucose from algal fucoidan (Ascophyllum nodosum)". In: *Glycobiology* 12.4, pp. 273–282.

Bielicki, J., V. Muller, M. Fuller, J. J. Hopwood, and D. S. Anson (2000). "Recombinant Canine α-L-Fucosidase: Expression, Purification, and Characterization". In: *Molecular Genetics and Metabolism* 69.1, pp. 24–32.

Blanz, J., S. Stroobants, R. Lüllmann-Rauch, W. Morelle, M. Lüdemann, R. D'Hooge, H. Reuterwall, J. C. Michalski, J. Fogh, C. Andersson, and P. Saftig (2008). "Reversal of peripheral and central neural storage and ataxia after recombinant enzyme replacement therapy in alpha-mannosidosis mice". In: *Human Molecular Genetics* 17.22, pp. 3437–3445.

Boado, R. J., E. K.-W. Hui, J. Z. Lu, Q.-H. Zhou, and W. M. Pardridge (2011). "Reversal of Lysosomal Storage in Brain of Adult MPS-I Mice with Intravenous Trojan Horse-Iduronidase Fusion Protein". In: *Molecular Pharmaceutics* 8.4, pp. 1342–1350.

Bosch, M. E. and T. Kielian (2015). "Neuroinflammatory paradigms in lysosomal storage diseases". In: *Frontiers in Neuroscience* 9.283, p. 8051.

Braulke, T. and J. S. Bonifacino (2009). "Sorting of lysosomal proteins". In: *Biochimica et Biophysica Acta (BBA) - Molecular Cell Research* 1793.4, pp. 605–614.

Braulke, T., H. J. Geuze, J. W. Slot, A. Hasilik, and K. von Figura (1987). "On the effects of weak bases and monensin on sorting and processing of lysosomal enzymes in human cells". In: *European journal of cell biology* 43.3, pp. 316–321.

Braulke, T., S. Tippmer, H. J. Chao, and K. von Figura (1990). "Regulation of mannose 6-phosphate/insulin-like growth factor II receptor distribution by activators and inhibitors of protein kinase C". In: *European journal of biochemistry / FEBS* 189.3, pp. 609–616.

Burrow, A. T. and G. A. Grabowski (2013). "Emerging Treatments and Future Outcomes". In: *Lysosomal Storage Disorders*. Ed. by Atul Mehta and Bryan Winchester. Oxford: John Wiley & Sons, Ltd, pp. 174–180.

Caimi, L., S. Marchesini, M. F. Aleo, R. Bresciani, E. Monti, A. Casella, M. L. Giudici, and A. Preti (1989). "Rapid preparation of a distinct lysosomal population from myelinating mouse brain using Percoll gradients". In: *Journal of neurochemistry* 52.6, pp. 1722–1728.

Canuel, M., A. Korkidakis, K. Konnyu, and C. R. Morales (2008). "Sortilin mediates the lysosomal targeting of cathepsins D and H". In: *Biochemical and biophysical research communications* 373.2, pp. 292–297.

Capecchi, M. R. (2005). "Gene targeting in mice: functional analysis of the mammalian genome for the twenty-first century". In: *Nature reviews. Genetics* 6.6, pp. 507–512.

Carmona-Gutierrez, D., A. L. Hughes, F. Madeo, and C. Ruckenstuhl (2016). "The crucial impact of lysosomes in aging and longevity". In: *Ageing research reviews*.

Chang, Y., J. S. Imam, and M. F. Wilkinson (2007). "The Nonsense-Mediated Decay RNA Surveillance Pathway". In: *Annual Review of Biochemistry* 76.1, pp. 51–74.

Chien, S. F. and G. Dawson (1980). "Purification and properties of two forms of human alpha-L-fucosidase". In: *Biochimica et biophysica acta* 614.2, pp. 476–488.

Chung, C., M. J. Elrick, J. M. Dell'Orco, Z. S. Qin, S. Kalyana-Sundaram, A. M. Chinnaiyan, V. G. Shakkottai, and A. P. Lieberman (2016). "Heat Shock Protein Beta-1 Modifies Anterior to Posterior Purkinje Cell Vulnerability in a Mouse Model of Niemann-Pick Type C Disease". In: *PLoS genetics* 12.5, e1006042.

Clarke, J. T.R. (2013). "The Gangliosidoses". In: *Lysosomal Storage Disorders*. Ed. by Atul Mehta and Bryan Winchester. Oxford: John Wiley & Sons, Ltd, pp. 63–69.

Condori, J., W. Acosta, J. Ayala, V. Katta, A. Flory, R. Martin, J. Radin, C. L. Cramer, and D. N. Radin (2016). "Enzyme replacement for GM1-gangliosidosis: Uptake, lysosomal

activation, and cellular disease correction using a novel β-galactosidase:RTB lectin fusion". In: *Molecular Genetics and Metabolism* 117.2, pp. 199–209.

Coutinho, M. F., M. J. Prata, and S. Alves (2012a). "A shortcut to the lysosome: the mannose-6-phosphate-independent pathway". In: *Molecular Genetics and Metabolism* 107.3, pp. 257–266.

Coutinho, M. F., M. J. Prata, and S. Alves (2012b). "Mannose-6-phosphate pathway: A review on its role in lysosomal function and dysfunction". In: *Molecular Genetics and Metabolism* 105.4, pp. 542–550.

Cox, T. M. (2013). "Current Treatments". In: *Lysosomal Storage Disorders*. Ed. by Atul Mehta and Bryan Winchester. Oxford: John Wiley & Sons, Ltd, pp. 151–165.

Cuppoletti, J., D. Aures-Fischer, and G. Sachs (1987). "The lysosomal H+ pump: 8-azido-ATP inhibition and the role of chloride in H+ transport". In: *Biochimica et biophysica acta* 899.2, pp. 276–284.

Damme, M., S. Stroobants, M. Lüdemann, M. Rothaug, R. Lüllmann-Rauch, H. C. Beck, A. Ericsson, C. Andersson, J. Fogh, R. D'Hooge, P. Saftig, and J. Blanz (2015). "Chronic enzyme replacement therapy ameliorates neuropathology in alpha-mannosidosis mice". In: *Annals of clinical and translational neurology* 2.11, pp. 987–1001.

Damme, Markus, Stijn Stroobants, Steven U. Walkley, Renate Lüllmann-Rauch, Rudi D'Hooge, Jens Fogh, Paul Saftig, Torben Lübke, and Judith Blanz (2011). "Cerebellar alterations and gait defects as therapeutic outcome measures for enzyme replacement therapy in α-mannosidosis". In: *Journal of neuropathology and experimental neurology* 70.1, pp. 83–94.

Dawson, G. and J. W. Spranger (1971). "Fucosidosis: a glycosphingolipidosis". In: *The New England journal of medicine* 285.2, p. 122.

d'Azzo, A. and E. J. Bonten (2013). "Defect in Protective Protein / Cathepsin A: Galactosialidosis". In: *Lysosomal Storage Disorders*. Ed. by A. Mehta and B. Winchester. Oxford: John Wiley & Sons, Ltd, pp. 115–120.

De Duve, C. (1963). "The Lysosome Concept". In: *Ciba Foundation Symposium - Lysosomes*. Ed. by de Reuck,A. V. S and Margrate P. Cameron. Novartis Foundation Symposia. Chichester and UK: John Wiley & Sons, Ltd, pp. 1–35.

De Duve, C. (1964). "From Cytases to Lysosomes". In: *Federation proceedings* 23, pp. 1045–1049.

De Duve, C, B. C. Pressman, R. Gianetto, R Wattiaux, and F. Appelmans (1955). "Tissue fractionation studies. 6. Intracellular distribution patterns of enzymes in rat-liver tissue". In: *The Biochemical journal* 60.4, pp. 604–617.

Desantos-Garcia, J. L., S. I. Khalil, A. Hussein, Y. Hu, and Y. Mechref (2011). "Enhanced sensitivity of LC-MS analysis of permethylated N-glycans through online purification". In: *Electrophoresis* 32.24, pp. 3516–3525.

Desnick, R. J. and E. H. Schuchman (2002). "Enzyme replacement and enhancement therapies: lessons from lysosomal disorders". In: *Nature reviews. Genetics* 3.12, pp. 954–966.

Deuschl, F., K. Kollmann, K. von Figura, and T. Lübke (2006). "Molecular characterization of the hypothetical 66.3-kDa protein in mouse: lysosomal targeting, glycosylation, processing and tissue distribution". In: *FEBS letters* 580.24, pp. 5747–5752.

Di Malta, C., J. D. Fryer, C. Settembre, and A. Ballabio (2012). "Astrocyte dysfunction triggers neurodegeneration in a lysosomal storage disorder". In: *Proceedings of the National Academy of Sciences of the United States of America* 109.35, E2334–42.

Dice, J. F. (2007). "Chaperone-mediated autophagy". In: *Autophagy* 3.4, pp. 295–299.

Durand, P., C. Borrone, G.Della Cella, and M. Philippart (1968). "Fucosidosis". In: *The Lancet* 291.7553, p. 1198.

Durand, P., C. Borrone, and G. Della Cella (1966). "A new mucopolysaccharide lipid-storage disease?" In: *The Lancet* 288.7476, pp. 1313–1314.

Durand, P., C. Borrone, and G. Della Cella (1969). "Fucosidosis". In: *The Journal of pediatrics* 75.4, pp. 665–674.

Elrick, M. J., C. D. Pacheco, T. Yu, N. Dadgar, V. G. Shakkottai, C. Ware, H. L. Paulson, and A. P. Lieberman (2010). "Conditional Niemann-Pick C mice demonstrate cell autonomous Purkinje cell neurodegeneration". In: *Human Molecular Genetics* 19.5, pp. 837–847.

Evers, M., P. Saftig, P. Schmidt, A. Hafner, D. B. McLoghlin, W. Schmahl, B. Hess, K. von Figura, and C. Peters (1996). "Targeted disruption of the arylsulfatase B gene results in mice resembling the phenotype of mucopolysaccharidosis VI". In: *Proceedings of the National Academy of Sciences of the United States of America* 93.16, pp. 8214–8219.

Flanagan-Steet, H., C. Matheny, A. Petrey, J. Parker, and R. Steet (2016). "Enzyme-specific differences in mannose phosphorylation between GlcNAc-1-phosphotransferase $\alpha\beta$ and γ subunit deficient zebrafish support cathepsin proteases as early mediators of mucolipidosis pathology". In: *Biochimica et Biophysica Acta (BBA) - General Subjects* 1860.9, pp. 1845–1853.

Fletcher, J. L., G. S. Kondagari, C. H. Vite, P. Williamson, and R. M. Taylor (2014). "Oligodendrocyte loss during the disease course in a canine model of the lysosomal storage disease fucosidosis". In: *Journal of neuropathology and experimental neurology* 73.6, pp. 536–547.

Fletcher, J. L., G. S. Kondagari, A. L. Wright, P. C. Thomson, P. Williamson, and R. M. Taylor (2011). "Myelin genes are downregulated in canine fucosidosis". In: *Biochimica et Biophysica Acta (BBA) - Molecular Basis of Disease* 1812.11, pp. 1418–1426.

Fraldi, A., A. D. Klein, D. L. Medina, and C. Settembre (2016). "Brain Disorders Due to Lysosomal Dysfunction". In: *Annual review of neuroscience* 39, pp. 277–295.

Freitag, F., K. Küchemann, and S. Blümcke (1971). "Hepatic ultrastructure in fucosidosis". In: *Virchows Archiv. B: Cell pathology* 7.2, pp. 99–113.

Galluzzi, P., A. Rufa, P. Balestri, A. Cerase, and A. Federico (2001). "MR brain imaging of fucosidosis type I". In: *AJNR. American journal of neuroradiology* 22.4, pp. 777–780.

Gieselmann, V., U. Matzner, B. Hess, R. Lüllmann-Rauch, R. Coenen, D. Hartmann, R. D'Hooge, P. DeDeyn, and G. Nagels (1998). "Metachromatic leukodystrophy: molecular genetics and an animal model". In: *Journal of inherited metabolic disease* 21.5, pp. 564–574.

Gramer, M. J., D. V. Schaffer, M. B. Sliwkowski, and C. F. Goochee (1994). "Purification and characterization of alpha-L-fucosidase from Chinese hamster ovary cell culture supernatant". In: *Glycobiology* 4.5, pp. 611–616.

Harvey, D. J. (2011). "Derivatization of carbohydrates for analysis by chromatography; electrophoresis and mass spectrometry". In: *Journal of chromatography. B, Analytical technologies in the biomedical and life sciences* 879.17-18, pp. 1196–1225.

Hayashi, H., S. Niinobe, Y. Matsumoto, and T. Suga (1981). "Effects of Triton WR-1339 on lipoprotein lipolytic activity and lipid content of rat liver lysosomes". In: *Journal of biochemistry* 89.2, pp. 573–579.

Hess, B., P. Saftig, D. Hartmann, R. Coenen, R. Lüllmann-Rauch, H. H. Goebel, M. Evers, K. von Figura, R. D'Hooge, G. Nagels, P. de Deyn, C. Peters, and V. Gieselmann (1996). "Phenotype of arylsulfatase A-deficient mice: relationship to human metachromatic leukodystrophy". In: *Proceedings of the National Academy of Sciences of the United States of America* 93.25, pp. 14821–14826.

Hopwood, J. J. (2013). "Genetics of Lysosomal Storage Disorders and Counselling". In: *Lysosomal Storage Disorders*. Ed. by Atul Mehta and Bryan Winchester. Oxford: John Wiley & Sons, Ltd, pp. 29–36.

Huang, L., D. Pike, D. E. Sleat, V. Nanda, and P. Lobel (2014). "Potential pitfalls and solutions for use of fluorescent fusion proteins to study the lysosome". In: *PloS one* 9.2, e88893.

Inui, K., M. Akagi, T. Nishigaki, T. Muramatsu, H. Tsukamoto, and S. Okada (2000). "A case of chronic infantile type of fucosidosis: clinical and magnetic resonance image findings". In: *Brain & development* 22.1, pp. 47–49.

Ioannou, Y. A., K. M. Zeidner, R. E. Gordon, and R. J. Desnick (2001). "Fabry disease: preclinical studies demonstrate the effectiveness of alpha-galactosidase A replacement in enzyme-deficient mice". In: *American journal of human genetics* 68.1, pp. 14–25.

Jain, P., S. Sharma, A. Kumar, and S. Aneja (2014). "Hypomyelination with T2-hypointense globi pallidi in a child with fucosidosis". In: *Journal of child neurology* 29.7, pp. 988–989.

Al-Jasmi, F. A., N. Tawfig, A. Berniah, B. R. Ali, M. Taleb, J. L. Hertecant, F. Bastaki, and A.-K. Souid (2013). "Prevalence and Novel Mutations of Lysosomal Storage Disorders in United Arab Emirates". In: *JIMD Reports - Volume 10*. Ed. by J. Zschocke, K. M. Gibson, G. Brown, E. Morava, and V. Peters. Vol. 10. JIMD Reports. Berlin and Heidelberg: Springer Berlin Heidelberg, pp. 1–9.

Jayapal, K. P., K. F. Waschlin, W.-S. Hu, and M. G. S. Yap (2007). *Recombinant protein therapeutics from CHO cells: 20 years and counting*. New York, NY, and ETATS-UNIS.

Johnson, S. W. and J. A. Alhadeff (1991). "Mammalian alpha-L-fucosidases". In: *Comparative biochemistry and physiology. B, Comparative biochemistry* 99.3, pp. 479–488.

Johnson, S. W., S. Piesecki, R. F. Wang, I. Damjanov, and J. A. Alhadeff (1992). "Analysis of purified human liver alpha-L-fucosidase by western-blotting with lectins and polyclonal and monoclonal antibodies". In: *The Biochemical journal* 282 (Pt 3), pp. 829–834.

Kanitakis, J., C. Allombert, B. Doebelin, M.-C. Deroo-Berger, S. Grande, S. Blanc, and A. Claudy (2005). "Fucosidosis with angiokeratoma. Immunohistochemical & electronmicroscopic study of a new case and literature review". In: *Journal of cutaneous pathology* 32.7, pp. 506–511.

Kau, T., C. Karlo, T. Güngör, V. Prietsch, C. J. Kellenberger, I. Scheer, and E. Boltshauser (2011). "Increased cerebellar volume in the early stage of fucosidosis: a case control study". In: *Neuroradiology* 53.7, pp. 509–516.

Kelly, W. R., A. E. Clague, R. J. Barns, M. J. Bate, and B. M. MacKay (1983). "Canine alpha-L-fucosidosis: a storage disease of Springer Spaniels". In: *Acta neuropathologica* 60.1-2, pp. 9–13.

Kollmann, K., M. Damme, S. Markmann, W. Morelle, M. Schweizer, I. Hermans-Borgmeyer, A. K. Rochert, S. Pohl, T. Lubke, J.-C. Michalski, R. Kakela, S. U. Walkley, and T. Braulke

(2012). "Lysosomal dysfunction causes neurodegeneration in mucolipidosis II 'knock-in' mice". In: *Brain* 135.9, pp. 2661–2675.

Kondagari, G. S., J. L. Fletcher, R. Cruz, P. Williamson, J. J. Hopwood, and R. M. Taylor (2015). "The effects of intracisternal enzyme replacement versus sham treatment on central neuropathology in preclinical canine fucosidosis". In: *Orphanet journal of rare diseases* 10.1, p. 143.

Kondagari, G. S., B. M. King, P. C. Thomson, P. Williamson, P. R. Clements, M. Fuller, K. M. Hemsley, J. J. Hopwood, and R. M. Taylor (2011a). "Treatment of canine fucosidosis by intracisternal enzyme infusion". In: *Experimental neurology* 230.2, pp. 218–226.

Kondagari, G. S., J. Yang, and R. M. Taylor (2011b). "Investigation of cerebrocortical and cerebellar pathology in canine fucosidosis and comparison to aged brain". In: *Neurobiology of disease* 41.3, pp. 605–613.

Kornfeld, R. and S. Kornfeld (1985). "Assembly of asparagine-linked oligosaccharides". In: *Annual review of biochemistry* 54, pp. 631–664.

Kornfeld, S. and I. Mellman (1989). "The biogenesis of lysosomes". In: *Annual review of cell biology* 5, pp. 483–525.

Kowalewski, B., P. Heimann, T. Ortkras, R. Lullmann-Rauch, T. Sawada, S. U. Walkley, T. Dierks, and M. Damme (2015). "Ataxia is the major neuropathological finding in arylsulfatase G-deficient mice: similarities and dissimilarities to Sanfilippo disease (mucopolysaccharidosis type III)". In: *Human Molecular Genetics* 24.7, pp. 1856–1868.

Kyrklund, T. (1987). "Two procedures to remove polar contaminants from a crude brain lipid extract by using prepacked reversed-phase columns". In: *Lipids* 22.4, pp. 274–277.

Lakomek, K., A. Dickmanns, M. Kettwig, H. Urlaub, R. Ficner, and T. Lübke (2009). "Initial insight into the function of the lysosomal 66.3 kDa protein from mouse by means of X-ray crystallography". In: *BMC structural biology* 9, p. 56.

Laury-Kleintop, L. D., I. Damjanov, and J. A. Alhadeff (1987). "Antibody-affinity purification of novel alpha-L-fucosidase from mouse liver". In: *The Biochemical journal* 245.2, pp. 589–593.

Leighton, F., B. Poole, H. Beaufay, P. Baudhuin, J. W. Coffey, S. Fowler, and C. de Duve (1968). "The large-scale separation of peroxisomes, mitochondria, and lysosomes from the livers of rats injected with triton WR-1339. Improved isolation procedures, automated analysis, biochemical and morphological properties of fractions". In: *The Journal of cell biology* 37.2, pp. 482–513.

Levvy, G. A. and A. McAllan (1961). "Mammalian fucosidases. 2. alpha-L-Fucosidase". In: *The Biochemical journal* 80, pp. 435–439.

Liu, S.-W., C.-S. Chen, S.-S. Chang, K.-K. T. Mong, C.-H. Lin, C.-W. Chang, C. Yi Tang, and Y.-K. Li (2009). "Identification of Essential Residues of Human α-l-Fucosidase and Tests of Its Mechanism". In: *Biochemistry* 48.1, pp. 110–120.

Lowry, O. H., N. J. Rosebrough, A. L. Farr, and R. J. Randall (1951). "Protein measurement with the Folin phenol reagent". In: *The Journal of biological chemistry* 193.1, pp. 265–275.

Lübke, T., P. Lobel, and D. E. Sleat (2009). "Proteomics of the lysosome". In: *Biochimica et biophysica acta* 1793.4, pp. 625–635.

Malm, D., H. M. F. Riise Stensland, and Ø. Nilssen (2013). "Glycoproteinoses". In: *Lysosomal Storage Disorders*. Ed. by Atul Mehta and Bryan Winchester. Oxford: John Wiley & Sons, Ltd, pp. 107–114.

Markmann, S., M. Thelen, K. Cornils, M. Schweizer, N. Brocke-Ahmadinejad, T. Willnow, J. Heeren, V. Gieselmann, T. Braulke, and K. Kollmann (2015). "Lrp1/LDL Receptor Play Critical Roles in Mannose 6-Phosphate-Independent Lysosomal Enzyme Targeting". In: *Traffic (Copenhagen, Denmark)* 16.7, pp. 743–759.

Martina, J. A., H. I. Diab, L. Lishu, L. Jeong-A, S. Patange, N. Raben, and R. Puertollano (2014). "The Nutrient-Responsive Transcription Factor TFE3 Promotes Autophagy, Lysosomal Biogenesis, and Clearance of Cellular Debris". In: *Science Signaling* 7.309, ra9.

Martinez-Pomares, L. (2012). "The mannose receptor". In: *Journal of leukocyte biology* 92.6, pp. 1177–1186.

Matzner, U. (2005). "Therapy of Lysosomal Storage Diseases". In: *Lysosomes*. Ed. by P. Saftig. Boston and MA: Springer US, pp. 112–129.

Matzner, U., R. Lüllmann-Rauch, S. Stroobants, C. Andersson, C. Weigelt, C. Eistrup, J. Fogh, R. D'Hooge, and V. Gieselmann (2009). "Enzyme replacement improves ataxic gait and central nervous system histopathology in a mouse model of metachromatic leukodystrophy". In: *Molecular therapy : the journal of the American Society of Gene Therapy* 17.4, pp. 600–606.

McGlynn, R., K. Dobrenis, and S. U. Walkley (2004). "Differential subcellular localization of cholesterol, gangliosides, and glycosaminoglycans in murine models of mucopolysaccharide storage disorders". In: *The Journal of comparative neurology* 480.4, pp. 415–426.

McIlvaine, T. C. (1921). "A buffer solution for colorimetric comparison". In: *Journal of Biological Chemistry* 49.1, pp. 183–186.

Meikle, P. J., D. A. Brooks, E. M. Ravenscroft, M. Yan, R. E. Williams, A. E. Jaunzems, T. K. Chataway, L. E. Karageorgos, R. C. Davey, C. D. Boulter, S. R. Carlsson, and J. J. Hopwood (1997). "Diagnosis of lysosomal storage disorders: evaluation of lysosome-associated membrane protein LAMP-1 as a diagnostic marker". In: *Clinical chemistry* 43.8 Pt 1, pp. 1325–1335.

Menéndez-Sainz, C., A. González-Quevedo, S. González-García, M. Peña-Sánchez, and R. Giugliani (2012). "High proportion of mannosidosis and fucosidosis among lysosomal storage diseases in Cuba". In: *Genetics and Molecular Research* 11.3, pp. 2352–2359.

Metz, B., G. F. A. Kersten, P. Hoogerhout, H. F. Brugghe, H. A. M. Timmermans, A. de Jong, H. Meiring, J. ten Hove, W. E. Hennink, D. J. A. Crommelin, and W. Jiskoot (2004). "Identification of formaldehyde-induced modifications in proteins: reactions with model peptides". In: *The Journal of biological chemistry* 279.8, pp. 6235–6243.

Miano, M., E. Lanino, R. Gatti, G. Morreale, P. Fondelli, M. E. Celle, M. Stroppiano, F. Crescenzi, and G. Dini (2001). "Four year follow-up of a case of fucosidosis treated with unrelated donor bone marrow transplantation". In: *Bone marrow transplantation* 27.7, pp. 747–751.

Michalski, J. C. and A. Klein (1999). "Glycoprotein lysosomal storage disorders: alpha- and beta-mannosidosis, fucosidosis and alpha-N-acetylgalactosaminidase deficiency". In: *Biochimica et biophysica acta* 1455.2-3, pp. 69–84.

Micsenyi, M. C. and S. U. Walkley (2013). "The Lysosomal System: Physiology and Pathology". In: *Lysosomal Storage Disorders*. Ed. by A. Mehta and B. Winchester. Oxford: John Wiley & Sons, Ltd, pp. 1–12.

Migneault, I., C. Dartiguenave, M. J. Bertrand, and K. C. Waldron (2004). "Glutaraldehyde: behavior in aqueous solution, reaction with proteins, and application to enzyme crosslinking". In: *BioTechniques* 37.5, pp. 790–6, 798–802.

Nishigaki, M., K. Yamashita, I. Matsuda, S. Arashima, and A. Kobata (1978). "Urinary oligosaccharides of fucosidosis. Evidence of the occurrence of X-antigenic determinant in serum-type sugar chains of glycoproteins". In: *Journal of biochemistry* 84.4, pp. 823–834.

Noronkoski, T. and I. Mononen (1997). "Influence of L-fucose attached alpha 1–>6 to the asparagine-linked N-acetylglucosamine on the hydrolysis of the N-glycosidic linkage by human glycosylasparaginase". In: *Glycobiology* 7.2, pp. 217–220.

Oner, A. Y., A. Cansu, S. Akpek, and A. Serdaroglu (2007). "Fucosidosis: MRI and MRS findings". In: *Pediatric radiology* 37.10, pp. 1050–1052.

Oriol, R., J. Le Pendu, and R. Mollicone (1986). "Genetics of ABO, H, Lewis, X and related antigens". In: *Vox sanguinis* 51.3, pp. 161–171.

Petersen, B., T. N. Petersen, P. Andersen, M. Nielsen, and C. Lundegaard (2009). "A generic method for assignment of reliability scores applied to solvent accessibility predictions". In: *BMC structural biology* 9, p. 51.

Pfaffl, M. W. (2001). "A new mathematical model for relative quantification in real-time RT-PCR". In: *Nucleic acids research* 29.9, e45.

Platt, F. M., B. Boland, and van der Spoel, A. C. (2012). "The cell biology of disease: Lysosomal storage disorders: The cellular impact of lysosomal dysfunction". In: *The Journal of Cell Biology* 199.5, pp. 723–734.

Pohlmann, R., A. Waheed, A. Hasilik, and K. von Figura (1982). "Synthesis of phosphorylated recognition marker in lysosomal enzymes is located in the cis part of Golgi apparatus". In: *The Journal of biological chemistry* 257.10, pp. 5323–5325.

Reczek, D., M. Schwake, J. Schröder, H. Hughes, J. Blanz, X. Jin, W. Brondyk, S. van Patten, Ti. Edmunds, and P. Saftig (2007). "LIMP-2 is a receptor for lysosomal mannose-6-phosphate-independent targeting of beta-glucocerebrosidase". In: *Cell* 131.4, pp. 770–783.

Robinson, D. and R. Thorpe (1973). "Human liver alpha-L-fucosidases". In: *Clinica chimica acta; international journal of clinical chemistry* 47.3, pp. 403–407.

Roces, D. P., R. Lüllmann-Rauch, J. Peng, C. Balducci, C. Andersson, O. Tollersrud, J. Fogh, A. Orlacchio, T. Beccari, P. Saftig, and K. von Figura (2004). "Efficacy of enzyme replacement therapy in alpha-mannosidosis mice: a preclinical animal study". In: *Human Molecular Genetics* 13.18, pp. 1979–1988.

Sambrook, J. and D. W. Russel (2001). *Molecular cloning: A laboratory manual*. 3. ed. Cold Spring Harbor and NY: Cold Spring Harbor Laboratory Press.

Sandhoff, K., K. Harzer, W. Wässle, and H. Jatzkewitz (1971). "Enzyme alterations and lipid storage in three variants of Tay-Sachs disease". In: *Journal of neurochemistry* 18.12, pp. 2469–2489.

Sardiello, M., M. Palmieri, A. Di Ronza, D. L. Medina, M. Valenza, V. A. Gennarino, C. Di Malta, F. Donaudy, V. Embrione, R. S. Polishchuk, S. Banfi, G. Parenti, E. Cattaneo, and A. Ballabio (2009). "A gene network regulating lysosomal biogenesis and function". In: *Science (New York, N.Y.)* 325.5939, pp. 473–477.

Schwake, M., B. Schröder, and P. Saftig (2013). "Lysosomal membrane proteins and their central role in physiology". In: *Traffic (Copenhagen, Denmark)* 14.7, pp. 739–748.

Schweingruber, C., S. C. Rufener, D. Zünd, A. Yamashita, and O. Mühlemann (2013). "Nonsense-mediated mRNA decay — Mechanisms of substrate mRNA recognition and degradation in mammalian cells". In: *Biochimica et Biophysica Acta (BBA) - Gene Regulatory Mechanisms* 1829.6-7, pp. 612–623.

Sleat, D. E., M. C. Della Valle, H. Zheng, D. F. Moore, and P. Lobel (2008). "The mannose 6-phosphate glycoprotein proteome". In: *Journal of proteome research* 7.7, pp. 3010–3021.

Sleat, D. E., H. Zheng, M. Qian, and P. Lobel (2005). "Identification of Sites of Mannose 6-Phosphorylation on Lysosomal Proteins". In: *Molecular & Cellular Proteomics* 5.4, pp. 686–701.

Sobkowicz, A. D., M. E. Gallagher, C. J. Reid, D. Crean, S. D. Carrington, and J. A. Irwin (2014). "Modulation of expression in BEAS-2B airway epithelial cells of α-L-fucosidase A1 and A2 by Th1 and Th2 cytokines, and overexpression of α-L-fucosidase 2". In: *Molecular and cellular biochemistry* 390.1-2, pp. 101–113.

Stanley, P. and R. D. Cummings (2009). "Structures Common to Different Glycans". In: *Essentials of glycobiology*. Ed. by Ajit Varki. Cold Spring Harbor and N.Y: Cold Spring Harbor Laboratory Press, Chapter 13.

Stinchi, S., R. Lüllmann-Rauch, D. Hartmann, R. Coenen, T. Beccari, A. Orlacchio, K. von Figura, and P. Saftig (1999). "Targeted disruption of the lysosomal alpha-mannosidase gene results in mice resembling a mild form of human alpha-mannosidosis". In: *Human molecular genetics* 8.8, pp. 1365–1372.

Thorpe, S. J. and T. Feizi (1984). "Species differences in the expression of carbohydrate differentiation antigens on mammalian blood cells revealed by immunofluorescence with monoclonal antibodies". In: *Bioscience reports* 4.8, pp. 673–685.

Tsay, G. C. and G. Dawson (1976). "Oligosaccharide storage in brains from patients with fucosidosis, GM1-gangliosidosis and GM2-gangliosidosis (Sandhoff's disease)". In: *Journal of neurochemistry* 27.3, pp. 733–740.

Tsay, G. C., G. Dawson, and S. S. Sung (1976). "Structure of the accumulating oligosaccharide in fucosidosis". In: *The Journal of biological chemistry* 251.19, pp. 5852–5859.

Turkia, B. H., N. Tebib, H. Azzouz, M. S. Abdelmoula, J. Bouguila, H. Sanhaji, N. Miladi, I. Maire, C. Caillaud, N. Kaabachi, and Ben Dridi, M F (2008). "Phenotypic spectrum of fucosidosis in Tunisia". In: *Journal of inherited metabolic disease* 31 Suppl 2, S313–6.

Turner, B. M. (1979). "Purification and characterisation of alpha-L-fucosidase from human placenta. pH-dependent changes in molecular size". In: *Biochimica et biophysica acta* 578.2, pp. 325–336.

Turner, B. M., N. G. Beratis, V. S. Turner, and K. Hirschhorn (1974). "Isozymes of human alpha-L-fucosidase detectable by starch gel electrophoresis". In: *Clinica chimica acta; international journal of clinical chemistry* 57.1, pp. 29–35.

Untergasser, A., I. Cutcutache, T. Koressaar, J. Ye, B. C. Faircloth, M. Remm, and S. G. Rozen (2012). "Primer3 - new capabilities and interfaces". In: *Nucleic acids research* 40.15, e115.

Van Patten, S. M., H. Hughes, M. R. Huff, P. A. Piepenhagen, J. Waire, H. Qiu, C. Ganesa, D. Reczek, P. V. Ward, J. P. Kutzko, and T. Edmunds (2007). "Effect of mannose chain length on targeting of glucocerebrosidase for enzyme replacement therapy of Gaucher disease". In: *Glycobiology* 17.5, pp. 467–478.

Van Hoof, F. and H. G. Hers (1968a). "Mucopolysaccharidosis by absence of alpha-fucosidase". In: *Lancet* 1.7553, p. 1198.

Van Hoof, F. and H. G. Hers (1968b). "The abnormalities of lysosomal enzymes in mucopolysaccharidoses". In: *European journal of biochemistry / FEBS* 7.1, pp. 34–44.

Van Meel, E. and J. Klumperman (2008). "Imaging and imagination: understanding the endo-lysosomal system". In: *Histochemistry and cell biology* 129.3, pp. 253–266.

Vitner, E. B., F. M. Platt, and A. H. Futerman (2010). "Common and uncommon pathogenic cascades in lysosomal storage diseases". In: *The Journal of biological chemistry* 285.27, pp. 20423–20427.

Von Bülow, R., B. Schmidt, T. Dierks, N. Schwabauer, K. Schilling, E. Weber, I. Usón, and K. von Figura (2002). "Defective oligomerization of arylsulfatase A as a cause of its instability in lysosomes and metachromatic leukodystrophy". In: *The Journal of biological chemistry* 277.11, pp. 9455–9461.

Walkley, S. U. (2004). "Secondary accumulation of gangliosides in lysosomal storage disorders". In: *Seminars in Cell & Developmental Biology* 15.4, pp. 433–444.

Walkley, S. U., J. Sikora, M. Micsenyi, C. Davidson, and K. Dobrenis (2010). "Lysosomal compromise and brain dysfunction: examining the role of neuroaxonal dystrophy". In: *Biochemical Society transactions* 38.6, pp. 1436–1441.

Walkley, S. U. and M. T. Vanier (2009). "Secondary lipid accumulation in lysosomal disease". In: *Biochimica et biophysica acta* 1793.4, pp. 726–736.

Wiederschain, G. Y., L. G. Kolibaba, and E. L. Rosenfeld (1973). "Human alpha-L-fucosidases". In: *Clinica chimica acta; international journal of clinical chemistry* 46.3, pp. 305–310.

Wiederschain, G. Y., E. L. Rosenfeld, A. I. Brusilovsky, and L. G. Kolibaba (1971). "-L-fucosidase and other glycosidases in human placenta, foetus liver and amniotic fluid at

various stages of gestation". In: *Clinica chimica acta; international journal of clinical chemistry* 35.1, pp. 99–107.

Willems, P. J., R. Gatti, J. K. Darby, G. Romeo, P. Durand, J. E. Dumon, and J. S. O'Brien (1991). "Fucosidosis revisited: a review of 77 patients". In: *American journal of medical genetics* 38.1, pp. 111–131.

Willems, P. J., H. C. Seo, P. Coucke, R. Tonlorenzi, and J. S. O'Brien (1999). "Spectrum of mutations in fucosidosis". In: *European journal of human genetics : EJHG* 7.1, pp. 60–67.

Winchester, B. (2005). "Lysosomal metabolism of glycoproteins". In: *Glycobiology* 15.6, 1R–15R.

Winchester, B. (2013a). "Classification of Lysosomal Storage Diseases". In: *Lysosomal Storage Disorders*. Ed. by Atul Mehta and Bryan Winchester. Oxford: John Wiley & Sons, Ltd, pp. 37–46.

Winchester, B. (2013b). "Laboratory Diagnosis of Lysosomal Storage Diseases". In: *Lysosomal Storage Disorders*. Ed. by Atul Mehta and Bryan Winchester. Oxford: John Wiley & Sons, Ltd, pp. 20–28.

Woloszynek, J. C., M. Roberts, T. Coleman, C. Vogler, W. Sly, C. F. Semenkovich, and M. S. Sands (2004). "Numerous transcriptional alterations in liver persist after short-term enzyme-replacement therapy in a murine model of mucopolysaccharidosis type VII". In: *The Biochemical journal* 379.Pt 2, pp. 461–469.

Wraith, E. J. and M. Beck (2013). "Clinical Aspects and Clinical Diagnosis". In: *Lysosomal Storage Disorders*. Ed. by Atul Mehta and Bryan Winchester. Oxford: John Wiley & Sons, Ltd, pp. 13–19.

Yamamoto, M., X. H. Lin, Y. Kominato, Y. Hata, R. Noda, N. Saitou, and F. Yamamoto (2001). "Murine equivalent of the human histo-blood group ABO gene is a cis-AB gene and encodes a glycosyltransferase with both A and B transferase activity". In: *The Journal of biological chemistry* 276.17, pp. 13701–13708.

Yamashita, K., Y. Tachibana, S. Takada, I. Matsuda, S. Arashima, and A. Kobata (1979). "Urinary glycopeptides of fucosidosis". In: *The Journal of biological chemistry* 254.11, pp. 4820–4827.

Yu, W. H., K. W. Zhao, S. Ryazantsev, N. Rozengurt, and E. F. Neufeld (2000). "Short-term enzyme replacement in the murine model of Sanfilippo syndrome type B". In: *Molecular Genetics and Metabolism* 71.4, pp. 573–580.

Zervas, M., K. Dobrenis, and S. U. Walkley (2001). "Neurons in Niemann-Pick disease type C accumulate gangliosides as well as unesterified cholesterol and undergo dendritic and

axonal alterations". In: *Journal of neuropathology and experimental neurology* 60.1, pp. 49–64.

Appendix

Sequences

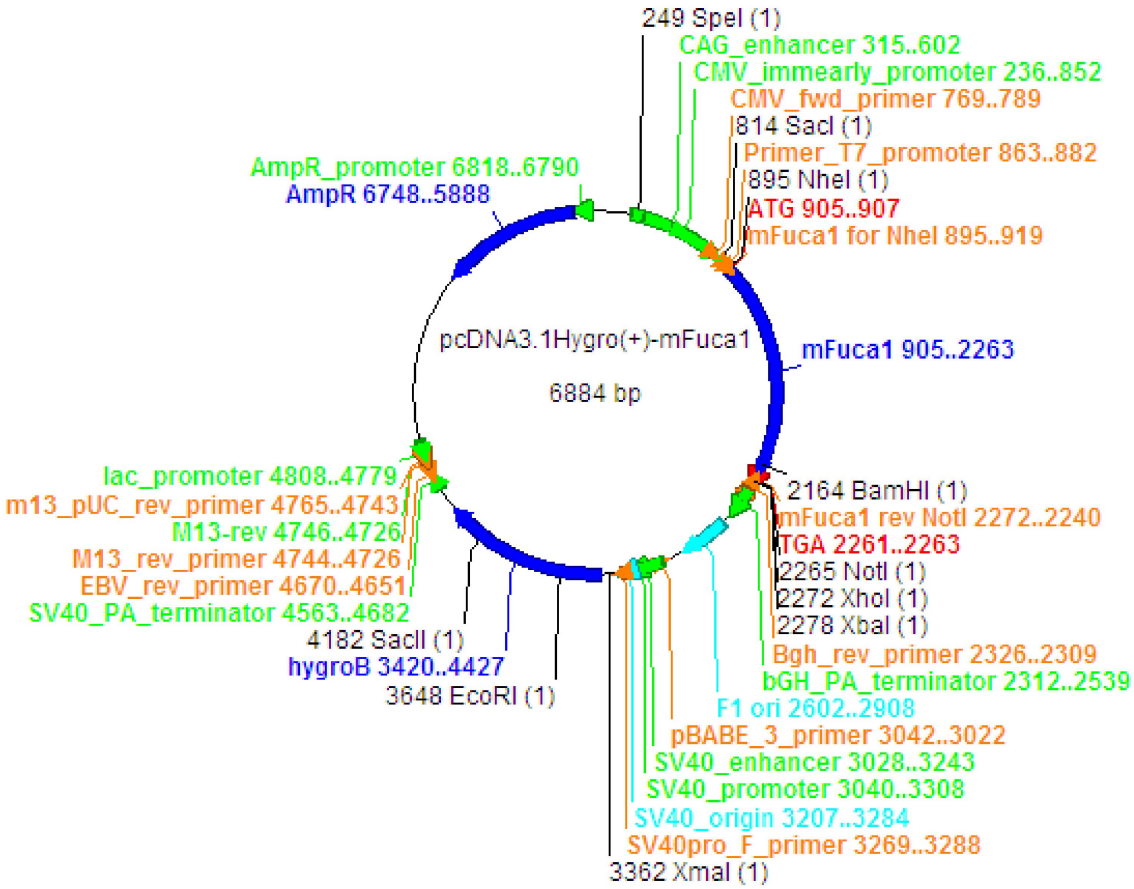

Figure A.1: Vector map of the expression plasmid for murine α-L-fucosidase

```
mFuca1    1>ATGCTGCTGCTGCTGCTGCTGCTAGTGGCTGCGGCCCAGGCAGTGGC>50
               M  L  L  L  L  L  L  L  L  V  A  A  A  Q  A  V  A

mFuca1   51>CCTGGCTCCGCGCCGCTTCACTCCGGACTGGCAGAGCTTGGACTCGCGGC>100
                  L  A  P  R  R  F  T  P  D  W  Q  S  L  D  S  R

mFuca1  101>CACTGCCGAGCTGGTTCGATGAGGCCAAGTTCGGGGTGTTCGTGCACTGG>150
                  P  L  P  S  W  F  D  E  A  K  F  G  V  F  V  H  W

mFuca1  151>GGGGTGTTCTCGGTGCCCGCCTGGGGCAGTGAATGGTTCTGGTGGCACTG>200
                  G  V  F  S  V  P  A  W  G  S  E  W  F  W  W  H  W

mFuca1  201>GCAGGGCGATCGGATGCCGGCCTACCAGCGCTTCATGACAGAAAACTACC>250
                  Q  G  D  R  M  P  A  Y  Q  R  F  M  T  E  N  Y

mFuca1  251>CGCCCGGCTTCAGCTACGCCGACTTCGCACCGCAGTTCACAGCGCGCTTC>300
                  P  P  G  F  S  Y  A  D  F  A  P  Q  F  T  A  R  F

mFuca1  301>TTCCACCCGGATCAGTGGGCCGAACTCTTTCAGGCTGCCGGGGCCAAGTA>350
                  F  H  P  D  Q  W  A  E  L  F  Q  A  A  G  A  K  Y

mFuca1  351>CGTCGTCCTGACCACAAAGCATCATGAAGGCTTCACAAACTGGCCAAGCC>400
                  V  V  L  T  T  K  H  H  E  G  F  T  N  W  P  S

mFuca1  401>CTGTGTCTTGGAACTGGAACTCGAAGGACGTGGGGCCCCACCGTGATTTG>450
                  P  V  S  W  N  W  N  S  K  D  V  G  P  H  R  D  L

mFuca1  451>GTCGGTGAGTTGGGAGCAGCTGTGCGGAAGAGGAACATACGCTACGGCCT>500
                  V  G  E  L  G  A  A  V  R  K  R  N  I  R  Y  G  L

mFuca1  501>CTACCACTCGCTCTTGGAATGGTTCCATCCACTCTACCTACTTGATAAGA>550
                  Y  H  S  L  L  E  W  F  H  P  L  Y  L  L  D  K

mFuca1  551>AAAATGGCTTCAAAACTCAGCATTTCGTCAGGGCAAAAACAATGCCAGAG>600
                  K  N  G  F  K  T  Q  H  F  V  R  A  K  T  M  P  E

mFuca1  601>CTGTATGACCTTGTTAACAGCTACAAGCCTGACCTGATCTGGTCCGACGG>650
                  L  Y  D  L  V  N  S  Y  K  P  D  L  I  W  S  D  G

mFuca1  651>GGAGTGGGAGTGTCCTGACACGTACTGGAACTCCACCAGCTTCCTTGCTT>700
                  E  W  E  C  P  D  T  Y  W  N  S  T  S  F  L  A

mFuca1  701>GGCTCTACAACGATAGCCCTGTCAAGGATGAGGTGATAGTGAATGACCGG>750
                  W  L  Y  N  D  S  P  V  K  D  E  V  I  V  N  D  R
```

Figure A.2: cDNA and protein sequences of murine α-L-fucosidase

```
mFuca1  751>TGGGGCCAGAACTGCTCCTGTCATCATGGAGGGTACTACAACTGTCAAGA>800
             W  G  Q  N  C  S  C  H  H  G  G  Y  Y  N  C  Q  D

mFuca1  801>CAAATACAAGCCACAGAGCTTGCCAGACCACAAGTGGGAGATGTGCACCA>850
              K  Y  K  P  Q  S  L  P  D  H  K  W  E  M  C  T

mFuca1  851>GCATGGACAGAGCATCCTGGGGCTATCGAAAAGACATGACCATGTCGACC>900
            S  M  D  R  A  S  W  G  Y  R  K  D  M  T  M  S  T

mFuca1  901>ATCGCCAAGGAAAATGAAATCATCGAGGAATTGGTTCAGACGGTAAGTTT>950
              I  A  K  E  N  E  I  I  E  E  L  V  Q  T  V  S  L

mFuca1  951>GGGAGGCAACTATCTTCTCAACATTGGACCAACTAAAGATGGTCTGATCG>1000
              G  G  N  Y  L  L  N  I  G  P  T  K  D  G  L  I

mFuca1 1001>TCCCCATCTTCCAAGAAAGGCTTCTTGCTGTCGGCAAGTGGCTGCAGATC>1050
            V  P  I  F  Q  E  R  L  L  A  V  G  K  W  L  Q  I

mFuca1 1051>AACGGGGAGGCCATCTATGCCTCCAAACCCTGGAGGGTGCAGTCGGAAAA>1100
              N  G  E  A  I  Y  A  S  K  P  W  R  V  Q  S  E  K

mFuca1 1101>GAACAAGACGGTTGTGTGGTACACTACTAAAAACGCAACTGTTTACGCCA>1150
              N  K  T  V  V  W  Y  T  T  K  N  A  T  V  Y  A

mFuca1 1151>CTTTCCTGTACTGGCCAGAAAATGGGATCGTGAACCTCAAATCCCCCAAA>1200
            T  F  L  Y  W  P  E  N  G  I  V  N  L  K  S  P  K

mFuca1 1201>ACGACCTCGGCCACAAAGATAACAATGCTAGGACTAGAAGGAGACCTGAG>1250
              T  T  S  A  T  K  I  T  M  L  G  L  E  G  D  L  S

mFuca1 1251>CTGGACCCAGGATCCACTGGAGGGCGTCCTCATCTCTCTGCCACAGTTGC>1300
              W  T  Q  D  P  L  E  G  V  L  I  S  L  P  Q  L

mFuca1 1301>CACCTACCGTTCTGCCGGTGGAGTTTGCGTGGACTCTGAAGCTGACAAAG>1350
            P  P  T  V  L  P  V  E  F  A  W  T  L  K  L  T  K

mFuca1 1351>GTGAACTGA>1359
              V  N  *
```

Figure A.2: cDNA and protein sequences of murine α-L-fucosidase (continued)

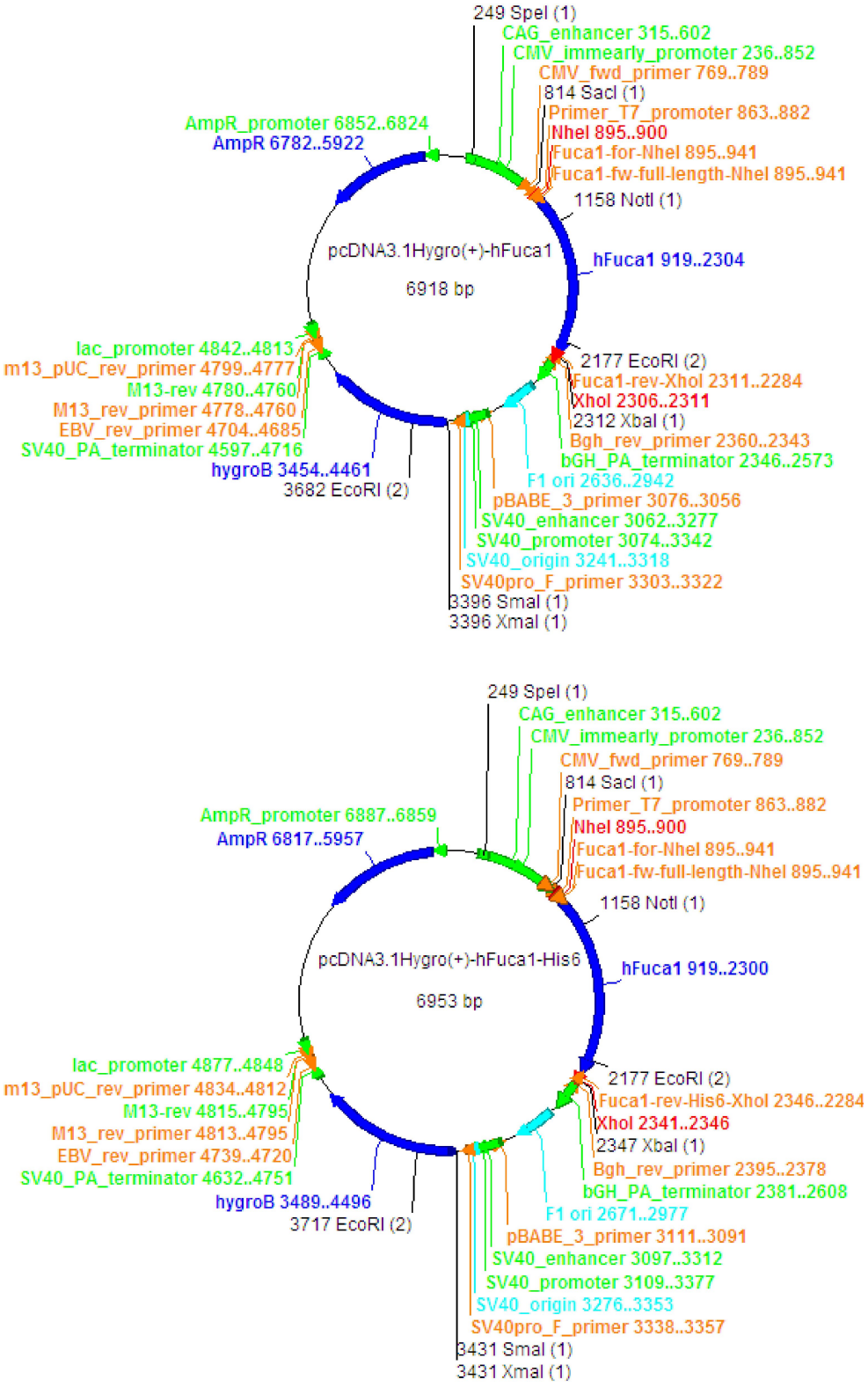

Figure A.3: Vector maps of the expression plasmids for untagged and His_6-tagged human α-L-fucosidase

```
hFuca1                1>ATGAGGTCGCGGCCGGCGGGTCCCGCGCTGTTGCTGCTGCTGCTCTTCCT>50
hFuca1-His6           1>ATGAGGTCGCGGCCGGCGGGTCCCGCGCTGTTGCTGCTGCTGCTCTTCCT>50
hFuca1-D230N-E294Q    1>ATGAGGTCGCGGCCGGCGGGTCCCGCGCTGTTGCTGCTGCTGCTCTTCCT>50
                        M  R  S  R  P  A  G  P  A  L  L  L  L  L  L  F  L

hFuca1               51>CGGAGCGGCCGAGTCGGTGCGTCGGGCCCAGCCTCCGCGCCGCTACACCC>100
hFuca1-His6          51>CGGAGCGGCCGAGTCGGTGCGTCGGGCCCAGCCTCCGCGCCGCTACACCC>100
hFuca1-D230N-E294Q   51>CGGAGCGGCCGAGTCGGTGCGTCGGGCCCAGCCTCCGCGCCGCTACACCC>100
                           G  A  A  E  S  V  R  R  A  Q  P  P  R  R  Y  T

hFuca1              101>CAGACTGGCCGAGCCTGGATTCTCGGCCGCTGCCGGCCTGGTTCGACGAA>150
hFuca1-His6         101>CAGACTGGCCGAGCCTGGATTCTCGGCCGCTGCCGGCCTGGTTCGACGAA>150
hFuca1-D230N-E294Q  101>CAGACTGGCCGAGCCTGGATTCTCGGCCGCTGCCGGCCTGGTTCGACGAA>150
                          P  D  W  P  S  L  D  S  R  P  L  P  A  W  F  D  E

hFuca1              151>GCCAAGTTCGGGGTGTTCATCCACTGGGGCGTGTTCTCGGTGCCCGCCTG>200
hFuca1-His6         151>GCCAAGTTCGGGGTGTTCATCCACTGGGGCGTGTTCTCGGTGCCCGCCTG>200
hFuca1-D230N-E294Q  151>GCCAAGTTCGGGGTGTTCATCCACTGGGGCGTGTTCTCGGTGCCCGCCTG>200
                           A  K  F  G  V  F  I  H  W  G  V  F  S  V  P  A  W

hFuca1              201>GGGCAGCGAGTGGTTCTGGTGGCACTGGCAGGGCGAGGGGCGGCCGCAGT>250
hFuca1-His6         201>GGGCAGCGAGTGGTTCTGGTGGCACTGGCAGGGCGAGGGGCGGCCGCAGT>250
hFuca1-D230N-E294Q  201>GGGCAGCGAGTGGTTCTGGTGGCACTGGCAGGGCGAGGGGCGGCCGCAGT>250
                           G  S  E  W  F  W  W  H  W  Q  G  E  G  R  P  Q

hFuca1              251>ACCAGCGCTTCATGCGCGACAACTACCCGCCCGGCTTCAGCTACGCCGAC>300
hFuca1-His6         251>ACCAGCGCTTCATGCGCGACAACTACCCGCCCGGCTTCAGCTACGCCGAC>300
hFuca1-D230N-E294Q  251>ACCAGCGCTTCATGCGCGACAACTACCCGCCCGGCTTCAGCTACGCCGAC>300
                          Y  Q  R  F  M  R  D  N  Y  P  P  G  F  S  Y  A  D

hFuca1              301>TTCGGACCGCAGTTCACTGCGCGCTTCTTCCACCCGGAGGAGTGGGCCGA>350
hFuca1-His6         301>TTCGGACCGCAGTTCACTGCGCGCTTCTTCCACCCGGAGGAGTGGGCCGA>350
hFuca1-D230N-E294Q  301>TTCGGACCGCAGTTCACTGCGCGCTTCTTCCACCCGGAGGAGTGGGCCGA>350
                           F  G  P  Q  F  T  A  R  F  F  H  P  E  E  W  A  D

hFuca1              351>CCTCTTCCAGGCCGCGGGCGCCAAGTATGTAGTTTTGACGACAAAGCATC>400
hFuca1-His6         351>CCTCTTCCAGGCCGCGGGCGCCAAGTATGTAGTTTTGACGACAAAGCATC>400
hFuca1-D230N-E294Q  351>CCTCTTCCAGGCCGCGGGCGCCAAGTATGTAGTTTTGACGACAAAGCATC>400
                           L  F  Q  A  A  G  A  K  Y  V  V  L  T  T  K  H

hFuca1              401>ACGAAGGCTTCACAAACTGGCCGAGTCCTGTGTCTTGGAACTGGAACTCC>450
hFuca1-His6         401>ACGAAGGCTTCACAAACTGGCCGAGTCCTGTGTCTTGGAACTGGAACTCC>450
hFuca1-D230N-E294Q  401>ACGAAGGCTTCACAAACTGGCCGAGTCCTGTGTCTTGGAACTGGAACTCC>450
                          H  E  G  F  T  N  W  P  S  P  V  S  W  N  W  N  S

hFuca1              451>AAAGACGTGGGGCCTCATCGGGATTTGGTTGGTGAATTGGGAACAGCTCT>500
hFuca1-His6         451>AAAGACGTGGGGCCTCATCGGGATTTGGTTGGTGAATTGGGAACAGCTCT>500
hFuca1-D230N-E294Q  451>AAAGACGTGGGGCCTCATCGGGATTTGGTTGGTGAATTGGGAACAGCTCT>500
                           K  D  V  G  P  H  R  D  L  V  G  E  L  G  T  A  L
```

Figure A.4: cDNA and protein sequences of untagged and His_6-tagged human α-L-fucosidase as well as of its active site mutant (D230N, E294Q)

```
hFuca1                501>CCGGAAGAGGAACATCCGCTATGGACTATACCACTCACTCTTAGAGTGGT>550
hFuca1-His6           501>CCGGAAGAGGAACATCCGCTATGGACTATACCACTCACTCTTAGAGTGGT>550
hFuca1-D230N-E294Q    501>CCGGAAGAGGAACATCCGCTATGGACTATACCACTCACTCTTAGAGTGGT>550
                           R  K  R  N  I  R  Y  G  L  Y  H  S  L  L  E  W

hFuca1                551>TCCATCCACTCTATCTACTTGATAAGAAAAATGGCTTCAAAACACAGCAT>600
hFuca1-His6           551>TCCATCCACTCTATCTACTTGATAAGAAAAATGGCTTCAAAACACAGCAT>600
hFuca1-D230N-E294Q    551>TCCATCCACTCTATCTACTTGATAAGAAAAATGGCTTCAAAACACAGCAT>600
                         F  H  P  L  Y  L  L  D  K  K  N  G  F  K  T  Q  H

hFuca1                601>TTTGTCAGTGCAAAAACAATGCCAGAGCTGTACGACCTTGTTAACAGCTA>650
hFuca1-His6           601>TTTGTCAGTGCAAAAACAATGCCAGAGCTGTACGACCTTGTTAACAGCTA>650
hFuca1-D230N-E294Q    601>TTTGTCAGTGCAAAAACAATGCCAGAGCTGTACGACCTTGTTAACAGCTA>650
                            F  V  S  A  K  T  M  P  E  L  Y  D  L  V  N  S  Y

hFuca1                651>TAAACCTGATCTGATCTGGTCTGATGGGGAGTGGGAATGTCCTGATACTT>700
hFuca1-His6           651>TAAACCTGATCTGATCTGGTCTGATGGGGAGTGGGAATGTCCTGATACTT>700
hFuca1-D230N-E294Q    651>TAAACCTGATCTGATCTGGTCTAATGGGGAGTGGGAATGTCCTGATACTT>700
                              K  P  D  L  I  W  S D/N G  E  W  E  C  P  D  T

hFuca1                701>ACTGGAACTCCACAAATTTTCTTTCATGGCTCTACAATGACAGCCCTGTC>750
hFuca1-His6           701>ACTGGAACTCCACAAATTTTCTTTCATGGCTCTACAATGACAGCCCTGTC>750
hFuca1-D230N-E294Q    701>ACTGGAACTCCACAAATTTTCTTTCATGGCTCTACAATGACAGCCCTGTC>750
                            Y  W  N  S  T  N  F  L  S  W  L  Y  N  D  S  P  V

hFuca1                751>AAGGATGAGGTGGTAGTAAATGACCGATGGGGTCAGAACTGTTCCTGTCA>800
hFuca1-His6           751>AAGGATGAGGTGGTAGTAAATGACCGATGGGGTCAGAACTGTTCCTGTCA>800
hFuca1-D230N-E294Q    751>AAGGATGAGGTGGTAGTAAATGACCGATGGGGTCAGAACTGTTCCTGTCA>800
                              K  D  E  V  V  V  N  D  R  W  G  Q  N  C  S  C  H

hFuca1                801>CCATGGAGGATACTATAACTGTGAAGATAAATTCAAGCCACAGAGCTTGC>850
hFuca1-His6           801>CCATGGAGGATACTATAACTGTGAAGATAAATTCAAGCCACAGAGCTTGC>850
hFuca1-D230N-E294Q    801>CCATGGAGGATACTATAACTGTGAAGATAAATTCAAGCCACAGAGCTTGC>850
                              H  G  G  Y  Y  N  C  E  D  K  F  K  P  Q  S  L

hFuca1                851>CAGATCACAAGTGGGAGATGTGCACCAGCATTGACAAGTTTTCCTGGGGC>900
hFuca1-His6           851>CAGATCACAAGTGGGAGATGTGCACCAGCATTGACAAGTTTTCCTGGGGC>900
hFuca1-D230N-E294Q    851>CAGATCACAAGTGGCAGATGTGCACCAGCATTGACAAGTTTTCCTGGGGC>900
                            P  D  H  K  W E/Q M  C  T  S  I  D  K  F  S  W  G

hFuca1                901>TATCGTCGTGACATGGCATTGTCTGATGTTACAGAAGAATCTGAAATCAT>950
hFuca1-His6           901>TATCGTCGTGACATGGCATTGTCTGATGTTACAGAAGAATCTGAAATCAT>950
hFuca1-D230N-E294Q    901>TATCGTCGTGACATGGCATTGTCTGATGTTACAGAAGAATCTGAAATCAT>950
                              Y  R  R  D  M  A  L  S  D  V  T  E  E  S  E  I  I

hFuca1                951>TTCGGAACTGGTTCAGACAGTAAGTTTGGGAGGCAACTATCTTCTGAACA>100
hFuca1-His6           951>TTCGGAACTGGTTCAGACAGTAAGTTTGGGAGGCAACTATCTTCTGAACA>100
hFuca1-D230N-E294Q    951>TTCGGAACTGGTTCAGACAGTAAGTTTGGGAGGCAACTATCTTCTGAACA>100
                              S  E  L  V  Q  T  V  S  L  G  G  N  Y  L  L  N
```

Figure A.4: cDNA and protein sequences of untagged and His_6-tagged human α-L-fucosidase as well as of its active site mutant (D230N, E294Q; continued)

```
hFuca1              1001>TTGGACCAACTAAAGATGGACTGATTGTTCCCATCTTCCAAGAAAGGCTT>1050
hFuca1-His6         1001>TTGGACCAACTAAAGATGGACTGATTGTTCCCATCTTCCAAGAAAGGCTT>1050
hFuca1-D230N-E294Q  1001>TTGGACCAACTAAAGATGGACTGATTGTTCCCATCTTCCAAGAAAGGCTT>1050
                          I  G  P  T  K  D  G  L  I  V  P  I  F  Q  E  R  L

hFuca1              1051>CTTGCTGTTGGGAAATGGCTGAGCATCAATGGGGAGGCTATCTATGCCTC>1100
hFuca1-His6         1051>CTTGCTGTTGGGAAATGGCTGAGCATCAATGGGGAGGCTATCTATGCCTC>1100
hFuca1-D230N-E294Q  1051>CTTGCTGTTGGGAAATGGCTGAGCATCAATGGGGAGGCTATCTATGCCTC>1100
                            L  A  V  G  K  W  L  S  I  N  G  E  A  I  Y  A  S

hFuca1              1101>CAAACCATGGCGGGTGCAATGGGAAAAGAACACAACATCTGTATGGTATA>1150
hFuca1-His6         1101>CAAACCATGGCGGGTGCAATGGGAAAAGAACACAACATCTGTATGGTATA>1150
hFuca1-D230N-E294Q  1101>CAAACCATGGCGGGTGCAATGGGAAAAGAACACAACATCTGTATGGTATA>1150
                             K  P  W  R  V  Q  W  E  K  N  T  T  S  V  W  Y

hFuca1              1151>CCTCAAAGGGATCGGCTGTTTATGCCATTTTTCTGCACTGGCCAGAAAAT>1200
hFuca1-His6         1151>CCTCAAAGGGATCGGCTGTTTATGCCATTTTTCTGCACTGGCCAGAAAAT>1200
hFuca1-D230N-E294Q  1151>CCTCAAAGGGATCGGCTGTTTATGCCATTTTTCTGCACTGGCCAGAAAAT>1200
                          T  S  K  G  S  A  V  Y  A  I  F  L  H  W  P  E  N

hFuca1              1201>GGAGTCTTAAACCTTGAATCCCCCATAACTACCTCAACTACAAAGATAAC>1250
hFuca1-His6         1201>GGAGTCTTAAACCTTGAATCCCCCATAACTACCTCAACTACAAAGATAAC>1250
hFuca1-D230N-E294Q  1201>GGAGTCTTAAACCTTGAATCCCCCATAACTACCTCAACTACAAAGATAAC>1250
                            G  V  L  N  L  E  S  P  I  T  T  S  T  T  K  I  T

hFuca1              1251>AATGCTGGGAATTCAAGGAGATCTGAAGTGGTCCACAGATCCAGATAAAG>1300
hFuca1-His6         1251>AATGCTGGGAATTCAAGGAGATCTGAAGTGGTCCACAGATCCAGATAAAG>1300
hFuca1-D230N-E294Q  1251>AATGCTGGGAATTCAAGGAGATCTGAAGTGGTCCACAGATCCAGATAAAG>1300
                             M  L  G  I  Q  G  D  L  K  W  S  T  D  P  D  K

hFuca1              1301>GTCTCTTCATCTCTCTACCCCAGTTGCCACCCTCTGCTGTCCCCGCAGAG>1350
hFuca1-His6         1301>GTCTCTTCATCTCTCTACCCCAGTTGCCACCCTCTGCTGTCCCCGCAGAG>1350
hFuca1-D230N-E294Q  1301>GTCTCTTCATCTCTCTACCCCAGTTGCCACCCTCTGCTGTCCCCGCAGAG>1350
                          G  L  F  I  S  L  P  Q  L  P  P  S  A  V  P  A  E

hFuca1              1351>TTTGCTTGGACTATAAAGCTGACAGGAGTGAAG----------------->1383
hFuca1-His6         1351>TTTGCTTGGACTATAAAGCTGACAGGAGTGAAGGGAAGAGGATCGCATCA>1400
hFuca1-D230N-E294Q  1351>TTTGCTTGGACTATAAAGCTGACAGGAGTGAAG----------------->1383
                             F  A  W  T  I  K  L  T  G  V  K  G  R  G  S  H  H

hFuca1              1384>----------------TAA>1386
hFuca1-His6         1401>CCATCACCATCACGGATAA>1419
hFuca1-D230N-E294Q  1384>----------------TAA>1386
                             H  H  H  H  G  *
```

Figure A.4: cDNA and protein sequences of untagged and His_6-tagged human α-L-fucosidase as well as of its active site mutant (D230N, E294Q; continued)

Additional results

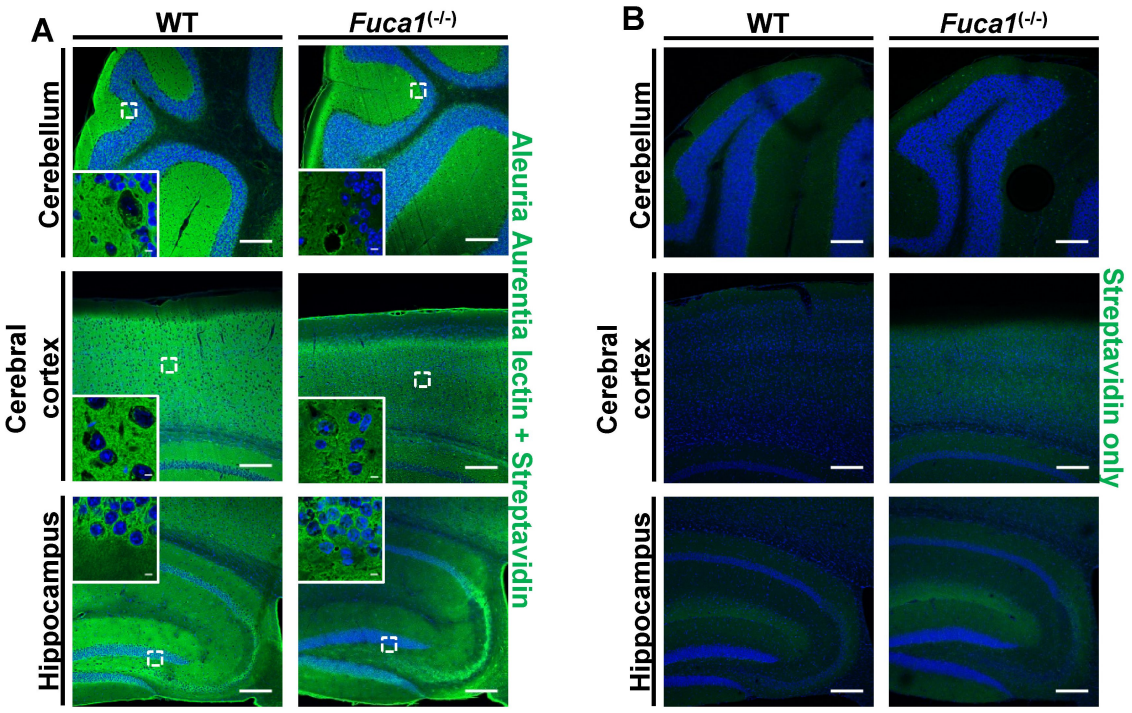

Figure A.5: ***Aleuria aurentia*** **lectin staining of the brain**
Semi-thin sections of the brain of 5-month-old wildtype and *Fuca1*$^{(-/-)}$ mice were stained with (**A**) biotinylated *Aleuria aurentia* lectin, which was detected using DyeLight® 594-conjungated straptavidin or (**B**) as internal control were incubated with DyeLight® 594-conjungated streptavidin only. Bars correspondent to 200 μm or 5 μm (inset). Cell nuclei were stained with DAPI (blue).

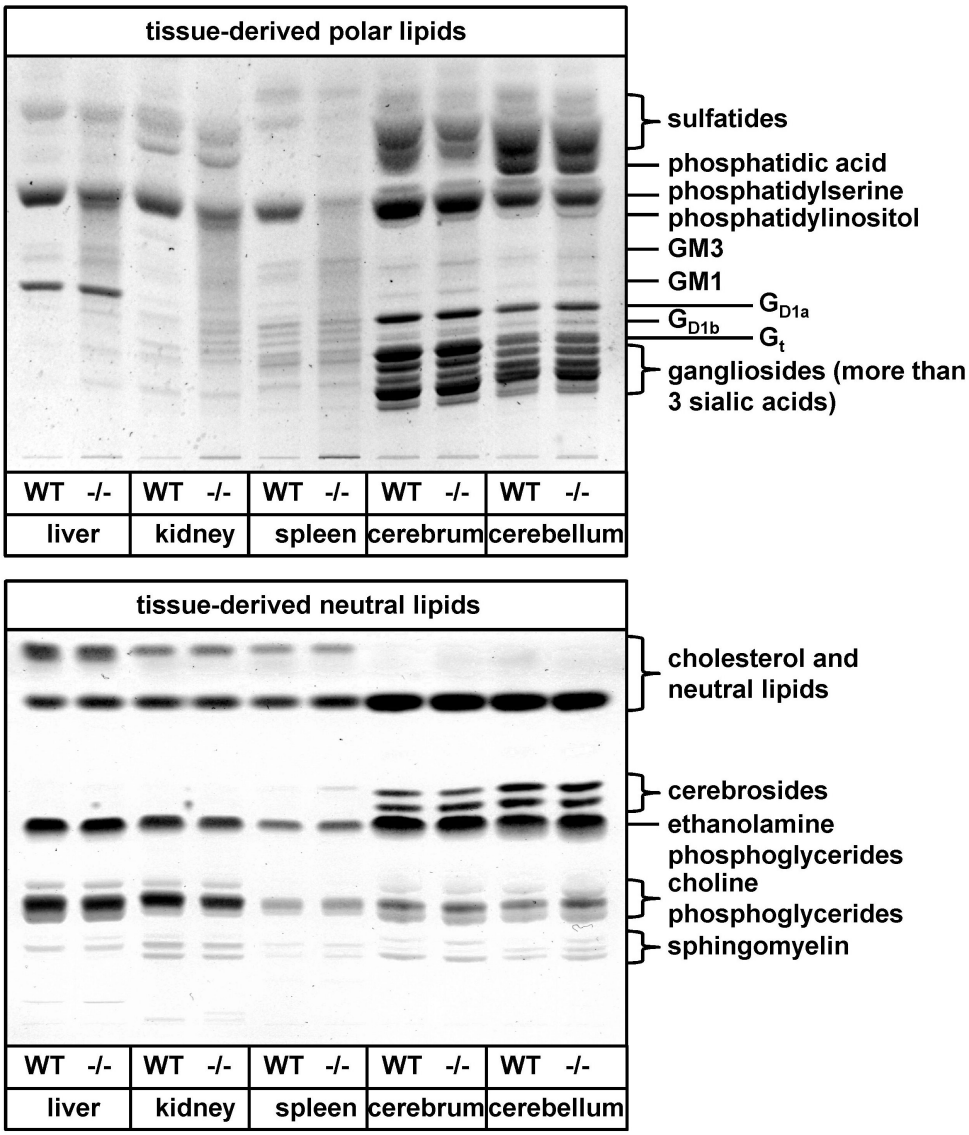

Figure A.6: Analysis of lipid-rich fractions from mouse tissues by TLC
Lipids were isolated from different tissues of 3-month-old wildtype and *Fuca1*$^{(-/-)}$ mice, were separated into polar and neutral lipids and were analyzed by TLC. Identification of the single lipid species was done by comparison with published results (Kyrklund 1987).

List of Abbreviations

4-MU	4-methylumbelliferone
4-MUF	4-methylumbelliferyl-α-L-fucopyranoside
αMan	α-mannosidase
βGal	β-galactosidase
βMan	β-mannosidase
aa	amino acid
APS	ammonium persulfate
Asn	asparagine
ATP	adenosine-5'-triphosphate
BMT	bone marrow transplantation
bp	base pair(s)
BSA	bovine serum albumin
CCD	charge coupled device
cDNA	complementary DNA
CHO	Chinese hamster ovary cell
CLEAR	coordinated lysosomal expression and regulation
CMA	chaperone-mediated autophagy
CNBr	cyanogen bromide
CNS	central nervous system
ConA	Concanavalin A
CtsB	cathepsin B
CtsD	cathepsin D
CV	column volume
DAPI	4',6-diamidino-2-phenylindole
DABCO	1,4-diazabicyclo[2.2.2]octane
DEAE	diethylaminoehtyl
DEPC	diethyl pyrocarbonate
dH2O	sterile Milli Q water
DHFR	dihydrofolate reductase
DMEM	Dulbecco's modified Eagle medium
DMSO	dimethyl sulfoxide
DNA	deoxyribonucleic acid
dNTP	deoxynucleoside triphosphate (dATP, dCTP, dGTP, dTTP)

E. coli	*Escherichia coli*
DTA	diphtheria toxin A
ECL	enhanced chemiluminescence
EDTA	ethylendiamine tetraacetic acid
EET	enzyme enhancement therapy
EndoH	endo-b-N-acetylglucosaminidase H
ER	endoplasmatic reticulum
ERT	enzyme replacement therapy
FCS	fetal calf serum
Fuc	L-fucose
Fuca1	α-L-fucosidase 1
Fuca1$^{(-/-)}$	*Fuca1* gene knock-out
Fuca2	α-L-fucosidase 2
fw	forward
g	earth's gravity
GAPDH	glycerinaldehyd-3-phosphat-dehydrogenase
GFAP	glial fibrillary acidic protein
GlcNAc	*N*-acetylglucosamine
GM2	monosialic ganglioside 2
GNTP	Golgi-*N*-acetylglucosamine-1-phosphotransferase
GTP	guanosine-5'-triphosphate
h	human
HexB	hexosaminidase subunit beta
HPLC	high performance liquid chromatography
HRP	horseradish peroxidase
Hsc	heat shock cognate
HSCs	haematopoetic stem cells
Iba1	ionized calcium-binding adapter molecule 1
IEX	ion exchange chromatography
IMAC	immobilized metal ion affinity chromatography
iPSCs	induced pluripotent stem cells
kb	kilobase(s)
kDa	kilodalton
LAMP	lysosomal-associated membrane protein
LB	Luria Bertani
LIMP	lysosomal integral membrane protein

LSD	lysosomal storage disease
m	murine
M6P	mannose-6-phosphate
Man	mannose
MBP	myelin basic protein
MEF	mouse embryonic fibroblasts
ML	mucolipidosis
MLD	metachromatic leukodystrophy
MPR 40 / 300	mannose-6-phosphate receptor (40 kDa or 300 kDa form)
MPS	mucopolysaccharidoses
mRNA	messenger RNA
MRS	magnetic resonance spectroscopy
MS	mass spectrometry
MSD	multiple sulfatase deficiency
mTORC1	rapamycin complex 1
MWCO	molecular weight cut-off
NCL	neuronal ceroid lipofuscinosis
NHS	N-hydroxysuccinimide
NMD	nonsense-mediated mRNA decay
NPC	Niemann-Pick disease type C
p. a.	pro analysis purity
PBS	phosphate buffered saline
PCR	polymerase chain reaction
PEI	polyethylenimine
PFA	*para*-formaldehyde
PLL	poly-L-lysine
Plp1	proteolipid protein 1
PMSF	phenylmethylsulfonyl fluoride
PNGase F	peptidyl-N-glycosidase F
pNP	para-nitrophenol
pNPF	*para*-nitrophenyl-α-L-fucopyranoside
PTC	premature termination codon
PVDF	polyvinylidene fluoride
rev	reverse
RGS-His_6	protein tag with the sequence Arg-Gly-Ser-His-His-His-His-His-His
RNA	ribonucleic acid

SCX	strong cation exchange chromatography
SDS	sodium dodecyl sulfate
SDS-PAGE	sodium dodecyl sulfate polyacrylamide gel electrophoresis
Ser	serine
S-PBS	PBS containing 0.2 % saponin
SUMF1	*sulfatase modifying factor 1*
T_M	melting temperature (PCR)
TAE	tris/acetate/EDTA buffer
TBS	tris buffered saline
TEM	transmission electron microscopy
TEMED	N,N,N',N'-tetramethylethylene diamine
TFE3	transcription factor E3
TFEB	transcription factor EB
Thr	threonine
TLC	thin-layer chromatography
Tris	tris-(hydroxymethyl)-aminomethane
UCE	uncovering enzyme
WT	wildtype
U	unit(s)
UV	ultraviolet
v/v	volume per volume
w/v	weight per volume

List of Figures

List of Tables

Selbstständigkeitserklärung

Erklärung gemäß §8 Abs. 1 der Rahmenpromotionsordnung der Universität Bielefeld

Die vorliegende Arbeit wurde in der Zeit von Oktober 2013 bis September 2016 in der Arbeitsgruppe Biochemie I an der Fakultät für Chemie der Universität Bielefeld unter der wissenschaftlichen Anleitung von Prof. Dr. Torben Lübke angefertigt.

Hiermit erkläre ich, dass mir die gegenwärtige Promotionsordnung der Fakultät für Chemie der Universität Bielefeld vom 01.07.2011 bekannt ist.

Hiermit versichere ich, dass ich die vorliegende Dissertation ohne fremde Hilfe selbstständig verfasst und nur die angegebenen Quellen und Hilfsmittel verwendet habe. Wörtlich oder dem Sinn nach aus Werken entnommene Stellen sind unter Angabe der Quellen kenntlich gemacht.

Ich bestätige, dass Dritte weder unmittelbar noch mittelbar geldwerte Leistungen von mir für Vermittlungstätigkeiten oder für Arbeiten erhalten haben, die im Zusammenhang mit dem Inhalt der vorgelegten Dissertation stehen.

Die vorliegende Dissertation wurde noch nicht als Prüfungsarbeit für eine staatliche oder andere wissenschaftliche Prüfung eingereicht und weder in der gegenwärtigen noch in einer anderen Fassung bei einer anderen Hochschule als Dissertation vorgelegt.

Bielefeld, den 06.09.2016